
The Quest of Radical Cations of the
Heavier Chalcogenides

INAUGURAL DISSERTATION

Towards the Academic Degree
Doctor Rerum Naturalium (Dr. rer. nat.)

Submitted to the
Department of Biology and Chemistry
of the Universität Bremen

by
Farzin Mostaghimi

from Shiraz

May 2021

This work was carried out under the supervision of Prof. Dr. Jens Beckmann from October 2014 to May 2021 at the Institute of Inorganic Chemistry and Crystallography, Department of Biology and Chemistry of the University of Bremen.

1st Referee: Prof. Dr. Jens Beckmann

2nd Referee: Prof. Dr. Petra Swiderek

Disputation: 03.09.2021

Acknowledgement

First of all I would like to express my gratitude to Prof. Dr. Jens Beckmann for the opportunity to work in his group, for mentoring and his support during that time.

Furthermore I want to thank Prof. Dr. Petra Swiderek for being the reviewer of this thesis.

I would also like to thank the members of the audit committee: Prof. Dr. Jens Beckmann, Prof. Dr. Petra Swiderek, Prof. Dr. Hans-Joachim Breunig, Dr. Malte Hesse, Daniel Duvinage and Björn Grabbet.

Moreover I would like to thank all the staff members of the service department of the University of Bremen for providing analytical data and technical support, especially Dr. Thomas Dülks and Dorit Kemken for measuring of numerous mass spectra and their help with the assignment. My special thanks go to the former and actual members of our work group for providing a good environment for work.

Moreover I would like to thank Peter Brackmann and Sarah Matz for measuring the crystals by X-ray crystallography and Dr. Enno Lork for solving the received data.

Last but not least I would like to thank my family, my parents Iraj and Farizeh, my brother Farhad and especially my wife Sayna who accompanied and supported me continuously through all the time.

List of Publications

Published Articles

- Chulanova, E. A.; Pritchina, E. A.; Malaspina, L. A.; Grabowsky, S.; Mostaghimi, F.; Beckmann, J.; Bagryanskaya, I. Y.; Shakhova, M. V.; Konstantinova, L. S.; Rakitin, O. A. et al. *New Charge-Transfer Complexes with 1,2,5-Thiadiazoles as Both Electron Acceptors and Donors Featuring an Unprecedented Addition Reaction*. *Chemistry, A European Journal* **2017**, 23, 852–864. DOI: 10.1002/chem.201604121.
- Wohltmann, W.; Mostaghimi, F.; Bolsinger, J.; Lork, E.; Mebs, S.; Beckmann, J. *Synthesis and halogenation of bis(8-methoxynaphthyl)ditelluride*. *Inorganica Chimica Acta* **2018**, 475, 73–82. DOI: 10.1016/j.ica.2017.08.011.
- Ramirez Y Medina, I.-M.; Rohdenburg, M.; Mostaghimi, F.; Grabowsky, S.; Swiderek, P.; Beckmann, J.; Hoffmann, J.; Dorcet, V.; Hissler, M.; Staubitz, A. *Tuning the Optoelectronic Properties of Stannoles by the Judicious Choice of the Organic Substituents*. *Inorganic chemistry* **2018**, 57, 12562–12575. DOI: 10.1021/acs.inorgchem.8b01649.
- Mostaghimi, F.; Lork, E.; Hong, I.; Roemmele, T. L.; Boéré, R. T.; Mebs, S.; Beckmann, J. *The reaction of phenoxatellurine with single-electron oxidizers revisited*. *New J. Chem.* **2019**, 43, 12754–12766. DOI: 10.1039/C9NJ02401H.
- Mostaghimi, F.; Bolsinger, J.; Lork, E.; Beckmann, J. *New insights into the oxidation of phenoxatellurine with sulphuric acid*. *Main Group Metal Chemistry* **2019**, 42, 150–152. DOI: 10.1515/mgmc-2019-0017.
- Mostaghimi, F.; Lork, E.; Beckmann, J. *fac-Bis(phenoxatellurine) tricarbonyl manganese(I) bromide*. *Main Group Metal Chemistry* **2020**, 43, 181–183. DOI: 10.1515/mgmc-2020-0022.
- Mostaghimi, F.; Duvinage, D; Lork, E.; Beckmann, J. *Synthesis and structure of 2,8-dimethyl-10,10-dichlorophenoxatellurine*. *Main Group Metal Chemistry* **2020**, 44, 9–11. DOI: <https://doi.org/10.1515/mgmc-2021-0002>.

Poster Presentations and Lectures at Conferences

- Mostaghimi, F.; Beckmann, J.; Lork, E.; *On the Single Electron Oxidation of Phenoxatellurine*, 18th Norddeutsches Doktorandenkolloquium **2015**, Goslar, Germany.
- Mostaghimi, F.; *On the Way to Te-containing Radicals* **2017**, Doktoranden-Seminar, GDCH JungChemikerForum, Bremen, Germany.

Contents

1. Introduction	1
1.1. Homoatomic Polycations	1
1.2. Radical Cations	2
2. Results	12
2.1. New Charge-Transfer Complexes with 1,2,5-Thiadiazoles as Both Electron Acceptors and Donors Featuring an Unprecedented Addition Reaction	12
2.1.1. Synopsis	12
2.1.2. Experimental Contributions	12
2.2. The reaction of phenoxatellurine with single-electron oxidizers revisited	26
2.2.1. Synopsis	26
2.2.2. Experimental Contributions	26
2.3. Trimorphism of the Dicationic Phenoxatellurine Triple Decker Triflate Salt	40
2.3.1. Introduction & Results	40
2.3.2. Experimental	47
2.4. New insights into the oxidation of phenoxatellurine with sulphuric acid	51
2.4.1. Synopsis	51
2.4.2. Experimental Contributions	51
2.5. <i>fac</i> -Bis(Phenoxatellurine) Tricarbonyl Manganese(I) Bromide	55
2.5.1. Synopsis	55
2.5.2. Experimental Contributions	55
2.6. Synthesis and Structure of 2,8-Dimethyl-10,10-dichlorophenoxatellurine	59
2.6.1. Synopsis	59
2.6.2. Experimental Contributions	59
2.7. Synthesis and Crystal Structure of Phenoxaiodonium Tosylate	63
2.7.1. Introduction & Results	63
2.7.2. Experimental	64
2.8. Synthesis and halogenation of bis(8-methoxynaphthyl)ditelluride	67
2.8.1. Synopsis	67
2.8.2. Experimental Contributions	67

2.9. Synthesis and characterization of 5-Diphenylphosphino-6-phenylchalcogenacenaphthyenes	78
2.9.1. Introduction & Results	78
2.9.2. Experimental	83
2.10. Synthesis and Single-Electron Oxidation of Bulky Bis(<i>m</i> -terphenyl)chalcogenes.....	88
2.10.1. Introduction & Results	88
2.10.2. Experimental	92
2.11. Synthesis and Characterization of Trimesityltelluronium hexafluorophosphate.....	96
2.11.1. Introduction & Results	96
2.11.2. Experimental	97
3. Conclusion	100
4. Zusammenfassung	102
5. References	104
6. Supporting Information	117

1. Introduction

Sulphur was already known in ancient times and used for example, as described in the Ebers Papyrus, an ancient Egyptian medical papyrus, in balms for fumigation. Due to its diversity and elemental occurrence sulphur belongs to the most extensively examined and used elements. The most common use of sulphur is the conversion to sulphuric acid.^[1] Other applications include sulphur as components of fertiliser^[2] or its conversion to rubber.^[3]

Apart from common usage, organosulphur compounds play an important role in chemistry, for example in the Asinger reaction for the formation of 3-thiazolines.^[4] The reaction of Grignard reagents with sulphur leads to thioether and thiols. Cyclohexane can be dehydrogenated to benzene by the use of hydrogen sulphide.^[5]

The discovery of selenium dates back to 1818 when both chemists, Jöns Jacob Berzelius and Johan Gottlieb Gahn, were producing sulphuric acid by the lead chamber process in Sweden.^[6] Almost 20 years later, in 1836 the first organoselenium compound was synthesized by Löwig.^[7] Due to the similar behaviour of organoselenium compounds towards organosulphur analogues, selenium was of little importance for the synthetic chemistry. Nowadays organoselenium compounds are used in specialized reactions, for example as vinylic selenides for the stereoselective functionalization of alkenes^[8] or as selenium dioxide for the Riley-Oxidation, a mild, selective oxidation reaction of ketones and alkenes.^[9] Tellurium was first discovered in 1782 by the Austrian mineralogist Müller von Reichenstein, although he was not able to identify it as a new element. A few years later, in 1798 Klaproth isolated the new element and named it tellurium after the Latin word for "earth", *tellus*.^[6] Based on the high prices, tellurium is mainly used in the metallurgy for increasing the corrosion resistance and making the resulting alloy more machinable. Moreover tellurium is used widely in the semiconductor industry, for example in the new phase change memory chips (PCM).^[10] In chemical synthesis tellurium compounds can be used as pigments for ceramics.^[11]

1.1. Homoatomic Polycations

Although it is well known for the elements of the 16th group to have a tendency to build cations and homoatomic polycations^[12,13], only little is known about their chemistry and behaviour. With conc. sulphuric acid the oxidation of sulphur cannot be realized^[14], whereas the heavier congeners selenium and tellurium can be oxidized easily to the intensely coloured Se_8^{2+} (green) and Te_4^{2+} (red) cations. Both reactions for generating the polycations are used as quantitative proof of those elements.

Not just the discovery of tellurium dates back to Klaproth in 1798, but also the disclosure of the probably smallest and oldest known polytellurium cation^[15], although the molecular structure

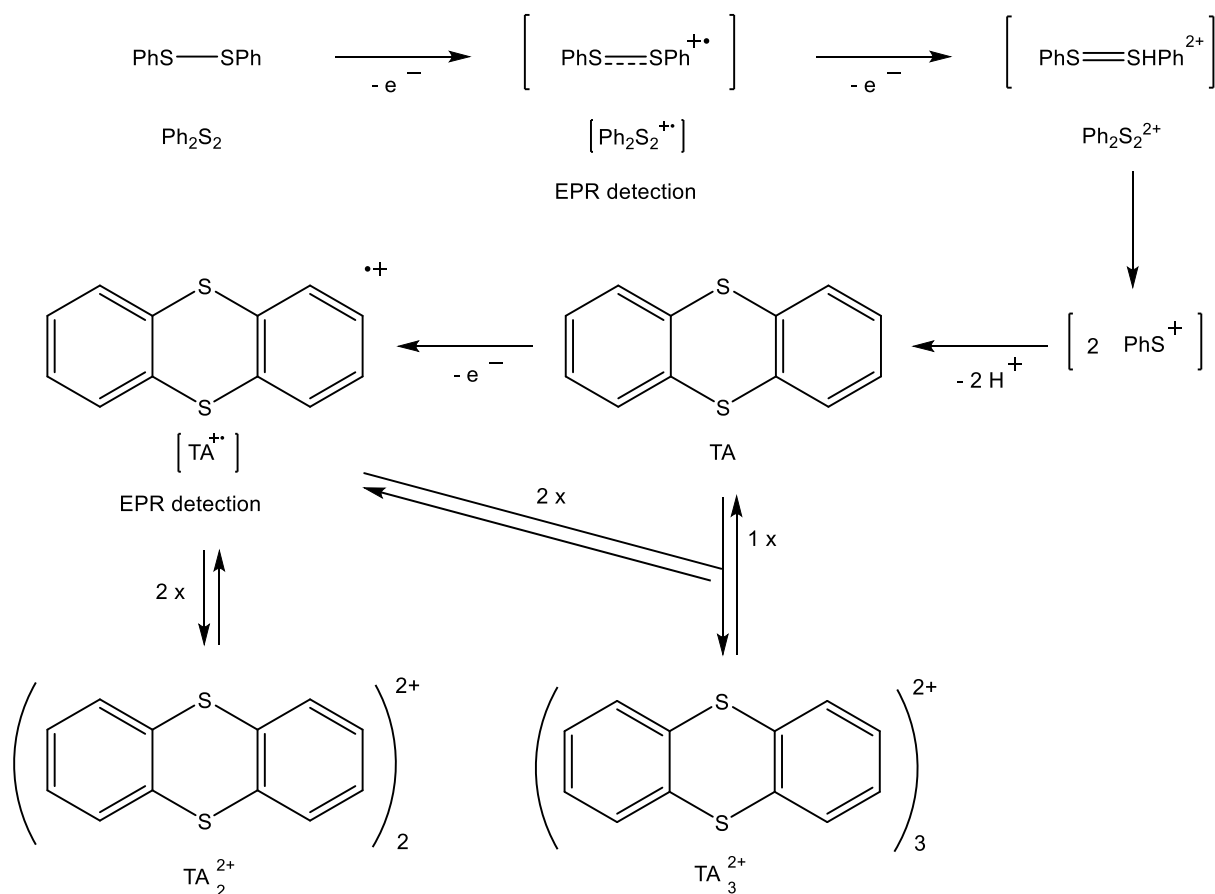
of the dication was unknown for a long time. In 1971 Barr et al. introduced the structure of a Te_4^{2+} cation with the help of $\text{Te}_4[\text{AsF}_6]_2$.^[16] The following years, different working groups focused on the characterization of the molecule via chemical analysis and vibrational spectroscopy^[17–19], but the crystal structure was hitherto unknown until 2003.^[20] Despite the fact that meanwhile various structures of Se_4^{2+} and Te_4^{2+} are known, there are only few S_4^{2+} structures^[19,21–25], for instance the resulting structure of the oxidation of $\text{S}_2\text{O}_6\text{F}_2$ with antimony pentafluoride to $\text{S}_4[\text{SbF}_6]_2$.^[26] The reason for the rarity is, that sulphur cations build bigger clusters, from S_8 to S_{19}^{2+} . Gillespie et al. presented a S_8^{2+} and S_{16}^{2+} species by the reaction of sulphur with arsenic pentafluoride.^[27]

The smallest cationic dichalcogen-building units E_2^+ ($\text{E} = \text{S}, \text{Se}, \text{Te}$) were, due to their instability, just exposed and proven in the gas phase.

In comparison to that, the heavier analogues R-E-E-R ($\text{E} = \text{S}, \text{Se}, \text{Te}$) of organic peroxides build stable and common compounds, which can be used as synthetic precursors in many reactions.

1.2. Radical Cations

In 1869 Stenhouse observed the evolution of an intense violet colour while dissolving thiophenol in conc. sulphuric acid.^[28,29] Although the intermediates could not be determined, he was able to isolate diphenyl disulphide (Ph_2S_2), which can be dissolved again in conc. sulphuric acid leading to the formation of thianthrene (TA), which is characterized by an intensely coloured solution, seen in Scheme 1. Thianthrene (TA) itself can also be dissolved in conc. sulphuric acid again, leading to intensely coloured solutions containing the thianthrene radical cation $(\text{TA})^{+\bullet}$.



Scheme 1. Oxidation of diphenyl disulphide in concentrated sulphuric acid (intermediate species in brackets have not been isolated).

Fries and Volk were able to set up a first connection between thiophenol and thianthrene, without recognizing the reaction as single electron oxidizing steps.^[30] In later times the usage of those intensely coloured salts as colouring agents were considered popular.^[31,32]

Gomberg's pioneering discovery on the stable free triphenylmethyl radical in 1900 led to a new understanding of radicals.^[33,34] The first proof of the radical character of the thianthrene radical cation (TA)^{•+} in conc. sulphuric acid was then worked out by Hirshon et al. in 1953.^[35] Both, diphenyl disulphide (Ph₂S₂) and thianthrene (TA), can have unpaired electrons by means of oxidation in solution, which is the reason for their intense colour. However, the synthesis was limited to the oxidation by mineral acids.^[36–39] The open-shell electronic structure of the thianthrene radical cation (TA)^{•+} was described in 1962 by the first EPR measurements.^[37,40–44] From then on many studies reported the synthesis, reactivity and use of those radicals in organic synthesis.^[45] Most conveniently, the thianthrene radical cation (TA)^{•+} has been prepared by single electron oxidation from its parent (TA) using various methods and reagents including HClO₄ / acetic anhydride^[41], SbCl₅ / HCCl₃^[46], ICl / CCl₄^[47], NO[B₄F₄]^[48,49], AlCl₃ / CH₂Cl₂^[50], the dodecamethylcarboranyl radical / hexane^[51], electrochemically with [NBu₄][PF₆] / SO₂^[52], AlCl₃ / SO₂^[53] and XeF₂, Me₃SiO₃SCF₃ / CH₂Cl₂.^[54] The molecular structure of a thianthrene radical

cation $(TA)^{+\bullet}$ was obtained by Bock et al. in 1994 with the reaction of its parent (TA) with aluminum chloride in dichloromethane. The oxidation of thianthrene (TA) results in a significant bending along the intramolecular S – S axis seen in Figure 1.

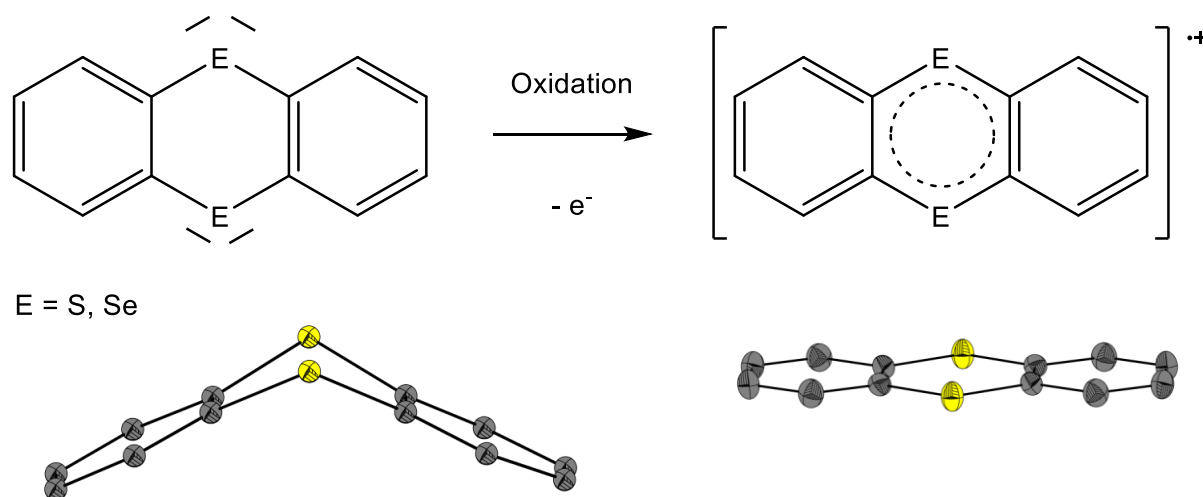


Figure 1. Change of the folding angle along the E – E axis through oxidation (E = S, Se).

The structural change enables electron pairing in the solid state and thus a reversible oligomerisation, so that intermolecular S – S interactions can proceed. A diamagnetic dimer $(TA)_2[AlCl_4]_2$ is formed (double-decker structure).^[50] Beck et al. described in 2009 a similar structure for $(TA)_2[PF_6]_2$.^[52] The same group was able to isolate a diamagnetic trimer $(TA)_3[Al_2Cl_7]_2$ (figure 2) with stacks of parallel and eclipsed TA units (parallel triple-decker structure)^[53], while a diamagnetic trimer $(TA)_3[C_{13}H_{36}B_{11}]_2$ containing stacks of parallel TA units, with an orthogonal central unit to the two outer eclipsed units (crossed triple-decker structure) was reported by Rosokha et al. in 2007.^[51]

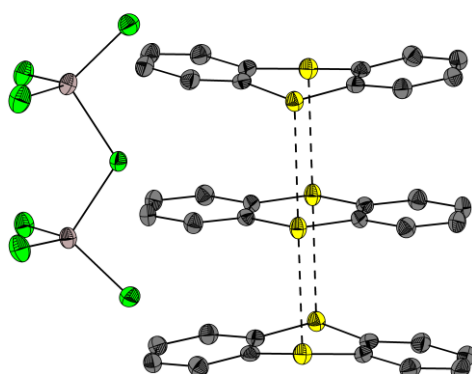


Figure 2. Crystal structure of the diamagnetic trimer $(TA)_3[Al_2Cl_7]_2$ with stacks of parallel and eclipsed TA units (parallel triple-decker structure).^[53]

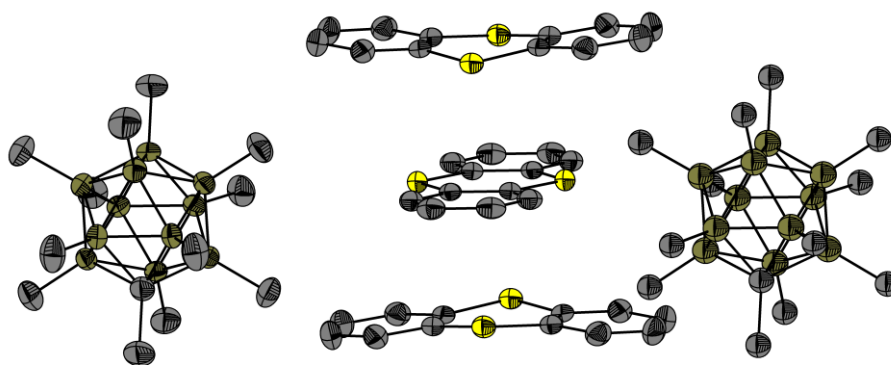
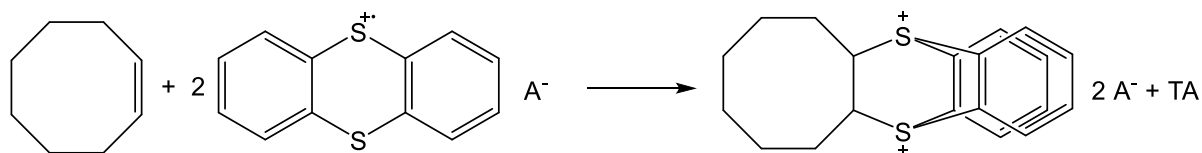


Figure 3. Crystal structure of the diamagnetic trimer $(TA)_3[C_{13}H_{36}B_{11}]_2$ containing stacks of parallel TA units, with an orthogonal central unit to the two outer eclipsed units (crossed triple-decker structure) (Solvent molecules are omitted).^[51]

As shown by UV-Vis spectro-electrochemistry, in solution the thianthrene radical cation $(TA)^{+\cdot}$ is in a concentration dependent equilibrium with its dimer $(TA)_2^{2+}$.^[44]

Connelly and Geiger described the use of the thianthrene radical cation $(TA)^{+\cdot}$ as single-oxidation reagent.^[55] The reaction can be followed visually by using the purple thianthrene radical cation $(TA)^{+\cdot}$, which turns colorless upon reduction.

Furthermore the addition of thianthrene radical cation $(TA)^{+\cdot}$ to alkenes and cycloalkenes has been investigated lately.^[56–59]



Scheme 2. Addition of thianthrene radical cation $(TA)^{+\cdot}$ to cyclohexene.^[56]

Although the thianthrene radical cation $(TA)^{+\cdot}$ has been studied in great detail, there is only little information accessible about the isotype dibenzodioxines with heavier chalcogens. The reaction of selenanthrene (SeA) with aluminium chloride carried out by Beck et al. in 2012 resulted in the double-decker structure $(SeA)_2[AlCl_4]_2$.^[53] Even though the synthesis of telluranthrene (TeA) is known, the respective radical cation $(TeA)^{+\cdot}$ has not been investigated yet. A first approach in describing the electronic reason for the aggregation of thianthrene in solid state was made by Nishinaga and Komatsu in 2005. They suggested that π -bonding of the aromatic rings is the reason for the aggregation.^[60]

The radical cations of 1,2,3,4,5,6,7,8-octamethylantracene (OMA) and 2,3,6,7-tetramethoxy-9,10-dimethylantracene (TMDMA) support their theory. Without the possibility of multicentre σ -bonding through the heteroatoms sulphur, selenium and tellurium, oligomerization takes

place and the molecules thus form double-decker^[61] and triple-decker^[62] structures, respectively.

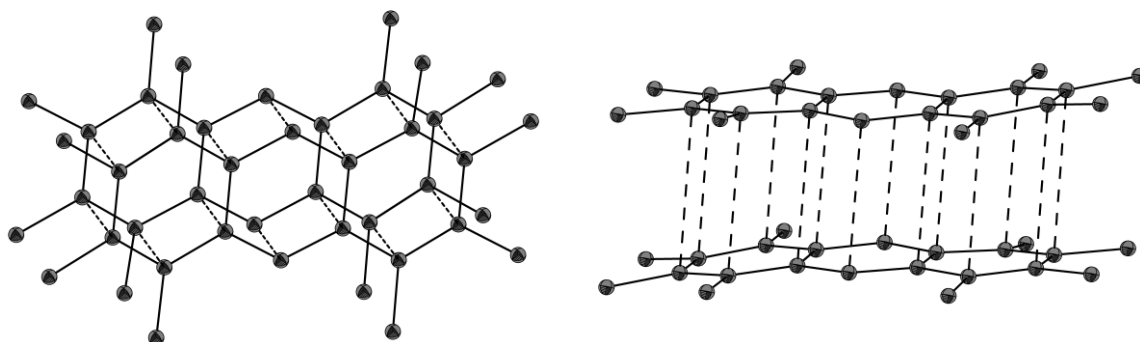


Figure 4. Crystal structure of the 1,2,3,4,5,6,7,8-octamethylantracene (OMA) radical cation double-decker structure (the counterions SbF_6 are omitted).^[61]

The paper of Plasseraud et al. on the reaction of a dimeric hydroxo di-*n*-butylstannane trifluoromethanesulphonato complex with phenazine (PA) established the fact, that not just radical cationic systems undergo oligomerisation.^[63] They reported a partly protonated double-decker $(\text{H-PA})_2[\text{O}_3\text{SCF}_3]_2$ and triple-decker structure $[(\text{H-PA})_2(\text{PA})][\text{O}_3\text{SCF}_3]_2$ seen in Figure 5.

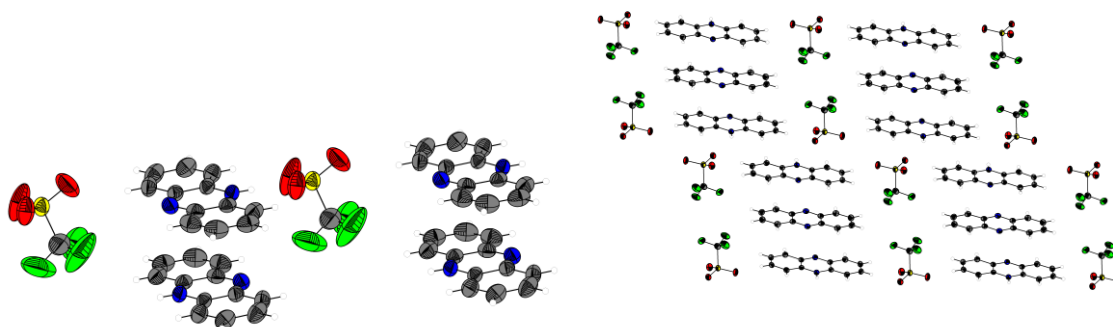
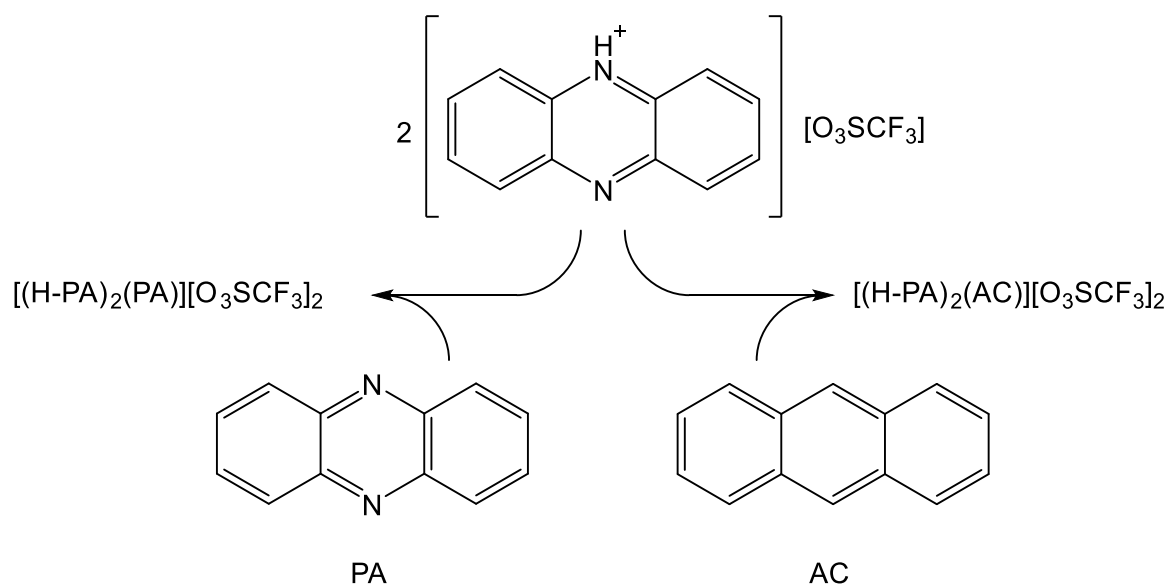


Figure 5. Unit cell of the double-decker structure (left) and the $[(\text{H-PA})_2(\text{PA})][\text{O}_3\text{SCF}_3]_2$ triple-decker structure (right).^[63]

Addition of anthracene (AC) leads to the mixed triple-decker structure $[(\text{H-PA})_2(\text{AC})][\text{O}_3\text{SCF}_3]_2$.^[64]



Scheme 3. Creation of the triple-decker structure $[(\text{H-PA})_2(\text{PA})][\text{O}_3\text{SCF}_3]_2$ (left) and the mixed triple-decker structure $[(\text{H-PA})_2(\text{AC})][\text{O}_3\text{SCF}_3]_2$ (right).^[64]

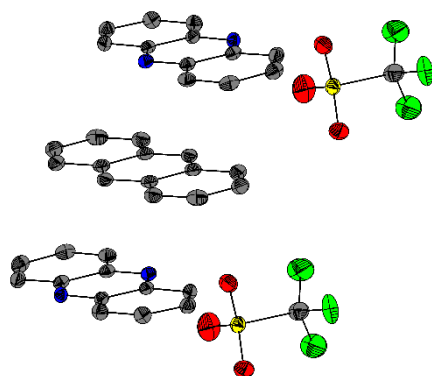
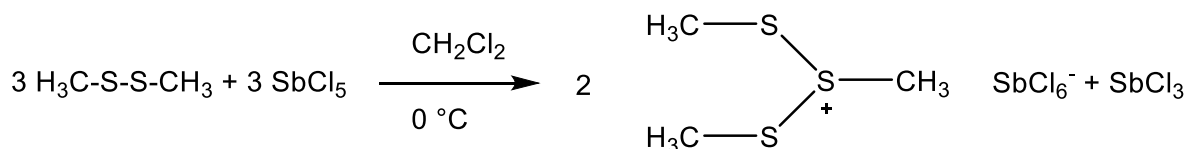


Figure 6. Crystal structure of the mixed triple-decker structure $[(\text{H-PA})_2(\text{AC})][\text{O}_3\text{SCF}_3]_2$.

Theoretical calculations on the thianthrene and selenanthrene double-decker structure ($(\text{TA})_2^{2+}$ and $(\text{SeA})_2^{2+}$) and both thianthrene triple-decker structures (parallel and crossed triple-decker structure) advise the presence of σ - and π -bonding for the oligomerisation. The results in all calculated structures indicate a singlet state as the ground state and intermolecular 2-electron-3 or 4-center (2e3c or 2e4c) bonds between the sulphur, respectively selenium atoms in the parallel stacks.^[53,65] In the crossed trimers, which stick together by London dispersion forces, these bonds are not provided.

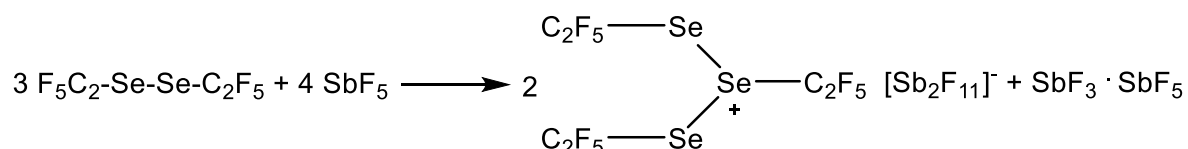
The missing intermediates seen in Scheme 1 were objectives of later researches. Roth et al. reported the isolation and characterization of the diphenyl disulphide radical cation $(\text{Ph}_2\text{S}_2)^{\cdot+}$ respectively the selenium congener by performing a single electron oxidation of diphenyl disulphide (Ph_2S_2) or diphenyl diselenide (Ph_2Se_2) in the straightened voids of the acidic zeolith matrix.^[66–68] The dication of diphenyl disulphide $(\text{Ph}_2\text{S}_2)^{2+}$ has been the objective of several

electrochemical and theoretical works.^[69-71] In earlier attempts the oxidation of dimethyl disulphide (Me_2S_2) with antimony pentachloride (SbCl_5) in dichloromethane at 0 °C resulted in a methyl sulphide stabilized sulphide cation ($(\text{CH}_3\text{S})_3^+$) as a hexachloroantimonate salt (Scheme 4).^[72]



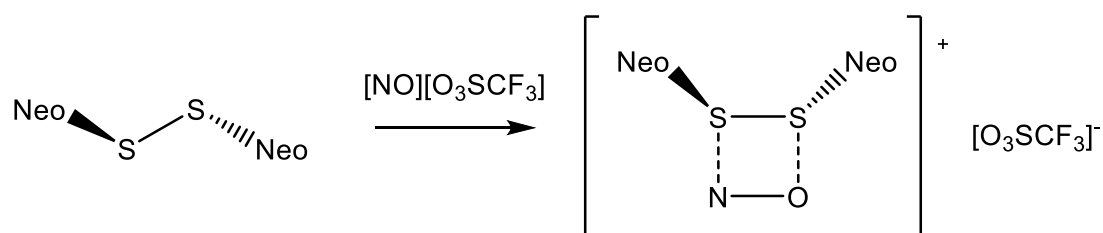
Scheme 4. Oxidation of dimethyl disulphide (Me_2S_2) with antimony pentachloride (SbCl_5).^[72]

The same year, 1976, Passmore et al. oxidized bis(perfluoroethyl) diselenide [$(\text{C}_2\text{F}_5)_2\text{Se}_2$] with antimony pentafluoride (SbF_5) and obtained similar results.^[73]



Scheme 5. Oxidation of bis(perfluoroethyl) diselenide [$(\text{C}_2\text{F}_5)_2\text{Se}_2$] with antimony pentafluoride (SbF_5).^[73]

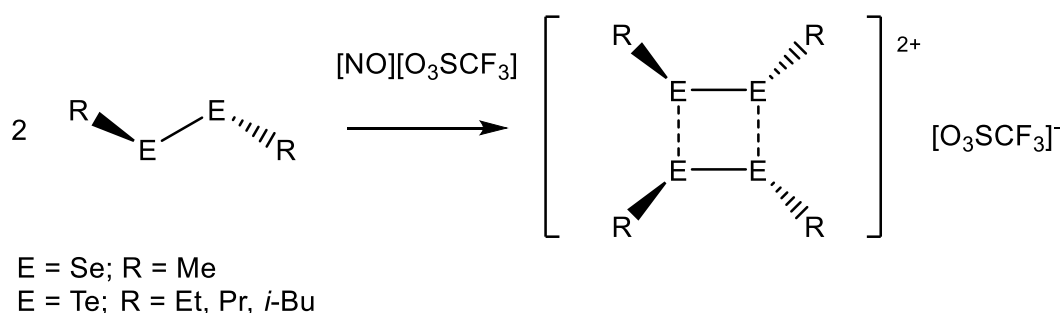
Seppelt et al. tried to prepare persistent dialkyl disulphide radical cations by oxidizing di-neopentyl disulphide (Neo_2S_2) with nitrosonium triflate ($[\text{NO}][\text{O}_3\text{SCF}_3]$) seen in Scheme 6.



Neo = neopentyl

Scheme 6. Single-electron oxidation of di-neo-pentyl disulphide (Neo_2S_2) with nitrosonium triflate ($[\text{NO}][\text{O}_3\text{SCF}_3]$).^[74]

The reaction resulted in the first diorgano disulphide-nitrosonium charge transfer adduct $[\text{Neo}_2\text{S}_2 \cdot \text{NO}]^+$ comprising a four-membered ring.^[74] Identical reactions with the heavier group 16 homologues selenium and tellurium gave diamagnetic dicationic ring structures $[(\text{MeSe})_4]^{2+}$ and $[(\text{EtTe})_4]^{2+}$.^[75]

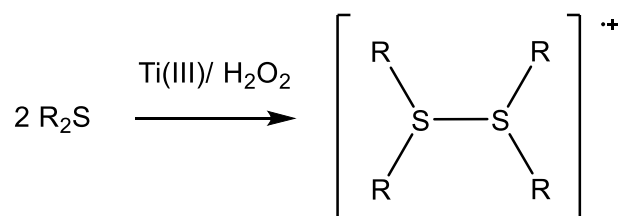


Scheme 7. Single-electron oxidation of dialkyl dichalcogenides Me_2Se_2 and R_2Te_2 (R = Et, Pr, *i*-Bu) with nitrosonium triflate ($[\text{NO}][\text{O}_3\text{SCF}_3]$).^[75,76]

The diamagnetic dicationic ring structures can be considered as dimeric, persistent radical cations with $\text{Se} \cdots \text{Se}$ and $\text{Te} \cdots \text{Te}$ bonds which can be seen as $\pi^* - \pi^*$ interaction. Both the shorter bond length of the chalcogen – chalcogen bond within the monomeric unit and the longer bonds between the monomers indicates a radical character of these compounds. Furthermore are the dicationic rings comparable with the isoelectronic dimers of the iodine dications $[\text{I}_4]^{2+}([\text{AsF}_6]^-)_2$, $[\text{I}_4]^{2+}[\text{Sb}_3\text{F}_{11}]^-[[\text{SbF}_6]^-]$ ^[77] and $[\text{I}_4]^{2+}([\text{SbF}_6]^-)_2$.^[78]

The study on the oxidation and electrochemistry of 1,2-dichalcogenides by Block et al.^[79] and the analysis of the resulting radical cations^[80] reveal the properties of cyclic varieties of the aliphatic dichalcogenides. The oxidation involves a flattening of the ring structure and shortening of the chalcogen – chalcogen bond, as seen for the thianthrene radical cation.

Another possibility to receive chalcogen radical cations is by the use of diorganochalcogenes. Houghton and Humffray first oxidized diphenyl sulphide with a controlled-potential oxidation at a platinum anode.^[81] A year later the oxidation of dialkyl sulphide species with titanium(III)-hydrogen peroxide or –persulphate resulted in dialkyl sulphide radical cations $(\text{R}_2\text{S})^{\cdot+}$ which dimerize to $[\text{R}_2\text{S}-\text{SR}_2]^{\cdot+}$ (Scheme 8).^[82] The obtained radical character was measured via ESR spectroscopy.



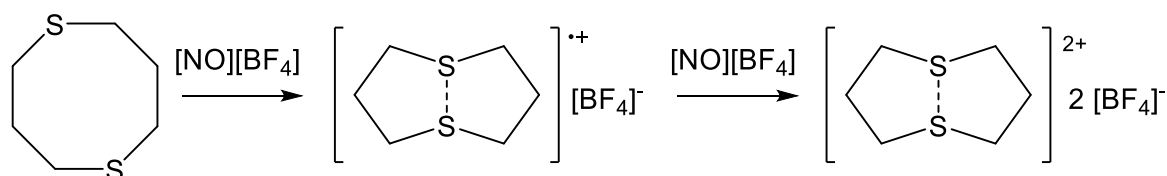
Scheme 8. Single-electron oxidation of dialkyl sulphide with titanium(III)-hydrogen peroxide.^[82]

Nishikida and Williams reported similar results by the irradiation of dimethyl sulphide (Me_2S) with γ - Rays.^[83] Many other complexed radical cations obtained by one-electron oxidation of dialkyl sulphides have been reported shortly after.^[84–86] Evidence of diorganoselenium based radical cations could also be shown by the comparison of proton coupling constants of dimethyl

selenide (Me_2Se) and its dimeric radical cation $[\text{Me}_2\text{Se}-\text{SeMe}_2]^{\bullet+}$.^[87] The first dialkyl tellurium dimer $[\text{R}_2\text{Te}-\text{TeR}_2]^{\bullet+}$ was approved by ESR measurement of γ - irradiated diluted solutions of dimethyl tellurium and diethyl tellurium at low temperature.^[88]

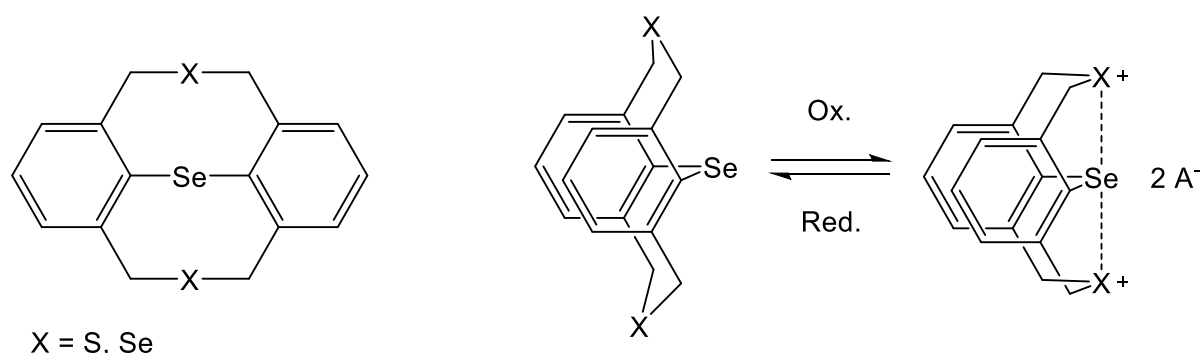
Long-living nonaromatic sulphur radical cations were obtained by Musker and Wolford in 1976. By the oxidation of 1,5-dithiacyclooctane (DTCO) with common single-electron oxidation reagents such as tetrakis(acetonitrile)copper(I) tetrafluoroborate $\text{Cu}(\text{CH}_3\text{CN})_4(\text{BF}_4)$, nitrosonium tetrafluoroborate $[\text{NO}][\text{BF}_4]$ and nitrosonium hexafluorophosphate $[\text{NO}][\text{PF}_6]$ in acetonitrile or nitromethane the desired radical cation can be formed (Scheme 9).^[89]

Analogous compounds with the heavier homologues selenium^[90–95] and tellurium^[94–97] have been reported ever since. Furthermore selenathia- and tellurathiamescocycles are accessible.^[98]



Scheme 9. Stepwise oxidation of 1,5-dithiacyclooctane (DTCO) with nitrosonium tetrafluoroborate $[\text{NO}][\text{BF}_4]$.^[89]

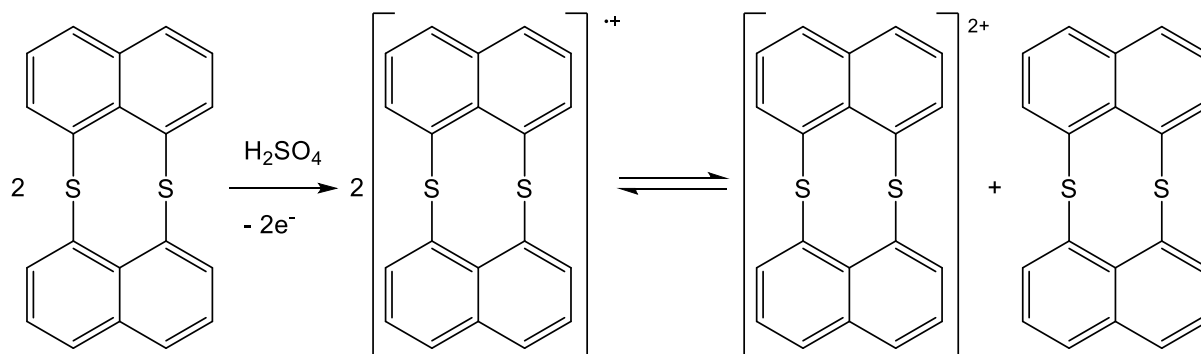
By the use of an equimolar amount of the oxidizing agent the received radical cation in Scheme 9 can be oxidized to the corresponding dication. A great number of studies investigated the extraordinary stability of the prepared radical cation. The unusual stability is attributed to transannular interactions within the mesocyclic dithioether, due to a slightly longer sulphur-sulphur bond length.^[99–107] Transannular bindings have also been used in other organochalcogen dications for stabilization, like in selenuranes and telluranes.^[108–110]



Scheme 10. Example of a selenurane and the stabilization of the dication.^[108]

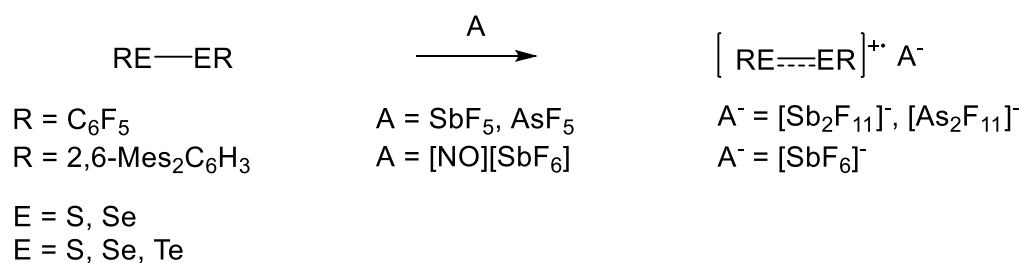
Fujihara et al. were able to show that dithio *peri*-bridged and diselenium *peri*-bridged naphthalene display the same behaviour as thianthrene when dissolved in conc. sulphuric acid, like

thianthrene before.^[111,112] When dissolved in conc. sulphuric acid dinaphtho[1,8-*b,c*]-1,5-dithiocin or dinaphtho[1,8-*b,c*]-1,5-diselenocin undergo single-electron oxidations and turn into radical cations (Scheme 11).



Scheme 11. Oxidation of dinaphtho[1,8-*b,c*]-1,5-dithiocin in conc. sulphuric acid.^[111]

Stable diaryldichalcogenide radical cations have been the objective of the work of Beckmann et al. in 2015.^[113] By the use of fluorinated aromatic substituents (C_6F_5) the oxidation of the respective dichalcogenides with antimony- or arsenic pentafluoride led to stable sulphur and selenium radical cations. By the use of bulky substituents on the aromatic scaffold, diarylditelurides could be converted to the tellurium radical cation via oxidation with nitrosonium hexafluoroantimonate the tellurium radical cation could also be made accessible.



Scheme 12. Synthesis of the diaryldichalcogenide radical cations.

2. Results

2.1. New Charge-Transfer Complexes with 1,2,5-Thiadiazoles as Both Electron Acceptors and Donors Featuring an Unprecedented Addition Reaction

2.1.1. Synopsis

The aim of this project was to synthesize novel charge-transfer complexes with 1,2,5-thiadiazole derivative as acceptor (A) and donor (D) molecule. With the cocrystalization of phenoxatellurine as a donor towards [1,2,5]thiadiazolo[3,4-c][1,2,5]thiadiazole as an acceptor, sublimed in gas phase, a complex with the ratio of 1:3 (D:A) was obtained.

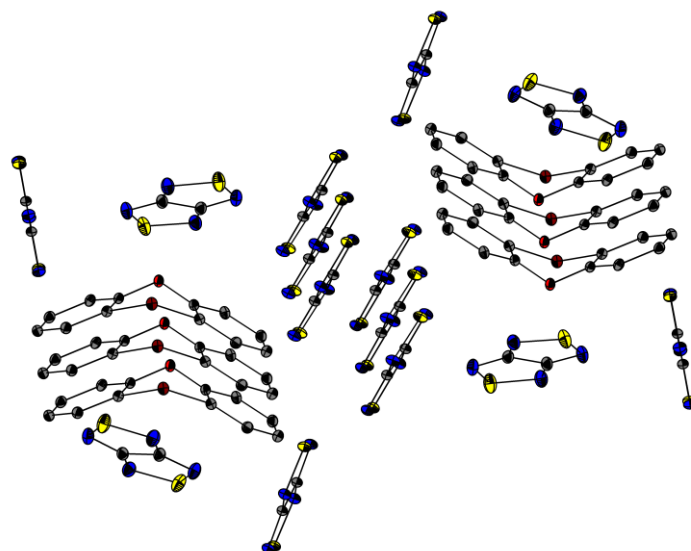


Figure 7. Molecular and crystal structure of the phenoxatellurine charge-transfer complex.

2.1.2. Experimental Contributions

In this work, I carried out the synthesis of the phenoxatellurine charge transfer complex. Prof. Dr. Jens Beckmann and Prof. Dr. Andrey V. Zibarev were the principal investigators, designed the concept and wrote the manuscript. Single crystal X-ray diffraction measurements and structure refinements have been made by Dr. Enno Lork. The article was published in the following journal:

Chulanova, E. A.; Pritchina, E. A.; Malaspina, L. A.; Grabowsky, S.; Mostaghimi, F.; Beckmann, J.; Bagryanskaya, I. Y.; Shakhova, M. V.; Konstantinova, L. S.; Rakitin, O. A. et al. *New Charge-Transfer Complexes with 1,2,5-Thiadiazoles as Both Electron Acceptors and Donors Featuring an Unprecedented Addition Reaction*. *Chemistry, A European Journal* **2017**, *23*, 852–864. DOI: 10.1002/chem.201604121.

Donor–Acceptor Systems

New Charge-Transfer Complexes with 1,2,5-Thiadiazoles as Both Electron Acceptors and Donors Featuring an Unprecedented Addition Reaction

Elena A. Chulanova,^[a, b, c] Elena A. Pritchina,^[a] Lorraine A. Malaspina,^[d] Simon Grabowsky,^{*,[d]} Farzin Mostaghimi,^[d] Jens Beckmann,^{*,[d]} Irina Yu. Bagryanskaya,^[a, b] Margarita V. Shakhova,^[e] Lidia S. Konstantinova,^[f, g] Oleg A. Rakitin,^[f, g] Nina P. Gritsan,^{*,[c, e]} and Andrey V. Zibarev^{*,[b, e]}

Abstract: The design and synthesis of novel charge-transfer (CT) complexes are of interest for fundamental chemistry and applications to materials science. In addition to the recently described first CT complex with both electron acceptor (A) and donor (D) groups belonging to the 1,2,5-thiadiazole series (1; A: 4-nitro-2,1,3-benzothiadiazole; D: 4-amino-2,1,3-benzothiadiazole), herein novel CT complexes **2** and **3** with 1,2,5-thiadiazoles as both A (4,6-dinitro-2,1,3-benzothiadiazole and [1,2,5]thiadiazolo[3,4-c][1,2,5]thiadiazole) and D (4-amino-2,1,3-benzothiadiazole) were synthesized. The series is completed by complex **4** with [1,2,5]thiadiazolo[3,4-c][1,2,5]thiadiazole as A and phenoxatellurine as D. Structures of complexes **2–4** were characterized by single-crystal X-ray diffraction (XRD), as well as solution and solid-state UV/Vis spectroscopy. Thermodynamics of their formation were obtained by density functional theory (DFT) calculations, their bonding situations were analyzed by quantum theory of atoms in molecules (QTAIM) calculations and dimer model energies of interactions quantified in the framework of the Hirshfeld surface (HS) analysis. With DFT

calculations, the largest value of CT between D and A was found for complex **2**, with 0.027 e in the XRD structure and 0.150 e in the optimized structure in MeCN. In the UV/Vis spectra, the λ_{max} of the CT bands of **2–4** varied in the range $\lambda = 517\text{--}705$ nm. Model energy calculations for **1–4** revealed the importance of both dispersion interactions and hydrogen bonding between D and A as contributors to CT in the crystalline state. In an attempt to enlarge the CT value with bis[1,2,5-thiadiazolo][3,4-b;3',4'-e]pyrazine as A and 4-amino-2,1,3-benzoselenadiazole as D, an unprecedented 1:1 addition reaction was observed upon formation of a C–N bond between atom C7 of D and pyrazine atom N4 of A, accompanied by hydrogen atom transfer from C7 to another pyrazine atom N8 (compound **5**). According to DFT calculations, the reaction is a multistep process featuring diradical intermediates and hydrogen atom intramolecular migration over four positions. Molecular and crystal structures of **5** (solvate with toluene) were elucidated by XRD and the crystal structure revealed a rather unusual porous framework.

Introduction

Fast progress in materials science on organic electronics and optoelectronics is predominantly related to organic semicon-

ductors. Generally, those are low- or high-molecular-weight π -delocalized compounds.^[1] Research into organic semiconductors began with small molecules, particularly with their charge-transfer (CT) complexes^[2] formed by interactions between π -

[a] E. A. Chulanova, E. A. Pritchina, Prof. I. Yu. Bagryanskaya
Department of Natural Sciences, Novosibirsk State University
630090 Novosibirsk (Russia)

[b] E. A. Chulanova, Prof. I. Yu. Bagryanskaya, Prof. A. V. Zibarev
Institute of Organic Chemistry, Russian Academy of Sciences
630090 Novosibirsk (Russia)
E-mail: zibarev@nioch.nsc.ru

[c] E. A. Chulanova, Prof. N. P. Gritsan
Institute of Chemical Kinetics and Combustion
Russian Academy of Sciences, 630090 Novosibirsk (Russia)
E-mail: gritsan@kinetics.nsc.ru

[d] L. A. Malaspina, Prof. S. Grabowsky, F. Mostaghimi, Prof. J. Beckmann
Institute for Inorganic Chemistry and Crystallography
University of Bremen, 28359 Bremen (Germany)
E-mail: simon.grabowsky@uni-bremen.de
j.beckmann@uni-bremen.de

[e] M. V. Shakhova, Prof. N. P. Gritsan, Prof. A. V. Zibarev
Department of Physics, Novosibirsk State University
630090 Novosibirsk (Russia)

[f] Prof. L. S. Konstantinova, Prof. O. A. Rakitin
Institute of Organic Chemistry, Russian Academy of Sciences
119991 Moscow (Russia)

[g] Prof. L. S. Konstantinova, Prof. O. A. Rakitin
Education and Research Center for Nanotechnology
South Ural State University, 454080 Chelyabinsk (Russia)

Supporting information for this article can be found under <http://dx.doi.org/10.1002/chem.201604121>. It includes additional results of DFT calculations, model energy calculations, HS analysis, and crystal lattice voids analysis.

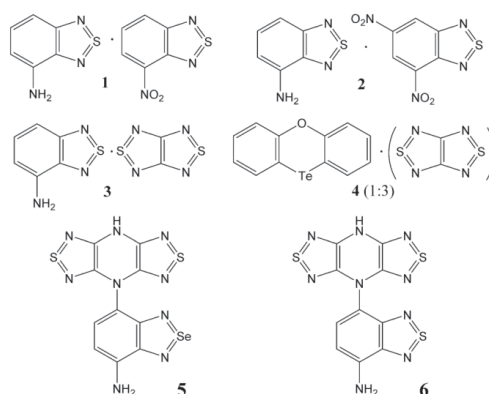
electron donor (D) and π -electron acceptor (A) molecules.^[3] Both low- and high-molecular-weight CT complexes are of interest to the field, including new applications covering ambipolar transport, metallicity, photoconductivity, ferroelectricity, or magnetoresistance.^[4,5] This stimulates further experimental and theoretical studies^[6] with special emphasis on the design, synthesis, and characterization of novel D–A systems. Beyond materials science, such systems are of clear interest to fundamental chemistry.

2,1,3-Benzothia-/selenadiazoles (i.e., benzo-fused 1,2,5-thia-/selenadiazoles) have been known for about 125 years.^[7] Nowadays, their chemistry is well developed in both hydrocarbon^[8] and fluorocarbon series.^[9] The chemistry of their tellurium congeners only began in the 1980s.^[10] Despite fast progress,^[11] this chemistry is still in its infancy compared with that of sulfur and selenium derivatives. One of the most interesting properties of 2,1,3-benzochalcogenadiazoles (chalcogen: S, Se, Te) is their positive electron affinity (EA), which makes them effective A compounds.^[12] Thus, 2,1,3-benzothia-/selenadiazoles (but not the less studied 2,1,3-benzotelluradiazoles^[11]) are widely used as A building blocks in the design and synthesis of numerous molecule-based functional materials for organic electronics,^[13] including CT complexes.^[14] Until recently, authentic (i.e., not highly polarized hybrid molecules)^[15] 2,1,3-benzothia-/selenadiazoles had never been used as D components of CT complexes. In 2014, it was, however, shown that substitution in the carbocycle of the parent 2,1,3-benzothiadiazole with amino and nitro groups allowed fine-tuning of the molecular EA and ionization energy (IE), leading to substituted derivatives that acted as D and A towards each other.^[16] As an example, the first CT complex **1** with both D and A components belonging to the 2,1,3-benzothiadiazole family, namely, 4-amino- and 4-nitro-2,1,3-benzothiadiazoles, respectively, was synthesized and characterized by single-crystal XRD, UV/Vis spectroscopy, and DFT and quantum theory of atoms in molecules (QTAIM) calculations.^[16] The main aim of the present work is to further exploit this finding.

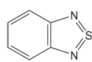
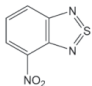
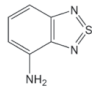
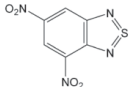
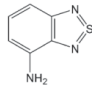
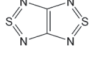
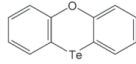
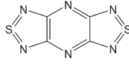
Herein, we report on the synthesis and characterization of novel CT complexes **2** and **3**, which are solely based on D and A molecules of fused 1,2,5-thiadiazole derivatives. Additionally, the first CT complex **4** between a 1,2,5-thiadiazole derivative as A and phenoxatellurine as a well-known D^[17] was prepared and characterized and showed a rather unusual 1:3 D–A stoichiometry. With bis[1,2,5-thiadiazolo][3,4-b;3',4'-e]pyrazine (the strongest known A in the 1,2,5-thiadiazole series)^[12] and 4-amino-2,1,3-benzoselenadiazole, an unprecedented addition product **5** was obtained instead of the target CT complex. A similar product **6** was also observed for the reaction between bis(thiadiazolo)pyrazine and 4-amino-2,1,3-benzothiadiazole.

Results and Discussion

For the synthesis of novel CT complexes, 4-amino-2,1,3-benzothiadiazole and its selenium congener were used as D, and 4,6-dinitro-2,1,3-benzothiadiazole, [1,2,5]thiadiazolo[3,4-c][1,2,5]thiadiazole, and bis[1,2,5-thiadiazolo][3,4-b;3',4'-e]pyrazine were used as A. Additionally, phenoxatellurine was ex-



ploited, for the first time, as D towards A of the 1,2,5-thiadiazole type. The adiabatic IEs and EAs of these compounds calculated at the (U)B3LYP/6-31+G(d) level of theory are displayed in Table 1. Previously, it was demonstrated that this method performed well for chalcogen–nitrogen heterocyclic compounds.^[12] CT complexes **2–4** were prepared by cocrystallization of their components from hexane. As in the cases of **2** and **3**, the initial D/A ratio in the syntheses of **4** was 1:1, whereas the stoichiometry of **4** was 1:3 in favor of A. Interestingly, complex **4** proved stable enough to be sublimed quantitatively in vacuo to give the same crystalline phase. Structures of complexes **2–4** were confirmed by single-crystal XRD (Figure 1). Molecular geometries of D and A components in complexes **2–4** were practically the same as those of the individual compounds.^[16,18a,b,19,20a] Similar to complex **1**,^[16] D–A π -stacked structures were revealed in the crystals of **2** and **3**, and both heterocycle–heterocycle and heterocycle–carbocycle π -stacking interactions were observed. In both complexes, π stacks are slightly tilted with a small offset of neighboring molecules. The interplanar separations in the stacks are 3.32–3.40 Å for **2** and 3.22–3.55 Å for **3**. The stacks are connected by shortened lateral contacts S··N of 2.99 Å in **2** and 3.05 Å in **3**—a normal van der Waals (VdW) contact S··N is 3.35 Å^[21]—together with hydrogen bonds N–H··O and N–H··N. In **4**, layers of stacked D and A molecules (shortest distances of C··N 3.45 and Te··N 3.82 Å) are intertwined with perpendicular layers of A molecules that form head-on S·· π contacts with S··C distances in the range of 3.41–3.56 Å. The 1:3 stoichiometry in **4** can be explained by the size difference between A and D molecules, in which smaller A molecules fit into channels opened perpendicularly to the plane of the D molecule. This can be visualized by a calculation of the voids^[22] left behind when two of the three symmetry-independent A molecules are removed from the structure (Figure 2). These voids extend as channels through the structure and may be interpreted as van der Waals (VdW) holes. However, some of the A molecules that fill these voids interact strongly with the D molecules, see the Hirshfeld surface (HS) analysis below.

Donor	IE [eV]	EA [eV]	Acceptor	IE [eV]	EA [eV]
	8.71	0.95		9.26	2.06
	7.44	0.80		9.84	2.86
1–3,6d			2a		
	7.29	0.83		9.99	2.14
5d			3,4a		
	6.81	-0.09		9.56	3.04
4d			5,6a		

[a] In the designations, letters **d** and **a** encode functionalities, namely, D and A, respectively, and numbers encode compounds 1–6 synthesized herein for which the functionalities were used.

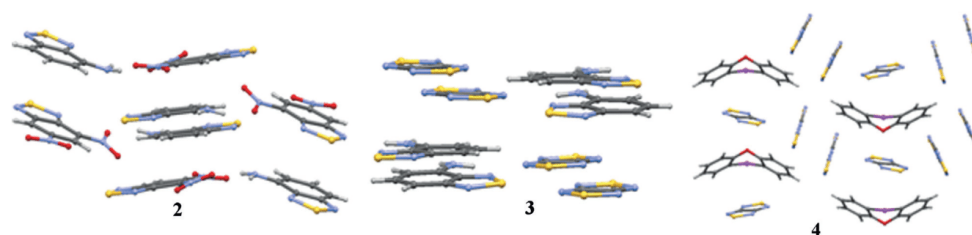


Figure 1. XRD structures of complexes 2–4.

For 1–4, HS analyses were performed.^[24] For reasons of comparability, the D molecule in each case was taken as the central unit to which the intermolecular interactions were referred. HSs were calculated for D and the property $d_{\text{norm}}^{[25]}$ was color coded onto them (Figure 3). If the sum of the distances of the closest atoms inside and outside a surface point is smaller than the sum of the VdW radii of the two atom types in contact, d_{norm} is negative and the HS is colored in red. For 1–4 (Figure 3), the closest atom–atom contacts (most intense red coloring) correspond to hydrogen bonds or electrostatic lateral interactions, for example, S...N and S...Te, but not to π -stacking interactions. Therefore, model energies of pairwise intermolecular interactions between two molecules were calculated in addition to the HS analysis^[26] (Section 2 in the Supporting Information). The total energy of intermolecular interactions in the crystal was expressed in terms of four key components, namely, electrostatic, polarization, dispersion, and exchange–repulsion: $E_{\text{tot}} = E_{\text{ele}} + E_{\text{pol}} + E_{\text{dis}} + E_{\text{rep}}$.^[26] In this way, the com-

plete situation of the dimer interaction is described and not only direct atom–atom contacts. It becomes clear (Figure 3 and Section 2 in the Supporting Information) that the total interaction energies between dimers exhibiting hydrogen bonding or lateral electrostatic contacts and between dimers involved in π stacking are comparable. Both types of interactions must play a role in the CT mechanism. In Figure 3, those bonding partners of the central D molecule that give rise to the highest total interaction energies are plotted (excluding the π -stacking partner below the HS surface for better visualization). The labeling of the molecules corresponds to that used in Tables S2–S6 in the Supporting Information, in which all interaction partners are shown and color coded. For 1 (Figure 3 and Section 2 in the Supporting Information), the strongest interactions are N–H...N bonds and lateral electrostatic interactions of the type S...N. The interaction between the central D (enclosed by the HS) and A molecules (A4) shows the closest contacts (most intensely colored red spots involving both hydrogen

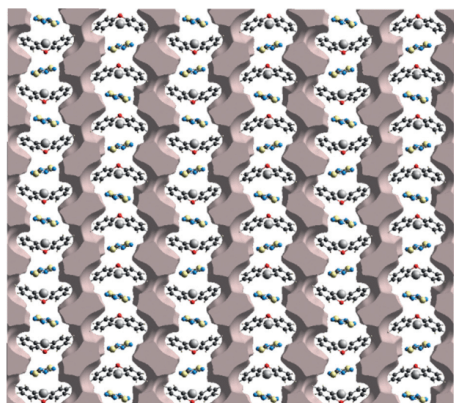


Figure 2. Voids in the crystal structure of **4** after artificially removing the A molecules that extend perpendicularly to the plane of the D molecule. Voids shown for all unit cells of the projection; the view is down the *a* axis. The percentage of voids relative to the unit cell volume is 27.3% (for voids only shown within the unit cell, see Section 1 and Figure S1 in the Supporting Information). The voids are calculated with the CrystalExplorer program^[23] according to ref. [22] at an electron-density isosurface of 0.0003 au, which corresponds to the solvent-accessible surface.

bonds and S...N contacts), which corresponds to a total interaction energy of $-35.4 \text{ kJ mol}^{-1}$ that is mainly constituted by the electrostatic energy term ($-37.5 \text{ kJ mol}^{-1}$) and to a lesser degree by the dispersive energy term ($-16.1 \text{ kJ mol}^{-1}$). Repulsion and exchange–correlation show positive values. Although the D–A contacts involving A1 (below the HS, not shown in Figure 3, but in Figure S3 in the Supporting Information) and A7 (above the HS) do not show close contacts and the electrostatic energy terms are significantly lower than those for the hydrogen-bonded dimers (-6.8 and -9.6 kJ mol^{-1} for A1 and A7, respectively), the total energies of these contacts are comparable to those of the hydrogen-bonded dimer (-27.5 and $-30.3 \text{ kJ mol}^{-1}$ for A1 and A7, respectively). The main stabilizing energy term is the dispersion one (-42.1 and $-44.6 \text{ kJ mol}^{-1}$ for A1 and A7, respectively), which is typical for π -stacking interactions. In summary, all major interactions of the central D molecule involve A molecules, whereas contacts with other D molecules are minor. In crystalline **1**, CT proceeds through two different mechanisms that are comparable in total energy: hydrogen bonding driven by electrostatic forces and π stacking driven by dispersive forces. For **2** (Figure 3; Section 2, Figure S4 and Table S3 in the Supporting Information), a similar situation is observed with all major interactions between the central D and A molecules being hydrogen-bonding (e.g., involving A7: N–H...O) and π -stacking (e.g., involving A2 and A8) interactions. The D–D interactions are negligible. The hydrogen-bonding interactions show prominent close atom–atom contacts (Figure 3, red spots on the HS), whereas π -stacking interactions do not produce such close contacts. The most significant difference between **2** and **1** is as follows: although the D molecule is identical in **1** and **2** (i.e., **1–3d**), the hydro-

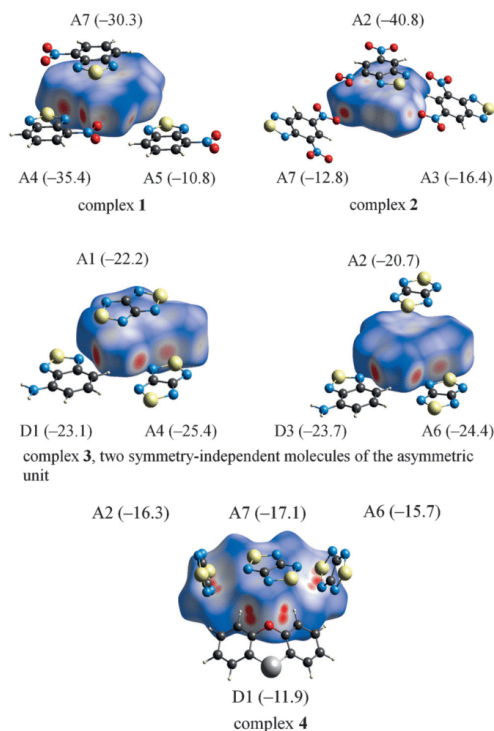


Figure 3. HSs of complexes **1–4** with d_{nom} mapped onto them. Color scale: -0.4 (red) to 0 (white) to 1.2 (blue). The closest atom–atom contacts in the complexes are represented by the red spots on the HSs. In addition, the interaction partners with the highest total interaction energies (kJ mol^{-1} ; Section 2 in the Supporting Information) are plotted (with exception of the π -stacking partners hidden below the surfaces).

gen-bonding interactions in **2** are much weaker, and the π -stacking interactions much stronger than those in **1**, with larger total (-40.8 and $-35.3 \text{ kJ mol}^{-1}$ for A2 and A8, respectively) and dispersion energies ($-52.6 \text{ kJ mol}^{-1}$ and $-50.0 \text{ kJ mol}^{-1}$ for A2 and A8, respectively). Therefore, CT for **2** in the crystalline state mainly proceeds through π -stacking interactions (cf. Figure 4). This is in agreement with a larger DFT-calculated CT value in the XRD structure of **2** than that in **1** (see below). For **3** (Figure 3; Section 2, Figures S5 and S6 and Tables S4 and S5 in the Supporting Information) with an asymmetric unit of two symmetry-independent D molecules, the interaction network around them is similar, but not identical. In both cases, there are hydrogen-bonding (N–H...N) and π -stacking interactions. Similar to **1** and in contrast to **2**, both interaction types are equally important in terms of their total energies. In contrast to both **1** and **2**, the total energies for the π -stacking interactions are lower, whereas the total energies for the hydrogen-bonding interactions are lower than that in **1**, but at the same level as that in **2**. A striking difference be-

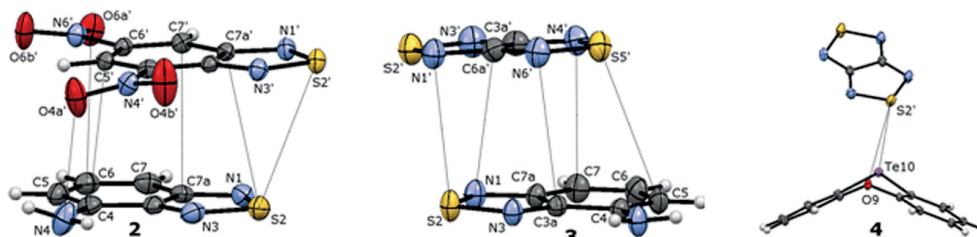


Figure 4. ORTEP plot of complexes 2–4 (displacement ellipsoids at 50%, H atoms are given as white circles) showing orientations of the neighboring molecules and the QTAIM intermolecular bond paths.

tween **3** and **1** and **2** is that in **3** the central D molecule exhibits significant interactions with other D molecules through N–H–N bonds (D1 and D3 for the first symmetry-independent molecule, and D3 and D5 for the second one). The interactions are of the same strength as that of the hydrogen-bonding dimeric interactions involving A4 for the first independent molecule and A6 for the second one. The π -stacking interactions involving A1 and A6 for the first independent D molecule, and A2 and A4 for the second one, are of the same total energy as that of the hydrogen-bonding interactions. Overall, for **3**, three different equally important types of intermolecular interactions are present: hydrogen bonding involving D–D contacts, hydrogen bonding involving D–A contacts, and π stacking involving D–A contacts.

For **4** (Figure 3; Section 2, Figure S7 and Table S6 in the Supporting Information), the intermolecular interactions are not directly comparable with those for **1–3** because of another D (i.e., **4d**), as well as the stoichiometry. In particular, hydrogen-bonding interactions are not possible due to the lack of suitable functional groups. The most important D–A interactions are those between the D molecule and A5 and A7 molecules bridging tellurium and oxygen atoms (cf. Figure 4). However, some other contacts show closer atom–atom arrangements (red spots on the HS) and similar dimeric interaction energies, for example, the contacts with A2 and A6 that are more head-on. For all D–A interactions, electrostatic and dispersion terms are of about the same importance. There is a single significant D–D interaction (with molecule D1) that can be assigned to a C–H–Te contact being mainly dispersive in nature. For **2–4**, the D–A π -stacking pair with the highest total interaction energy was selected to investigate the atom–atom interactions involved in the stacking in more detail through QTAIM analysis (Figure 4).^[27] Dimer calculations were performed at the experimental geometries manifested in the XRD crystal structures. For **2**, six bond critical points (BCPs) representing the dispersion bonding interactions between the D and A molecules were identified. Two of them belong to S2...S2' and S2...C7a' bond paths and the others to N4...O4a', C6...O6a', C7a...C7', and C4...C5' bond paths (Figure 4). For **3**, five BCPs with corresponding bond paths were localized: two belonging to S2...N1' and C5...S5'; the others to C7...N4', C3a...N6', and N1...C6a' (Figure 4). For complex **4**, only two BCPs were obtained; these represent the Te10...S2' and O9...S2' interactions (Figure 4). All

BCPs are characterized by very low values of electron density ($\rho \approx 0.004$ – 0.006 au) and Laplacian ($\Delta\rho \approx 0.013$ – 0.022 au) and a positive total electronic energy density ($H_{BCP} \approx 0.001$ au). These values indicate very low energy of the atom–atom non-covalent-bonding interactions in the complexes.^[27] However, the model energy discussion above has shown that significant dispersion and total energies are related to these dimers. This means that the electron-density topology is only one aspect of the total interaction between two molecules, but it can show preferred channels of exchange within these CT complexes.^[28] Previously, it was shown that the UV/Vis spectrum of the polycrystalline samples of complex **1** contains a pronounced CT band in the range of $\lambda = 550$ – 650 nm, corresponding to electron promotion from the D-localized HOMO to the A-localized LUMO.^[16] Figure 5 displays solution and solid-state UV/Vis spectra of individual D and A precursors and complexes **2–4**. The solid-state spectra were obtained for polycrystalline samples of compounds dispersed in BaSO₄ and represented in the form of a Kubelka–Munk function.^[29] The solution and solid-state spectra of the individual D and A compounds are very similar. For **3**, a weak absorbance is observed in the range of $\lambda = 560$ – 700 nm. The spectrum of **4** has a weak absorption band in the range of $\lambda = 425$ – 650 nm with a maximum at $\lambda \approx 475$ nm. The time-dependent (TD) DFT calculations at the M06-HF level of theory, which is known to reproduce the CT transitions well,^[30] for **3** and those at the B2PLYP level for **4** are in agreement with the solid-state UV/Vis spectra of the complexes (Figure 5). The calculations suggest that the long-wavelength transitions in **3** and **4** correspond to electron promotion from the D-localized HOMO into the A-localized LUMO (Figure 6). For **4**, two long-wavelength transitions at $\lambda = 508$ and 351 nm were predicted to correspond to electron promotion from the combinations of the mainly D-localized HOMO and HOMO–1 into the A-localized LUMO (Figure 6). Thus, absorption bands in the visible region of the polycrystalline samples of **3** and **4** are indeed the CT bands. In the spectrum of **2**, an absorption was observed in the range of $\lambda = 450$ – 700 nm that was remarkably strong for the series of compounds investigated. The experimental spectrum, which was the same for several independently prepared and measured samples, contradicts the results of TD-DFT calculations for **2** (Figure 5). The reasons for this are not entirely clear. Diffuse reflectance spectroscopy is known to be very sensitive to the sample surface. It cannot be excluded

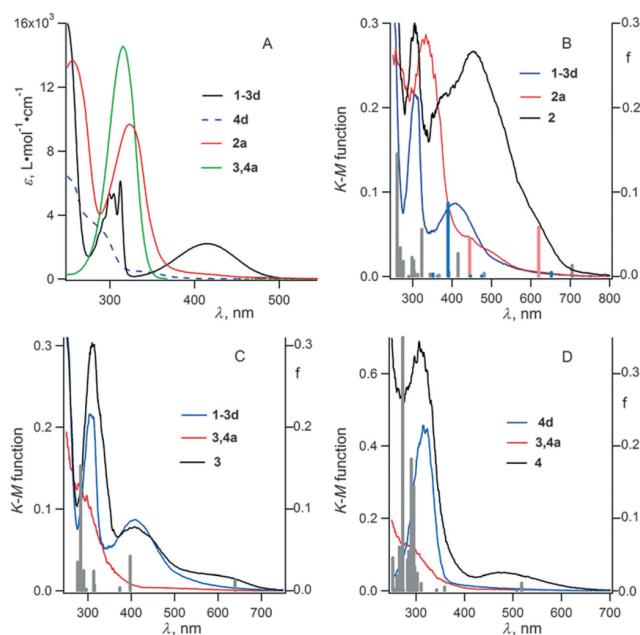


Figure 5. A) UV/Vis spectra of individual D and A in CH_2CN (for designations, see Table 1). B–D) Solid-state UV/Vis spectra in the form of Kubelka–Munk functions for individual D and A and their CT complexes **2–4** (0.02 mol fraction of the corresponding species in BaSO_4). Vertical gray bars indicate the positions and oscillator strengths (f , right axis) of the electronic transitions calculated at the TD-M06-HF/def2-TZVP level for the CT complexes **2** (B) and **3** (C), and at the TD-B2PLYP/def2-TZVP level (with ECP for Te) for **4** (D) in their XRD geometries. In B), the electronic transitions calculated at the TD-M06-HF/def2-TZVP level for the putative radical cation [1-3d]⁺ (blue bars) and the radical anion [2a]⁻ (red bars) are also depicted.

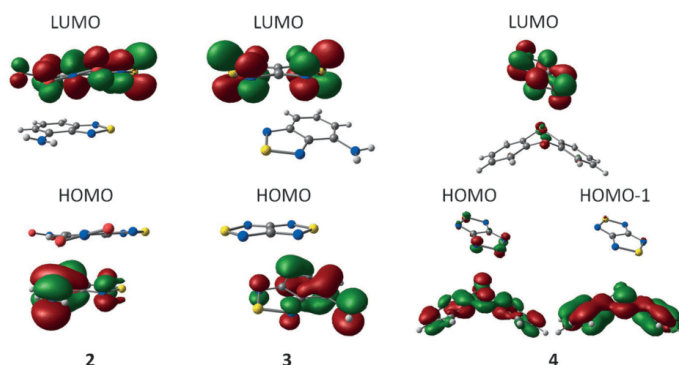


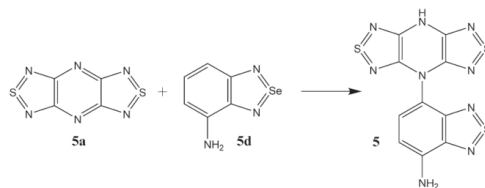
Figure 6. The HOMOs and LUMOs of complexes **2** and **3** calculated at the M06-HF/def2-TZVP level of theory, and the HOMO, HOMO-1, and LUMO of complex **4** calculated at the B2PLYP/def2-TZVP level (with ECP for Te). The LUMOs are localized on the A components and the HOMOs on the D components of the CTs.

that some uncontrolled products are formed on the surfaces of the measured samples. Particularly, the formation of a radical ion salt [1-3d][2a] (cf. ref. [31]) from CT complex **2** could be possible on the surface of the samples during the UV/Vis measurements because the calculations predict that this

salt possesses an intense absorption in the visible region (Figure 5). At the same time, bulk formation of salt [1-3d][2a] under the influence of grinding with BaSO_4 ^[32] can be rejected because the samples were EPR silent. A more detailed study is required to explain unambiguously the solid-state UV/Vis data

obtained for **2**. Similar to complex **1**,^[16] solution UV/Vis spectra of **2–4** in CH₃CN are superpositions of those of the D and A precursors. Moreover, solutions with a concentration of A that is much larger than that of D (up to 5×10^{-2} and $\sim 10^{-3}$ mol L⁻¹, respectively) do not absorb in the visible region at $\lambda > 500$ nm.

According to TD-DFT calculations (Table 2), complexes **2–4** with optimized solution structures have CT absorption bands with maxima at $\lambda \approx 700$ nm and moderate oscillator strengths $f = (1–4) \times 10^{-2}$. Thus, the equilibrium constants for CT complex



Scheme 1. Synthesis of compound **5**.

	2		3		4	
	CH ₃ CN	Hexane	CH ₃ CN	Hexane	CH ₃ CN	Hexane
ΔG_{CT} [kJ mol ⁻¹]	7.1	-4.2	11.3	9.2	15.0	10.9
Δq [e]	0.15	0.10	0.08	0.04	0.03	0.03
λ_{max} [nm] (f)	671 (0.015)	735 (0.040)	694 (0.037)	666 (0.037)	705 (0.009)	680 (0.009)

[a] Maxima (λ_{max}) and oscillator strengths (f) of the long-wavelength CT bands for the optimized structures of **2–4** are calculated at the TD-M06-HF/def2-TZVP level for **2** and **3** and at the B2PLYP/def2-TZVP level (with ECP for Te) for **4**.

formation in CH₃CN can be roughly estimated at $K_{CT} < 1$ L mol⁻¹, and the Gibbs free energies of complex formation at $\Delta G_{CT} > 0$ kJ mol⁻¹. This estimation is in agreement with positive ΔG_{CT} values for complex formation of **2–4** calculated for solutions in CH₃CN and hexane at the B97-D3/def2-TZVP level of theory (Table 2). For the XRD structures, the DFT-calculated CT values are 0.023 e for **1**,^[16] 0.027 e for **2**, 0.009 e for **3**, and 0.014 e for **4**. For structures of **2–4** optimized in solution, the calculated CT values are noticeably higher, especially in CH₃CN, although still small (Table 2). For the 1:1 complex between tetrathiafulvalene (TTF) and **3,4a** and the 1:2 complex between TTF and 3,4-dicyano-1,2,5-telluradiazole, the CT values were calculated in CH₃CN to be 0.24 and 0.39 e, respectively (onto two molecules of telluradiazole dimerized by in-plane Te–N contacts).^[14a] In an attempt to enlarge the CT value and to determine exothermal CT complex formation, compounds **5d** and **5a** were tested as D and A, respectively (Table 1). However, instead of the target CT complex, in toluene at reflux, an unprecedented 1:1 addition reaction was observed, leading to C–N cross-coupled product **5** (Scheme 1). The structure of **5** (solvate with disordered toluene) was confirmed by XRD; the results of which featured a rather unusual porous framework in the crystalline state with hexagonal honeycomb-shaped voids (Figure 7). The ¹H NMR spectrum of **5** confirmed addition accompanied by hydrogen atom transfer from **5d** onto **5a**, since it contained an H–N signal at $\delta = 12.10$, which was close to that of the H–N signal in the same-solvent spectrum of 4,8-dihydro[bis[1,2,5]thiadiazolo][3,4-b:3',4'-e]pyrazine ($\delta = 10.11$).^[8b] Other signals of **5** correspond to 7-R-substituted **5d** and are downfield-shifted relative to those of **5d**^[18c] due to the electron-withdrawing character of substituent R. The long-wavelength band in the UV/Vis spectrum of **5** is noticeably weaker

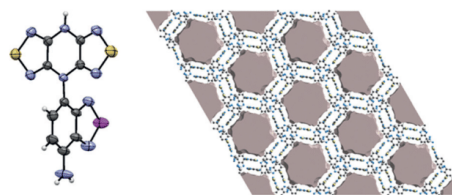
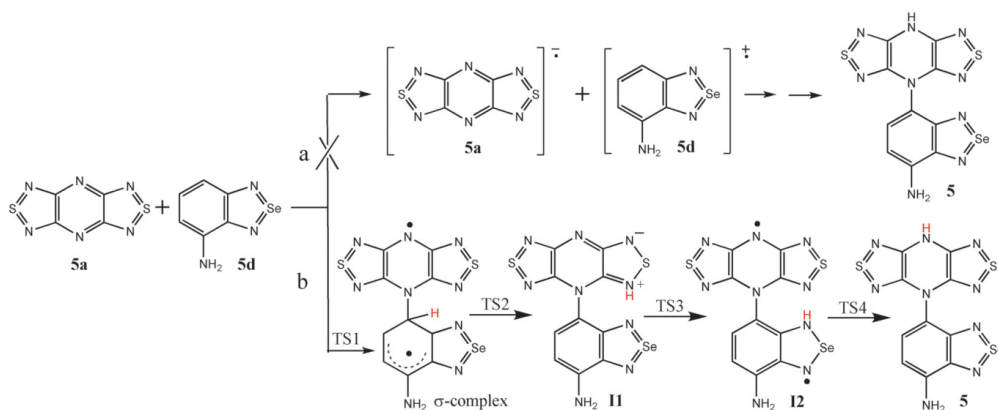


Figure 7. Left: ORTEP plot of **5** (displacement ellipsoids at 50%, H atoms are shown as white circles). Right: voids in the crystal structure of **5** after artificially removing the disordered solvent molecules. Voids shown for all unit cells of the projection; the view is down the *c* axis. The percentage of voids relative to the unit cell volume is 40.0% (for voids only shown within the unit cell, see Section 1 and Figure S2 in the Supporting Information). The voids were calculated with the CrystalExplorer program,^[23] according to ref. [22], at an electron density isosurface of 0.0003 au, corresponding to the solvent-accessible surface.

and blueshifted compared with that of **5a** (λ_{max} [nm] ($\log \epsilon$): **5**, 370 (1.6); **5a**, 470 (3.4)^[33]); this reflects destruction of perimetrical π -delocalization of **5a** upon transforming into **5**.

In the crystal, space filling by molecules of **5** is only 60%, whereas 40% of the unit cell volume (i.e., 4346.7 Å³) is accessible to solvent molecules (Figure 7). This space is occupied by heavily disordered toluene molecules that could not be modeled by a set of discrete atomic sites. The main structural motifs are as follows: by virtue of shortened S–N contacts of about 3.09 Å, the molecules of **5** form cyclic arrays in the crystallographic *ab* plane (Figure 7). The arrays are connected by π -stacking interactions (interplanar separation 3.21–3.28 Å) along the crystallographic *c* axis to give infinite channels with diameters of about 19.5 Å hosting disordered toluene molecules. The molar ratio of **5**/toluene is 1:1. It should be noted that porous organic molecular crystals currently attract much attention as promising alternatives to polymeric framework materials, such as zeolites and metal–organic frameworks.^[34] Formally, the reaction in Scheme 1 can be considered an arylation of pyrazine. It should be noted that known examples of arylation of pyrazine are rare and based on very different organometallic chemistry.^[35]

For the formation of **5** from **5d** and **5a**, two hypothetical pathways were considered (Scheme 2). First, thermodynamics of full electron transfer (ET) from **5d** onto **5a** were analyzed and DFT calculations found them to be very endothermic with $\Delta G^0 = 152.3$ kJ mol⁻¹. The energy of Coulomb interactions in the ion pair was estimated by using their collision diameters



Scheme 2. Hypothetical mechanisms of reactions between **5a** and **5d** to give **5** (migrating H atom is depicted in red).

calculated as suggested previously (for details, see Section 3 in the Supporting Information).^[36] The rate constant (k_{ET}) and activation energy (E_{ET}) of the ET were estimated in the framework of the classical Marcus approach^[37] by using Equation (1), in which k_{B} is the Boltzmann constant, ΔG^0 is the free energy of the ET reaction, and λ is the reorganization energy.

$$k_{\text{ET}} = A \times \exp \left[\frac{-(\Delta G^0 + \lambda)^2}{4\lambda k_{\text{B}} T} \right] = A \times \exp(-E_{\text{ET}}/k_{\text{B}} T) \quad (1)$$

The reorganization energy, λ , in Equation (1) is the sum of two components: the intramolecular reorganization energy, λ_{in} , and the solvent reorganization energy, λ_{s} . The latter term can be estimated by applying Equation (2), proposed by Marcus,^[37a,b] with effective radii obtained from DFT calculations.

$$\lambda_{\text{s}} = e^2 \left[\frac{1}{2R_{\text{A}}} + \frac{1}{2R_{\text{D}}} - \frac{1}{(R_{\text{A}} + R_{\text{D}})} \right] \cdot \left(\frac{1}{n^2} - \frac{1}{\epsilon_0} \right) \quad (2)$$

The value of λ_{s} was estimated to be 0.063 eV or 6.3 kJ mol⁻¹, that is, very small. The value of $\lambda_{\text{in}} = 0.29$ eV or 28.5 kJ mol⁻¹ was obtained from DFT calculations. With these values, E_{ET} was estimated to be about 268 kJ mol⁻¹, that is, very large. Thus, a pathway to **5** starting with ET (Scheme 2) cannot be realized. Intermediates and transition states (TSs) of the alternative pathway were localized through DFT calculations (Figure 8). The first step is an addition of **5a** to **5d** upon formation of the diradical σ -complex via TS1.^[38] The geometry of the complex was optimized in the triplet state of the diradical, and the electronic energy of the singlet state was calculated by using the spin-unrestricted broken-symmetry (BS) approach.^[39] The singlet-triplet splitting for the σ complex was estimated at -440 cm⁻¹. In the triplet state, the spin density is mainly localized as displayed in Scheme 2. Notably, the value of $\langle \hat{S}^2 \rangle$ for the BS state was 0.89. Transformation of the σ complex into **5** was found to be a three-step intramolecular transfer of a hydrogen atom for which intermediates I1 and I2 and TS2–TS4 were

localized (Scheme 2 and Figure 8). Similar to the σ complex, intermediate I2 is a diradical species with a singlet-triplet splitting of -540 cm⁻¹ and the $\langle \hat{S}^2 \rangle$ value of the BS state equals 0.85. In contrast to I2, the restricted wave function for the ground state of I1 was stable. Although the restricted wave functions of TS2 and TS3 (Figure 8) were also unstable, the calculated energy differences between the closed-shell singlet and BS states were 2.38 and 3.18 kJ mol⁻¹, respectively, that is, minor. Therefore, structure optimizations for these TS were performed by using the restricted DFT approach. Calculations revealed that the limiting step of the reaction under discussion was hydrogen atom transfer from the benzoselenadiazole C atom onto the thiadiazole N atom via TS2. The next step is an almost barrier-free migration of this atom to the selenadiazole N atom via TS3, and the final one is the migration to the pyrazine N atom via TS4 with a barrier similar to that of the first step (Figure 8). The activation energy of the whole process is close to the relative enthalpy of TS2. It was estimated at about 100 kJ mol⁻¹, which corresponded to the rather harsh reaction conditions. Solvation-free energies for reagents, intermediates, and TSs were calculated at (-26 ± 5) kJ mol⁻¹. Therefore, accounting for the solvation-free energy should not noticeably affect the thermodynamics and kinetics of this reaction. With **5a** and **1-3d** instead of **5d**, the reaction proceeded much more slowly under the same conditions. Nevertheless, compound **6**, that is, the all-sulfur congener of **5**, possessing better solubility in toluene, was detected in the reaction mixture by GC-MS. Furthermore, the interaction of **5a** and **1-3d** in [D₈]toluene instead of toluene gave the same product **6** without deuterium, according to the GC-MS data. This finding confirms the intramolecular hydrogen atom transfer in the reaction under discussion (Scheme 2 and Figures 7 and 8), in which toluene is not involved. For both samples of **6**, negative-ion mode ESI-MS measurements revealed the same base signal at m/z 345.976 (m/z calcd for [C₁₀H₄N₂S₃]⁻: 345.98), corresponding to the product of H⁺ abstraction from **6**, seemingly from the N–H bond of the pyrazine fragment as the most acidic one in

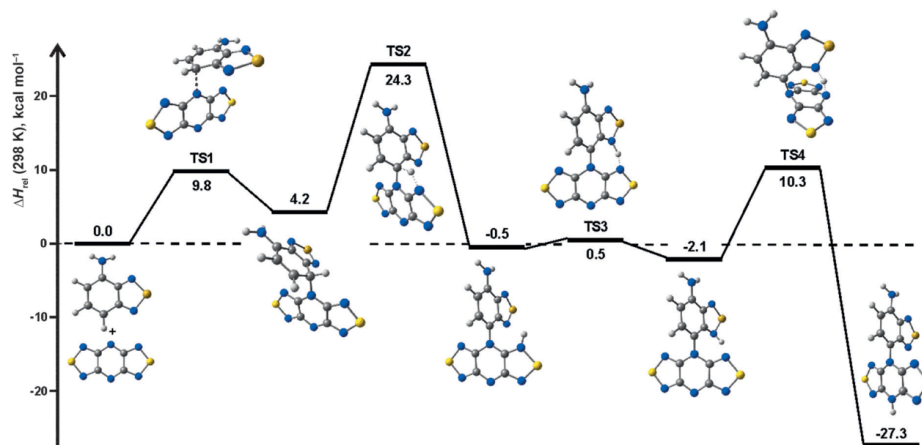


Figure 8. Relative enthalpies (ΔH_{rel} for convenience in kcal mol⁻¹; 1 kcal = 4.184 kJ) of the stationary points on the potential energy surface for the reaction between **5d** and **5a** to form **5** calculated with the B97-D3/TZVP method for $T=298$ K. Color code: C: black, H: white, N: blue, S: yellow, Se: orange.

the compound. These data do not provide evidence of either the absence or presence of deuterium in **6** synthesized in $[D_8]$ toluene, but independently confirm the authenticity of **6**.

Conclusions

Novel CT complexes **2** and **3** were prepared and characterized by single-crystal XRD; UV/Vis spectroscopy; DFT and QTAIM calculations; and, together with **1**, by HS analysis and model energy calculations. This proved that the recently described CT complex **1**,^[16] the D (4-amino-2,1,3-benzothiadiazole) and A (4-nitro-2,1,3-benzothiadiazole) components of which belonged to the 1,2,5-chalcogenadiazole family, was not a singularity. Additionally, the novel CT complex **4**, with a 1,2,5-thiadiazole derivative as A and phenoxatellurine as D, was synthesized and characterized in the same way. Investigations of other relevant combinations of D and A are in progress and the results will be published elsewhere.

The complexes are rather weakly bonded with DFT-calculated CT values for the XRD structures not exceeding 0.027 e (**2**). Model energy analysis revealed the importance of dispersion interactions and hydrogen bonding between D and A as contributors to the CT mechanism in the crystalline state. Whereas the pairwise intermolecular interactions between D and A are the strongest for **1–4** and dispersive in nature, isolated directional atom–atom interactions, for example, S \cdots N and hydrogen bridges, are stronger than single contacts related to the dispersion. This methodology combining XRD and solid-state UV/Vis spectroscopy with DFT and QTAIM calculations, HS analysis, and model energy calculations looks promising for further investigations of CT complexes in the crystalline state.

The attempt to enlarge the CT value with a bis(thiadiazolo)pyrazine derivative as A and a 2,1,3-benzoselenadiazole derivative as D resulted in a 1:1 addition reaction to give C–N cross-

coupled product **5**, which exhibited a rather unusually porous framework in the crystalline state. According to the DFT calculations, the addition is a multistep process, featuring diradical intermediates and hydrogen atom intramolecular migration between D and A moieties over four positions. All of these findings create new possibilities in the field beyond the recently described CT processes covering reduction of 1,2,5-chalcogenadiazoles into radical anions isolated in the form of thermally stable salts^[12,19,31] and D–A hypercoordination of anions to heavier chalcogen centers of these heterocycles.^[11a,b,d,e,40] Moreover, our discovery of hydrogen atom transfer from formal D to formal A for 1,2,5-chalcogenadiazoles, which leads to D–A cross-coupled products, is worth further investigation.

Experimental Section

General

¹H NMR spectra (500.13 MHz) were measured with a Bruker DRX-500 spectrometer for solutions in $[D_4]$ DMSO; chemical shifts are given with respect to Me₄Si. GC-MS measurements were performed with an Agilent 6890N device with an Agilent 5973N GC-MS system for solutions in CH₃CN. Negative-ion mode ESI-MS measurements were performed with a Bruker Customer microOTOF-Q hybrid quadrupole time-of-flight spectrometer equipped with ESI sources. Nitrogen was used as a drying gas at 190 °C at a flow rate of 4 L min⁻¹. The nebulizer pressure was set to 1.0 bar. IR spectra were recorded with a Bruker Tensor 27 spectrometer in KBr. Elemental analyses for C, H, N, and S were performed with a CHNS-Analyzer Euro EA 3000 instrument.

Solvents were dried by common drying agents and redistilled. Starting materials **1–3**,^{6d},^[16a] **5d**,^[18c] **2a**,^[18a] **5,6a**,^[18b] **3,4a**,^[14a,18a,19] and **4d**^[20b] were prepared by using procedures reported in the literature.

Synthesis

Complexes 2–4: A 1:1 mixture of D and A components was dissolved in boiling hexane and cooled to room temperature. The precipitate was filtered off and dried in air. Complexes **2–4** were obtained in the form of dark crystals suitable for XRD; complex **4** was stable enough to be sublimed quantitatively in vacuo to give the same crystalline phase. **2:** Dark brown solid; yield 47%; m.p. 141–143 °C. **3:** Dark red solid; yield 67%; m.p. 59–60 °C. **4:** Dark red solid; yield 83%; m.p. 77–79 °C.

Compound 5: A mixture of **5d** (50 mg, 0.25 mmol) and **5a** (49.5 mg, 0.25 mmol) was heated at reflux in toluene (40 mL) for 8 h. The precipitate was filtered off and washed with hexane. Compound **5**, solvate with toluene, was obtained in the form of dark crystals (yield 35%) suitable for XRD. The sample for elemental analysis and spectral measurements was carefully dried in vacuo. M.p. > 260 °C; UV/Vis: λ_{\max} (log ϵ) = 355 (1.64), 372 nm (1.55); $^1\text{H NMR}$: δ = 12.10 (s, 1H; H-N), 7.68 (d, J = 8.06 Hz, 1H; H-C), 7.53 (d, J = 8.06 Hz, 1H; H-C), 6.50 ppm (s, 2H; H₂N); IR: $\tilde{\nu}$ = 3356 m, 3230 m, 3169 m, 3103 m, 2993 m, 2906 m, 2852 m, 2731 m, 1618 vs, 1568 s, 1516 s, 1477 s, 1462 s, 1433 s, 1335 m, 1304 m, 1136 s, 955 w, 856 w, 795 m, 764 m, 743 m, 625 m, 586 w, 538 w, 509 w, 465 cm⁻¹ w; elemental analysis calcd (%) for C₁₀H₈N₆S₂Se: C 30.5, H 1.3, N 32.0, S 16.3; found: C 30.5, H 1.4, N 31.3, S 16.6.

Detection of compound 6

A mixture of **1–3d** (12.5 mg, 0.08 mmol) and **5a** (15.7 mg, 0.08 mmol) was heated at reflux in toluene or [D₆]toluene (10 mL) for 60 h. GC-MS measurements on both samples revealed the same product with m/z 347 [C₁₀H₈N₆S₂], corresponding to deuterium-free **6**. Negative-ion mode ESI-MS measurements revealed the same base signal at m/z 345.976 (m/z calcd for [C₁₀H₈N₆S₂]⁻: 345.98), corresponding to the product of H⁺ abstraction from **6**.

Crystal structure elucidation

XRD studies (Table 3) were carried out with a Bruker Kappa Apex II CCD diffractometer for **2**, **3**, and **5** and a Bruker Venture D8 diffractometer for **4** by using φ , ω scans of narrow (0.5°) frames and graphite-monochromated MoK α radiation (λ = 0.71073 Å). The structures were solved by direct methods and refined by a full-matrix least-squares anisotropic (isotropic for H atoms) procedure by using the SHELX program set.^[41] Generally, the H atom positions were calculated with the riding model and those for NH₂ groups located from difference Fourier maps. Absorption corrections were applied by using the empirical multiscan method with the SADABS program.^[42] In the refinement of **5**, which contained heavily disordered solvate molecules of toluene, the PLATON SQUEEZE program^[43] was used to calculate the contribution to the diffraction from the solvent region and thereby obtain a set of solvent-free diffraction intensities. The final crystal structures were analyzed for shortened contacts between nonbonded atoms by using the

Table 3. XRD data for compounds 2–5.^[a]

	2	3	4	5
formula	C ₁₀ H ₈ N ₆ O ₂ S·C ₆ H ₆ N ₂ S	C ₁₀ H ₈ N ₆ S·C ₂ N ₂ S ₂	C ₁₂ H ₈ OTe·3C ₂ N ₂ S ₂	C ₁₀ H ₈ N ₆ S ₂ Se·C ₇ H ₈
formula weight	377.37	295.37	728.32	486.44
T [K]	199(2)	199(2)	100(2)	296(2)
λ [Å]	0.71073	0.71073	0.71073	0.71073
crystal system	monoclinic	monoclinic	monoclinic	trigonal
space group	<i>P</i> 2 ₁ / <i>n</i>	<i>P</i> 2 ₁ / <i>c</i>	<i>P</i> 2 ₁ / <i>c</i>	<i>R</i> 3
<i>a</i> [Å]	7.1714(3)	13.3784(3)	6.5111(2)	38.8802(16)
<i>b</i> [Å]	13.8669(6)	23.4746(7)	23.5753(7)	38.8802(16)
<i>c</i> [Å]	14.6026(7)	7.3072(2)	15.8810(5)	8.2905(4)
α [°]	90	90	90	90
β [°]	102.148(2)	93.636(1)	94.484(1)	90
γ [°]	90	90	90	120
<i>V</i> [Å ³]	1419.6(1)	2290.2(1)	2430.29(13)	10853.5(8)
<i>Z</i>	4	8	4	18
ρ_{calcd} [mg m ⁻³]	1.766	1.713	1.991	1.086
μ [mm ⁻¹]	0.415	0.639	1.783	1.750
<i>F</i> (000)	768	1200	1424	3492
crystal size [mm ³]	0.05 × 0.15 × 0.9	0.20 × 0.30 × 0.60	0.80 × 0.50 × 0.50	0.05 × 0.10 × 0.60
θ range for data collection [°]	2.05–27.48	1.53–27.51	2.57–42.04	1.05–25.01
index ranges	–9 ≤ <i>h</i> ≤ 9 –17 ≤ <i>k</i> ≤ 16 –18 ≤ <i>l</i> ≤ 18	–16 ≤ <i>h</i> ≤ 17 –29 ≤ <i>k</i> ≤ 28 –9 ≤ <i>l</i> ≤ 9	–12 ≤ <i>h</i> ≤ 12 –44 ≤ <i>k</i> ≤ 44 –30 ≤ <i>l</i> ≤ 29	–46 ≤ <i>h</i> ≤ 45 –46 ≤ <i>k</i> ≤ 46 –9 ≤ <i>l</i> ≤ 9
reflins collected	14683	28531	87798	47273
independent reflins	3165 <i>R</i> (int) = 0.042	5102 <i>R</i> (int) = 0.040	17152 <i>R</i> (int) = 0.0315	4255 <i>R</i> (int) = 0.069
completeness to θ_{\max} [%]	100.0 ($\theta \leq 50^\circ$)	100.0 ($\theta \leq 50^\circ$)	99.8 ($\theta \leq 42.2^\circ$)	100.0 ($\theta \leq 50^\circ$)
data/restraints/parameters	3165/3/232	5102/6/337	17152/0/343	4255/0/199
goodness-of-fit on <i>F</i> ²	1.09	1.14	1.071	1.01
final <i>R</i> indices [<i>I</i> > 2 σ (<i>I</i>)]	<i>R</i> ₁ = 0.0407 <i>wR</i> ₂ = 0.1100	<i>R</i> ₁ = 0.0334 <i>wR</i> ₂ = 0.0889	<i>R</i> ₁ = 0.0291 <i>wR</i> ₂ = 0.0631	<i>R</i> ₁ = 0.0371 <i>wR</i> ₂ = 0.0869
final <i>R</i> indices (all data)	<i>R</i> ₁ = 0.0596 <i>wR</i> ₂ = 0.1292	<i>R</i> ₁ = 0.0498 <i>wR</i> ₂ = 0.1083	<i>R</i> ₁ = 0.0398 <i>wR</i> ₂ = 0.0668	<i>R</i> ₁ = 0.0719 <i>wR</i> ₂ = 0.0923
largest diff. peak/hole [e Å ⁻³]	0.43/–0.45	0.44/–0.33	1.866/–0.662	0.34/–0.38

[a] For XRD structure of **1**, see ref. [16].

PLATON^[44] and MERCURY programs.^[45] After artificially removing part of the molecules (C₂N₄S₂ for **4** and C₇H₈ for **5**, see Table 1), voids in the crystal lattices of **4** and **5** were analyzed with the CrystalExplorer 3.3 program,^[23] according to the procedure outlined in ref. [22] (see the Supporting Information).

CCDC 1501102 (**2**), 1501103 (**3**), 1501104 (**4**) and 1501105 (**5**) contain the supplementary crystallographic data for this paper. These data are provided free of charge by The Cambridge Crystallographic Data Centre.

HS and model energy analysis

The HS and energy analyses were performed with the CrystalExplorer 3.3 program.^[23] All model energy calculations for **1–3** were performed at the B3LYP/6-31G(d,p) level of theory, and those for **4** at the B3LYP/DGDZVP level by using previously suggested^[26] calibrations and scale factors for all energy components (Table S1 in the Supporting Information).

UV/Vis spectroscopy

The diffuse reflectance UV/Vis spectra were obtained with a Shimadzu UV-3101 PL spectrophotometer. Samples for the diffuse reflectance measurements were prepared by a thorough grinding of a mixture of the compounds under study with BaSO₄, which was used also as a standard. Spectral dependence of the diffuse reflectance was converted into a spectrum of a Kubelka–Munk function.^[29] Solution UV/Vis spectra were obtained with a Shimadzu UV-2401 PC spectrophotometer for solutions in CH₃CN.

Solid-state EPR

Solid-state EPR measurements on samples of complex **2** ground with BaSO₄, as described above, were conducted at ambient temperature with a Bruker EMX spectrometer (microwave (MW) power: 0.5 mW, modulation frequency: 100 KHz, modulation amplitude: 0.5 mT).

Quantum chemical calculations

The geometries of compounds studied were optimized at the B97-D3 level of theory^[46,47] with the def2-TZVP basis set^[48] for Te the def2-TZVP basis set with ECP was employed. The Becke–Johnson damping function was used in all dispersion-corrected calculations.^[49] The Grimme geometrical counterpoise (gCP) correction scheme was used to semiempirically treat the basis set superposition error (BSSE) effects.^[50] The COSMO solvation model^[51] was employed to take into account the solvent influence on the geometry. The resolution-of-the-identity approximation (RI) was used to speed up the GGA computations.^[52]

The thermodynamics of the formation of the CT complexes in solution was estimated as follows. Thermochemical corrections were obtained from the gas-phase optimization/frequency calculations at the B97-D3/def2-TZVP level of theory with gCP correction. Single-point calculations were performed for solutions in CH₃CN and hexane by using the COSMO solvation model, and energies after outlying charge correction were used to calculate enthalpies and Gibbs free energies. Notably, the standard state for the calculations of Gibbs free energy was chosen to be a 1 M solution.

Positions of the maxima and oscillator strengths in the UV/Vis spectra of complexes **2**, **3**, and their precursors were calculated at the TD M06-HF/TZVP level^[30,53] by using the corresponding XRD geometries, as well as those optimized in CH₃CN and hexane. In the case of **4**, calculations of the spectra were performed at the

double-hybrid B2PLYP level^[52,54] with def2-TZVP basis set (with ECP for Te).

The adiabatic EA and IE of D and A were calculated at the (U)B3LYP/6-31+G(d) level of theory.^[55] The CT values of the complexes were calculated from the Mulliken charges of partner D and A molecules.

The stationary points on the potential energy surface for the reaction between **5d** and **5a** to give **5**, that is, intermediates and TSs, were localized by using B97-D3/TZVP calculations (for details, see Section 3 in the Supporting Information).

For TD M06-HF calculations, the Gaussian 09 suite of programs was used,^[56] for all other calculations, the ORCA suite of programs were used.^[57]

Acknowledgements

The authors are grateful to Dr. Vitaly G. Kiselev for valuable discussions and Mr. Andrei A. Kuzhelev for solid-state EPR measurements, and to the Deutsche Forschungsgemeinschaft (projects nos. BE 3716/3-1 and GR 4451/1-1), Russian Federal Agency of Scientific Organizations (projects nos. 0302-2016-0002 and 0304-2014-0003), Russian Foundation for Basic Research (projects nos. 16-33-60173 and 16-33-00415), Russian Science Foundation (project no. 15-13-10022), Presidium of the Russian Academy of Sciences (projects nos. 0302-2014-0011 and 0304-2015-0005), and the Ministry of Education and Science of the Russian Federation (project of joint Laboratories of Siberian Branch of the Russian Academy of Sciences and National Research Universities) for financial support of various experimental parts of this work and HS analysis. N.P.G., E.A.C., E.A.P. and M.V.S. acknowledge the Russian Science Foundation for a financial support of the quantum chemical part of the work (project no. 16-13-10155). E.A.C. thanks the Ministry for the President of the Russian Federation's scholarship for post-graduate research abroad, and the BP Company for post-graduate scholarship. The Collective Instrumental and Analytical Center of Novosibirsk Institute of Organic Chemistry and the Computer Center of Novosibirsk State University are gratefully acknowledged for providing instrumental and computational facilities, respectively.

Keywords: donor–acceptor systems · chalcogens · charge transfer · quantum chemistry · X-ray diffraction

[1] Relevant literature is too abundant to be cited completely, for selected recent references, see: a) *Materials and Energy, Vol. 7, The WSPC Reference on Organic Electronics: Organic Semiconductors, Vols. 1 (Basic Concepts) and 2 (Fundamental Aspects of Materials and Applications)*, (Eds.: J. L. Bredas, S. R. Marder), World Scientific, **2016**; b) G. Schweicher, Y. Olivier, V. Lemaire, Y. H. Geerts, *Isr. J. Chem.* **2014**, *54*, 595–620, and other articles of this themed issue; c) S. Pola, C. H. Kuo, W. T. Peng, M. M. Islam, I. Chao, Y. T. Tao, *Chem. Mater.* **2012**, *24*, 2566–2571; d) C. Wang, H. Dong, W. Hu, Y. Liu, D. Zhu, *Chem. Rev.* **2012**, *112*, 2208–2267; e) Y. Zhao, W. Z. Liang, *Chem. Soc. Rev.* **2012**, *41*, 1075–1087; f) A. Mishra, P. Bauerle, *Angew. Chem. Int. Ed.* **2012**, *51*, 2020–2067; *Angew. Chem.* **2012**, *124*, 2060–2109; g) T. M. Figueira-Duarte, K. Muellen, *Chem. Rev.* **2011**, *111*, 7260–7314; h) L. Zhang, S. M. Fakhouri, F. Liu, J. C. Timmons, N. A. Ran, A. L. Briseno, *J. Mater. Chem.* **2011**, *21*, 1329–1337; i) J. E. Anthony, A. Facchetti, M. Heeney, S. R. Marder, X. Zhan, *Adv. Mater.* **2010**, *22*, 3876–3892, and other articles of this themed issue;

- j) V. Coropceanu, J. Cornil, D. A. da Silva Filho, Y. Olivier, R. Silbey, J. L. Bredas, *Chem. Rev.* **2007**, *107*, 926–952; k) A. R. Murphy, J. M. J. Frechet, *Chem. Rev.* **2007**, *107*, 1066–1096; l) H. Hoppe, N. S. Sariciftci, *J. Mater. Res.* **2004**, *19*, 1924–1945.
- [2] The term CT complex was coined by R. S. Mulliken. By definition, the CT complex is a D–A complex characterized by electronic transitions to an excited state, in which there is a partial transfer of electronic charge from D to A: a) R. S. Mulliken, *J. Am. Chem. Soc.* **1950**, *72*, 600–608; b) R. S. Mulliken, W. B. Pearson, *Molecular Complexes*, Wiley, New York, **1969**; c) R. Foster, *Charge Transfer Complexes*, Academic Press, London, **1969**; d) *IUPAC Compendium of Chemical Terminology (The Gold Book)* (Eds.: A. D. McNaught, A. R. Wilkinson), Blackwell Scientific Publications, Oxford, **1997**.
- [3] F. Gutmann, L. E. Lyons, *Organic Semiconductors*, Wiley, New York, **1967**.
- [4] a) E. Espildora, J. L. Delgado, N. Martin, *Isr. J. Chem.* **2014**, *54*, 429–439; b) G. Saito, Y. Yoshida, *Bull. Chem. Soc. Jpn.* **2007**, *80*, 1–137; c) *Organic Conductors, Superconductors, and Magnets: From Synthesis to Molecular Electronics* (Eds.: L. N. Ouahab, E. Yagubskii), Kluwer, Dordrecht, **2004**; d) *Extended Linear Chain Compounds* (Ed.: J. S. Miller), Plenum, New York, **1982**.
- [5] a) K. P. Goetz, D. Vermeulen, M. E. Payne, C. Kloc, L. E. McNeil, O. D. Jurchescu, *J. Mater. Chem. C* **2014**, *2*, 3065–3076; b) A. Yu. Sosorev, D. Yu. Paraschuk, *Isr. J. Chem.* **2014**, *54*, 650–673.
- [6] a) A. Rondi, Y. Rodriguez, T. Feurer, A. Cannizzo, *Acc. Chem. Res.* **2015**, *48*, 1432–1440; b) D. Wang, X. Zhang, W. Ding, X. Zhao, Z. Geng, *Comput. Theor. Chem.* **2014**, *1029*, 68–78; c) H. Phillips, E. Geva, B. D. Dunietz, *J. Chem. Theory Comput.* **2012**, *8*, 2661–2668; d) B. Baumeier, D. Andrienko, Y. Ma, M. Rohlfing, *J. Chem. Theory Comput.* **2012**, *8*, 997–1002; e) J. L. Brédas, D. Beljonne, V. Coropceanu, J. Cornil, *Chem. Rev.* **2004**, *104*, 4971–5003.
- [7] a) O. Hinsberg, *Ber. Dtsch. Chem. Ges.* **1889**, *22*, 862–866; b) O. Hinsberg, *Ber. Dtsch. Chem. Ges.* **1889**, *22*, 2895–2902.
- [8] a) B. A. D. Neto, P. H. P. R. Carvalho, J. R. Correa, *Acc. Chem. Res.* **2015**, *48*, 1560–1569; b) L. S. Konstantinova, E. A. Knyazeva, O. A. Rakitin, *Molecules* **2015**, *20*, 14522–14532; c) L. S. Konstantinova, I. E. Bobkova, Yu. V. Nelyubina, E. A. Chulanova, I. G. Irtegora, N. V. Vasilieva, P. S. Camacho, S. E. Ashbrook, G. Hua, A. M. Z. Slawin, J. D. Woollins, A. V. Zibarev, O. A. Rakitin, *Eur. J. Org. Chem.* **2015**, 5585–5593; d) L. S. Konstantinova, E. A. Knyazeva, A. A. Nefyodov, P. S. Camacho, S. E. Ashbrook, J. D. Woollins, A. V. Zibarev, O. A. Rakitin, *Tetrahedron Lett.* **2015**, *56*, 1107–1110; e) L. S. Konstantinova, E. A. Knyazeva, O. A. Rakitin, *Org. Prep. Proced.* **2014**, *46*, 475–544; f) B. A. D. Neto, A. A. M. Lapis, E. N. da Silva Junior, J. Dupont, *Eur. J. Org. Chem.* **2013**, 228–255; g) Z. V. Todress, *Chalcogenadiazoles: Chemistry and Applications*, CCR Press/Taylor & Francis, London, **2012**; h) P. A. Koutentis, in *Comprehensive Heterocyclic Chemistry III* (Eds.: A. R. Katritzky, C. A. Ramsden, E. F. V. Scriven, R. J. K. Taylor), Elsevier, Oxford, **2008**, Vol. 5, pp. 516–564; i) S. Yamazaki, in *Comprehensive Heterocyclic Chemistry III* (Eds.: A. R. Katritzky, C. A. Ramsden, E. F. V. Scriven, R. J. K. Taylor), Elsevier, Oxford, **2008**, Vol. 6, pp. 518–580; j) P. A. Koutentis, in *Science of Synthesis* (Eds.: R. C. Storr, T. L. Gilchrist), Thieme, Stuttgart, **2003**, Vol. 13, pp. 297–348; k) R. A. Aitken, in *Science of Synthesis* (Eds.: R. C. Storr, T. L. Gilchrist), Thieme, Stuttgart, **2003**, Vol. 13, pp. 777–822.
- [9] a) T. F. Mikhailovskaya, A. G. Makarov, N. Yu. Selikhova, A. Yu. Makarov, E. A. Pritchina, I. Yu. Bagryanskaya, E. V. Vorontsova, I. D. Ivanov, V. D. Tikhova, N. P. Gritsan, Yu. G. Slizhov, A. V. Zibarev, *J. Fluorine Chem.* **2016**, *183*, 44–58; b) A. G. Makarov, N. Yu. Selikhova, A. Yu. Makarov, V. S. Malkov, I. Yu. Bagryanskaya, Yu. V. Gatilov, A. S. Knyazeva, Yu. G. Slizhov, A. V. Zibarev, *J. Fluorine Chem.* **2014**, *165*, 123–131; c) N. V. Vasilieva, I. G. Irtegora, N. P. Gritsan, A. V. Lonchakov, A. Yu. Makarov, L. A. Shundrin, A. V. Zibarev, *J. Phys. Org. Chem.* **2010**, *23*, 536–543; d) A. V. Zibarev, I. V. Beregovaya, *Rev. Heteroatom. Chem.* **1992**, *7*, 171–190; e) A. V. Zibarev, A. O. Miller, *J. Fluorine Chem.* **1990**, *50*, 359–363.
- [10] In contrast to the situation with S and Se congeners, the archetypal 1,2,5-telluradiazole and its derivatives were synthesized first, and only then their annelated derivatives, including benzo-fused ones that is, 2,1,3-benzotelluradiazoles: a) V. Bertini, F. Lucchesini, A. De Munno, *Synthesis* **1982**, 681–683; b) V. Bertini, P. Dapporto, F. Lucchesini, A. Segà, A. De Munno, *Acta Crystallogr. Sect. A* **1984**, *40*, 653–655; c) R. Neidlein, D. Knecht, A. Gieren, C. Ruiz-Perez, *Z. Naturforsch. B* **1987**, *42*, 84–90; d) R. Neidlein, D. Knecht, *Helv. Chim. Acta* **1987**, *70*, 1076–1078; e) T. Chivers, X. Gao, M. Parvez, *Inorg. Chem.* **1996**, *35*, 9–15; f) V. N. Kovtonyuk, A. Yu. Makarov, M. M. Shakirov, A. V. Zibarev, *Chem. Commun.* **1996**, 1991–1992.
- [11] a) G. E. Garrett, G. L. Gibson, R. N. Straus, D. S. Seferos, M. S. Taylor, *J. Am. Chem. Soc.* **2015**, *137*, 4126–4133; b) N. A. Semenov, A. V. Lonchakov, N. P. Gritsan, A. V. Zibarev, *Russ. Chem. Bull.* **2015**, *64*, 499–510; c) J. Svec, P. Zimcik, L. Novakova, O. A. Rakitin, S. A. Amelichev, P. A. Stuzhin, V. Novakova, *Eur. J. Org. Chem.* **2015**, 596–604; d) N. A. Semenov, A. V. Lonchakov, N. A. Pushkarevsky, E. A. Suturina, V. V. Korolev, E. Lork, V. G. Vasiliev, S. N. Konchenko, J. Beckmann, N. P. Gritsan, A. V. Zibarev, *Organometallics* **2014**, *33*, 4302–4314; e) N. A. Semenov, N. A. Pushkarevsky, J. Beckmann, P. Finke, E. Lork, R. Mews, I. Yu. Bagryanskaya, Yu. V. Gatilov, S. N. Konchenko, V. G. Vasiliev, A. V. Zibarev, *Eur. J. Inorg. Chem.* **2012**, 3693–3703; f) A. F. Cozzolino, P. J. W. Elder, I. Vargas-Baca, *Coord. Chem. Rev.* **2011**, *255*, 1426–1438.
- [12] A. V. Lonchakov, O. A. Rakitin, N. P. Gritsan, A. V. Zibarev, *Molecules* **2013**, *18*, 9850–9900.
- [13] Relevant literature is too abundant to be cited completely; for selected recent reviews, see: a) D. M. Stoltzfus, D. E. Donaghey, A. Armin, P. E. Shaw, P. L. Burn, P. Meredith, *Chem. Rev.* **2016**, *116*, 12920–12955; b) L. Dou, Y. Liu, Z. Hang, G. Li, Y. Yang, *Chem. Rev.* **2015**, *115*, 12633–12665.
- [14] a) N. A. Pushkarevsky, A. V. Lonchakov, N. A. Semenov, E. Lork, L. I. Buravov, L. S. Konstantinova, T. G. Silber, N. Robertson, N. P. Gritsan, O. A. Rakitin, J. D. Woollins, E. B. Yagubskii, J. Beckmann, A. V. Zibarev, *Synth. Met.* **2012**, *162*, 2267–2276; b) T. Linder, E. Badiola, T. Baumgartner, T. C. Sutherland, *Org. Lett.* **2010**, *12*, 4520–4523; c) T. Suzuki, Y. Yamashita, T. Fukushima, T. Miyashi, *Mol. Cryst. Liq. Cryst.* **1997**, *296*, 165–180; d) T. Suzuki, H. Fujii, Y. Yamashita, C. Kabuto, S. Tanaka, M. Harasawa, T. Mukai, T. Miyashi, *J. Am. Chem. Soc.* **1992**, *114*, 3034–3043; e) Y. Yamashita, T. Suzuki, T. Mukai, G. Saito, *Chem. Commun.* **1985**, 1044–1045; f) Y. Yamashita, T. Suzuki, G. Saito, T. Mukai, *Chem. Lett.* **1985**, *14*, 1759–1762; g) A. Gieren, V. Lamm, T. Huebner, M. Rabben, R. Neidlein, D. Droste, *Chem. Ber.* **1984**, *117*, 1940–1953.
- [15] Y. Yamashita, M. Tomura, *J. Mater. Chem.* **1998**, *8*, 1933–1944.
- [16] a) D. A. Bashirov, T. S. Sukhikh, N. V. Kuratieva, E. A. Chulanova, I. V. Yushina, N. P. Gritsan, S. N. Konchenko, A. V. Zibarev, *RSC Adv.* **2014**, *4*, 28309–28316; b) E. A. Chulanova, *Diploma Dissertation*, Novosibirsk State University, Novosibirsk, Russia, **2014**.
- [17] a) D. P. Rainville, R. A. Zingaro, J. P. Ferrais, *Can. J. Chem.* **1980**, *58*, 1133–1137; b) C. A. Heller, R. A. Zingaro, E. A. Meyers, *Can. J. Chem.* **1974**, *52*, 3814–3824.
- [18] a) L. S. Konstantinova, E. A. Knyazeva, N. V. Obruchnikova, Yu. V. Gatilov, A. V. Zibarev, O. A. Rakitin, *Tetrahedron Lett.* **2013**, *54*, 3075–3078; b) L. S. Konstantinova, E. A. Knyazeva, N. V. Obruchnikova, N. V. Vasilieva, I. G. Irtegora, Yu. V. Nelyubina, I. Yu. Bagryanskaya, L. A. Shundrin, Z. Yu. Sosnovskaya, A. V. Zibarev, O. A. Rakitin, *Tetrahedron* **2014**, *70*, 5558–5568; c) M. Bella, M. Schultz, V. Milata, K. Konarikova, M. Breza, *Tetrahedron* **2010**, *66*, 8169–8174.
- [19] A. Yu. Makarov, I. G. Irtegora, N. V. Vasilieva, I. Yu. Bagryanskaya, T. Borrmann, Yu. V. Gatilov, E. Lork, R. Mews, W. D. Stohrer, A. V. Zibarev, *Inorg. Chem.* **2005**, *44*, 7194–7199.
- [20] a) M. R. Smith, M. M. Mangion, R. A. Zingaro, E. A. Meyers, *J. Heterocycl. Chem.* **1973**, *10*, 527–531; b) H. D. K. Drew, *J. Chem. Soc.* **1926**, *129*, 223–231.
- [21] a) R. S. Rowland, R. Taylor, *J. Phys. Chem.* **1906**, *100*, 7384–7391; b) M. Mantina, A. C. Chamberlin, R. Valero, C. J. Cramer, D. G. Truhlar, *J. Phys. Chem. A* **2009**, *113*, 5806–5812.
- [22] M. J. Turner, J. J. McKinnon, D. Jayatilaka, M. A. Spackman, *CrystEngComm* **2011**, *13*, 1804–1813.
- [23] M. J. Turner, J. J. McKinnon, S. K. Wolff, D. J. Grimwood, P. R. Spackman, D. Jayatilaka, M. A. Spackman, *CrystalExplorer 3.3*, The University of Western Australia, Crawley, Australia, **2005–2016**.
- [24] a) M. A. Spackman, D. Jayatilaka, *CrystEngComm* **2009**, *11*, 19–32; b) J. J. McKinnon, M. A. Spackman, A. S. Mitchell, *Acta Crystallogr. Sect. A* **2004**, *60*, 627–668; c) J. J. McKinnon, A. S. Mitchell, M. A. Spackman, *Chem. Eur. J.* **1998**, *4*, 2136–2141; d) M. A. Spackman, P. G. Byrom, *Chem. Phys. Lett.* **1997**, *267*, 215–220.
- [25] J. J. McKinnon, D. Jayatilaka, M. A. Spackman, *Chem. Commun.* **2007**, 3814–3816.
- [26] M. J. Turner, S. Grabowsky, D. Jayatilaka, M. A. Spackman, *J. Phys. Chem. Lett.* **2014**, *5*, 4249–4255.

- [27] a) *The Quantum Theory of Atoms in Molecules* (Eds.: C. F. Mottaand, R. J. Boid), Wiley-VCH, Weinheim, 2007; b) R. F. W. Bader, *Monatsh. Chem.* 2005, 136, 819–854; c) R. F. W. Bader, *Atoms in Molecules: A Quantum Theory*, Oxford University Press, Oxford, 1990.
- [28] A. M. Pendás, E. Francisco, M. A. Blanco, C. Gatti, *Chem. Eur. J.* 2007, 13, 9362–9371.
- [29] P. Kubelka, *J. Opt. Soc. Am.* 1948, 38, 448–457.
- [30] a) Y. Zhao, D. G. Truhlar, *J. Phys. Chem. A* 2006, 110, 13126–13130; b) Y. Zhao, D. G. Truhlar, *Acc. Chem. Res.* 2008, 41, 157–167; c) F. Weigend, R. Ahlrichs, *Phys. Chem. Chem. Phys.* 2005, 7, 3297–3305.
- [31] a) N. A. Pushkarevsky, N. A. Semenov, A. A. Dmitriev, N. V. Kuratieva, A. S. Bogomyakov, I. G. Irtegora, N. V. Vasilieva, B. E. Bode, N. P. Gritsan, L. S. Konstantinova, J. D. Woollins, O. A. Rakitin, S. N. Konchenko, V. I. Ovcharenko, A. V. Zibarev, *Inorg. Chem.* 2015, 54, 7007–7013; b) N. A. Semenov, N. A. Pushkarevsky, E. A. Suturina, E. A. Chulanova, N. V. Kuratieva, A. S. Bogomyakov, I. G. Irtegora, N. V. Vasilieva, L. S. Konstantinova, N. P. Gritsan, O. A. Rakitin, V. I. Ovcharenko, S. N. Konchenko, A. V. Zibarev, *Inorg. Chem.* 2013, 52, 6654–6663; c) A. V. Zibarev, R. Mews, in *Selenium and Tellurium Chemistry: From Small Molecules to Biomolecules and Materials* (Eds.: J. D. Woollins, R. S. Laitinen), Springer, Berlin, 2011, pp. 123–149; d) N. P. Gritsan, A. V. Zibarev, *Russ. Chem. Bull.* 2011, 60, 2131–2140; e) N. A. Semenov, N. A. Pushkarevsky, A. V. Lonchakov, A. S. Bogomyakov, E. A. Pritchina, E. A. Suturina, N. P. Gritsan, S. N. Konchenko, R. Mews, V. I. Ovcharenko, A. V. Zibarev, *Inorg. Chem.* 2010, 49, 7558–7564; f) S. N. Konchenko, N. P. Gritsan, A. V. Lonchakov, U. Radius, A. V. Zibarev, *Mendeleev Commun.* 2009, 19, 7–9; g) S. N. Konchenko, N. P. Gritsan, A. V. Lonchakov, I. G. Irtegora, R. Mews, V. I. Ovcharenko, U. Radius, A. V. Zibarev, *Eur. J. Inorg. Chem.* 2008, 3833–3838; h) N. P. Gritsan, A. V. Lonchakov, E. Lork, R. Mews, E. A. Pritchina, A. V. Zibarev, *Eur. J. Inorg. Chem.* 2008, 1994–1998; i) I. Yu. Bagryanskaya, Yu. V. Gatilov, N. P. Gritsan, V. N. Ikorskii, I. G. Irtegora, A. V. Lonchakov, E. Lork, R. Mews, V. I. Ovcharenko, N. A. Semenov, N. V. Vasilieva, A. V. Zibarev, *Eur. J. Inorg. Chem.* 2007, 4751–4761; j) V. N. Ikorskii, I. G. Irtegora, E. Lork, A. Yu. Makarov, R. Mews, V. I. Ovcharenko, A. V. Zibarev, *Eur. J. Inorg. Chem.* 2006, 3061–3067.
- [32] According to the maximum hardness principle, any distortion of the equilibrium geometry of a molecule reduces its absolute hardness (η), that is, the energy gap between its frontier molecular orbitals (2 η); normally, the HOMO increases and the LUMO decreases the energy). In a mechanochemical situation, impacted energy, which narrows the gaps of reaction partners through distortions of their molecular geometries, facilitates ET from D onto A, which might lead to radical ion salts: a) R. G. Pearson, *Chemical Hardness*, Wiley-VCH, Weinheim, 1997; b) W. Jones, M. D. Eddleston, *Faraday Discuss.* 2014, 170, 9–34; c) E. V. Boldyreva, *Chem. Soc. Rev.* 2013, 42, 7719–7736, and other articles of this themed issue; d) J. Ribas-Arino, D. Marx, *Chem. Rev.* 2012, 112, 5412–5487; e) S. L. James, C. J. Adams, C. Bolm, D. Braga, P. Collier, T. Friscic, F. Greppioni, R. D. M. Harries, G. Hayett, W. Jones, A. Krebs, J. Mack, L. Maini, A. G. Orpen, I. V. Parkin, W. C. Shearose, J. W. Steed, D. C. Waddell, *Chem. Soc. Rev.* 2012, 41, 413–447; see also the observation that grinding of a mixture of TTF (D) and [1,2,5]thiadiazolo[1,2,5]thiadiazole (A; in this work, 3,4a) led to the formation of the CT complex (ref. [14a]).
- [33] Y. Yamashita, R. Saito, T. Suzuki, C. Kabuto, T. Mikai, T. Myashi, *Angew. Chem. Int. Ed. Engl.* 1988, 27, 434–435; *Angew. Chem.* 1988, 100, 428–429.
- [34] a) J. D. Evans, D. M. Huang, M. Haranczyk, A. W. Thornton, C. J. Sumby, C. J. Doonan, *CrystEngComm* 2016, 18, 4133–4141; b) U. Diaz, A. Corma, *Coord. Chem. Rev.* 2016, 311, 85–124.
- [35] E. Terada, T. Okamoto, M. Kozaki, M. E. Masaki, D. Shiomi, K. Sato, T. Takui, K. Okada, *J. Org. Chem.* 2005, 70, 10073–10081.
- [36] A. S. Sharipov, B. I. Loukhovitski, C. J. Tsai, A. M. Starik, *Eur. Phys. J. D* 2014, 68, 99.
- [37] a) R. A. Marcus, *Rev. Mod. Phys.* 1993, 65, 599–610; b) M. D. Newton, N. Sutin, *Ann. Rev. Phys. Chem.* 1984, 35, 437–480; c) M. D. Newton, *Chem. Rev.* 1991, 91, 767–792.
- [38] Notably, there is growing interest in the current literature to main-group radicals and diradicals/diradicaloids and borders between the latter and closed-shell species: a) M. Abe, *Chem. Rev.* 2013, 113, 7011–7088; b) S. Tolstikov, E. Tretyakov, S. Fokin, E. Suturina, G. Romanenko, A. Bogomyakov, D. Stass, A. Maryasov, M. Fedin, N. Gritsan, V. Ovcharenko, *Chem. Eur. J.* 2014, 20, 2793–2803; c) R. T. Boere, in *Electron Paramagnetic Resonance*, RSC, Cambridge, 2013, Vol. 23, pp. 22–57; d) A. Yu. Makarov, F. Blockhuys, I. Yu. Bagryanskaya, Yu. V. Gatilov, M. M. Shakirov, A. V. Zibarev, *Inorg. Chem.* 2013, 52, 3699–3710; e) S. Gonzalez-Gallardo, F. Breher, in *Comprehensive Inorganic Chemistry II* (Eds.: J. Reedijk, K. Poepelmeier), Elsevier, Amsterdam, 2013, Vol. 1, pp. 413–455; f) F. Breher, *Coord. Chem. Rev.* 2007, 251, 1007–1043.
- [39] a) L. Noodleman, *J. Chem. Phys.* 1981, 74, 5737–5743; b) L. Noodleman, E. R. Davidson, *Chem. Phys.* 1986, 109, 131–143; c) H. Nagao, M. Nishino, Y. Shigeta, T. Soda, Y. Kitagawa, T. Onishi, Y. Yoshioka, K. Yamaguchi, *Coord. Chem. Rev.* 2000, 198, 265–295.
- [40] E. A. Suturina, N. A. Semenov, A. V. Lonchakov, I. Yu. Bagryanskaya, Yu. V. Gatilov, I. G. Irtegora, N. V. Vasilieva, E. Lork, R. Mews, N. P. Gritsan, A. V. Zibarev, *J. Phys. Chem. A* 2011, 115, 4851–4860.
- [41] a) G. M. Sheldrick, *Acta Crystallogr. Sect. A* 2015, 71, 3–8; b) G. M. Sheldrick, SHELX-97, Programs for Crystal Structure Analysis (Release 97–2), University of Göttingen, Germany, 1997.
- [42] SADABS, Version 2008–1, Bruker AXS, Madison, WI, USA, 2008.
- [43] A. L. Spek, *Acta Crystallogr. Sect. A* 2015, 71, 9–18.
- [44] a) A. L. Spek, PLATON, A Multipurpose Crystallographic Tool (Version 10M), Utrecht University, Utrecht, The Netherlands, 2003; b) A. L. Spek, *J. Appl. Crystallogr.* 2003, 36, 7–13.
- [45] C. F. Macrae, P. R. Edgington, P. McCabe, E. Pidcock, G. P. Shields, R. Taylor, M. Towler, J. van de Stree, *J. Appl. Crystallogr.* 2006, 39, 453–457.
- [46] S. Grimme, *J. Comput. Chem.* 2006, 27, 1787–1799.
- [47] S. Grimme, J. Antony, S. Ehrlich, H. Krieg, *J. Chem. Phys.* 2010, 132, 154104.
- [48] F. Weigend, R. Ahlrichs, *Phys. Chem. Chem. Phys.* 2005, 7, 3297–3305.
- [49] S. Grimme, S. Ehrlich, L. Goerigk, *J. Comput. Chem.* 2011, 32, 1456–1465.
- [50] D. A. Pantazis, X. Y. Chen, C. R. Landis, F. Neese, *J. Chem. Theory Comput.* 2008, 4, 908–919.
- [51] S. Sinnecker, A. Rajendran, A. Klant, M. Diedenhofen, F. Neese, *J. Phys. Chem. A* 2006, 110, 2235–2245.
- [52] F. Neese, *J. Comput. Chem.* 2003, 24, 1740–1747.
- [53] A. Dreuw, M. Head-Gordon, *Chem. Rev.* 2005, 105, 4009–4037.
- [54] S. Grimme, F. Neese, *J. Chem. Phys.* 2007, 127, 154116.
- [55] A. D. Becke, *J. Chem. Phys.* 1993, 98, 5648–5652.
- [56] Gaussian 09, Revision A.01, M. J. Frisch, G. W. Trucks, H. B. Schlegel, G. E. Scuseria, M. A. Robb, J. R. Cheeseman, G. Scalmani, V. Barone, B. Menonucci, G. A. Petersson, H. Nakatsuji, M. Caricato, X. Li, H. P. Hratchian, A. F. Izmaylov, J. Bloino, G. Zheng, J. L. Sonnenberg, M. Hada, M. Ehara, K. Toyota, R. Fukuda, J. Hasegawa, M. Ishida, T. Nakajima, Y. Honda, O. Kitao, H. Nakai, T. Vreven, J. A. Montgomery, Jr., J. E. Peralta, F. Ogliaro, M. Bearpark, J. J. Heyd, E. Brothers, K. N. Kudin, V. N. Staroverov, R. Kobayashi, J. Normand, K. Raghavachari, A. Rendell, J. C. Burant, S. S. Iyengar, J. Tomasi, M. Cossi, N. Rega, J. M. Millam, M. Klene, J. E. Knox, J. B. Cross, V. Bakken, C. Adamo, J. Jaramillo, R. Gomperts, R. E. Stratmann, O. Yazyev, A. J. Austin, R. Cammi, C. Pomelli, J. W. Ochterski, R. L. Martin, K. Morokuma, V. G. Zakrzewski, G. A. Voth, P. Salvador, J. J. Dannenberg, S. Dapprich, A. D. Daniels, O. Farkas, J. B. Foresman, J. V. Ortiz, J. Cioslowski, D. J. Fox, Gaussian, Inc., Wallingford CT, 2009.
- [57] F. Neese, *WIREs* 2012, 2, 73–78.

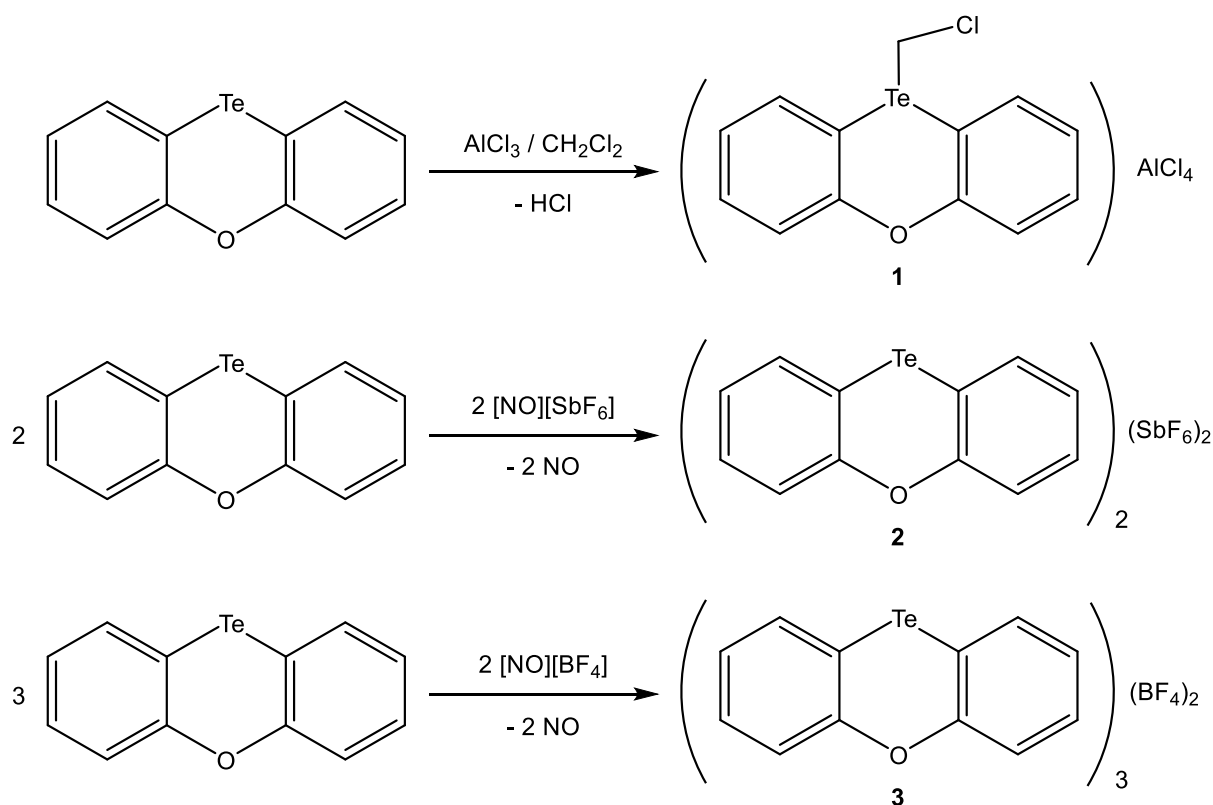
Manuscript received: August 31, 2016

Final Article published: December 13, 2016

2.2. The reaction of phenoxatellurine with single-electron oxidizers revisited

2.2.1. Synopsis

The reaction of phenoxatellurine (PT) upon known single-electron oxidizers, namely $\text{AlCl}_3/\text{CH}_2\text{Cl}_2$, $[\text{NO}][\text{SbF}_6]$ and $[\text{NO}][\text{BF}_4]$ was investigated providing diamagnetic double-decker and triple-decker structures. The represented dications $[\text{PT}_2]^{2+}$ and $[\text{PT}_3]^{2+}$ can be regarded as dimers of the radical cation $[\text{PT}]^{\cdot+}$ or as adduct between this dimer and neutral PT (Scheme 13).



Scheme 13. Reaction of phenoxatellurine with $\text{AlCl}_3/\text{CH}_2\text{Cl}_2$ (1), $[\text{NO}][\text{SbF}_6]$ (2) and $[\text{NO}][\text{BF}_4]$ (3).

2.2.2. Experimental Contributions

In this study, I carried out the synthesis of the compounds and their characterization. Moreover I wrote the experimental section and the manuscript with Prof. Dr. Jens Beckmann. Prof. Dr. René Boere and his group were responsible for the cyclic voltammetry measurements. X-ray analysis and structure refinements have been made by Dr. Enno Lork. The article was published in the following journal:

Mostaghimi, F.; Lork, E.; Hong, I.; Roemmele, T. L.; Boéré, R. T.; Mebs, S.; Beckmann, J. *The reaction of phenoxatellurine with single-electron oxidizers revisited*. *New J. Chem.* **2019**, 43, 12754–12766. DOI: 10.1039/C9NJ02401H.



The reaction of phenoxatellurine with single-electron oxidizers revisited†

Farzin Mostaghimi,^a Enno Lork,^a Intek Hong,^b Tracey L. Roemmele,^b René T. Boeré,^c Stefan Mebs^c and Jens Beckmann^c*

Cite this: *New J. Chem.*, 2019, 43, 12754

Received 9th May 2019,
Accepted 16th July 2019

DOI: 10.1039/c9nj02401h

rsc.li/njc

The reaction of phenoxatellurine (PT) with the known single-electron oxidizers $\text{AlCl}_3/\text{CH}_2\text{Cl}_2$, $[\text{NO}][\text{SbF}_6]$ and $[\text{NO}][\text{BF}_4]$ provided the diamagnetic products $[(\text{PT})\text{CH}_2\text{Cl}][\text{AlCl}_4]$ (**1**), $[\text{PT}_2][\text{SbF}_6]_2$ (**2**) and $[\text{PT}_3][\text{BF}_4]_2$ (**3**), respectively, which were fully characterized by X-ray crystallography. The dications $[\text{PT}_2]^{2+}$ and $[\text{PT}_3]^{2+}$ present in **2** and **3** can be regarded as dimers of the elusive radical cation $[\text{PT}]^{\bullet+}$ or as adduct between this dimer and neutral PT, respectively. The stacking between the aromatic layers of $[\text{PT}_2]^{2+}$ and $[\text{PT}_3]^{2+}$ can be best described using the pancake bonding (PB) model. The computational analysis uncovers the essential role of London dispersion effects for the stacking process and reveals the Te–Te interactions to be dominated by non-covalent bonding. The results are compared with those of the related thianthrene (TA) system.

Introduction

As early as 1868, it was noticed that diphenyl disulfide dissolves in conc. sulfuric acid to give intensely colored solutions. Though unknown at the time, the colour stems from the thianthrene (TA) radical cation $[\text{TA}]^{\bullet+}$, which forms after a series of single-electron oxidation steps (Scheme 1).¹

The recognition of the TA radical cation $[\text{TA}]^{\bullet+}$ as member of a unique compound class with unpaired electrons² arose only a few years after Gomberg's seminal discovery of the triphenylmethyl radical in 1900.³ Unambiguous proof for the open-shell electronic structure was provided by the first EPR measurements in 1962.^{4–9} Since that time, a great number of studies dealing with the synthesis, reactivity and its extensive use in organic synthesis have been reported.¹⁰ The thianthrene radical cation, $[\text{TA}]^{\bullet+}$, is conveniently prepared by single electron oxidation from parent thianthrene, TA, using various methods and reagents including $\text{HClO}_4/\text{acetic anhydride}$,⁵ $\text{SbCl}_5/\text{CHCl}_3$,¹¹ ICl/CCl_4 ,¹² $[\text{NO}][\text{BF}_4]$,¹³ $\text{AlCl}_3/\text{CH}_2\text{Cl}_2$,¹⁴ the dodecamethylcarboranyl radical/hexane,¹⁵ by electrolysis in $[\text{tBu}_4\text{N}][\text{PF}_6]/\text{SO}_2$,¹⁶ $\text{AlCl}_3/\text{SO}_2$,¹⁷ and XeF_2 , $\text{Me}_3\text{SiO}_3\text{SCF}_3/\text{CH}_2\text{Cl}_2$.¹⁸

Structural characterization of the obtained salts was only achieved much later and revealed (reversible) oligomerisation

and electron pairing in the solid state (Fig. 1). In 1994, Bock *et al.* isolated a diamagnetic dimer in $[\text{TA}_2][\text{AlCl}_4]_2$ comprised of stacks of parallel and eclipsed TA units (double-decker structure).¹⁴ A very similar structural arrangement was found in 2009 by Beck *et al.* in $[\text{TA}_2][\text{PF}_6]_2$.¹⁶ In 2012, the same group described a diamagnetic trimer in $[\text{TA}_3][\text{Al}_2\text{Cl}_7]_2$ comprised of stacks of parallel and eclipsed TA units (parallel triple-decker structure),¹⁷ whereas Kochi *et al.* in 2007 reported a diamagnetic trimer in $[\text{TA}_3][\text{C}_{13}\text{H}_{36}\text{B}_{11}]_2$ comprised of stacks of parallel TA rings, in which the central unit is rectangular to two eclipsed outer units (crossed triple-decker structure).¹⁵ It has been shown by UV-vis spectroelectrochemistry that, in solution, $[\text{TA}]^{\bullet+}$ is in a concentration-dependent equilibrium with its dimer $[\text{TA}_2]^{2+}$.⁹

While the TA radical cation has been studied exhaustively, rather little information is available about radical cations based on dibenzo-1,4-dioxin type heterocycles containing the heavier chalcogens. A notable exception involves the one-electron oxidation of 9,10-selenanthrene $[\text{SeA}_2]$, carried out by Beck *et al.* in 2012, which provided a dimer $[\text{SeA}][\text{AlCl}_4]$ of the corresponding yet undetected (by EPR) radical cation $[\text{SeA}]^{\bullet+}$.¹⁷

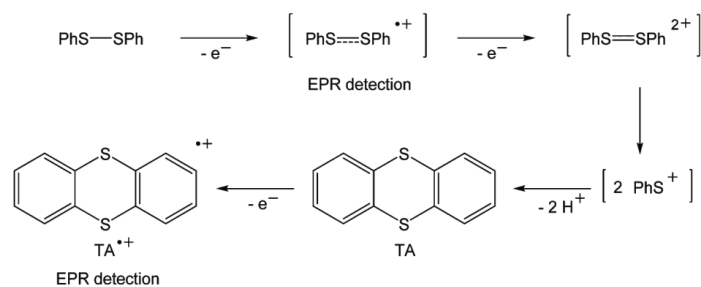
Although these dimeric and trimeric solid-state structures have been established unambiguously, the electronic reason for the aggregation remains unclear: in 2005, Nishinaga and Komatsu proposed in their review that multicentre π -bonding between the aromatic rings is responsible for the aggregation rather than multicentre σ -bonding between the chalcogen atoms.¹⁹ This idea is supported by the fact that substituted anthracene radical cations lacking heteroatoms also undergo oligomerisation, *e.g.* $[\text{OMA}_2][\text{SbCl}_6]_2$ (OMA = 1,2,3,4,5,6,7,8-octamethylanthracene)²⁰ and $[\text{TMDMA}_3][\text{SbCl}_6]_2$ (TMDMA = 2,3,6,7-tetramethoxy-9,10-dimethylanthracene).²¹ Nowadays, it is understood that the multicentre π -bonding in radical dimers is mostly due to the

^a Institut für Anorganische Chemie und Kristallographie, Universität Bremen, Leobener Straße 7, 28359 Bremen, Germany. E-mail: j.beckmann@uni-bremen.de

^b Department of Chemistry and Biochemistry, University of Lethbridge, Lethbridge, AB, Canada T1K 3M4. E-mail: boere@uleth.ca

^c Institut für Chemie und Biochemie, Freie Universität Berlin, Fabeckstraße 36a, 14195 Berlin, Germany. E-mail: stebs@chemie.fu-berlin.de

† Electronic supplementary information (ESI) available. CCDC 1895454–1895458. For ESI and crystallographic data in CIF or other electronic format see DOI: 10.1039/c9nj02401h



Scheme 1 Serial single-electron oxidation of diphenyl disulfide eventually provides $[TA]^{•+}$ (intermediate species in square brackets have not been isolated).

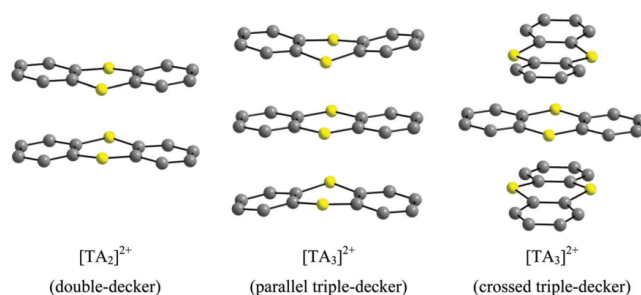


Fig. 1 Known structures of $[TA_2]^{2+}$ and $[TA_3]^{2+}$ dications.

SOMO-SOMO stabilization, which is commonly referred to as pancake bonding (PB).²² However, unpaired electrons are not even required for the oligomerisation. For example, partly protonated phenazine (PA) gives rise to a double-decker structure $[H-PA_2][O_3SCF_3]_2$ and a triple-decker structure $[(H-PA_2)(PA)][O_3SCF_3]_2$.²³ In the presence of anthracene (AC) a triple-decker structure $[(H-PA_2)(AC)][O_3SCF_3]_2$ with different polycyclic aromatic hydrocarbons was even formed.²⁴ For these examples a SOMO-SOMO stabilization can be clearly ruled out and London dispersion²⁵ might be exclusively responsible for the π -bonding. Sophisticated *ab initio* calculations of the dimers $[TA_2]^{2+}$ and $[SeA_2]^{2+}$ as well as the parallel and crossed trimers $[TA_3]^{2+}$ suggest that both (multicentre) σ - and π -bonding are operative. In all calculated structures, the ground states are singlets and, in the parallel stacks, intermolecular two-electron/three- or four-center (2e3c or 2e4c) bonds are formed between the S and Se atoms.²⁶

In 1926, Drew discovered a facile route for the synthesis to phenoxatellurin(e) (PT).²⁷ He noticed that upon contact with conc. sulfuric acid or nitric acid, intensely colored species evolve some of which he was able to isolate. While these compounds were characterized only by combustion analyses at the time, no reference was made to either the parallel behavior of TA nor to radicals in general. However, in 1929 Witzinger recognized the link between these dibenzodioxin type heterocycles and suggested that the intensely colored species are radical cations $[PT]^{•+}$,²⁸ a view that was later reinforced by Gioabă and Gioabă.²⁹

However, all attempts to structurally characterize these intensely colored species were deemed unsuccessful and provided only the tellurium(IV) species $[PT](NO_3)_2$ and $[PT]_2O(NO_3)_2$.³⁰ Rotated-disk voltammetry (RDE) studies on PT by Cauquis and Maurey-Mey in 1973³¹ and cyclic-voltammetry (CV) on related alkoxyated derivatives by Engman *et al.* in 1988³² confirmed single-electron oxidation processes, but EPR characterization of the radical cations was not achieved. Cauquis and Maurey-Mey concluded not only that dimerisation occurred very rapidly but also that the equilibrium constant, unlike for $[TA]^{•+}$, must be very large. The same authors also succeeded in the isolation of the salt $[PT_3][ClO_4]_2$, which was, however, never structurally characterized.

We have now reinvestigated the oxidation of PT using the reagents $AlCl_3/CH_2Cl_2$, $[NO][BF_4]$ and $[NO][SbF_6]$ which were previously employed to prepare salts of $[TA]^{•+}$ and similar species. These reactions provided the salts $[(PT)CH_2Cl][AlCl_4]$ (1), $[PT_2][SbF_6]_2 \cdot 3.5MeCN$ (2-3.5MeCN) and $[PT_3][BF_4]_2 \cdot 3MeCN$ (3-3MeCN), which have been fully characterized by X-ray crystallography and feature $[PT_2]^{2+}$ and $[PT_3]^{2+}$ dications deriving from dimerisation of the elusive radical cation $[PT]^{•+}$ (along with an additional molecule of PT in the latter case). The bonding situation of phenoxatellurin(e) based species PT, $[PT]^{•+}$, $[PT_2]^{2+}$ and $[PT_3]^{2+}$ has been computationally analyzed by a set of real-space bonding indicators (RSBIs), which complement orbital-based studies in comparison with the thianthrene based species TA, $[TA]^{•+}$, $[TA_2]^{2+}$ and $[TA_3]^{2+}$.^{17,26}

Table 1 Voltammetric data for PT in solution

Experiment	E_{p1}^a/V	E_{p1}^c/V	$\Delta E^{a-c}/mV$	$I_{p1}^a/\mu A$	$I_{p1}^c/\mu A$	I^c/I^a	E_1^{SWV}/V	E_2^{SWV}/V	E_{23}^{SWV}/V
GC, CH ₂ Cl ₂ , 0.50 mM	+0.561	+0.409	152	13	-13	1.00	+0.60 ^d	+1.65 ^d	
GC, CH ₂ Cl ₂ , 4.0 mM	+0.567	+0.192	375	+115	-99	0.86			
GC, CH ₂ Cl ₂ , 5.0 mM	+0.623	+0.101	522	+148	-60	0.41			
GC, CH ₃ CN, 1.0 mM	+0.409	+0.327	82	+33	-13	0.39	+0.38	+1.93	-2.68 ^b
GC, CH ₃ CN, 2.0 mM	+0.415	+0.307	108	+68	-18	0.26	+0.36	+1.97	-2.68 ^b
Pt, CH ₂ Cl ₂ , 0.50 mM	+0.590	+0.299	291	+5	-3	0.6	+0.46	+1.61	
Pt, CH ₃ CN, 1.0 mM	+0.441	+0.267	175	+9	-3	0.33	+0.41	+1.87	
Pt, CH ₃ CN, 3.0 mM	+0.543	+0.069	474	+28	-7	0.25	+0.41	+1.87	

^a 1.00 mM, in a separate experiment. ^b Process only observed at this electrode in this solvent.

Results and discussion

Electrochemical studies

The electrochemical oxidation of PT and, for comparison, TA was studied by CV at a platinum (Pt) electrode using [^tBu₄N][PF₆] as electrolyte in CH₂Cl₂, at concentrations relevant to the chemical oxidation reactions. Under these conditions, both PT and TA show irreversible oxidations with anodic peak potentials $E_{p1}^a = 0.52$ V and 0.81 V vs. Fc⁺⁰ (Fc = ferrocene), respectively (Fig. S2, ESI[†]). The magnitude of the oxidation peak potentials suggests that all oxidizing reagents suitable for TA can be also used for PT.³³ A thorough investigation of the voltammetric behaviour of PT at analytical concentrations was then undertaken in both CH₂Cl₂/[^tBu₄N][PF₆] and CH₃CN/[^tBu₄N][PF₆] using square-wave voltammetry (SWV) and CV at both glassy carbon (GC) and Pt electrodes (Table 1). The experiments in CH₂Cl₂ are referenced to internal cobaltocenium hexafluorophosphate (Cc), which is known to appear at -1.35 ± 0.01 V vs. Fc⁺⁰.³⁴ The experiments in CH₃CN are referenced to internal Fc. A typical SWV is presented in Fig. 2.

At the GC electrode, first and second oxidations are observed within the accessible window for CH₂Cl₂/[^tBu₄N][PF₆] at $E_1^{SWV} = +0.60$ and $E_2^{SWV} = +1.65$ V. In CH₃CN, two oxidations are also observed at +0.38 and +1.93 V, but this medium also allows observation of a single reduction peak, E_3^{SWV} , at -2.68 V.

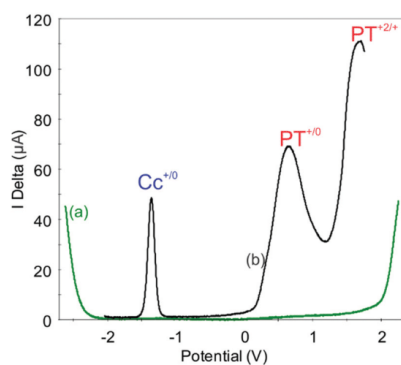


Fig. 2 SWV of PT (1.0 mM) at a GC electrode in CH₂Cl₂/[^tBu₄N][PF₆] (0.4 M) at RT vs. Fc⁺⁰. (a) Background scans showing the accessible solvent/electrolyte window. (b) Anodic scan on the PT solution.

Surprisingly on the Pt electrode, $E_1^{SWV} = +0.46$ in CH₂Cl₂/[^tBu₄N][PF₆], i.e. almost the same value as in CH₃CN (+0.41 V) whereas at GC $E_1^{SWV} = +0.22$ V. To further probe this difference in behaviour, a detailed concentration- and scan rate-dependent CV study was undertaken. Insight into the voltammetric behaviour is provided by the concentration dependence, illustrated for example at a GC electrode in CH₂Cl₂ (Fig. 3).

At sub-analytical concentrations, as in trace (a) at 0.50 mM, the CV response appears quasi-reversible (QR) with $I^c/I^a = 1.0$ but $\Delta E^{a-c} = 152$ mV. The QR nature of the response is confirmed by the increase of ΔE^{a-c} with increasing scan rate (Fig. S4, ESI[†]). In the case of PT, a straightforward explanation for QR behaviour is a slowed heterogeneous electron transfer rate associated with the large structural changes attending the one-electron oxidation (bent PT vs. planar PT⁺, see below); this corresponds to a large activation energy for the forward and reverse electron transfer due to flattening or bending, respectively. However, increasing the concentrations to as little as 1.0 and up to 5.0 mM induces a significant change to an irreversible CV response (Fig. 3b and c), resulting in a strong offset of especially the cathodic peak potentials E_{p1}^c and an I^c/I^a ratio significantly less than 1.0. Chemical and spectroelectrochemical evidence (see below) confirms that the cation radical [PT]^{•+} is not destroyed by oxidation, but rather that it associates to dimers [PT₂]²⁺ and trimers [PT₃]²⁺. Hence, the CV behaviour

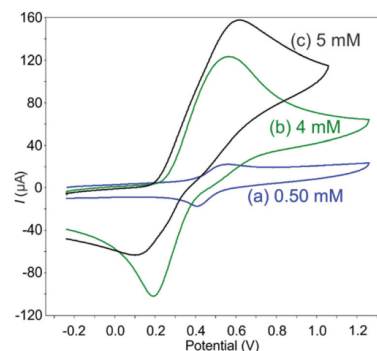
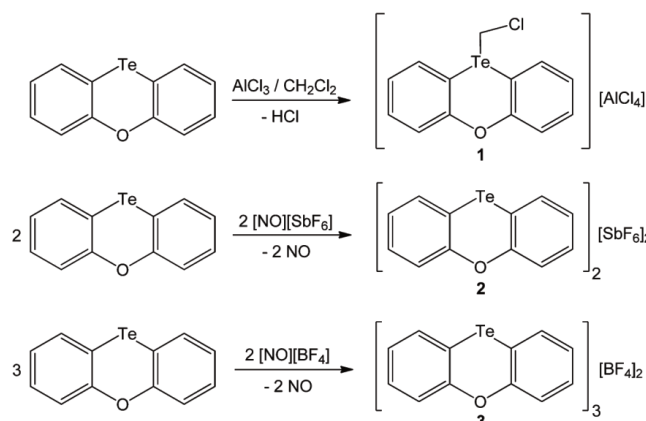


Fig. 3 Anodic scan CVs (0.2 V s^{-1} , starting and ending at -0.18 V vs. Fc⁺⁰) of PT in CH₂Cl₂/[^tBu₄N][PF₆] (0.4 M) at RT on a GC electrode showing the changes with increasing concentration. Referenced using added internal Cc⁺⁰ (not shown).



Scheme 2 Reaction of PT with one-electron oxidizing agents.

at higher (and synthetically relevant) concentrations is fully consistent with an electrochemically irreversible but chemically reversible ($E_{\text{irr}}C_{\text{rev}}$) mechanism. The cathodic peak therefore increasingly reflects reduction of the oligomeric species as their equilibrium concentrations increase. However, in view of the complexity of the isolated oligomers (dimer and trimer dicationic species), implying that the existence of the dimeric radical cation $[\text{PT}_2]^{\bullet+}$ as an undetected intermediate cannot be excluded, no attempt has been made in this work to analyze the mechanism in detail. We note that a similar mechanistic proposal was put forward by Cauquis and Maurey-Mey to explain their rotated-disk voltammetry and bulk electrolysis experiments.³¹ There is a strong electrode material influence on the CV behaviour so that at a Pt electrode the electrochemical irreversibility is already observed at 0.50 mM and the scan-rate dependent experiments display almost double the values for $\Delta E^{\text{a-c}}$ for the same scan-rate range (Fig. S5, ESI[†]). In view of the somewhat complex $E_{\text{irr}}C_{\text{rev}}$ behaviour, direct comparison of the peak potentials between electrodes is of limited value. However, the data in Table 1 generally indicate that oxidation in CH_3CN should be about 200 mV more facile than in CH_2Cl_2 .

Spectroelectrochemistry

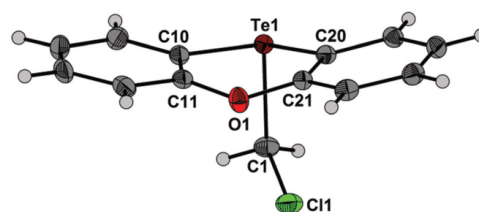
UV-vis spectroelectrochemical measurements of PT and TA reveal new absorptions in the visible spectrum upon oxidation at $\lambda_{\text{max}} = 380$ and 570 nm for PT and at $\lambda_{\text{max}} = 545$ nm for TA, which disappear again upon reduction (Fig. S6, ESI[†]). This confirms the voltammetric evidence for an $E_{\text{irr}}C_{\text{rev}}$ mechanism for the 1 e oxidation process. All attempts to generate the $[\text{PT}]^{\bullet+}$ radical cation *via in situ* spectroelectrochemistry and detect it by EPR spectroscopy failed. A high association constant for the $[\text{PT}_2]^{2+}$ diamagnetic dimer has been used to rationalize these results.³¹

Synthetic aspects

The reaction of PT with $\text{AlCl}_3/\text{CH}_2\text{Cl}_2$, a known single-electron oxidizer with an estimated $E^{\circ} = +1.1$ V vs. $\text{Fc}^{\bullet}/0$,^{14,35} proceeded *via*

a two-electron oxidative addition providing the telluronium ion in $[(\text{PT})\text{CH}_2\text{Cl}][\text{AlCl}_4]$ (**1**), a compound isolated as a brown crystalline solid in yields of 56% (Scheme 2). Nitrosyl ions, $[\text{NO}]^+$, are also common single-electron oxidizers with an $E^{\circ} = +1.00$ V vs. $\text{Fc}^{\bullet}/0$ in CH_2Cl_2 .³³ The reaction of PT with $\text{NO}(\text{SbF}_6)$ and $\text{NO}(\text{BF}_4)$ gave intensely violet-blue solutions, from which $[\text{PT}_2][\text{SbF}_6]_2 \cdot 3.5\text{MeCN}$ (**2**·3.5MeCN) and $[\text{PT}_3][\text{BF}_4]_2 \cdot 3\text{MeCN}$ (**3**·3MeCN) were isolated as crystalline materials in yields of 35% and 31%, respectively (Scheme 2). Compounds **2**·3.5MeCN and **3**·3MeCN are pleochromic. They are violet with an orange luster and dark-blue in reflective light, whereas smaller fragments are red in transmitted light. All compounds are essentially ionic. The molecular structures of the $[(\text{PT})\text{CH}_2\text{Cl}]^+$ cation present in **1** and the $[\text{PT}_2]^{2+}$ and $[\text{PT}_3]^{2+}$ dicationic species present in **2** and **3**, respectively, are shown in Fig. 4–6.

In the first coordination sphere, the Te atom of the $[(\text{PT})\text{CH}_2\text{Cl}]^+$ cation present in **1** is coordinated by 3 C atoms. The exocyclic Te–C bond length of **1** (2.171(2) Å) is longer than the endocyclic Te–C bond lengths (2.077(2), 2.083(2) Å), which are slightly shorter than those of the parent PT (2.095(2), 2.099(2) Å). The endocyclic C–Te–C angle of **1** (91.90(8)°) is slightly increased compared to the parent PT (88.98(6)°). In the crystal lattice, the $[(\text{PT})\text{CH}_2\text{Cl}]^+$ cations and $[\text{AlCl}_4]^-$ anions of **1** are associated by secondary Te···Cl interactions (3.385(2), 3.401(2), 3.449(1) Å). Considering

Fig. 4 Molecular structure of the $[(\text{PT})\text{CH}_2\text{Cl}]^+$ cation present in **1** drawn with 50% probability ellipsoids ($[\text{AlCl}_4]^-$ omitted).

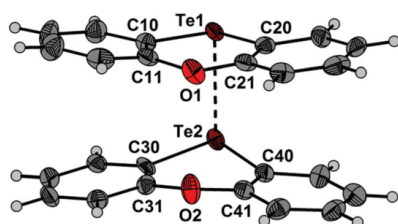


Fig. 5 Molecular structure of the $[PT_2]^{2+}$ dication present in **2** drawn with 50% probability ellipsoids ($[SbF_6]^-$ omitted).

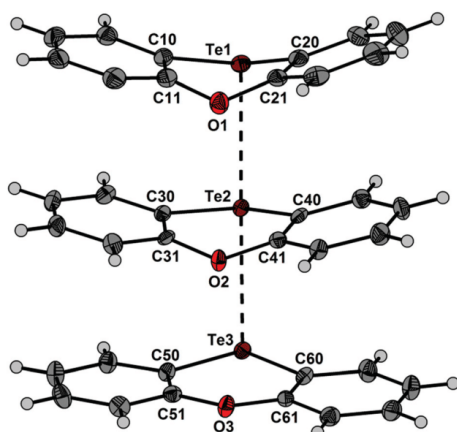


Fig. 6 Molecular structure of the $[PT_3]^{2+}$ dication present in **3** drawn with 50% probability ellipsoids ($[BF_4]^-$ omitted).

the first and second coordination spheres, the spatial arrangement at the Te atom is distorted octahedral. The structures of **2** and **3** feature the $[PT_2]^{2+}$ and $[PT_3]^{2+}$ dications, respectively, possessing stacks of parallel PT moieties, similar to those reported for $[TA_2]^{2+}$,^{14,16} and $[TA_3]^{2+}$,¹⁷ (Fig. 1).

The interlayer Te–Te bond lengths of $[PT_2]^{2+}$, containing two crystallographically independent, albeit similar, conformers (2.897(1), 2.903(1) Å) and $[PT_3]^{2+}$ (3.1034(7), 3.1381(7) Å), are substantially longer than the Te–Te single bond length in PhTeTePh (2.712(2) Å) and point to bond orders smaller than 1.³⁶ This situation is typical for PB in radical dimers.²³ The Te–C bond lengths and the C–Te–C angles of the $[PT_2]^{2+}$ and $[PT_3]^{2+}$ dications fall within the range observed for the structures of parent PT and the $[(PT)CH_2Cl]^+$ cation (see above). In the crystal lattice, the Te atoms of the $[PT_2]^{2+}$ and $[PT_3]^{2+}$ dications are associated with F atoms of the $[SbF_6]^-$ and $[BF_4]^-$ counterions, as well as N atoms of CH_3CN solvate molecules. The secondary Te...N and Te...F contacts range from 2.882(8) to 3.278(7) Å and from 2.996(9) to 3.257(7) Å, respectively, in **2** and from 2.951(8) to 3.593(9) Å and from 2.983(8) to 3.483(6) Å, respectively, in **3**. In all structures the PT moieties are significantly flatter than the parent

PT, which adopts a butterfly conformation. The extent of folding within the butterfly structure can be quantitatively expressed by the fold angle α of the two planes defined by phenyl rings plus the Te and O atoms (for coplanar rings, α is zero). For the parent PT^{37} and **1** the fold angles α are 37.5° and 17.8°, respectively. The fold angles α of the two independent $[PT_2]^{2+}$ conformers of **2** (Te1: 10.8°, Te2: 15.1° and Te3: 3.4°, Te4: 20.8°) and $[PT_3]^{2+}$ of **3** (Te1: 1.1°, Te2: 22.2°, Te3: 33.6°) spread over a larger range, which points to a flat bending potential.

Compounds **1–3** are only sparingly soluble in non-polar solvents. The highest solubility was observed in acetonitrile, from which the NMR data were acquired. The ^{125}Te NMR spectra ($MeCN-D_3$) of **1–3** display only one signal each at $\delta = 562.8$, 1896.4 and 1697.1 ppm, respectively, which are shifted to lower frequency compared to the parent PT ($\delta = 420.0$ ppm). The observation that **3** gives rise to only one ^{125}Te resonance points to a dynamic exchange process in solution that occurs fast on the NMR time scale. This is also supported by the ^{13}C NMR spectrum (CH_3CN-D_3) of **3** that shows only one set of signals suggesting that the PT moieties are equivalent in solution. We hypothesize that this dynamic exchange process involves the reversible dissociation of $[PT_3]^{2+}$ into $[PT_2]^{2+}$ and neutral PT. This hypothesis is supported by the fact that no EPR signals could be detected from solutions of **2** and **3** in CH_3CN . In order to predict what such spectra could look like, simulations of EPR spectra were made for $[TA]^{*+}$ and $[PT]^{*+}$ based on DFT calculated hyperfine splitting (HFS) values (Tables S2 and S3, ESI[†]). The predicted ^{125}Te HFS is extremely small despite a high spin-density at this nucleus, possibly due to an inadequacy of the basis set. Nevertheless, the low natural abundance (7%) of ^{125}Te could produce only weak ‘satellites’ of the main signal. For both radicals, the splitting of the high-abundance signals are to aromatic H atoms and thus are very small. The expected strong spin-orbit coupling to Te with its large spin density (SD) is likely to cause extensive line-broadening and potentially to weaken the signal intensity much more than the simple prediction shown in Table S3 (ESI[†]). In contrast to the materials isolated by Drew,²⁵ **2** and **3** are extremely sensitive to air exposure, both in solution and in the solid-state. Upon contact with air, the violet and blue colors fade within seconds. Even when the crystals were covered by perfluorinated oil, fading of the colour was observed after a few minutes.

Computational analysis

PT, TA and their radical cations $[PT]^{*+}$ and $[TA]^{*+}$ were fully optimized in the gas phase. As anticipated, the neutral parent molecules PT and TA display butterfly structures, whereas the radical cations $[PT]^{*+}$ and $[TA]^{*+}$ possess planar structures. Results of the atoms-in-molecules (AIM) analysis,³⁸ Electron-Localizability-Indicator (ELI-D)³⁹ iso-surfaces as well as electrostatic potentials (ESPs) are shown in Fig. 7 and 8. Topological bond descriptors derived from AIM theory are listed in Table 2. Basin integration provided atomic and fragmental AIM charges, which are collected in Table 3. The SD of the radical cations $[PT]^{*+}$ and $[TA]^{*+}$ is shown in Fig. 9.

The vertical and adiabatic ionization energies of PT (703.13 and 674.02 $KJ mol^{-1}$) and TA (731.69 and 684.67 $KJ mol^{-1}$) are

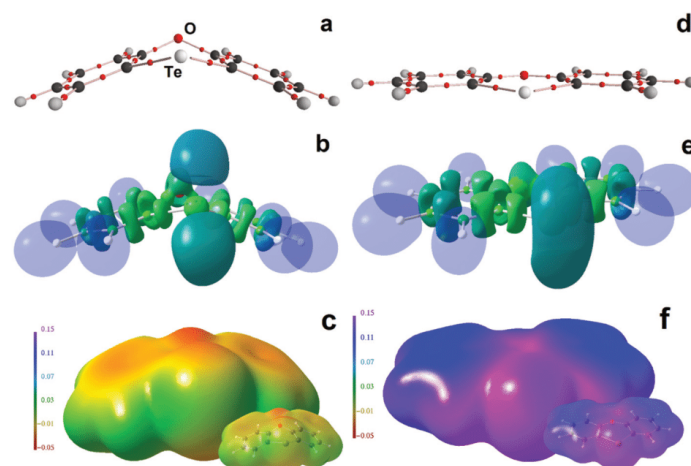


Fig. 7 (a and d) AIM-topology, (b and e) ELI-D iso-surface ($Y = 1.3$), and (c and f) ESP (in a.u.) mapped on the 0.001 a.u. ED surface for compounds PT (left) and [PT]^{•+} (right). For the ESP, solid and transparent modes are shown.

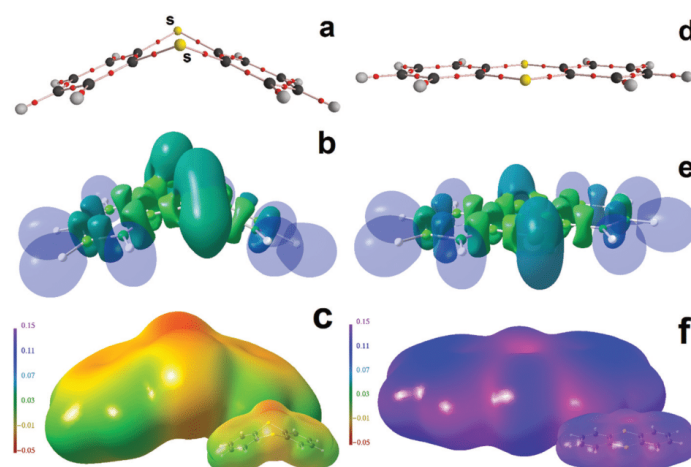


Fig. 8 (a and d) AIM-topology, (b and e) ELI-D iso-surface ($Y = 1.3$), and (c and f) ESP (in a.u.) mapped on the 0.001 a.u. ED surface for compounds TA (left column) and [TA]^{•+} (right column). For the ESP, solid and transparent modes are shown.

surprisingly similar, but overall confirm the trend established by voltammetry that PT can be oxidized more easily than TA. During the change from a butterfly to a planar structure upon oxidation, the C–E (E = O, S, Te) bonds become shorter by 0.02 to 0.04 Å. The ELI-D iso-surfaces display regions of increased electron localizability, e.g. bonding electrons or lone-pairs. The parent PT and TA monomers show two spatially separated lone pairs at each chalcogen atom, which shrink and almost fuse together upon one-electron oxidation to form [TA]^{•+} and [PT]^{•+}. The electron population within these basins decreases by 0.2 *e* (S),

0.5 *e* (O) and 0.7 *e* (Te), which is counter balanced by increased electron population of ca. 0.2 *e* in each E–C bonding basin (E = O, S, Te).

AIM provides a complementary picture. The basin integration shows that each C₆H₄-fragment has lost ca. 0.4 *e* in [TA]^{•+} and 0.3 *e* in [PT]^{•+}, whereas quite different values of 0.2 *e* (S), 0.0 *e* (O), and 0.4 *e* (Te) are obtained for the chalcogen atoms (Table 3). The electrostatic potential (ESP) shows negative areas (in red) at the central ring of neutral PT and TA close to the chalcogen atoms, which after one-electron oxidation turns into the most positive

Table 2 Topological bond descriptors derived from AIM theory^a

Model	Contact	d [Å]	$\rho(\mathbf{r})_{\text{bcp}}$ [$\text{e} \text{Å}^{-3}$]	$\nabla^2 \rho(\mathbf{r})_{\text{bcp}}$ [$\text{e} \text{Å}^{-5}$]	ϵ	$G/\rho(\mathbf{r})_{\text{bcp}}$ [a.u.]	$H/\rho(\mathbf{r})_{\text{bcp}}$ [a.u.]
[PT] ^b	Te–C	2.070	0.90	–0.6	0.16	0.52	–0.56
[PT] ^b	O–C	1.361	1.94	–9.2	0.04	1.21	–1.54
[TA] ^b	S–C	1.735	1.41	–9.0	0.18	0.31	–0.76
[PT ₂] ²⁺	Te...Te	3.090	0.30	0.2	0.04	0.25	–0.19
[PT ₂] ²⁺	Te...Te	3.203	0.25	0.4	0.04	0.27	–0.15
[PT ₃] ²⁺	Te...Te	3.239	0.23	0.5	0.05	0.28	–0.14
[PT ₃] ²⁺	O...O	3.101	0.04	0.6	0.79	0.87	0.14
[PT ₃] ²⁺	O...O	3.173	0.04	0.6	4.34	0.91	0.17
[TA ₂] ²⁺	S...S	2.982	0.19	1.0	0.05	0.45	–0.07
[TA ₃] ²⁺	S...S	3.103	0.15	1.0	0.06	0.47	–0.04
[PT ₃] ²⁺	O4...C20	3.095	0.05	0.6	1.50	0.75	0.15
[PT ₃] ²⁺	C5...C17	3.321	0.05	0.6	2.64	0.57	0.14
[PT ₃] ²⁺	C9...C22	3.464	0.04	0.4	4.25	0.55	0.14
[TA ₃] ²⁺	C3...C25	3.255	0.05	0.5	2.52	0.59	0.16
[TA ₃] ²⁺	C9...C31	3.316	0.05	0.5	4.31	0.58	0.15

^a d is the bond distance, $\rho(\mathbf{r})_{\text{bcp}}$ is the ED at the bcp, $\nabla^2 \rho(\mathbf{r})_{\text{bcp}}$ is the Laplacian of the ED, ϵ is the bond ellipticity, $G/\rho(\mathbf{r})_{\text{bcp}}$ and $H/\rho(\mathbf{r})_{\text{bcp}}$ are the respective kinetic and total energy density over $\rho(\mathbf{r})_{\text{bcp}}$ ratios. ^b Averaged values for all compounds of this group including PT, [PT₂]²⁺, and [PT₃]²⁺, or TA, [TA₂]²⁺, and [TA₃]²⁺. For atom labels, see ESI.

area (in purple) for [PT]^{•+} and [TA]^{•+} (Fig. 7c, f and 8c, f). This is reflected by the SD distribution, which is also mostly localized at the central ring (Fig. 9). The double decker structures of [PT₂]²⁺ and [TA₂]²⁺ as well as the triple decker structures [PT₃]²⁺ and [TA₃]²⁺ were fully characterized in the gas phase, with and without an empirical dispersion correction, which revealed the importance of London dispersion for the stabilization of the π -stacked structures.

Results of the AIM analysis, ELI-D iso-surfaces as well as the non-covalent interaction (NCI)⁴⁰ iso-surface analysis are shown

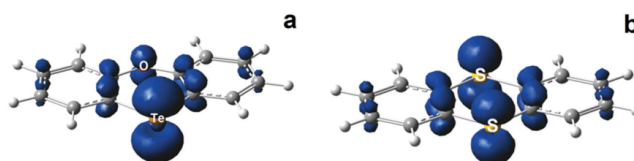
in Fig. 10 and 11. Stacking of [PT]^{•+} and [TA]^{•+} radical cations and related compounds is governed by chalcogen–chalcogen interactions as well as by C _{π} –C _{π} -contacts. The importance of the latter becomes especially apparent in simple gas-phase calculations of dimers and trimers, which are not restricted by crystal field of solvation effects. The inclusion of an empirical dispersion correction in the computations afforded the desired stacked clusters, whereas the organic C₆H₄-fragments try to avoid each other if such a dispersion correction is lacking. For [TA₂]²⁺ and [TA₃]²⁺, this leads to increased intermolecular S–S distances and increased fold angles α within each molecule (Fig. 11a and b).

The two S–S contacts connecting each pair of molecules prevent rotation along the stacking axis so that the molecules nevertheless remain on top of each other. The individual molecules in [PT₂]²⁺ and [PT₃]²⁺, however, are rotated along the Te–Te axis by ca. 90° and 180°, respectively, since the O–O contacts are too weak to prevent rotation (Fig. 10a and b). Taking into account the dispersion correction, the optimized structures of [PT₂]²⁺, [PT₃]²⁺, [TA₂]²⁺ and [TA₃]²⁺ resemble the parallel stacking also found by X-ray diffraction (Fig. 10c, d and 11c, d). [TA₂]²⁺ and [TA₃]²⁺ are observed to be centrosymmetric, whereas asymmetric stacking is observed for [PT₂]²⁺ and [PT₃]²⁺.

For [TA₂]²⁺, this leads to the formation of two identical fragments, each of which exhibit a fold angle α of 10.8°, which is between values observed for TA in the gas-phase ($\alpha = 46.1^\circ$) and the corresponding radical cation [TA]^{•+} ($\alpha = 0^\circ$). For [TA₃]²⁺ the outer molecules are similarly tilted ($\alpha = 14.5^\circ$), whereas the central molecule is flat. By contrast, the existence of two different chalcogen atoms, Te and O, in TA reduces the symmetry of its monomers (e.g. from C_{2v} in TA to C_s in PT), dimers and trimers. For [PT]^{•+} the fold angle α is 39.7°. In [PT₂]²⁺, fold angles α of 21.5° and 4.2° are observed. Corresponding angles α

Table 3 AIM atomic and fragmental charges (in e)

	PT	[PT] ^{•+}	[PT ₂] ²⁺	[PT ₃] ²⁺		TA	[TA] ^{•+}	[TA ₂] ²⁺	[TA ₃] ²⁺
ph(1)	0.30	0.59	0.60	0.47	ph(1)	–0.13	0.22	0.13	0.07
Te	0.56	0.97	1.00	0.78	S	0.11	0.27	0.37	0.22
O	–1.17	–1.16	–1.17	–1.18					
ph(2)			0.57	0.51	ph(2)			0.13	0.09
Te			0.98	0.94	S			0.37	0.32
O			–1.17	–1.18					
ph(3)				0.50	ph(3)				0.07
Te				0.84	S				0.24
O				–1.17					
Frag1	0.00	0.99	1.04	0.54	Frag1	–0.03	0.97	1.00	0.59
Frag2			0.95	0.78	Frag2			1.00	0.82
Frag3				0.67	Frag3				0.62
Tot	0.00	0.99	2.00	2.00	Tot	–0.03	0.97	2.01	2.04

Fig. 9 SD of the radical cations [PT]^{•+} (left) and [TA]^{•+} (right).

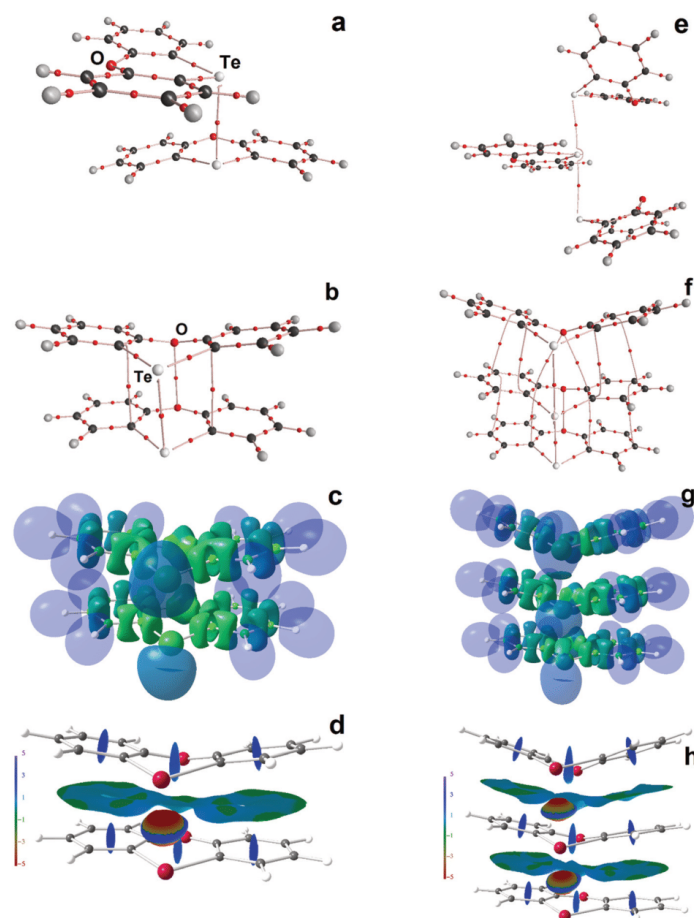


Fig. 10 AIM-topology of $[PT_2]^{2+}$ and $[PT_3]^{2+}$ without (a and e) and with (b and f) empirical dispersion correction, (c and g) ELI-D iso-surface ($Y = 1.3$), and (d and h) NCI iso-surface ($s(r) = 0.5$) for compounds $[PT_2]^{2+}$ (left column) and $[PT_3]^{2+}$ (right column).

for $[PT_3]^{2+}$ are 36.8° , 23.4° , and 7.9° . These trends are reflected in the electronic bond descriptors (see below). Interestingly, the basis-set superposition error (BSSE) corrected complexation energies (E_{compl}) are found to be larger for the dimers $[PT_2]^{2+}$ (-201 kJ mol^{-1}) and $[TA_2]^{2+}$ (-232 kJ mol^{-1}) than for the trimers $[PT_3]^{2+}$ (-94 kJ mol^{-1}) and $[TA_3]^{2+}$ (-161 kJ mol^{-1}). Bond path analyses according to the topological AIM approach reveal S-S, O-O, or Te-Te interactions in compounds $[TA_2]^{2+}$, $[TA_3]^{2+}$, $[PT_2]^{2+}$ and $[PT_3]^{2+}$ (Fig. 10c, d and 11c, d). Additional intermolecular C-C bond paths reflect π - π -contacts. Electronic bonding parameters at the bond critical points (bcp) for relevant bonds are collected in Table 2. They include polar-covalent E-C contacts (E = Te, S, O), which are characterized by significant concentration of electron density at the bcp (ED or $\rho(\mathbf{r})_{\text{bcp}} = 0.9\text{--}1.9 \text{ e } \text{\AA}^3$), a negative Laplacian ($\nabla^2\rho(\mathbf{r})_{\text{bcp}} = -9.2$ to

$-0.6 \text{ e } \text{\AA}^3$), and a largely negative total energy density over ED ratio ($H/\rho(\mathbf{r})_{\text{bcp}} = -0.6$ to -1.5 a.u.). With increasing difference of the electronegativity, bond polarization increases, which is reflected in the kinetic energy density over ED ratio ($G/\rho(\mathbf{r})_{\text{bcp}} = 0.3$ (S-C)– 1.2 (O-C) a.u.). Since all E-C bonds are involved in the π -system, bond ellipticities (ϵ) are larger than 0.1 for Te-C and S-C bonds. As the E-C bonds are almost unaffected by the stacking, values have been averaged. Long-ranging E-E contacts ($d > 3 \text{ \AA}$) are characterized by significantly lower ED values ($\rho(\mathbf{r})_{\text{bcp}} = 0.1\text{--}0.3 \text{ e } \text{\AA}^3$), a positive Laplacian ($\nabla^2\rho(\mathbf{r})_{\text{bcp}} = 0.2\text{--}1.0 \text{ e } \text{\AA}^3$), and a small negative or even positive $H/\rho(\mathbf{r})_{\text{bcp}} = -0.1\text{--}0.2 \text{ a.u.}$ Whereas some degree of covalency remains in the S-S and Te-Te contacts, the bond characteristics of the O-O contacts already resemble those of the weak C_π - C_π contacts, which are dominated by non-covalent bonding aspects. The C_π - C_π contacts

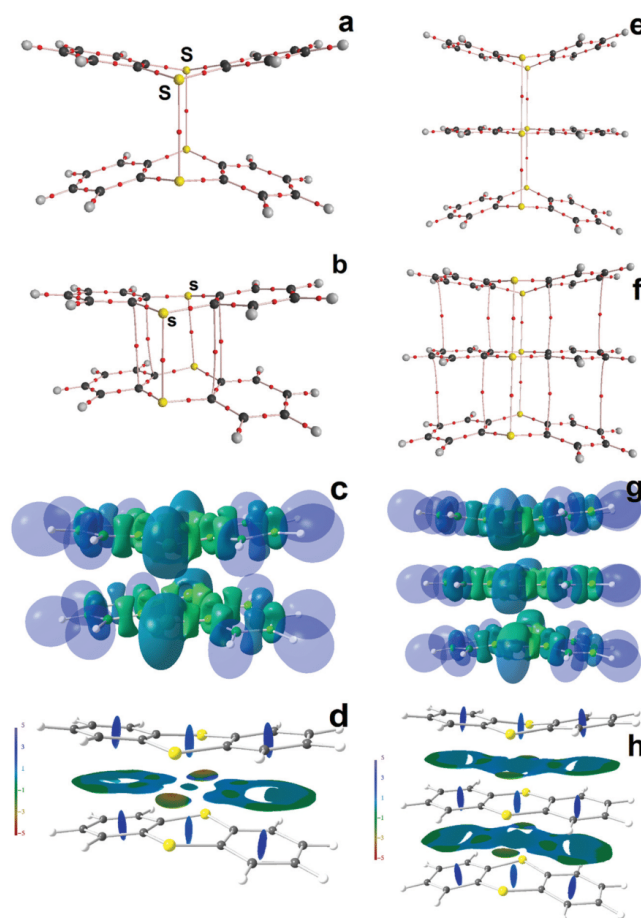


Fig. 11 AIM-topology of $[TA_2]^{2+}$ and $[TA_3]^{2+}$ without (a and e) and with (b and f) empirical dispersion correction, (c and g) ELI-D iso-surface ($Y = 1.3$), and (d and h) NCI iso-surface ($s(r) = 0.5$) for compounds $[TA_2]^{2+}$ (left column) and $[TA_3]^{2+}$ (right column).

are visible in NCI iso-surfaces as flat and long-ranging light-green and blue regions between the molecules (Fig. 10g, h and 11g, h). Small NCI basins are also obtained for S–S and O–O contacts, whereas large, convex and red-colored basins are visible along the Te–Te axis, suggesting attractive non-covalent Te–Te-bond contributions.

Conclusion

The oxidation of PT using $AlCl_3/CH_2Cl_2$, $[NO][SbF_6]$ and $[NO][BF_4]$ afforded the diamagnetic salts $[(PT)CH_2Cl][AlCl_4]$ (1), $[PT_2][SbF_6]_2$ (2) and $[PT_3][BF_4]_2$ (3), which have been fully characterized. The dications $[PT_2]^{2+}$ and $[PT_3]^{2+}$ of 2 and 3 can be regarded as the dimer of the elusive radical cation $[PT]^{+\bullet}$ or as an adduct

between this dimer and neutral PT, respectively. The dications crystallize with parallel stacks of PT moieties that are significantly more planar than their neutral parent PT. These stacks are held together by SOMO–SOMO interactions and non-covalent Te–Te interactions (PB) as well as London dispersion interactions.

Experimental section

General aspects

Reagents were obtained commercially (Sigma-Aldrich, Germany) and were used as received. Dry solvents were collected from a SPS800 mBraun solvent system. PT was prepared in two steps according to slightly modified literature procedures (see ESI† for details).²⁷ 1H -, ^{13}C - and ^{125}Te -NMR spectra were recorded at RT

(unless otherwise stated) using a Bruker Avance-360 spectrometer and are referenced to tetramethylsilane (^1H , ^{13}C) and telluric acid (^{125}Te). Chemical shifts are reported in parts per million (ppm) and coupling constants (J) are given in Hertz (Hz). Electron impact mass spectrometry (EI-MS) was carried out using a Finnigan MAT 95. The spectra were collected for one minute and averaged. The electrospray ionization mass spectrometry (ESI-MS) spectrum was also obtained on the Bruker Impact II. Acetonitrile solutions were injected directly into the spectrometer at a flow rate of $3\ \mu\text{l}\ \text{min}^{-1}$. Nitrogen was used both as a drying gas and for nebulization with flow rates of approximately $4\ \text{L}\ \text{min}^{-1}$ and a pressure of 0.4 bar. The spectrum was collected for one minute and averaged. UV/vis spectra were recorded on a JASCO V-570 spectrometer.

Electrochemistry and spectroelectrochemistry

CV and UV-vis spectroelectrochemical experiments in Bremen were undertaken in a TSC 1600 "Sealable Measuring Cell" provided by rhd instruments GmbH & Co (Darmstadt, Germany) at glass-sealed Pt wire working and auxiliary electrodes and a silver wire *pseudo* reference electrode with added internal Fc for determining the zero of potential. Experiments were controlled with an Autolab PGSTAT101 supported by Nova 2.1 software (Metrohm AG, Herisau, Switzerland). In a glovebox under Ar atmosphere, 5.5 mg of PT or 5.7 mg of TA were dissolved in 1.0 ml of $0.1\ \text{M}\ [\text{Bu}_4\text{N}][\text{PF}_6]$ solutions in CH_2Cl_2 and transferred to the measuring cell. The cell was sealed and connected to the potentiostat. The measurements were realized with a scan rate of $0.2\ \text{V}\ \text{s}^{-1}$. CV and SWV experiments in Lethbridge used a three-electrode cell with 1.6 mm diameter Pt or 3.0 mm diameter GC working electrodes (BASi, West Lafayette IN, USA) and Pt wires for both the auxiliary and *pseudo* reference electrodes in a nitrogen-filled glove box loaded with the indicated concentrations of PT in either $\text{CH}_2\text{Cl}_2/[\text{Bu}_4\text{N}][\text{PF}_6]$ (0.4 M) or $\text{CH}_3\text{CN}/[\text{Bu}_4\text{N}][\text{PF}_6]$ (0.1 M). CV and SWV experiments were performed using a PARSTAT 2273 potentiostat via PowerSuite 2.58 software (AMETEK Scientific Instruments, USA). CVs were performed using scan rates of $0.20\text{--}10.0\ \text{V}\ \text{s}^{-1}$, with all potentials being reported *versus* the $\text{Fe}^{3/0}$ redox couple. The electrodes were polished with $0.05\ \mu\text{m}$ alumina, rinsed with distilled water and dried with a tissue before use. *In situ* EPR spectroelectrochemical experiments were carried out using a miniature quartz flat cell (Wilmad WG-808) with a Pt foil working electrode, and Pt wires as the reference and auxiliary electrodes.⁴¹ The measurements were obtained on a Bruker EMXplus spectrometer operating at X-band frequencies (9.8 GHz). Electrolysis was controlled using a BAS CV50 potentiostat (BASi).

Synthesis of $[(\text{PT})\text{CH}_2\text{Cl}][\text{AlCl}_4]$ (1)

A 100 ml Schlenk flask was charged with AlCl_3 (140 mg, 1.01 mmol) and a solution of PT (300 mg, 1.01 mmol) in dichloromethane (20 ml) was slowly added. Immediately, the yellow solution turned brown. The solution was stirred for 30 min and was then left standing overnight. The brown crystals that formed were collected by filtration to give **1** (290 mg, 0.56 mmol, 56%).

$^1\text{H-NMR}$ (360 MHz, $\text{d}_3\text{-MeCN}$): $\delta = 7.40\text{--}7.93$ (m, 12H, $\text{C}_{\text{Ar-H}}$), 4.74 (s, 2H, $\text{Te-CH}_2\text{-Cl}$) ppm. $^{13}\text{C-NMR}$ (90 MHz, $\text{d}_3\text{-MeCN}$):

$\delta = 154.8$ ($\text{C}_{\text{Ar-CH-O}}$), 121.1, 126.9, 136.0, 137.2 (C_{Ar}), 103.7 ($\text{C}_{\text{Ar-CH-Te}}$), 41.1 ($\text{Te-CH}_2\text{-Cl}$) ppm. $^{125}\text{Te-NMR}$ (110 MHz, $\text{d}_3\text{-MeCN}$): $\delta = 562.8$ ppm. ESI-MS (CH_3CN , positive mode): m/z (rel. int.) = 347 (100) $[\text{M}]^+$, 298 (98) $[\text{C}_{12}\text{H}_8\text{OTe}]^+$. ESI-MS (CH_3CN , negative mode): m/z (rel. int.) = 169 (100) $[\text{AlCl}_4]^-$. UV/VIS (CH_2Cl_2): $\lambda_{\text{max}} = 279\ \text{nm}$, 323 nm.

Synthesis of $[\text{PT}_2][\text{SbF}_6]_2$ (2)

A 100 ml Schlenk flask was charged with $[\text{NO}][\text{SbF}_6]$ (900 mg, 3.38 mmol) and a solution of PT (1.00 g, 3.38 mmol) in diethyl ether (20 ml) was slowly added. Immediately, the yellow solution turned dark violet-blue. The solution was stirred for 30 min and was then left standing overnight. The dark violet single crystals (orange lustre) that formed were collected by filtration to give 2-3.5NCMe (1.42 g, 0.591 mmol, 35%).

$^1\text{H-NMR}$ (360 MHz, $\text{d}_3\text{-MeCN}$): $\delta = 7.06\text{--}7.91$ (m, 12H, $\text{C}_{\text{Ar-H}}$), 1.94 (s, 3H, $\text{CH}_3\text{-CN}$) ppm.

$^{13}\text{C-NMR}$ (90 MHz, $\text{d}_3\text{-MeCN}$): $\delta = 120.7$, 126.4, 135.6, 136.7 (C_{Ar}), 102.4 ($\text{C}_{\text{Ar-CH-Te}}$), 152.7 ($\text{C}_{\text{Ar-CH-O}}$), 1.3 (CH_3CN), 117.9 (CH_3CN) ppm. $^{125}\text{Te-NMR}$ (110 MHz, $\text{d}_3\text{-MeCN}$): $\delta = 1896.4$ ppm. ESI-MS ($\text{CH}_3\text{CN}/\text{CH}_3\text{OH}$ 1:10, positive mode): m/z (rel. int.) = 329 (100) $[(\text{C}_{12}\text{H}_8\text{OTe})\text{H}^+(\text{CH}_3\text{OH})]^+$, 315 (18) $[\text{C}_{12}\text{H}_8\text{OTeOH}]^+$, 298 (73) $[\text{C}_{12}\text{H}_8\text{OTe}]^+$. ESI-MS ($\text{CH}_3\text{CN}/\text{CH}_3\text{OH}$ 1:10, negative mode): m/z (rel. int.) = 495 (95) $[\text{Na}(\text{SbF}_6)_2]^-$, 235 (100) $[\text{SbF}_6]^-$. UV/VIS (CH_2Cl_2): $\lambda_{\text{max}} = 286\ \text{nm}$.

Synthesis of $[\text{PT}_3][\text{BF}_4]_2$ (3)

A 100 ml Schlenk flask was charged with $[\text{NO}][\text{BF}_4]$ (120 mg, 1.01 mmol) and a solution of PT (300 mg, 1.01 mmol) in diethyl ether (20 ml) was slowly added. Immediately, the yellow solution turned dark violet blue. The solution was stirred for 30 min and was then left standing overnight. The dark blue crystals that formed were collected by filtration to give 2-3NCMe (370 mg, 0.104 mmol, 31%).

$^1\text{H-NMR}$ (360 MHz, $\text{d}_3\text{-MeCN}$): $\delta = 7.40\text{--}8.05$ (m, 12H, $\text{C}_{\text{Ar-H}}$), 1.94 (s, 3H, $\text{CH}_3\text{-CN}$) ppm. $^{13}\text{C-NMR}$ (90 MHz, $\text{d}_3\text{-MeCN}$): $\delta = 120.2$, 124.1, 131.5, 132.1 (C_{Ar}), 118.4 ($\text{C}_{\text{Ar-CH-Te}}$), 151.2 ($\text{C}_{\text{Ar-CH-O}}$), 1.3 (CH_3CN), 118.2 (CH_3CN) ppm. $^{125}\text{Te-NMR}$ (110 MHz, $\text{d}_3\text{-MeCN}$): $\delta = 1697.1$ ppm. ESI-MS (CH_3CN , positive mode): m/z (rel. int.) = 627 (100) $[\text{M} + (\text{C}_{12}\text{H}_8\text{OTeOH})^+ + \text{CH}_3\text{OH}]^+$, 329 (66) $[\text{M}^{2+} + \text{CH}_3\text{O}^-]^+$, 315 (100) $[\text{M}^{2+} + \text{OH}^-]^+$, 298 (23) $[\text{M}^+]$. ESI-MS (CH_3CN , negative mode): m/z (rel. int.) = 436 (16) $[(\text{C}_{12}\text{H}_8\text{OTeOH}) + \text{BF}_4 + \text{Cl}]^-$, 87 (100) $[\text{BF}_4]^-$. UV/VIS (CH_2Cl_2): $\lambda_{\text{max}} = 283\ \text{nm}$.

Crystallography

Intensity data of **1**, 2-3.5NCMe, and 2-3NCMe were collected on a Bruker Venture D8 diffractometer at 100 K with graphite-monochromated Mo-K α (0.7107 Å) radiation. All structures were solved by direct methods and refined based on F^2 using the SHELX program package as implemented in WinGX.⁴² All non-hydrogen atoms were refined using anisotropic displacement parameters. Hydrogen atoms attached to carbon were included in geometrically calculated positions using a riding model. Crystal and refinement data are collected in Table 4. Figures were created using DIAMOND.⁴³

Table 4 Crystal data and structure refinement of **1**, **2**:3.5NCMe and **3**:3NCMe

	1	2 :3.5NCMe	3 :3NCMe
Formula	C ₁₃ H ₁₀ AlCl ₅ OTe	C ₆₂ H ₅₃ F ₂₄ N ₇ O ₄ Sb ₄ Te ₄	C ₄₂ H ₃₃ B ₂ F ₈ N ₃ O ₃ Te ₃
Formula weight, g mol ⁻¹	514.04	2413.51	1184.13
Crystal system	Monoclinic	Triclinic	Triclinic
Crystal size, mm	0.15 × 0.05 × 0.03	0.07 × 0.06 × 0.05	0.09 × 0.09 × 0.07
Space group	P2 ₁ /c	P1	P1
a, Å	10.4998(5)	7.8579(4)	11.2438(6)
b, Å	13.2979(7)	13.2378(7)	13.7621(8)
c, Å	13.2281(7)	36.414(2)	14.1152(7)
α, °	90	87.470(2)	92.195(3)
β, °	107.021(2)	89.732(2)	104.598(3)
γ, °	90	84.874(2)	101.316(3)
V, Å ³	1766.1(2)	3769.0(3)	2063.7(2)
Z	4	2	2
ρ _{calcd} , Mg m ⁻³	1.933	2.127	1.906
μ (Mo Kα), mm ⁻¹	2.484	3.044	2.187
F(000)	984	2268	1136
θ range, deg	2.22 to 28.37	2.33 to 27.61	2.42 to 30.10
Index ranges	-14 ≤ h ≤ 14 -17 ≤ k ≤ 17 -17 ≤ l ≤ 17	-10 ≤ h ≤ 10 -16 ≤ k ≤ 17 -47 ≤ l ≤ 47	-15 ≤ h ≤ 15 -19 ≤ k ≤ 19 -19 ≤ l ≤ 19
No. of reflns collected	46 773	83 412	76 825
Completeness to θ _{max}	99.5%	98.2%	99.5%
No. indep. reflns	4398	17 186	10 990
No. obsd reflns with (I > 2σ(I))	3918	13 959	7531
No. refined params	190	948	553
Goof (F ²)	1.044	1.097	1.285
R ₁ (F) (I > 2σ(I))	0.0214	0.0550	0.0644
wR ₂ (F ²) (all data)	0.0519	0.1210	0.1102
Largest diff peak/hole, e Å ⁻³	1.022/-0.457	2.105/-1.615	1.545/-1.013
CCDC number	1895454	1895455	1895456

Crystallographic data for the structural analyses have been deposited with the Cambridge Crystallographic Data Centre.

Computational methodology

Starting from XRD atomic coordinates, geometry optimizations of PT, [PT]⁺, [PT₂]²⁺ and [PT₃]²⁺ as well as TA, [TA]⁺, [TA₂]²⁺ and [TA₃]²⁺, in the gas phase were performed at the B3PW91/6-311+G(2df,p)⁴⁴ level of theory using Gaussian09.⁴⁵ For the Te atoms, effective core potentials (ECP28MDF) and a corresponding cc-pVTZ basis set were applied.⁴⁴ The resulting wavefunction files were used for topological analysis of the electron density (ED) according to the Atoms-In-Molecules³⁸ space-partitioning scheme using AIM2000,⁴⁵ whereas DGRID⁴⁶ was used to generate and analyze the ELI-D related real-space bonding descriptors applying a grid step size of 0.05 a.u. NCI grids were computed with NCIPLOT.⁴⁷ Bond paths are displayed with AIM2000,⁴⁵ ELI-D, ESP, and NCI figures are displayed with Moliso.⁴⁸ AIM affords atomic basins which can be integrated to give volumes and charges. In addition, a bond paths motif is provided, which resembles the molecular structure and uncovers all kind of atom-atom interactions, from very weak to strong.⁴⁹ Other RSBI derived from the ED include spin densities (SDs), the electrostatic potential (ESP), and the reduced density gradient, $s(\mathbf{r}) = [1/2(3\pi^2)^{1/3}]|\nabla\rho|/\rho^{4/3}$, following to the Non-Covalent Interactions (NCI) index⁵⁰ method. The latter is especially useful to uncover non-covalent bonding regions. Mapping the ED times the sign of the second eigenvalue of the Hessian ($\text{sign}(\lambda_2)\rho$) on iso-surfaces of $s(\mathbf{r})$ facilitates the assignment of different contact types including non-bonding/repulsive ($\lambda_2 > 0$), van der Waals like ($\lambda_2 \approx 0$), and

attractive ($\lambda_2 < 0$). A proper tool for the investigation of covalent (including dative) bonds is given by the topological dissection of the pair-density according to ELI-D³⁹ approach, which provides core, bonding and lone-pair basins. Notably, ELI-D and NCI iso-surfaces often show complementary spatial distribution suggesting spatial separation of covalent and non-covalent bonding aspects.⁵¹ The combination of all RSBI allows to monitor electronic rearrangements due to structural changes, which is highly relevant e.g. for strained systems, ligand variation, or unusual bonds.⁵²

Conflicts of interest

There are no conflicts to declare.

Acknowledgements

The Deutsche Forschungsgemeinschaft (DFG) and the Natural Sciences and Engineering Research Council (NSERC-Canada) are gratefully acknowledged for financial support.

References

- (a) G. Stenhouse, *Proc. R. Soc. London*, 1868, **17**, 62;
(b) G. Stenhouse, *Justus Liebigs Ann. Chem.*, 1869, **149**, 247.
- (a) K. Fies and W. Volk, *Chem. Ber.*, 1909, **42**, 1170–1176;
(b) K. Fries, H. Koch and H. Stuckebrock, *Justus Liebigs Ann. Chem.*, 1929, **468**, 162.

- 3 (a) M. Gomberg, *Ber. Dtsch. Chem. Ges.*, 1900, **33**, 3150; (b) M. Gomberg, *J. Am. Chem. Soc.*, 1900, **22**, 757.
- 4 M. Kinoshita, *Bull. Chem. Soc. Jpn.*, 1962, **35**, 1137.
- 5 E. A. C. Lucken, *J. Chem. Soc.*, 1962, 4963.
- 6 H. J. Shine and L. Piette, *J. Am. Chem. Soc.*, 1962, **84**, 4798.
- 7 J. Giordan and H. Bock, *Chem. Ber.*, 1982, **115**, 2548.
- 8 A. G. Davies and D. C. McGuchan, *Organometallics*, 1991, **10**, 329.
- 9 P. Raptas, L. Kress, P. Hapiot and L. Dunsch, *Phys. Chem. Chem. Phys.*, 2002, **4**, 4181.
- 10 P. Rangappa and H. J. Shine, *J. Sulfur Chem.*, 2006, **27**, 617 and other reviews and original work cited therein.
- 11 Y. Sato, M. Kinoshita, M. Sano and H. Akamatu, *Bull. Chem. Soc. Jpn.*, 1967, **40**, 2539.
- 12 Y. Murata, L. Hughes and H. J. Shine, *Inorg. Nucl. Chem. Lett.*, 1968, **4**, 573.
- 13 (a) B. K. Bandlish and H. J. Shine, *J. Org. Chem.*, 1977, **42**, 561; (b) B. Boduszek and H. J. Shine, *J. Org. Chem.*, 1988, **53**, 5142.
- 14 H. Bock, A. Rauschenbach, C. Näther, M. Kleine and Z. Havlas, *Chem. Ber.*, 1994, **127**, 2043.
- 15 S. V. Rosokha, J. Lu, T. Y. Rosokha and J. K. Kochi, *Acta Crystallogr., Sect. C: Cryst. Struct. Commun.*, 2007, **63**, o347.
- 16 J. Beck, T. Bredow and R. T. Tjahjanto, *Z. Naturforsch.*, 2009, **64b**, 145.
- 17 R. T. Tjahjanto, M. F. Peintinger, T. Bredow and J. Beck, *Eur. J. Inorg. Chem.*, 2012, 3625.
- 18 H. Poleschner and K. Seppelt, *Angew. Chem., Int. Ed.*, 2013, **52**, 12838.
- 19 T. Nishinaga and K. Komatsu, *Org. Biomol. Chem.*, 2005, **3**, 561–569.
- 20 R. Sebastiano, J. D. Korp and J. K. Kochi, *J. Chem. Soc., Chem. Commun.*, 1991, 1481–1482.
- 21 M. J. Modjewski, R. Shukla, S. V. Lindeman and R. Rathore, *Tetrahedron Lett.*, 2009, **50**, 6687–6690.
- 22 (a) S. Suzuki, Y. Morita, K. Fukui, K. Sato, D. Shiomi, T. Takui and K. Nakatsuji, *J. Am. Chem. Soc.*, 2006, **128**, 2530–2531; (b) K. E. Preuss, *Polyhedron*, 2014, **79**, 1–15; (c) R. T. Boéré, *ACS Omega*, 2018, **3**, 18170–18180; (d) M. Kertesz, *Chem. – Eur. J.*, 2019, **25**, 400–416.
- 23 L. Plasseraud, H. Cattey, P. Richard and D. Ballivet-Tkatchenko, *J. Organomet. Chem.*, 2009, **694**, 2386–2394.
- 24 L. Plasseraud, B. Therrien, A. Růžička and H. Cattey, *Inorg. Chim. Acta*, 2012, **380**, 50–56.
- 25 (a) D. J. Liptrot and P. P. Power, *Nat. Rev. Chem.*, 2017, **1**, 0004; (b) J. P. Wagner and P. R. Schreiner, *Angew. Chem., Int. Ed.*, 2015, **54**, 12274–12296; (c) J.-D. Guo, D. J. Liptrot, S. Nagase and P. P. Power, *Chem. Sci.*, 2015, **6**, 6235–6244; (d) J. P. Wagner and P. R. Schreiner, *J. Chem. Theory Comput.*, 2016, **12**, 231–237.
- 26 M. F. Peintinger, J. Beck and T. Bredow, *Phys. Chem. Chem. Phys.*, 2013, **15**, 18702–18709.
- 27 (a) H. D. K. Drew, *J. Chem. Soc.*, 1926, 223–231; (b) H. D. K. Drew, *J. Chem. Soc.*, 1926, 3054–3071; (c) H. D. K. Drew and R. W. Thomason, *J. Chem. Soc.*, 1927, 116–125; (d) H. D. K. Drew, *J. Chem. Soc.*, 1928, 506–510; (e) H. D. K. Drew, *J. Chem. Soc.*, 1928, 511–524.
- 28 K. Witzinger, *Z. Angew. Chem.*, 1929, **42**, 668–670.
- 29 A. N. Gioabă and A. A. Gioabă, *Roum. Chem. Q. Rev.*, 1995, **3**, 303–327.
- 30 (a) M. M. Mangion, M. R. Smith and E. A. Meyers, *J. Heterocycl. Chem.*, 1973, 533–536; (b) M. M. Mangion, M. R. Smith and E. A. Meyers, *J. Heterocycl. Chem.*, 1973, 543–549.
- 31 G. Cauquis and M. Maurey-Mey, *Bull. Soc. Chim. Fr.*, 1973, 2870.
- 32 L. Engman, J. Hellberg, C. Ishag and S. J. Söderholm, *J. Chem. Soc., Perkin Trans. 1*, 1988, 2095–2101.
- 33 N. G. Connelly and W. E. Geiger, *Chem. Rev.*, 1996, **96**, 877–910.
- 34 R. S. Stojanovic and A. M. Bond, *Anal. Chem.*, 1993, **65**, 56–64.
- 35 H. Bock and U. Lechner-Knoblauch, *J. Organomet. Chem.*, 1985, **294**, 295–304.
- 36 A. L. Fuller, L. A. S. Scott-Hayward, Y. Li, M. Bühl, A. M. Z. Slawin and J. D. Woollins, *J. Am. Chem. Soc.*, 2010, **132**, 5799–5802.
- 37 M. R. Smith, M. M. Mangion, R. A. Zingaro and E. A. Meyer, *J. Heterocycl. Chem.*, 1973, **10**, 527–531.
- 38 R. W. F. Bader, *Atoms in Molecules. A Quantum Theory*, Cambridge University Press, Oxford, UK, 1991.
- 39 M. Kohout, F. R. Wagner and Y. Grin, *Theor. Chem. Acc.*, 2008, **119**, 413–420.
- 40 E. R. Johnson, S. Keinan, P. Mori-Sanchez, J. Contreras-García, A. J. Cohen and W. Yang, *J. Am. Chem. Soc.*, 2010, **132**, 6498–6506.
- 41 R. T. Boéré, A. M. Bond, T. Chivers, S. W. Feldberg and T. L. Roemmele, *Inorg. Chem.*, 2007, **46**, 5596–5607.
- 42 (a) G. M. Sheldrick, *Acta Crystallogr., Sect. A: Found. Crystallogr.*, 2008, **64**, 112–122; (b) G. M. Sheldrick, *Acta Crystallogr., Sect. C: Struct. Chem.*, 2015, **71**, 3–8; (c) L. J. Farrugia, *J. Appl. Crystallogr.*, 1999, **32**, 837–838.
- 43 K. Brandenburg, *DIAMOND version 3.2i*, Crystal Impact GbR, Bonn Germany, 2012.
- 44 (a) J. P. Perdew, J. A. Chevary, S. H. Vosko, K. A. Jackson, M. R. Pederson, D. J. Singh and C. Fiolhais, *Phys. Rev. B: Condens. Matter Mater. Phys.*, 1992, **46**, 6671–6687; (b) A. D. Becke, *J. Chem. Phys.*, 1993, **98**, 5648–5652; (c) K. A. Peterson, D. Figgen, E. Goll, H. Stoll and M. Dolg, *J. Chem. Phys.*, 2003, **119**, 11113–11123; (d) B. Metz, H. Stoll and M. Dolg, *J. Chem. Phys.*, 2000, **113**, 2563–2569; (e) K. A. Peterson, *J. Chem. Phys.*, 2003, **119**, 11099–11112.
- 45 M. J. Frisch, G. W. Trucks, H. B. Schlegel, G. E. Scuseria, M. A. Robb, J. R. Cheeseman, G. Scalmani, V. Barone, B. Mennucci, G. A. Petersson, H. Nakatsuji, M. Caricato, X. Li, H. P. Hratchian, A. F. Izmaylov, J. Bloino, G. Zheng, J. L. Sonnenberg, M. Hada, M. Ehara, K. Toyota, R. Fukuda, J. Hasegawa, M. Ishida, T. Nakajima, Y. Honda, O. Kitao, H. Nakai, T. Vreven, J. A. Montgomery Jr., J. E. Peralta, F. Ogliaro, M. Bearpark, J. J. Heyd, E. Brothers, K. N. Kudin, V. N. Staroverov, R. Kobayashi, J. Normand, K. Raghavachari, A. Rendell, J. C. Burant, S. S. Iyengar, J. Tomasi, M. Cossi, N. Rega, J. M. Millam, M. Klene, J. E. Knox, J. B. Cross, V. Bakken,

- C. Adamo, J. Jaramillo, R. Gomperts, R. E. Stratmann, O. Yazyev, A. J. Austin, R. Cammi, C. Pomelli, J. W. Ochterski, R. L. Martin, K. Morokuma, V. G. Zakrzewski, G. A. Voth, P. Salvador, J. J. Dannenberg, S. Dapprich, A. D. Daniels, O. Farkas, J. B. Foresman, J. V. Ortiz, J. Cioslowski and D. J. Fox, *Gaussian09, revision B.01*, Gaussian, Inc., Wallingford, CT, 2010.
- 46 F. Biegler-König, J. Schönbohm and D. Bayles, *J. Comput. Chem.*, 2001, **22**, 545–559.
- 47 M. Kohout, *DGRID-4.6*, Radebeul, 2011.
- 48 J. Contreras-García, E. Johnson, S. Keinan, R. Chaudret, J.-P. Piquemal, D. Beratan and W. Yang, *J. Chem. Theory Comput.*, 2011, **7**, 625–632.
- 49 C. B. Hübschle and P. Luger, *J. Appl. Crystallogr.*, 2006, **39**, 901–904.
- 50 C. Gatti, *Z. Kristallogr.*, 2005, **220**, 399–457.
- 51 (a) M. Kohout, *Int. J. Quantum Chem.*, 2004, **97**, 651–658; (b) M. Kohout, F. R. Wagner and Y. Grin, *Theor. Chem. Acc.*, 2008, **119**, 413–420.
- 52 S. Mebs, *Chem. Phys. Lett.*, 2016, **651**, 172–177.

2.3. Trimorphism of the Dicationic Phenoxatellurine Triple Decker Triplate Salt

2.3.1. Introduction & Results

The reaction of phenoxatellurine (PT) with triflic acid has been examined. Phenoxatellurine (PT) undergoes a single-electron oxidation with triflic acid resulting in the oligomerization of the PT units leading to relatively air stable triple-decker structures.

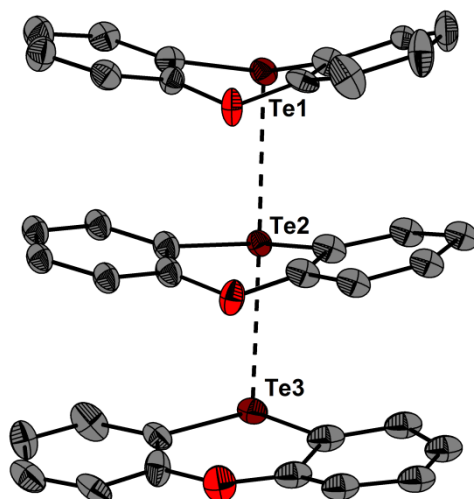
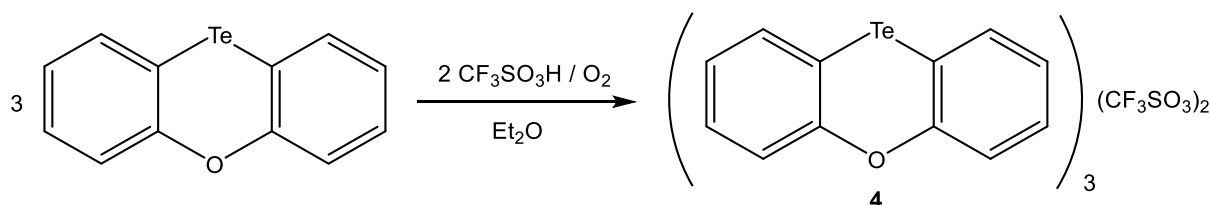


Figure 8. Molecular structure of the one $[PT_3]^{2+}$ dication of monoclinic $[PT_3](O_3SCF_3)_2$ showing 50 % probability ellipsoids ($[CF_3SO_3]^-$ omitted).

The characteristics of this reaction is that three different colors (violet, red and golden) and thus modifications of the crystal structure, monoclinic, triclinic and orthorhombic were observed. However, any efforts in synthesizing only one modification failed.

Scheme 14 depicts the reaction of phenoxatellurine (PT) in diethyl ether with triflic acid and gaseous oxygen.



Scheme 14. Reaction of phenoxatellurine (PT) with triflic acid and gaseous oxygen.

Upon oxidation with triflic acid in the presence of gaseous oxygen passing through the solution an immediate colorchange from colorless to dark violet occurs, signalling the presence of radical bonding situations. Evaporation of the solvent and recrystallization from dry acetonitrile gave rise to the different modifications.

The following table (Table 1) presents the tellurium bond parameters of the $[\text{PT}_3]^{2+}$ dications.

Table 1. Selected bond parameters of the $[\text{PT}_3]^{2+}$ dications within the three modifications.

	<i>Triclinic 1</i>	<i>Triclinic 2</i>	<i>Monoclinic</i>	<i>Orthorhombic</i>	<i>BF₄ salt</i>
$\alpha(\text{Te1}) / ^\circ$	30.1	32.2	30.5	32.0	33.6
$\alpha(\text{Te2}) / ^\circ$	20.5	21.6	20.9	22.4	22.2
$\alpha(\text{Te3}) / ^\circ$	1.2	4.7	4.4	4.7	1.1
Te1-Te2 / Å	3.122(8)	3.152(8)	3.132(2)	3.177(1)	3.138(1)
Te2-Te3 / Å	3.051(8)	3.045(7)	3.056(2)	3.096(1)	3.103(1)

The fold angles α of all modifications are smaller than the parent PT of 37.5° ^[114] and spread over a large range. The same behavior was already reported for the $[\text{PT}]_3(\text{BF}_4)_2$ structure.^[115] The Te-Te bond lengths of 3.122(8) – 3.177(1) Å for Te1-Te2 and 3.045(7) – 3.096(1) Å for Te2-Te3 are also comparable to the ones of $[\text{PT}]_3(\text{BF}_4)_2$ (3.138(1), 3.103(1) Å).

The crystallization of a molecular compound in different polymorphs containing different conformers is called conformational polymorphism^[116,117], where the relative orientation of the molecules in the crystal structure is determined by the type and strength of the intermolecular non-covalent forces.^[118–121] With missing hydrogen or any strong non-covalent interactions, London dispersion may be considered as an explanation for the packing of the molecules. The phenoxatellurine triflate salt $[\text{PT}_3](\text{O}_3\text{SCF}_3)_2$ reveals three modifications with four independent conformers (triclinic 1 and 2, monoclinic and orthorhombic). Other conformational polymorphisms in organotellurium chemistry have been reported earlier.^[122–126] The packing diagrams of all three modifications are given in Figure 9.

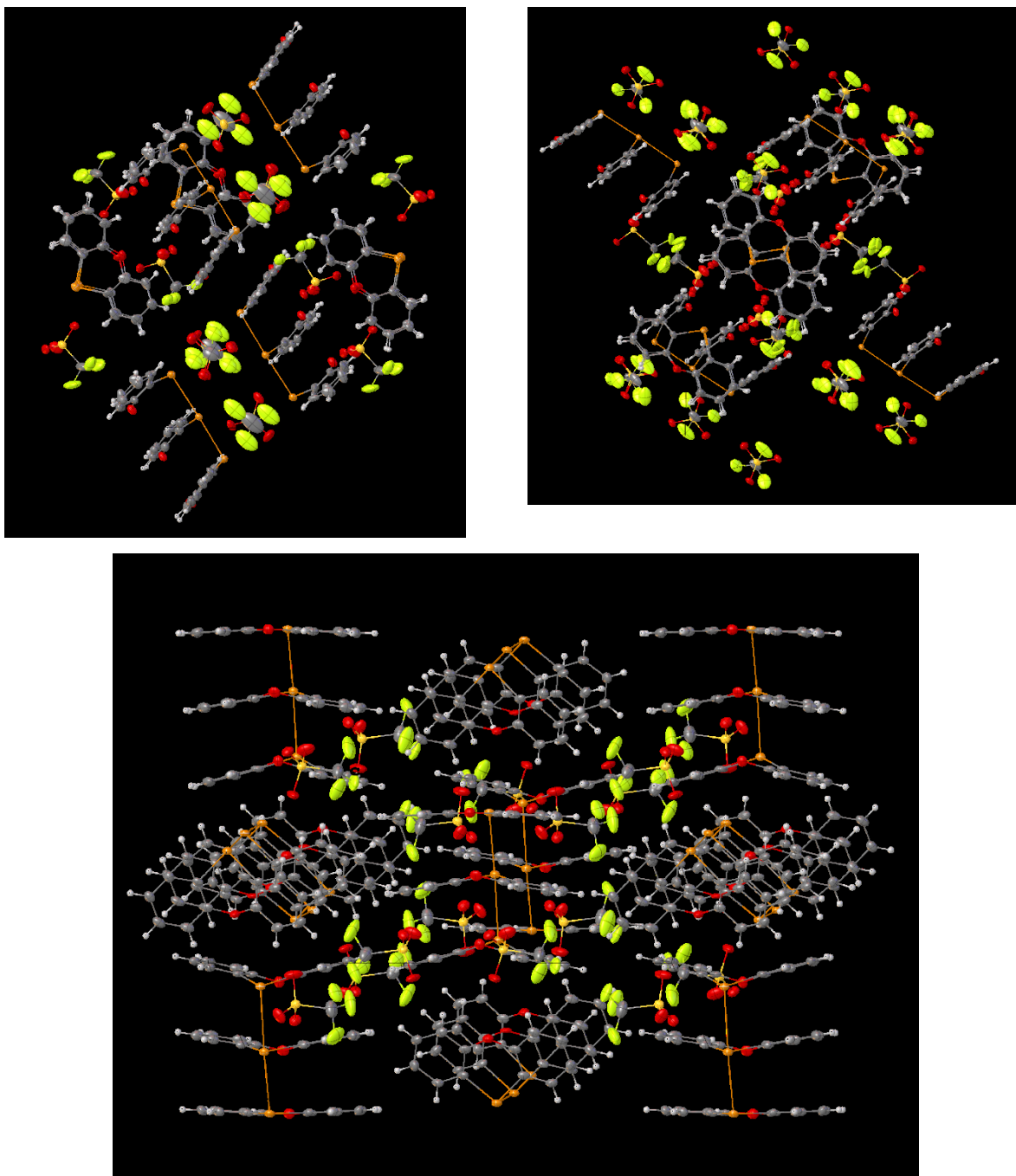


Figure 9. 2D-packing motifs of the $[PT_3]^{2+}$ dication in triclinic (top left), monoclinic (bottom) and orthorhombic (top right).

For the calculation of intermolecular non-covalent forces, a Hirshfeld surface analysis was carried out with Crystal Explorer.^[127–130] Here the red spots on the Hirshfeld Surface (HS) that are color coded with the property d_{norm} ^[131] describing close atom–atom contacts.

The percentage contributions of all atom-atom interactions are displayed in Table 2.

Table 2. Percentage contributions of atom–atom interactions between a central [PT₃]²⁺ dication with adjacent [PT₃]²⁺ dications and triflate ions in the crystal lattice for all three modifications (^aconformer 1, ^bconformer 2).

	<i>triclinic (%)</i>	<i>monoclinic (%)</i>	<i>orthorhombic (%)</i>
<i>C-All</i>	12.1 ^a 11.4 ^b	12.2	12.0
<i>H-E</i>	74.0 ^a 74.1 ^b	73.6	74.3
<i>O-E</i>	3.0 ^a 3.1 ^b	3.1	1.9
<i>Te-E</i>	10.9 ^a 11.4 ^b	11.0	11.8
<i>Te-O</i>	8.7 ^a 9.2 ^b	8.7	8.8

All three compounds are dominated by H · · · E interactions with approximately 74 % and show similar interactions with small differences. The triclinic conformer 2 reveals slightly higher Te · · · O contact contributions than the others by about 0.4 % and in the orthorhombic conformer the O · · · E interactions are the smallest with 1.9 %.

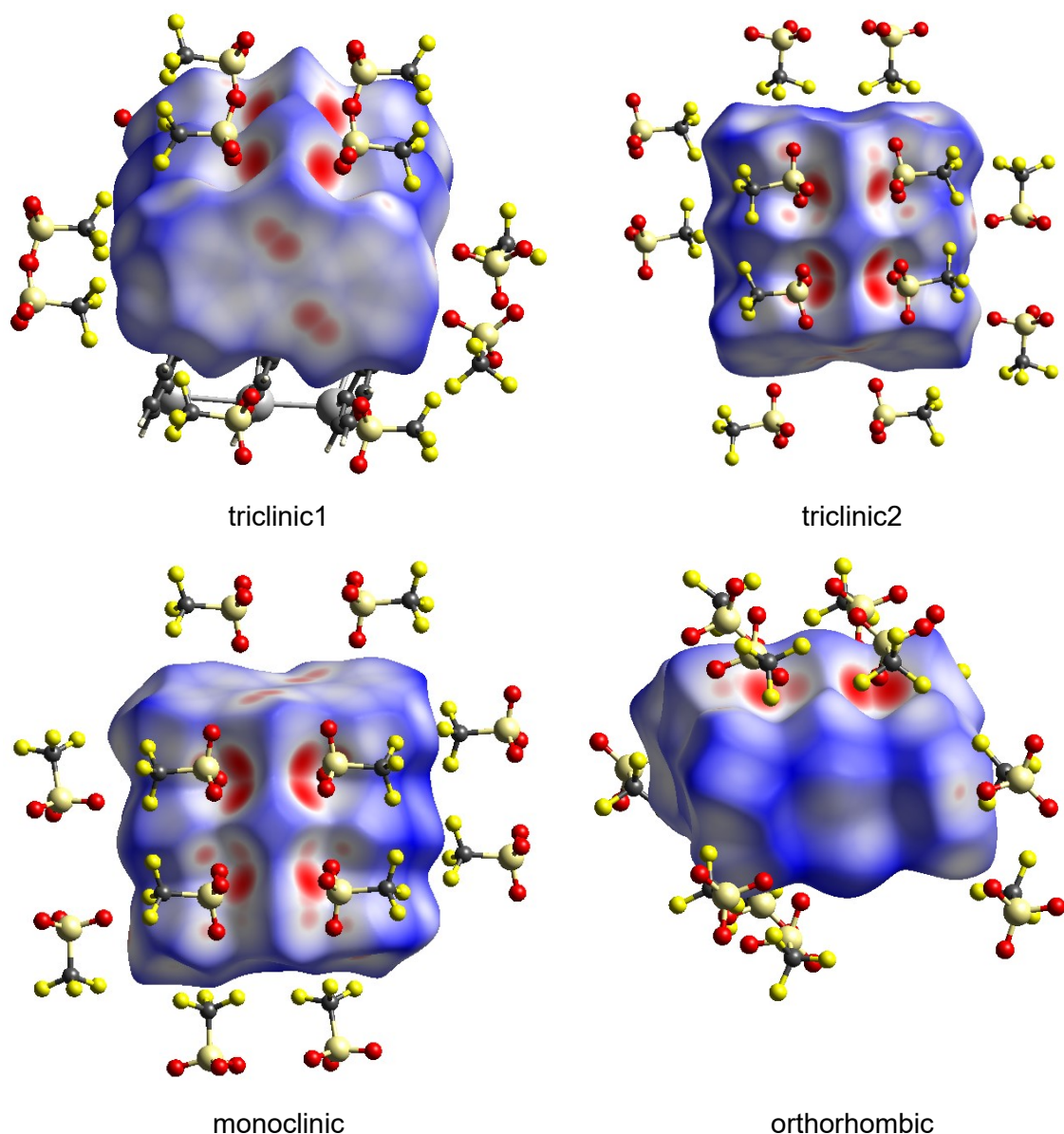


Figure 10. Hirshfeld Surfaces of the conformer in the triclinic, conformer 1 and 2, the monoclinic and the orthorhombic crystal structure. Significant interaction partners are shown if existent, d_{norm} mapped.

The fingerprint plots (Figure 11) depict the HS-mediated close contacts in a 2D picture showing the interactions of every surface point of the closest interior atom (d_i) to the closest exterior atom (d_e)^[128,129] and confirm the small differences in the crystal packings of all three polymorph conformers.

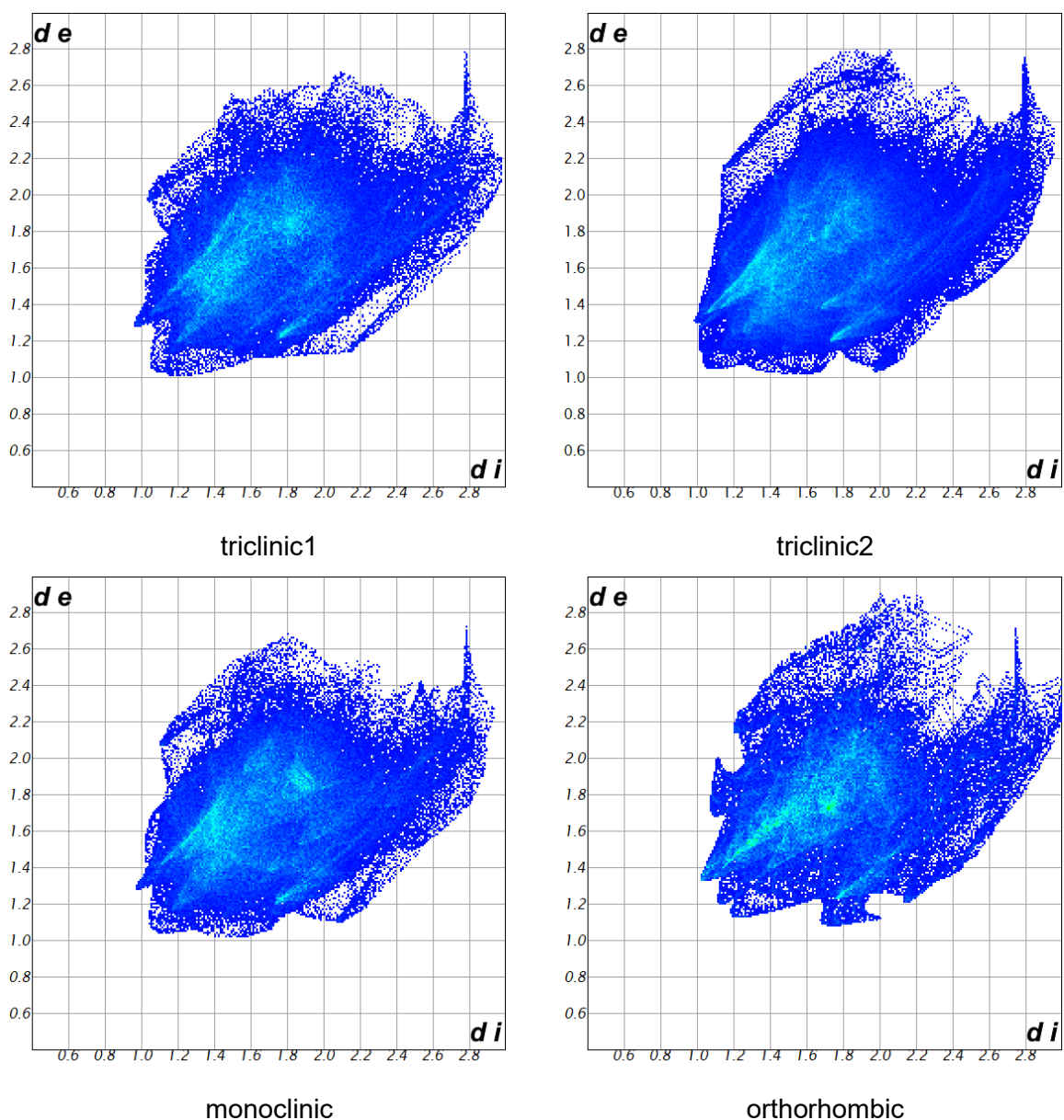
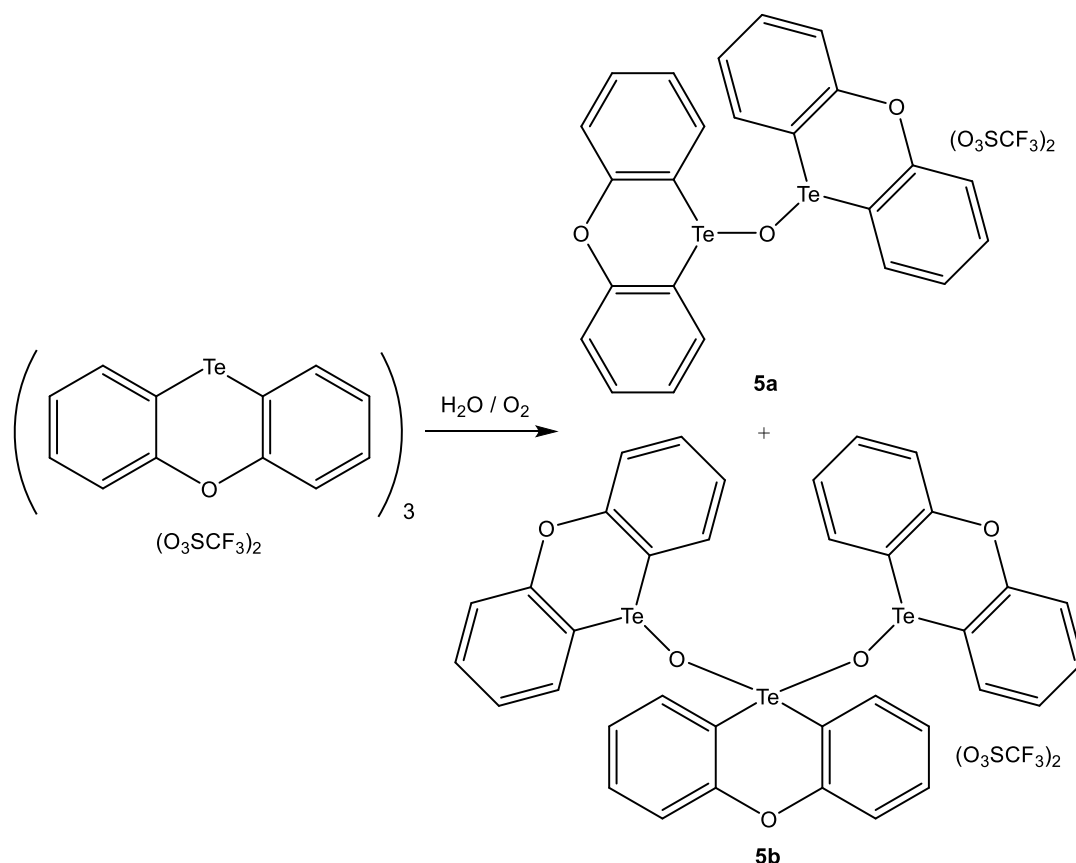


Figure 11. Hirshfeld surface fingerprint plots of $[\text{PT}_3]^{2+}$.

The monoclinic conformer, compared to the triclinic and orthorhombic species, has the highest density of 2.047 mg m^{-3} (Table 5) and indicates thus the thermodynamic stability at low temperatures according to the density rule, which correlates the highest density with a maximum of van-der-Waals interactions. At absolute zero where the entropy is negligible the monoclinic conformer is consequently the most stable form.^[132,133]

The trend in crystal densities coincides to the crystal voids, where the modification with the lowest density (orthorhombic conformer) has the highest percentage of voids and the monoclinic form has the lowest percentage of voids.

Exposure to air for several weeks results in an oxo-bridged dimer $[\text{PT}]_2\text{O}(\text{O}_3\text{SCF}_3)_2$ (**5a**) or trimer $[\text{PT}]_3\text{O}_2(\text{O}_3\text{SCF}_3)_2$ (**5b**) with the loss of the intense color (Scheme 15).



This reaction is rather slow, since there are still violet crystals in the mixture. The molecular structures of both oxo-bridged species are shown in Figure 12.

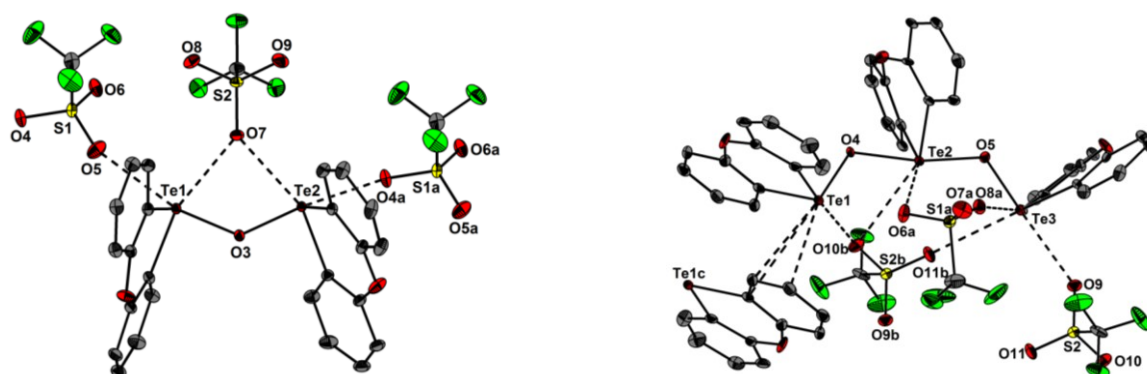


Figure 12. Crystal structures of $[PT]_2O(O_3SCF_3)_2$ (left) and $[PT]_3O_2(O_3SCF_3)_2$ (right) showing 50 % probability ellipsoids and the essential numbering scheme.

Selected bond parameters of $[PT]_2O(O_3SCF_3)_2$ and $[PT]_3O_2(O_3SCF_3)_2$ are listed in Table 3. The interactions to the triflic anions can be seen in Table 4.

Table 3. Selected bond parameters for the oxo-bridged species $[\text{PT}]_2\text{O}(\text{O}_3\text{SCF}_3)_2$ and $[\text{PT}]_3\text{O}_2(\text{O}_3\text{SCF}_3)_2$.

	$[\text{PT}]_2\text{O}$ $(\text{O}_3\text{SCF}_3)_2$		$[\text{PT}]_3\text{O}_2$ $(\text{O}_3\text{SCF}_3)_2$
α (Te1-O3-Te2) / °	56.5	α (Te1-O4-Te2) / °	60.3
		α (Te2-O5-Te3) / °	60.2
Te1-O3 / Å	1.951(6)	Te1-O4 / Å	1.900(5)
Te2-O3 / Å	1.978(5)	Te2-O4 / Å	2.157(6)
		Te2-O5 / Å	2.084(6)
		Te3-O5 / Å	1.912(6)

The oxo-bridged dimer $[\text{PT}]_2\text{O}(\text{O}_3\text{SCF}_3)_2$ has nearly identical intramolecular Te-O bond lengths and an Te-O-Te angle of 56.5°. The molecular structure of $[\text{PT}]_3\text{O}_2(\text{O}_3\text{SCF}_3)_2$ reveals an angle of 60.2 and 60.3 with slightly shorter Te-O bond lengths between the “outer” PT units.

Table 4. Te...O bond lengths of the PT units towards the triflic anions.

	$[\text{PT}]_2\text{O}$ $(\text{O}_3\text{SCF}_3)_2$		$[\text{PT}]_3\text{O}_2$ $(\text{O}_3\text{SCF}_3)_2$
Te1...O5 / Å	2.970(0)	Te1...O10b / Å	2.997(9)
Te1...O7 / Å	3.001(8)	Te2...O10b / Å	3.319(8)
Te2...O7 / Å	3.140(6)	Te2...O6a / Å	3.171(4)
Te2...O4a / Å	2.532(9)	Te3...O8a / Å	3.027(0)
		Te3...O11b / Å	3.250(5)
		Te3...O9 / Å	2.823(6)

2.3.2. Experimental

Reagents were obtained commercially (Sigma-Aldrich, Germany) and used as received. Dry solvents were collected from a SPS800 mBraun solvent system. Diethyl ether was dried over potassium hydroxide and distilled of sodium/benzophenone. PT was prepared in two steps according to slightly modified literature procedures.^[134–138] ^1H -, ^{13}C - and ^{125}Te -NMR spectra were recorded at RT (unless otherwise stated) using a Bruker Avance-360 spectrometer and are referenced to tetramethylsilane (^1H , ^{13}C) and telluric acid (^{125}Te). Chemical shifts are reported in parts per million (ppm) and coupling constants (J) are given in Hertz (Hz). Air sensitive substances were handled in gloveboxes “Labmaster” by M. Braun. The electrospray ionization mass spectrometry (ESI-MS) spectrum was obtained on the Bruker Impact II. Acetonitrile solutions were injected directly into the spectrometer at a flow rate of 3 $\mu\text{l min}^{-1}$. Nitrogen was used both as a drying gas and for nebulization with flow rates of approximately 4 L min^{-1} and a pressure of 0.4 bar. The spectrum was collected for one minute and averaged. UV/vis spectra were recorded on a JASCO V-570 spectrometer. Crystal Explorer^[139] was used for the calculation and visualization of Hirshfeld surfaces and fingerprint plots.^[129]

2.3.2.1 Synthesis of [PT]₃(O₃SCF₃)₂

In a dried schlenk-tube under argon atmosphere phenoxatellurine (1.00 g (3.38 mmol) was dissolved in 20 ml of dry diethyl ether and treated with gaseous oxygen. 0.3 ml (3.38 mmol) trifluoromethanesulphonic acid was added slowly and the solution was stirred for 30 minutes. The resulting solid was filtered off and the residue dried in vacuum, leaving 0.96 g (2.16 mmol, 64 %) of the crude product. Recrystallization from acetonitrile gave crystals in three different modifications. m.p. > 230 °C

¹H-NMR (360 MHz, CD₃CN): δ = 6.97 – 7.57 (m, 12H, C_{Ar}-H) ppm. **¹³C-{¹H}-NMR (90 MHz, CD₃CN):** δ = 120.9, 126.5, 137.0, 136.7 (C_{Ar}), 118.1 (C_{Ar}-CH-Te), 150.9 (C_{Ar}-CH-O) ppm. **¹²⁵Te-NMR (110 MHz, CD₃CN):** δ = 1611.8 ppm. **MS (ESI, CH₃CN, positive mode):** m/z (rel. Int.) = 447 (9) [(C₁₂H₈OTe⁺)(CF₃SO₃⁻)⁺, 315 (100) [C₁₂H₈OTe-OH]⁺, 298 (100) [C₁₂H₈OTe]⁺, 168 (13) [C₁₂H₈O]⁺. **MS (ESI, CH₃CN, negative mode):** m/z (rel. Int.) = 825 (100) [(C₁₂H₈OTe⁺)(CF₃SO₃⁻)₂(CH₃CN)₂]⁻, 487 (64) [(C₁₂H₈OTe⁺)(CF₃SO₃⁻)-H⁺(CH₃CN)]⁻, 149 (95) [CF₃SO₃]⁻. **UV/VIS (CH₂Cl₂):** λ_{max} = 276 nm, 338 nm und 455 nm. **Molar Conductivity (CH₃CN, c = 5 × 10⁻⁷ mol L⁻¹):** Λ = 480 Ω⁻¹ cm² mol.

X-ray crystallography. Intensity data of [PT]₃(O₃SCF₃)₂, [PT]₂O(O₃SCF₃)₂ and [PT]₃O₂(O₃SCF₃)₂ were collected on a Bruker Venture D8 diffractometer with graphite-monochromated Mo-Kα (0.7107 Å) radiation. The structures were solved by direct methods and difference Fourier synthesis with subsequent Full-matrix least-squares refinements on *F*², using all data.^[140] All non-hydrogen atoms were refined using anisotropic displacement parameters. Hydrogen atoms were included in geometrically calculated positions using a riding model. Crystal and refinement data are collected in Table 5 and 6. Figures were created using DIAMOND.^[141]

Table 5. Crystal data and structure refinement of [PT]₃(O₃SCF₃)₂ (three modifications).

Formula	C ₃₈ H ₂₄ F ₆ O ₉ S ₂ Te ₃	C ₃₈ H ₂₄ F ₆ O ₉ S ₂ Te ₃	C ₃₈ H ₂₄ F ₆ O ₉ S ₂ Te ₃
Formula weight, g mol ⁻¹	1185.49	1185.49	1185.49
Crystal system	triclinic	monoclinic	orthorhombic
Crystal size, mm	0.07 × 0.07 × 0.05	0.10 × 0.05 × 0.05	0.08 × 0.05 × 0.05
Space group	P-1	C2/c	Cmca
a, Å	14.032(1)	24.072(1)	22.900(1)
b, Å	14.294(1)	14.355(7)	20.4206(8)
c, Å	20.207(2)	22.309(1)	16.7235(7)
α, °	85.227(5)	90	90
β, °	86.118(4)	93.735(2)	90
γ, °	73.007(5)	90	90
V, Å ³	3858.6(6)	7692.8(6)	7820.5(6)
Z	4	8	8
ρ _{calcd} , Mg m ⁻³	2.041	2.047	2.014
Void volume, Å ³	498.9 ^a	944.9 ^a	1095.3 ^a
Percentage of voids	12.9%	12.2%	14.0%
μ (Mo Kα), mm ⁻¹	2.446	2.454	2.414
F(000)	2264	4528	4528
θ range, deg	2.43 to 25.71	2.41 to 27.55	4.43 to 26.03
Index ranges	-16 ≤ h ≤ 9	-31 ≤ h ≤ 31	-29 ≤ h ≤ 29
	-17 ≤ k ≤ 17	-18 ≤ k ≤ 18	-26 ≤ k ≤ 26
	-24 ≤ l ≤ 24	-28 ≤ l ≤ 27	-21 ≤ l ≤ 19
No. of reflns collected	85616	71136	22143
Completeness to θ _{max}	97.6%	99.8%	99.8%
No. indep. Reflns	14011	8873	4607
No. obsd reflns with (I > 2σ(I))	11485	7258	3901
No. refined params	811	523	271
GooF (F ²)	1.162	1.117	1.211
R ₁ (F) (I > 2σ(I))	0.0604	0.0540	0.0498
wR ₂ (F ²) (all data)	0.1371	0.1275	0.1148
Largest diff peak/hole, e Å ⁻³	2.561 / -2.470	2.959 / -1.150	2.301 / -1.964

Table 6. Crystal data and structure refinement of [PT]₂O(O₃SCF₃)₃ and [PT]₃O₂(O₃SCF₃)₃.

<i>Formula</i>	<i>C₂₆H₁₆F₆O₉S₂Te₂</i>	<i>C₃₈H₂₄F₆O₁₁S₂Te₃</i>
<i>Formula weight, g mol⁻¹</i>	905.71	1217.49
<i>Crystal system</i>	triclinic	monoclinic
<i>Crystal size, mm</i>	0.05 × 0.05 × 0.05	0.21 × 0.11 × 0.05
<i>Space group</i>	P-1	P2 ₁ /c
<i>a, Å</i>	10.2882(4)	14.797(3)
<i>b, Å</i>	12.5699(5)	21.598(4)
<i>c, Å</i>	13.4601(5)	12.977(2)
<i>α, °</i>	63.7570(10)	90
<i>β, °</i>	74.9890(10)	101.347(5)
<i>γ, °</i>	66.0680(10)	90
<i>V, Å³</i>	1420.29(9)	4066.3(13)
<i>Z</i>	2	4
<i>ρ_{calcd}, Mg m⁻³</i>	2.118	1.989
<i>Void volume, Å³</i>	868	2328
<i>F(000)</i>	2.295	2.328
<i>θ range, deg</i>	2.37 to 42.48	2.62 to 27.50
<i>Index ranges</i>	-19 ≤ h ≤ 18	-17 ≤ h ≤ 17
	-23 ≤ k ≤ 23	-25 ≤ k ≤ 19
	-25 ≤ l ≤ 25	-15 ≤ l ≤ 15
<i>No. of reflns collected</i>	96357	33258
<i>Completeness to θ_{max}</i>	99.1%	99.5%
<i>No. indep. Reflns</i>	20378	7190
<i>No. obsd reflns with (I > 2σ(I))</i>	16023	4073
<i>No. refined params</i>	406	541
<i>GooF (F²)</i>	1.085	0.974
<i>R₁ (F) (I > 2σ(I))</i>	0.0367	0.0428
<i>wR₂ (F²) (all data)</i>	0.0683	0.1204
<i>Largest diff peak/hole, e Å⁻³</i>	2.798 / -1.714	0.967 / -0.801

2.4. New insights into the oxidation of phenoxatellurine with sulphuric acid

2.4.1. Synopsis

Comparable to the reaction of thianthrene (TA) in conc. sulphuric acid, phenoxatellurine (PT) forms intensely colored species. Drew was able to isolate some of those intense red crystals and suggested that diphenoxtellurylium dibisulphate disulphuric acid trihydrate $(PT)_2(SO_4H)_2(H_2SO_4)_2(H_2O)_3$ evolved.^[134] Furthermore he noticed that the exposure to moist air on a porous tile causes the loss of, what he called, “attached free” sulphuric acid, resulting in an intensely violet species, the diphenoxtellurylium dibissulphate di- or trihydrate $(PT)_2(SO_4H)_2(H_2O)_{2-3}$.

The aim of this project was to reinvestigate the synthesis and characterization of the intensely red and the resulting violet species from phenoxatellurine (PT). The molecular structure was determined via X-ray analysis and, due to their poor solubility. The characterization has been done only by elemental analysis.

2.4.2. Experimental Contributions

In this study, I carried out the synthesis of the compounds and their characterization. Moreover I wrote the experimental section. The manuscript was written by Prof. Dr. Jens Beckmann. X-ray analysis and structure refinements have been made by Dr. Enno Lork. The article was published in the following journal:

Mostaghimi, F.; Bolsinger, J.; Lork, E.; Beckmann, J. *New insights into the oxidation of phenoxatellurine with sulphuric acid*. Main Group Metal Chemistry **2019**, 42, 150–152. DOI: 10.1515/mgmc-2019-0017.

Short Communication

Open Access

Farzin Mostaghimi, Jens Bolsinger, Enno Lork and Jens Beckmann*

New insights into the oxidation of phenoxatellurine with sulfuric acid

https://doi.org/10.1515/mgmc-2019-0017
Received May 10, 2019; accepted July 29, 2019.

Abstract: The oxidation of phenoxatellurine (PT) with conc. H_2SO_4 was reinvestigated. Two crystalline products, namely $[\text{PT}_2][\text{H}_3\text{O}][\text{SO}_4\text{H}_3]$ (**1**) and $[\text{PT}][\text{SO}_4]$ (**2**) were isolated and fully characterized by X-ray crystallography. The structure of **1** features $[\text{PT}_2]^{2+}$ dications giving rise to double-decker structures with two parallel PT layers that arise from dimerisation of two radical cations $[\text{PT}]^{\cdot+}$. The $[\text{PT}_2]^{2+}$ dications and the hydrogensulfate ions are associated via secondary $\text{Te}\cdots\text{O}$ interactions. The oxonium ion and the hydrogensulfate ions are involved in hydrogen bonding. The structure of **2** comprises ion pairs consisting of $[\text{PT}]^{2+}$ dications and sulfate ions, which form a 2D coordination polymer. In addition, adjacent sulfate ions in the crystal lattice bind to tellurium atoms via secondary secondary $\text{Te}\cdots\text{O}$ interactions.

Keywords: tellurium; pancake bonding; radical dimer

Phenoxatellurine (PT) is a well-defined dibenzodioxine-type heterocycle (Scheme 1, in which one oxygen atom has been formally replaced by tellurium (Drew, 1926a). Unlike planar dibenzodioxine, PT comprises a butterfly-type structure in the solid-state (Smith et al., 1973). Upon contact with mineral acids, such as sulfuric acid and nitric acids, PT forms intensely colored substances, which remained a curiosity for a long time (Drew, 1926b). There was early suspicion that the color arose from single-electron oxidation of PT (Witzinger, 1929), which

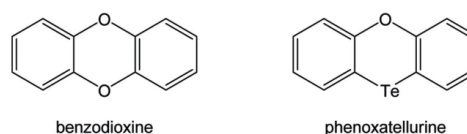
was later confirmed by cyclovoltammetry (Cauquis and Maurey-Mey, 1973). However, the exact nature of the colored substances still remained unclear at the time. Very recently, we investigated the single-electron oxidation of PT using nitrosonium salts, $[\text{NO}][\text{SbF}_6]$ and $[\text{NO}][\text{BF}_4]$, which produced the well-defined products $[\text{PT}_2][\text{SbF}_6]_2$ and $[\text{PT}_3][\text{BF}_4]_2$, respectively, possessing so-called double-decker and triple-decker structures (Mostaghimi et al., 2019). Indeed, the aggregation within these layered structures stemmed from SOMO-SOMO interaction between two radical cations $[\text{PT}]^{\cdot+}$, commonly referred to as pancake bonding (Kertesz, 2019), but also from significant London dispersion interactions and non-covalent multi-centre bonding between the tellurium atoms.

In this work we reinvestigated the reaction of PT with sulfuric acid. We were now able to isolate and structurally characterize two compounds, namely, $[\text{PT}_2][\text{H}_3\text{O}][\text{SO}_4\text{H}_3]$ (**1**) and $[\text{PT}][\text{SO}_4]$ (**2**), that are closely related to Drew's original work (Drew, 1926b). Following the described procedure, PT was dissolved in concentrated sulfuric acid to give a deep red solution, from which sulfur dioxide evolved. The solution was carefully diluted with water and allowed to stand. After three days, bright red single crystals (**1**) had formed, which were characterized by X-ray crystallography. Accordingly, the composition of the red crystals is $[\text{PT}_2][\text{H}_3\text{O}][\text{SO}_4\text{H}_3]$ (**1**). Drew's original report suggests that in his case the red crystals were composed of $[\text{PT}_2][\text{H}_3\text{O}][\text{SO}_4\text{H}_3(\text{H}_2\text{O})]$ (denoted **III** in his work). Upon exposure to moist air on porous tile, he also obtained products "free" of sulfuric acid, namely, $[\text{PT}_2][\text{SO}_4\text{H}_3(\text{H}_2\text{O})_3]$ (denoted **IV** in his work) and $[\text{PT}_2][\text{SO}_4\text{H}_3(\text{H}_2\text{O})_2]$ (denoted **V** in his work), which were intensely blue-violet in colour (Drew, 1926b). We were able to confirm his observation.

* Corresponding author: Jens Beckmann, Institut für Anorganische Chemie und Kristallographie, Universität Bremen, Leobener Straße 7, 28359 Bremen, Germany; Institut für Chemie und Biochemie Freie Universität Berlin, Fabeckstraße 34-36, 14195 Berlin, Germany, e-mail: j.beckmann@uni-bremen.de.

Farzin Mostaghimi and Enno Lork, Institut für Anorganische Chemie und Kristallographie, Universität Bremen, Leobener Straße 7, 28359 Bremen, Germany

Jens Bolsinger, Institut für Chemie und Biochemie Freie Universität Berlin, Fabeckstraße 34-36, 14195 Berlin, Germany



Scheme 1: Lewis formulas of benzodioxine and phenoxatellurine.

However, no single crystals were obtained from any of these intensely blue-violet products. The crystal structure of **1** is shown in Figure 1. Like $[\text{PT}_2][\text{SbF}_6]_2$ (Mostaghimi et al., 2019), **1** contains $[\text{PT}_2]^{2+}$ dications with a layered double-decker structure. The Te-Te bond length of **1** (2.928(1) Å) are slightly larger than those of $[\text{PT}_2][\text{SbF}_6]_2$ (2.897(1), 2.903(1) Å) having two conformers in the asymmetric unit. The degree of folding of the butterfly-structure can be quantified using the fold angle α between the planes defined by the two phenyl rings and the Te and O atoms. The fold angles α of **1** (3.5°, 21.9°) closely resembles values of one conformer of $[\text{PT}_2][\text{SbF}_6]_2$ (3.4°, 20.8°). These very similar structural features strongly suggest that the pancake bonding situation including London dispersion and non-covalent Te...Te interactions are also similar (Mostaghimi et al., 2019).

The $[\text{PT}_2]^{2+}$ dication is associated with six $[\text{SO}_4\text{H}]^-$ ions via a total of eight Te...O contacts (2.910(1)-3.465(1) Å, dashed blue lines in Figure 1) that are significantly shorter than the primary Te-O bonds in $[(4\text{-MeOC}_6\text{H}_4)_2\text{TeO}]_n$

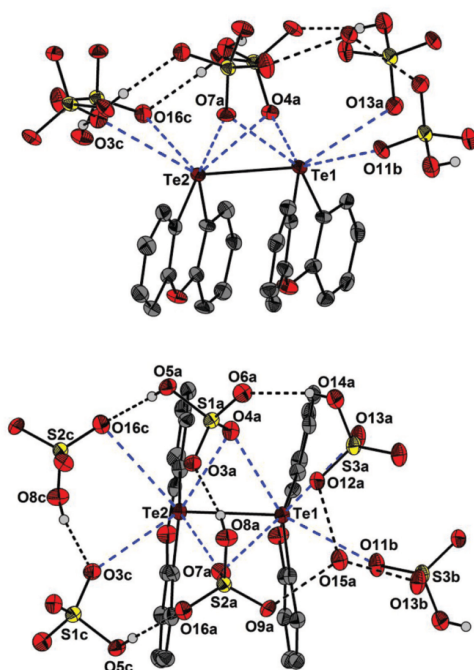


Figure 1: Crystal structure of **1** (from two perspectives) showing 30% probability ellipsoids and the atomic numbering. The dashed black and blue lines show secondary Te...O contacts and hydrogen bonds, respectively.

(2.025(2) and 2.100(2) Å) (Beckmann et al., 2003). The $[\text{H}_3\text{O}]^+$ ion and the $[\text{SO}_4\text{H}]^-$ ions give rise to rather strong hydrogen bonds, as evidenced by the short O...O donor-acceptor distances (2.535(1)-2.644(1) Å, dashed black lines).

Recrystallization of the red crystals (**1**) from hot water at the air, furnished colorless crystals (**2**), which were also investigated by X-ray crystallography. The composition of the colorless crystals is $[\text{PT}][\text{SO}_4]$ (**2**), which is apparently the same material Drew obtained by recrystallisation from glacial acid (denoted **VII** in his work). The crystal structure of **2** is shown in Figure 2.

The structure consists of ion pairs alternating $[\text{PT}]^{2+}$ dications and sulfate ions that build a 1D coordination polymer. The $[\text{PT}]^{2+}$ dication of **2** is almost planar (fold $\alpha = 7.7^\circ$). The spatial arrangement of the Te atom is defined by two slightly elongated primary Te...O bonds (2.153(4), 2.249(5) Å; dashed black lines in Figure 2) and three secondary Te...O bonds (2.940(4), 2.989(5), 3.099(5) Å; dashed blue lines in Figure 2).

Almost 100 years after the discovery that phenoxatellurine (PT) dissolves in conc. sulfuric acid to give intensely colorful solutions (Drew, 1926b), the nature of one species, namely $[\text{PT}_2][\text{H}_3\text{O}][\text{SO}_4\text{H}]_3$ (**1**), which is responsible for the red color has been unraveled. A related colorless species, namely $[\text{PT}][\text{SO}_4]$ (**2**), was also obtained and fully characterized.

X-ray crystallography. Intensity data were collected using a STOE IPDS 2T diffractometer (**1**) and a Bruker Venture D8 diffractometer (**2**) with graphite-monochromated Mo-K α (0.7107 Å) radiation. The structures were solved by direct methods and difference Fourier synthesis using SHELXS-97 implemented in

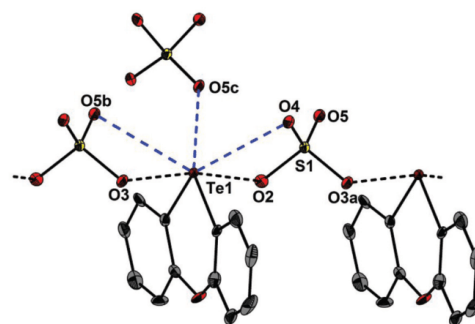


Figure 2: Crystal structure of **2** showing 30% probability ellipsoids and the atomic numbering. The dashed black and blue lines show slightly elongated primary Te...O bonds and secondary Te...O contacts, respectively.

Table 1: Crystal data and structure refinement of **1** and **2**.

	1	2
Formula	C ₂₆ H ₂₂ O ₁₅ S ₃ Te ₂	C ₁₂ H ₈ O ₅ STe
Formula weight, g mol ⁻¹	901.80	391.84
Crystal system	triclinic	monoclinic
Crystal size, mm	0.5 × 0.5 × 0.5	0.08 × 0.07 × 0.04
Space group	P $\bar{1}$	P2 ₁ /n
a, Å	10.997(2)	8.414(2)
b, Å	12.523(2)	6.224(1)
c, Å	12.689(2)	22.629(6)
α , °	66.41(1)	90
β , °	78.10(1)	96.175(9)
γ , °	65.83(1)	90
V, Å ³	1459.1(4)	1178.18(5)
Z	2	4
ρ_{calc} , Mg m ⁻³	2.053	2.715
μ (Mo K α), mm ⁻¹	2.288	2.209
F(000)	876	752
θ range, deg	1.75 to 29.26	2.50 to 27.50
Index ranges	-15 ≤ h ≤ 15 -17 ≤ k ≤ 15 -17 ≤ l ≤ 17	-10 ≤ h ≤ 10 -7 ≤ k ≤ 8 -29 ≤ l ≤ 29
No. of reflns collected	16726	28767
Completeness to θ_{max}	97.9%	97.3%
No. indep. Reflns	7776	2640
No. obsd reflns with (I > 2 σ (I))	4479	1816
No. refined params	406	127
Goof (F ²)	0.943	1.048
R ₁ (F) (I > 2 σ (I))	0.0608	0.0535
wR ₂ (F ²) (all data)	0.1759	0.0788
Largest diff peak/hole, e Å ⁻³	1.007 / -3.305	1.631 / -1.398
CCDC number	1915290	1915291

the program WinGX 2002 (Farrugia, 1999). Full-matrix least-squares refinements on F^2 , using all data. All non-hydrogen atoms were refined using anisotropic displacement parameters. Hydrogen atoms attached to carbon atoms were included in geometrically calculated positions using a riding model and were refined isotropically. The hydrogen atoms attached to the oxygen atoms (expect O15) of **1** were located during the last

refinement cycle and refined isotropically. Crystal and refinement data are collected in Table 1. Figures were created using DIAMOND (Brandenburg and Putz, 2006). Crystallographic data for the structural analyses have been deposited with the Cambridge Crystallographic Data Centre. Copies of this information may be obtained free of charge from The Director, CCDC, 12 Union Road, Cambridge CB2 1EZ, UK (Fax: +44-1223-336033; e-mail: deposit@ccdc.cam.ac.uk or http://www.ccdc.cam.ac.uk).

Acknowledgements: The Deutsche Forschungsgemeinschaft (DFG) is gratefully acknowledged for financial support.

References

- Beckmann J., Dakternieks D., Duthie A., Ribot F., Schürmann M., Lewcenko N.A., New Insights into the Structures of Diorganotellurium Oxides. The First Polymeric Diorganotelluroxane [(p-MeOC₆H₄)₂TeO]_n. *Organometallics*, 2003, 22, 3257-3261.
- Brandenburg K., Putz H., DIAMOND V3.1d. Crystal Impact GbR, Bonn, Germany, 2006.
- Cauquis G., Maurey-Mey M., Formation d'un sel complexe par oxidation de la phénoxatellurine. *Bull. Soc. Chim. Fr.*, 1973.
- Drew H.D.K., Cyclic Organometallic Compounds. Part I. Compounds of Tellurium. *J. Chem. Soc.*, 1926a, 223-231.
- Drew H.D.K., Cyclic Organometallic Compounds. Part II. Tellurylium Compounds, a New Series of Intensely Coloured Tellurium Derivatives. The Migration of Anions in Solids. *J. Chem. Soc.*, 1926b, 3054-3071.
- Farrugia L.J., Win GX suite for small-molecule single-crystal crystallography. *J. Appl. Crystallogr.*, 1999, 32, 837-838.
- Kertesz M., Pancake Bonding: An Unusual Pi-Stacking Interaction. *Chem. Eur. J.*, 2019, 25, 400-416.
- Mostaghimi F., Lork E., Hong I., Roemmele T.L., Boeré R.T., Mebs S., et al., The Reaction of Phenoxatellurine with Single-Electron Oxidizers Revisited. *New J. Chem.*, 2019, 43, 12754-12766.
- Smith M.R., Mangion M.M., Zingaro R.A., Meyer E.A., The crystal structure of phenoxatellurine, C₁₂H₈O₅Te. *J. Heterocyclic Chem.*, 1973, 10, 527-531.
- Witzinger R., Neue Ergebnisse der Auxochromtheorie: II Über amphotere Auxochrome. *Z. Angew. Chem.*, 1929, 42, 668-670.

2.5. *fac*-Bis(Phenoxatellurine) Tricarbonyl Manganese(I) Bromide

2.5.1. Synopsis

The reaction of phenoxatellurine (PT) with manganese pentacarbonyl chloride leads to bis-(phenoxatellurin)-tricarbonyl-manganese(I)-chloride ($\text{Mn}(\text{PT})_2(\text{CO})_3\text{Cl}$).^[142] Due to the characterization via infrared absorption the position of the phenoxatellurine (PT) units could only be assumed as presented in Figure 13.

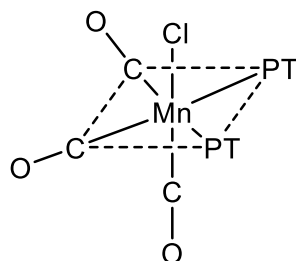


Figure 13. Suggested orientation of the substituents in the bis-(phenoxatellurin)-tricarbonyl-manganese(I)-bromide ($\text{Mn}(\text{PT})_2(\text{CO})_3\text{Cl}$) structure.^[142]

The aim of this work was to report the spatial arrangement of the substituents within the structure using the closely related $(\text{CO})_5\text{MnBr}$. Via X-ray analysis, the crystal structure was determined showing the arrangement predicted by Hieber and Kuck.

2.5.2. Experimental Contributions

In this study, I carried out the synthesis of the compounds and their characterization. Moreover I wrote the experimental section and the manuscript with Prof. Dr. Jens Beckmann. X-ray analysis and structure refinements have been made by Dr. Enno Lork. The article was published in the following journal:

Mostaghimi, F.; Lork, E.; Beckmann, J. *fac*-Bis(phenoxatellurine) tricarbonyl manganese(I) bromide. *Main Group Metal Chemistry* **2020**, 43, 181–183. DOI: 10.1515/mgmc-2020-0022.

Short Communication

Open Access

Farzin Mostaghimi, Enno Lork and Jens Beckmann*

fac-Bis(phenoxatellurine) tricarbonyl manganese(I) bromide

<https://doi.org/10.1515/mgmc-2020-0022>

Received July 22, 2020; accepted September 22, 2020.

Abstract: The reaction of $(\text{CO})_5\text{MnBr}$ with phenoxatellurine (PT) provided the octahedral complex *fac*- $(\text{CO})_3(\text{PT})_2\text{MnBr}$ in which the two PT ligands are situated in *cis*-position.

Keywords: manganese; tellurium; metal carbonyl complex; phenoxatellurine

Hieber's pioneering work on metal carbonyls laid the foundation for the field of organometallic chemistry (Hieber, 1970). Whilst researching the substitution of CO by alternative ligands, his group also studied the reaction of $(\text{CO})_5\text{MnCl}$ with phenoxatellurine (PT), which provided $(\text{CO})_3(\text{PT})_2\text{MnCl}$ (**1**) as octahedral complex with an unknown constitution (Scheme 1) (Hieber and Kruck, 1962).

Recently, we (re-)investigated the single-electron oxidation of PT (Mostaghimi et al., 2019a, 2019b) and the preparation of charge-transfer complexes with PT (Chulanova et al., 2017), which prompted us study the closely related reaction of $(\text{CO})_5\text{MnBr}$ with PT that afforded an analogous complex *fac*- $(\text{CO})_3(\text{PT})_2\text{MnBr}$ (**2**) as colourless, low-melting solid (Scheme 1). Although **2** was reasonably soluble in many solvents including chloroform and dichloromethane, no reasonable NMR spectra were acquired, which was tentatively attributed to the paramagnetic nature of the sample. The molecular structure of **2** is shown in Figure 1 and selected bond parameters are collected in the caption of the figure. Crystal and refinement data are listed in Table 1.

The spatial arrangement of the manganese atom is octahedral and defined by a $\text{C}_3\text{Te}_2\text{Br}$ donor set. The three CO ligands are arranged in a facial manner, which is consistent with the observation of three intense CO stretching vibrations at $\tilde{\nu} = 2007$, 1943 and 1905 cm^{-1} . For the starting material $(\text{CO})_5\text{MnBr}$, the IR spectrum

shows two intense CO stretching vibrations at $\tilde{\nu} = 2055$ and 1999 cm^{-1} and in addition six minor intense CO stretching vibrations (Kaes, et al., 1967). The two PT ligands adopt butterfly conformations and are situated in *cis*-position to each other. The degree of folding within the butterfly conformation may be quantified by the fold angle α between the planes defined by the two phenyl rings and the Te and O atoms. The fold angles α of **2** (Te1: 34.4°, Te2: 37.8°) are very similar to than in the free PT (37.5°) (Mostaghimi et al., 2019a). The Te-Mn bond lengths of **2** (2.612(8) and 2.650(6) Å) are substantially longer than those of *peri*-substituted acenaphthyl (Ace)-based complexes *fac*- $(6\text{-Ph}_2\text{P-Ace-5-})_2\text{TeMn}(\text{CO})_3\text{Br}$ (2.599(1) Å) and $(6\text{-Ph}_2\text{P-Ace-5-})_2\text{Mn}(\text{CO})_2\text{Br}$ (2.546(1) Å) (Do et al., 2018).

Experimental

Synthesis of *fac*- $(\text{CO})_3(\text{PT})_2\text{MnBr}$ (**2**)

In a 25 mL J. Young tube, a solution of PT (470 mg, 1.6 mmol) in absolute ethanol (20 mL) was added to $(\text{CO})_5\text{MnBr}$ (200 mg, 0.7 mmol). The mixture was heated to 50°C. After the $(\text{CO})_5\text{MnBr}$ had entirely dissolved, the solvent was evaporated to dryness. The solid residue was dissolved in the minimum amount of dry dichloromethane. This solution was carefully layered by the same volume of hexane. Slow diffusion of the solvents induced crystallization of the product, which was obtained as orange needles (450 mg, 79% yield; Mp.: 75°C dec.).

MS (ESI, positive, $\text{CH}_2\text{Cl}_2/\text{CH}_3\text{CN}$ 1:10, 3 $\mu\text{L}/\text{min}$): m/z (rel. Int) = 537 (100%) [$\text{M}\cdot\text{PT}+\text{Na}$], 521 (56%) [$\text{M}\cdot\text{PT}+\text{Li}$], 437 (55%) [$\text{Mn}(\text{CO})_3\text{PT}$].

X-ray crystallography

Intensity data of **2** was collected on a Bruker Venture D8 diffractometer with graphite-monochromated Mo-K α (0.7107 Å) radiation. The structure was solved by

*Corresponding author: Jens Beckmann, Institut für Anorganische Chemie, Universität Bremen, Leobener Straße 7, 28359 Bremen, Germany; e-mail: j.beckmann@uni-bremen.de

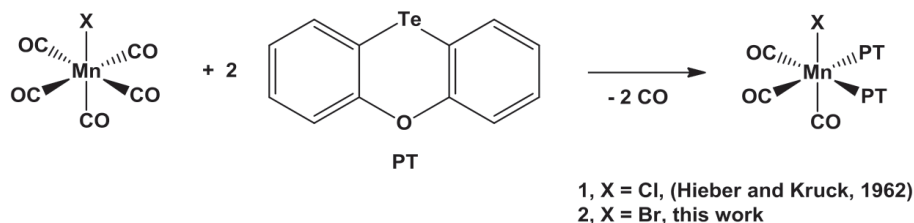
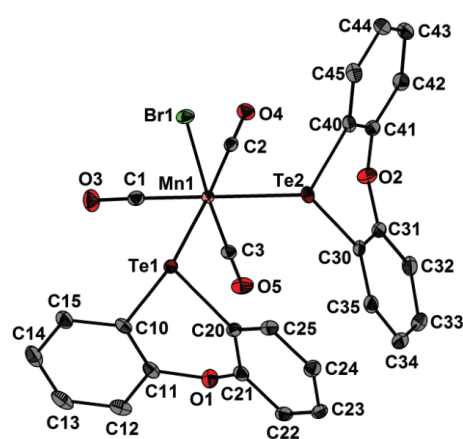
Scheme 1: Reaction of $(\text{CO})_3\text{MnX}$ ($X = \text{Cl}, \text{Br}$) with phenoxatellurine (PT).

Figure 1: Molecular structure of *fac*-(CO)₃(PT)₂MnBr (2) showing 50% probability ellipsoids and the crystallographic numbering scheme. Selected bond parameters [Å]: Mn1-Te1 2.650(6), Mn1-Te2 2.612(8), Mn1-C1 1.814(4), Mn1-C2 1.811(1), Mn1-C3 1.774(4), Mn1-Br1 2.524(2), Te1-Mn1-Te2 89.01(6), Te1-Mn1-Br1 86.19(0), Te1-Mn1-C1 87.61(4), Te1-Mn1-C2 175.32(5), Te1-Mn1-C3 95.18(0), Te2-Mn1-Br1 83.52(7), Te2-Mn1-C1 175.64(3), Te2-Mn1-C2 91.26(5), Te2-Mn1-C3 92.91(9).

direct methods and difference Fourier synthesis with subsequent Full-matrix least-squares refinements on F^2 , using all data (Dolomanov, 2009). All non-hydrogen atoms were refined using anisotropic displacement parameters. Hydrogen atoms were included in geometrically calculated positions using a riding model. Crystal and refinement data are collected in Table 1. Figure 1 was created using DIAMOND (Brandenburg and Putz, 2006). Crystallographic data for the structural analysis has been deposited with the Cambridge Crystallographic Data Centre, CCDC numbers 2017546.

Table 1: Crystal data and structure refinement of $(\text{C}_{12}\text{H}_8\text{OTe})_2(\text{CO})_3\text{MnBr}$.

Formula	$\text{C}_{27}\text{H}_{16}\text{BrMnO}_5\text{Te}_2$
Formula weight, g mol^{-1}	810.45
Crystal system	orthorhombic
Crystal size, mm	$0.60 \times 0.60 \times 0.50$
Space group	$Pna2_1$
a , Å	19.208(5)
b , Å	20.513(5)
c , Å	6.428(5)
V , Å ³	2533(2)
Z	4
ρ_{calc} , Mg m^{-3}	2.125
T , K	100
μ (Mo $K\alpha$), mm^{-1}	4.394
$F(000)$	1528
θ range, deg	2.25 to 30.08
Index ranges	$-27 \leq h \leq 27$ $-28 \leq k \leq 28$ $-9 \leq l \leq 9$
No. of reflns collected	229503
Completeness to θ_{max}	99.9%
No. indep. Reflins	7419
No. obsd reflns with $(I > 2\sigma(I))$	7227
No. refined params	130
Goof (F^2)	1.047
R_1 (F) ($I > 2\sigma(I)$)	0.0119
wR_2 (F^2) (all data)	0.0252
Flack parameter	0.008(2)
$(\Delta/\sigma)_{\text{max}}$	< 0.001
Largest diff peak/hole, $\text{e} \text{ \AA}^{-3}$	0.261 / -0.492

Copies of this information may be obtained free of charge from The Director, CCDC, 12 Union Road, Cambridge CB2 1EZ, UK (Fax: +44-1223-336033; e-mail: deposit@ccdc.cam.ac.uk or <http://www.ccdc.cam.ac.uk>).

Conflict of interest: One of the authors (Jens Beckmann) is a member of the Editorial Board of Main Group Metal Chemistry.

References

- Brandenburg K., Putz H., DIAMOND V3.1d, Crystal Impact GbR, 2006.
- Chulanova E.A., Pritchina E.A., Malaspina L.A., Grabowsky S., Mostaghimi F., Beckmann J., et al., Novel Charge-Transfer Complexes with 1,2,5-Thiadiazoles as Both Electron Acceptors and Donors Featuring an Unprecedented Addition Reaction. *Chem. Eur. J.*, 2017, 23, 852-864.
- Do T.G., Hupf E., Lork E., Beckmann J., Bis(6-diphenylphosphino-acenaphth-5-yl)telluride as Ligand Towards Manganese and Rhenium Carbonyls. *Molecules*, 2018, 23, 2805.
- Dolomanov O.V., Bourhis L.J., Gildea R.J., Howard A.K., Puschmann H., OLEX2: a complete structure solution, refinement and analysis program. *J. Appl. Cryst.*, 2009, 42, 339-341.
- Hieber W., Kruck T., Tellurorganyl-haltige Metallcarbonyle. *Chem. Ber.*, 1962, 95, 2027-2041.
- Hieber W., Metal Carbonyls, forty years of research. *Adv. Organomet. Chem.*, 1970, 8, 1-28.
- Kaeszi H.D., Bau R., Hendrickson D., Smith J.M., Spectroscopic Studies of Isotopically Substituted Metal Carbonyls. I. Vibrational Analysis of Metal Pentacarbonyl Halides. *J. Am. Chem. Soc.*, 1967, 89, 2844-2851.
- Mostaghimi F., Bolsinger J., Lork E., Beckmann J., New Insights into the Oxidation of Phenoxatellurine with Sulfuric Acid. *Main Group Met. Chem.*, 2019a, 42, 150-152.
- Mostaghimi F., Lork E., Hong I., Roemmele T.L., Boeré R.T., Mebs S., et al., The Reaction of Phenoxatellurine with Single-Electron Oxidizers Revisited. *New J. Chem.*, 2019b, 43, 12754-12766.

2.6. Synthesis and Structure of 2,8-Dimethyl-10,10-dichlorophenoxatellurine

2.6.1. Synopsis

The synthesis and characterization of 2,8-dimethyl-10,10-dichlorophenoxatellurine is described in this work. Unlike phenoxatellurine and 10,10-dichlorophenoxatellurine, 2,8-dimethyl-10,10-dichlorophenoxatellurine reveals a planar ring structure.

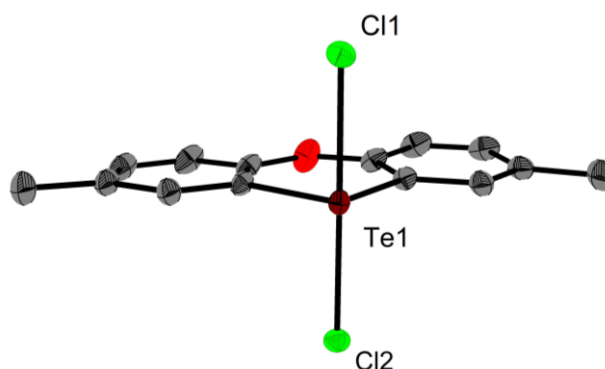


Figure 14. Molecular structure of 2,8-Dimethyl-10,10-dichlorophenoxatellurine.

2.6.2. Experimental Contributions

In this study, I carried out the synthesis of the compounds. The characterization was carried out with the help of Daniel Duvinage. Moreover I wrote the experimental section and the manuscript with Prof. Dr. Jens Beckmann. X-ray analysis and structure refinements have been made by Dr. Enno Lork. The article was published in the following journal:

Mostaghimi, F.; Duvinage, D; Lork, E.; Beckmann, J. *Synthesis and structure of 2,8-dimethyl-10,10-dichlorophenoxatellurine*. *Main Group Metal Chemistry* **2020**, 44, 9–11. DOI: <https://doi.org/10.1515/mgmc-2021-0002>.

Rapid Communication

Open Access

Farzin Mostaghimi, Daniel Duvinage, Enno Lork, and Jens Beckmann*

Synthesis and structure of 2,8-dimethyl-10,10-dichlorophenoxatellurine

<https://doi.org/10.1515/mgmc-2021-0002>
received July 22, 2020; accepted October 01, 2020

Abstract: The condensation of 4,4'-dimethyldiphenylether with tellurium tetrachloride yielded 2,8-dimethyl-10,10-dichlorophenoxatellurine (**3**), which was characterized by X-ray diffraction. Unlike the parent phenoxatellurine (**1**) and the 10,10-dichlorophenoxatellurine (**2**) showing butterfly conformations, **3** reveals a planar ring structure.

Keywords: tellurium, phenoxatellurine, diaryltellurium dichloride, secondary bonding

The chemistry of phenoxatellurine (**1**, Scheme 1), a heterocycle formally derived from dibenzodioxine in which one of the two oxygen atoms was replaced by a tellurium atom, has a long history that was covered in a review until 1995 (Gioabă and Gioabă, 1995).

It is assessable by reduction of 10,10-dichlorophenoxatellurine (**2**, Scheme 1), which can be easily obtained by condensation of diphenylether with tellurium tetrachloride (Drew, 1926). With 2-phenoxyphenyltellurium trichloride an intermediate of this condensation reaction was recently isolated and fully characterized (Toma, et al., 2016). We recently studied the electronic properties of a charge transfer complex between **1** and [1,2,5]thiadiazolo[3,4-c][1,2,5]thiadiazole (Chulanova et al., 2017) and (re-)investigated the single-electron oxidation of **1** giving rise to the formation of dicationic double- and triple-decker complexes (Mostaghimi et al., 2019a, 2019b). In context of this work, we also studied the condensation reaction of 4,4'-dimethyldiphenylether with tellurium tetrachloride, which afforded 2,8-dimethyl-10,10-dichlorophenoxatellurine (**2**) as slightly yellow crystalline product in 93% yield (Scheme 2).

* **Corresponding author: Jens Beckmann**, Institut für Anorganische Chemie, Universität Bremen, Leobener Straße 7, 28359 Bremen, Germany, e-mail: j.beckmann@uni-bremen.de

Farzin Mostaghimi, Daniel Duvinage, Enno Lork: Institut für Anorganische Chemie, Universität Bremen, Leobener Straße 7, 28359 Bremen, Germany

The ^{125}Te NMR chemical shift of **3** ($\delta = 596.4$ ppm) is nearly identical with that of **2** ($\delta = 594.4$ ppm). The crystal and molecular structure of **3** is shown in Figure 1. The key feature is the crystallographically imposed planarity of the 2,8-dimethylphenoxatellurine scaffold, which is in sharp contrast to the butterfly structures of the unsubstituted phenoxatellurine scaffolds of **1** (Smith et al., 1973), **2** (Korp et al., 1980), and **2**·1/2 NCMc (Mostaghimi, 2019b).

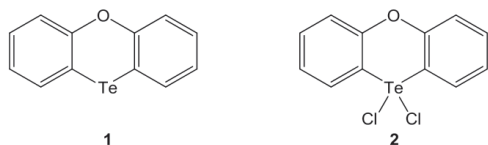
Like **2** (Korp et al., 1980) and other diaryltellurium dichlorides (Zukerman-Schpector and Haiduc, 2001), the spatial arrangement of the Te atom of **3** is trigonal bipyramidal when bearing in mind the stereochemically active lone pair. In this arrangement, the two crystallographically equivalent Cl atoms occupy the axial positions, whereas the two C atoms and the lone pair are situated in the equatorial positions. Without the lone pair, the structure can be also described as 'seesaw' arrangement. The primary Te–Cl bond length of **3** (2.537(1) Å) is consistent with those of **2** (2.478(3)–2.576(3) Å, Korp et al., 1980) and other diaryltellurium dichlorides (Zukerman-Schpector and Haiduc, 2001). In the crystal lattice, **3** forms a 2D coordination polymer defined by secondary Te...Cl interactions, unlike **2**, which give rise to discrete tetramers with 'cubane' like structures (Korp et al., 1980). The equivalent secondary Te1...Clb contacts of **3** (3.558(1) Å) are again comparable with those of **2** (3.368(4)–2.576(3) Å) and other diaryltellurium dichlorides (Zukerman-Schpector and Haiduc, 2001).

Experimental

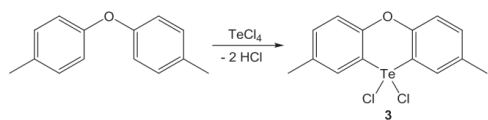
Synthesis of **3**

In a dried two necked flask equipped with a condenser and a moist guard 5.55 g (20.6 mmol, 1.00 eq.) tellurium tetrachloride and 4.08 g (20.6 mmol, 1.00 eq.) *p*-tolyl ether are heated slowly over the course of 4 h to 200°C under reflux. After cooling to room temperature the reddish brown solid is mortared into a fine powder and stirred

Open Access. © 2021 Farzin Mostaghimi et al., published by De Gruyter. This work is licensed under the Creative Commons Attribution 4.0 International License.



Scheme 1: Phenoxatellurine (1) and 10,10-dichlorophenoxatellurine (2).



Scheme 2: Condensation reaction of 4,4'-dimethyldiphenyl ether with tellurium tetrachloride providing 2,8-dimethyl-10,10-dichlorophenoxatellurine (3).

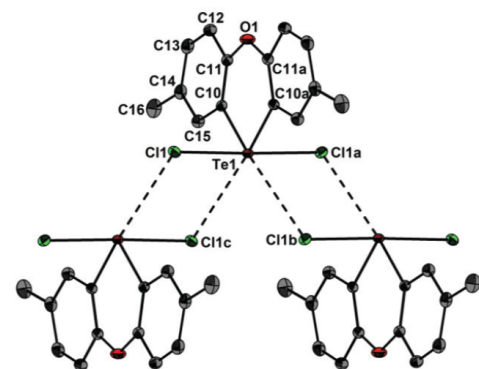


Figure 1: Crystal and molecular structure of **3** showing 30% probability ellipsoid and the essential atomic numbering. Symmetry codes: $a = 1-x, y, 0.5-z$; $b = x, 1-y, -0.5+z$; $c = 1-x, 1-y, 1-z$. Selected bond parameters [\AA , $^\circ$]: Te1-Cl1 2.536(8), Te1-Clb 3.558(1), Te1-C10 2.078(3), Cl1-Te1-Cl1a 178.37(4), C10-Te1-C10a 92.68(2).

in diethyl ether to dissolve unreacted *p*-tolyl ether. The solid is filtered off and the remaining product with traces of elemental tellurium is stirred in acetone and filtered again. Evaporation of the solvent gives 7.53 g (19.1 mmol, 93%) of **3** as a deep red crystalline solid.

^1H NMR (600 MHz, CDCl_3): $\delta = 7.67$ (s, 2H, $\text{C}_{\text{Ar}}\text{-H}$), 7.49 (d, $^3J_{\text{H-H}} = 8.45$ Hz, 2H, $\text{C}_{\text{Ar}}\text{-H}$), 7.39 (dd, $^3J_{\text{H-H}} = 8.45$ Hz, $^4J_{\text{H-H}} = 2.00$ Hz, 2H, $\text{C}_{\text{Ar}}\text{-H}$), 2.41 (s, 6H, CH_3) ppm. $^{13}\text{C}\{^1\text{H}\}$ NMR (151 MHz, CDCl_3): $\delta = 148.65$ (s, $\text{C}_{\text{Ar}}\text{-O}$), 135.55 (s, C_{Ar}), 135.23 (s, C_{Ar}), 135.23 (s, C_{Ar}), 132.28 (s, C_{Ar}), 119.87 (s, C_{Ar}), 115.72 (s, $\text{C}_{\text{Ar}}\text{-Te}$), 20.53 (s, CH_3) ppm. ^{125}Te NMR (190 MHz, CD_2Cl_2): $\delta = 596.40$ (s) ppm. EI-MS (70 eV, 200 $^\circ\text{C}$, direct injection) m/z (rel. Int.) = 367 (7) $[\text{M}]^+$, 361 (17) $[\text{M-Cl}]^+$, 326 (57)

Table 1: Crystal data and structure refinement of **3**

Formula	$\text{C}_{14}\text{H}_{12}\text{Cl}_2\text{O}\text{Te}$
Formula weight, g mol^{-1}	394.74
Crystal system	monoclinic
Crystal size, mm	$0.08 \times 0.06 \times 0.04$
Space group	$\text{C2}/c$
a , \AA	18.6738(7)
b , \AA	10.0086(3)
c , \AA	7.7964(3)
α , $^\circ$	90.00
β , $^\circ$	97.676(1)
γ , $^\circ$	90.00
V , \AA^3	1444.08(9)
Z	4
ρ_{calcd} , Mg m^{-3}	1.816
T , K	100
μ (Mo $K\alpha$), mm^{-1}	1.966
$F(000)$	760
θ range, deg	2.31 to 35.03
Index ranges	$-30 \leq h \leq 30$ $-16 \leq k \leq 16$ $-12 \leq l \leq 12$
No. of refls collected	22659
Completeness to θ_{max}	98.4%
No. indep. Reflins	3181
No. obsd refls with ($>2\sigma(I)$)	2788
No. refined params	84
Goof (F^2)	1.113
R_1 (F) ($I > 2\sigma(I)$)	0.0267
wR_2 (F^2) (all data)	0.0808
$(\Delta/\sigma)_{\text{max}}$	< 0.001
Largest diff peak/hole, e \AA^{-3}	0.898/−1.479

$[\text{M-2Cl}]^+$, 196 (100) $[\text{M-Te}]^+$. UV/Vis (CH_2Cl_2): λ_{max} 275 nm, 305 nm, 386 nm, 518 nm.

HRMS ESI ($\text{CH}_2\text{Cl}_2/\text{MeCN}$ 1:10 + 1% water): $[\text{M-2Cl+OH}]^+$ calculated for $\text{C}_{14}\text{H}_{13}\text{O}_2\text{Te}$, $m/z = 342.99723$; found, 342.99711. No signal was found without the addition of water.

Decomp. point: 263 $^\circ\text{C}$

X-ray crystallography

Intensity data of **3** was collected on a Bruker Venture D8 diffractometer with graphite-monochromated Mo- $K\alpha$ (0.7107 \AA) radiation. The structure was solved by direct methods and difference Fourier synthesis with subsequent Full-matrix least-squares refinements on F^2 , using all data (Farrugia, 1999). All non-hydrogen atoms were refined using anisotropic displacement parameters. Hydrogen atoms attached to carbon atoms were included in geometrically calculated positions using a riding model. Crystal and refinement data are collected in Table 1. Figures were

created using DIAMOND (Brandenburg and Putz, 2006). Crystallographic data for the structural analysis has been deposited with the Cambridge Crystallographic Data Centre, CCDC number 1976524. Copies of this information may be obtained free of charge from The Director, CCDC, 12 Union Road, Cambridge CB2 1EZ, UK (Fax: +44-1223-336033; e-mail: deposit@ccdc.cam.ac.uk or <http://www.ccdc.cam.ac.uk>).

Conflict of interest: One of the authors (Jens Beckmann) is a member of the Editorial Board of Main Group Metal Chemistry.

References

- Brandenburg K., Putz H., DIAMOND V3.1d, Crystal Impact GbR, 2006.
- Chulanova E.A., Pritchina E.A., Malaspina L.A., Grabowsky S., Mostaghimi F., Beckmann J., et al., New Charge-Transfer Complexes with 1,2,5-Thiadiazoles as Both Electron Acceptors and Donors Featuring an Unprecedented Addition Reaction. *Chem. Eur. J.*, 2017, 23, 852-864.
- Drew H.D.K., Cyclic organo-metallic compounds. Part I. Compounds of tellurium. *J. Chem. Soc.*, 1926, 129, 223-231.
- Farrugia L.J., WinGX suite for small-molecule single-crystal crystallography. *J. Appl. Crystal.*, 1999, 32, 837-838.
- Gioabă A.N., Gioabă A.A., Chemistry of phenoxatellurine. *Roum. Chem. Q. Rev.*, 1995, 3, 303-327.
- Korp J.D., Bernal I., Turley J.C., Martin G.E., Crystal and Molecular Structure of Phenoxatellurine 10,10-Dichloride. *Inorg. Chem.*, 1980, 19, 2556-2560.
- Mostaghimi F., Bolsinger J., Lork E., Beckmann J., New insights into the oxidation of phenoxatellurine with sulfuric acid. *Main Group Met. Chem.*, 2019a, 42, 150-152.
- Mostaghimi F., Lork E., Hong I., Roemmele T.L., Boeré R., Mebs S., Beckmann J., The reaction of phenoxatellurine with single-electron oxidizers revisited. *New. J. Chem.*, 2019b, 43, 12754-12766.
- Smith M.R., Mangion M.M., Zingaro R.A., Meyer E.A., The crystal structure of phenoxatellurine, C₁₂H₈O₂Te. *J. Heterocycl. Chem.*, 1973, 10, 527-531.
- Toma A.M., Nicorară A., Silvestru A., Ruffer T., Lang H., Mehring M., Bis(2-phenoxyphenyl)dichalcogenides and their chemical reactivity. *J. Organomet. Chem.*, 2016, 810, 33-39.
- Zukerman-Schpector J., Haiduc I., Diorganotellurium(IV) dihalides and secondary bonding: revisiting the coordination polyhedral. *Phosphorus Sulfur*, 2001, 171, 73-112.

2.7. Synthesis and Crystal Structure of Phenoxaiodonium Tosylate

2.7.1. Introduction & Results

The synthesis and structure of the title compound, dibenzo[*b,e*][1,4]iodaoxin-5-ium 4-methylbenzenesulphonate $[\text{C}_{12}\text{H}_8\text{OI}][\text{O}_3\text{S}(p\text{-C}_6\text{H}_4\text{Me})]$, was reported. The phenoxaiodonium cation $[\text{C}_{12}\text{H}_8\text{OI}]^+$ **[6]**⁺ was compared to the isoelectronic neutral phenoxatellurine $\text{C}_{12}\text{H}_8\text{OTe}$. In recent years diaryliodonium salts received considerable attention as building blocks in organic synthesis and pharmacology.^[143] The phenoxaiodonium ion, $[\text{C}_{12}\text{H}_8\text{OI}]^+$ **[6]**⁺, a potent inhibitor of flavin-containing enzymes^[144], was first prepared 55 years ago but never fully characterized.^[145] The phenoxaiodonium ion is isoelectronic with the neutral phenoxatellurine, $\text{C}_{12}\text{H}_8\text{OTe}$, possessing a butterfly structure.^[114] Upon single electron oxidation, phenoxatellurine gives rise to the planar radical cation, $[\text{C}_{12}\text{H}_8\text{OTe}]^+$, which rapidly undergoes aggregation to form double-decker and triple-decker structures.^[115,146]

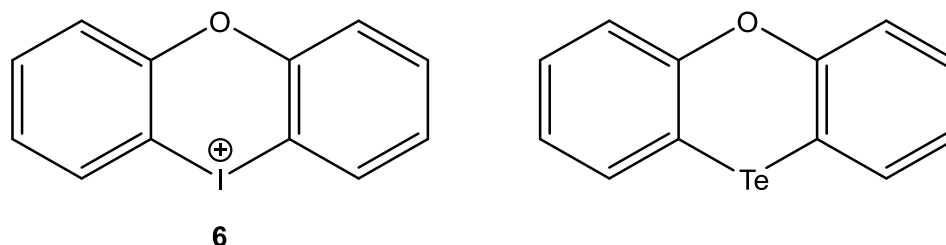
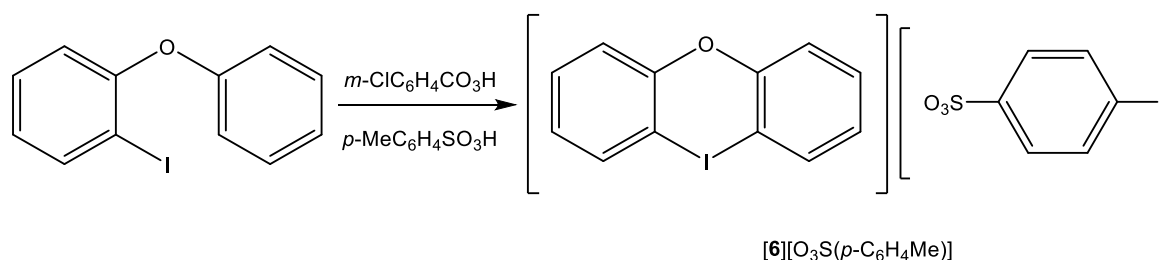


Figure 15. Phenoxaiodonium cation (left) and isoelectronic neutral phenoxatellurine (right).

In this work, the phenoxaiodonium ion **[6]**⁺ was obtained by oxidation of *o*-iodophenyl phenyl ether with *m*-chlorobenzoic peracid in the presence of *p*-toluene sulphonic acid and isolated as colourless crystalline tosylate salt **[6][O₃S(*p*-C₆H₄Me)]** in nearly quantitative yield (Scheme 16).



Scheme 16. Synthesis of phenoxaiodonium tosylate.

The crystal structure of **[6][O₃S(*p*-C₆H₄Me)]** is displayed in Figure 16. Selected bond parameters are collected in the caption of the figure. The phenoxaiodonium ion **[6]**⁺ adopts a butterfly conformation (fold angle $\alpha = 54.0^\circ$), which is more pronounced than in phenoxatellurine (fold angle $\alpha = 37.5^\circ$).^[115] The mean I-C bond length (2.096(2) Å) is identical within the experimental

error with the Te-C bond length (2.096(2) Å) and the C-I-C angle 87.66(7)° is only marginally smaller than the C-Te-C angle (88.98(6)°). In the crystal lattice, two phenoxaiodonium ions [6]⁺ and two tosylate ions are associated by secondary I ··· O contacts (2.726(2), 2.667(2) Å) via a crystallographic centre of inversion.

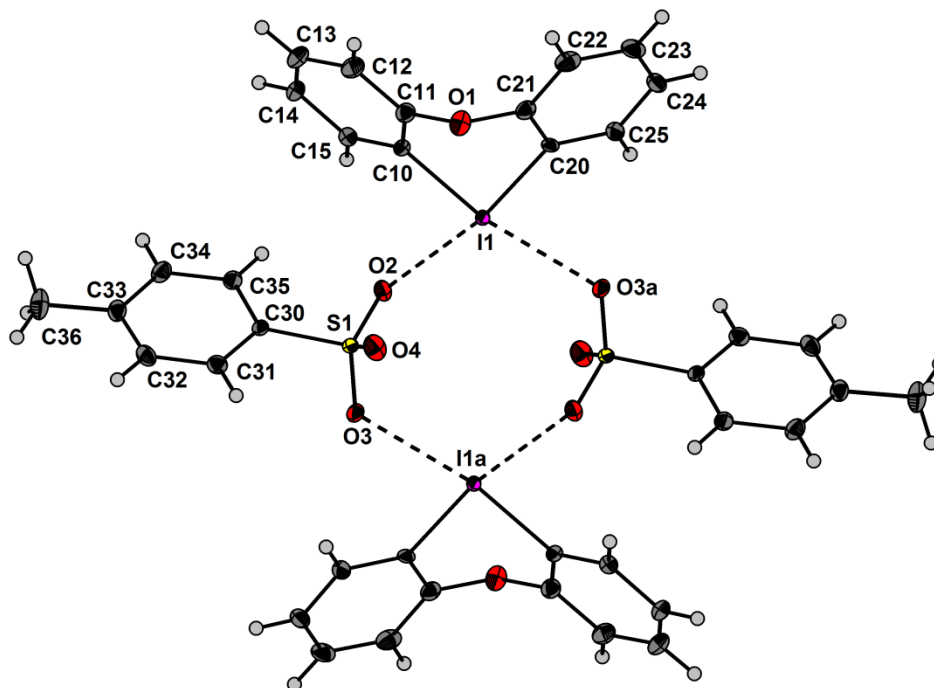


Figure 16. Crystal structure of [6][O₃S(*p*-C₆H₄Me)]. Selected bond parameters [°, Å]: I1-C10 2.098(2), I1-C20 2.093(2), C10-I1-C20 87.66(7), I1···O2 2.726(2), I1···O3a 2.667(2).

2.7.2. Experimental

Reagents were obtained commercially (Sigma-Aldrich, Germany) and were used as received. Dry solvents were collected from a SPS800 mBraun solvent system. Diethyl ether was dried over potassium hydroxide and distilled of sodium/benzophenone. The electrospray ionization mass spectrometry (ESI-MS) spectrum was obtained on the Bruker Impact II. Acetonitrile solutions were injected directly into the spectrometer at a flow rate of 3 µl min⁻¹. Nitrogen was used both as a drying gas and for nebulization with flow rates of approximately 4 L min⁻¹ and a pressure of 0.4 bar. The spectrum was collected for one minute and averaged. UV/vis spectra were recorded on a JASCO V-570 spectrometer.

2.7.2.1 Synthesis of [6][O₃S(*p*-C₆H₄Me)]

O-iodophenyl phenyl ether was prepared by the lithiation of diphenyl ether with *n*-butyllithium in THF at 0 °C for 4h and the subsequent addition of iodine in THF at -78 °C.^[147] O-iodophenyl phenyl ether was oxidized similar to examples in the literature by *meta*-chlorperoxybenzoic acid in the presence of *p*-toluene sulphonic acid to form the cyclic aryliodonium tosylate^[148]:

O-iodophenyl phenyl ether (200 mg, 0.68 mmol, 1.00 eq.) and *p*-toluenesulphonic acid (161 mg, 0.84 mmol, 1.25 eq.) were suspended in dry CH₂Cl₂ (20 ml) and stirred for 1 h, while the suspension turns yellow. Afterwards the suspension was cooled to 0 °C and *m*-chloroperoxybenzoic acid (146 mg, 0.84, 1.25 eq) was added, which turns the reaction mixture to dark violet and a white precipitate forms. After stirring overnight the solvent was removed under reduced pressure. The residue was washed with cold dry diethyl ether (3 × 10 ml) to remove remaining acids, dissolved again in a mixture of dry CH₂Cl₂ and dry *n*-hexane (1:1) and decanted off of possible remaining solids. Upon cooling the solution to –78 °C, [6][O₃S(*p*-C₆H₄Me)] (300 mg, 0.64 mmol, 94 %) was obtained as colourless crystals.

X-ray crystallography. Intensity data of [6][O₃S(*p*-C₆H₄Me)] was collected on a Bruker Venture D8 diffractometer with graphite-monochromated Mo-K α (0.7107 Å) radiation. The structure was solved by direct methods and difference Fourier synthesis with subsequent Full-matrix least-squares refinements on F^2 , using all data.^[140] All non-hydrogen atoms were refined using anisotropic displacement parameters. Hydrogen atoms were included in geometrically calculated positions using a riding model. Crystal and refinement data are collected in Table 7. Figures were created using DIAMOND.^[141]

Table 7. Crystal data and structure refinement of [6][O₃S(*p*-C₆H₄Me)].

<i>Formula</i>	<i>C₁₉H₁₅O₄S</i>
<i>Formula weight, g mol⁻¹</i>	466.29
<i>Crystal system</i>	triclinic
<i>Crystal size, mm</i>	0.08 × 0.07 × 0.06
<i>Space group</i>	<i>P</i> $\bar{1}$
<i>a, Å</i>	7.457(2)
<i>b, Å</i>	10.197(0)
<i>c, Å</i>	12.388(9)
<i>α, °</i>	100.423(1)
<i>β, °</i>	104.868(1)
<i>γ, °</i>	97.276(1)
<i>V, Å³</i>	880.5(3)
<i>Z</i>	2
<i>ρ_{calcd}, Mg m⁻³</i>	1.759
<i>T, K</i>	100
<i>μ (Mo Kα), mm⁻¹</i>	1.958
<i>F(000)</i>	460
<i>θ range, deg</i>	2.39 to 32.61
<i>Index ranges</i>	-11 ≤ <i>h</i> ≤ 11 -15 ≤ <i>k</i> ≤ 15 -18 ≤ <i>l</i> ≤ 18
<i>No. of reflns collected</i>	32469
<i>Completeness to θ_{max}</i>	99.9%
<i>No. indep. Reflns</i>	6418
<i>No. obsd reflns with (I > 2σ(I))</i>	5609
<i>No. refined params</i>	227
<i>GooF (F²)</i>	1.050
<i>R₁ (F) (I > 2σ(I))</i>	0.0279
<i>wR₂ (F²) (all data)</i>	0.0583
<i>(Δ/σ)_{max}</i>	< 0.001
<i>Largest diff peak/hole, e Å⁻³</i>	0.930 / -1.300

2.8. Synthesis and halogenation of bis(8-methoxynaphthyl)ditelluride

2.8.1. Synopsis

The utilization of diaryltellurides as starting materials in various organometallic reactions are well known. Bis(naphthyl)ditelluride and naphthytellurides with intramolecular coordinated N-donor substituents in *peri*-position to the tellurium atoms has been already described throughoutly.^[149,150]

This work reports naphthylbased telluriumorganyles with intramolecular O-donor substituents in *peri*-position, starting from 8-methoxynaphthyl lithium.

2.8.2. Experimental Contributions

In this work, I carried out part of the synthesis and characterization of the compounds and wrote the experimental section with Wiebke Wohltmann and Jens Bolsinger. Prof. Dr. Jens Beckmann was the principal investigator, designed the concept and wrote the manuscript. Single crystal X-ray diffraction measurements and structure refinements have been made by Dr. Enno Lork. Stefan Mebs did the DFT-calculations. The article was published in the following journal:

Wohltmann, W.; Mostaghimi, F.; Bolsinger, J.; Lork, E.; Mebs, S.; Beckmann, J. *Synthesis and halogenation of bis(8-methoxynaphthyl)ditelluride*. *Inorganica Chimica Acta* **2018**, 475, 73–82. DOI: 10.1016/j.ica.2017.08.011.



Contents lists available at ScienceDirect

Inorganica Chimica Acta

journal homepage: www.elsevier.com/locate/ica

Research paper

Synthesis and halogenation of bis(8-methoxynaphthyl)ditelluride

Wiebke Wohltmann^a, Farzin Mostaghimi^a, Jens Bolsinger^b, Enno Lork^a, Stefan Mebs^{c,*}, Jens Beckmann^{a,b,*}^a Institut für Anorganische Chemie und Kristallographie, Universität Bremen, Leobener Straße 7, 28359 Bremen, Germany^b Institut für Chemie und Biochemie, Freie Universität Berlin, Fabbeckstr. 34–36, 14195 Berlin, Germany^c Institut für Experimentalphysik, Freie Universität Berlin, Arnimallee 14, 14195 Berlin, Germany

ARTICLE INFO

Article history:

Received 29 June 2017

Received in revised form 1 August 2017

Accepted 3 August 2017

Available online 18 August 2017

1 Dedicated to Professor Ionel Haiduc on the occasion of his 80th birthday.

ABSTRACT

The intramolecularly coordinated 8-methoxytellurium compounds (8-MeOC₁₀H₆)₂Te₂ (**3**), 8-MeOC₁₀H₆TeCl₃ (**7a**), 8-MeOC₁₀H₆TeBr₃ (**7b**) and 5-Br-8-MeOC₁₀H₆TeBr₃ (**7c**) were prepared and fully characterized by multinuclear NMR spectroscopy, MS spectrometry and X-ray crystallography. The intramolecular Te–O coordination of **7a** and the related 6-diphenylphosphinoxy-acenaphthyl-5-tellurium trichloride (**6a**) as well as the related Te–N coordination of the 8-(dimethylamino)-naphthyltellurium trichloride (**5a**) were analyzed using a set of real-space bond indicators derived from DFT calculations and the electron density-based theories AIM, ELI-D and NCI. Similar electronic parameters were obtained for the weak Te–N and Te–O interactions in **5a** and **7a**, which are governed by σ -hole bonding. Additional electrostatic interactions between the terminal O atom and the Te atom in **6a** result in a significantly shorter and stronger Te–O contact compared to that in **7a**. This, in turn, leads to an elongation of the Te–Cl bond opposite to the Te–O bond.

© 2017 Elsevier B.V. All rights reserved.

1. Introduction

Diarylditellurides are versatile starting materials in organotellurium chemistry [1]. Well-known naphthyl-based examples include bis(naphthyl)ditelluride (**1**) [2] and bis(8-dimethylaminonaphthyl)ditelluride (**2**) [3], which contains intramolecularly coordinating N-donor substituents in *peri*-position to the Te atoms (Scheme 1). In this work, we describe the related bis(8-methoxynaphthyl)ditelluride (**3**), having intramolecularly coordinating O-donor substituents to compare the effect of the different donor atoms (Scheme 1).

The exhaustive halogenation of diarylditellurides usually gives rise to aryltellurium trihalides, which due to the enhanced Lewis acidity are often aggregated and as a result show a low solubility in most organic solvents [1]. Intramolecularly coordinating donor substituents reduce the Lewis acidity in aryltellurium trihalides by formation of intramolecular donor acceptor bonds and by blocking off potential coordination sites at the Te atom [4]. From the set of available intramolecularly coordinating donor substituents, those comprising *peri*-substituted (ace)-naphthyl scaffolds are considered very rigid, which permanently prevents dissociation of the intramolecular donor acceptor bonds [5]. Well-known (ace)naph-

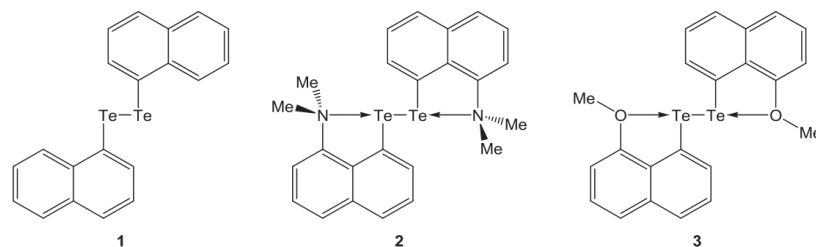
thyl-based examples include naphthyltellurium trichloride (**4a**) [6] and tribromide (**4b**) [7], 8-dimethylamino-naphthyltellurium trichloride (**5a**) [8] and tribromide (**5b**) [3] as well as the 6-diphenylphosphinoxy-acenaphthyl-5-tellurium trichloride (**6a**) and tribromide (**6b**) [9], which to the best of our knowledge have not yet been compared to examine the effect of the intramolecular coordination (Scheme 2). In this work, we extend this series by chlorination and bromination of the **3**, which provided 8-methoxynaphthyltellurium trichloride (**7a**) and tribromide (**7b**) and the related 8-methoxy-4-bromo-naphthyltellurium tribromide (**7c**), in which the bromination took place also at the aromatic ring (Scheme 2). The intramolecular donor-acceptor interactions of **5a–7a** are investigated with density functional theory (DFT) computations and subsequent analysis of a set of real-space bonding indicators (RSBI). Topological dissection of the calculated electron density (ED) according to the Atoms-in-Molecules (AIM) [10] space-partitioning scheme provides a bond paths motif, which resembles the molecular structure, as well as atomic/fragmental charges and volumes. The electronic properties at the bond critical points (bcps) connecting two adjacent atoms are used to characterize all types of chemical bonds [11]. Non-covalent interactions can be determined and visualized by the reduced electron density gradient, $s(\mathbf{r}) = [1/2(3\pi^2)^{1/3}|\nabla\rho|/\rho^{4/3}]$, according to the Non-Covalent Interactions Indicator (NCI) [12] approach. Mapping the second eigenvalue of the electron density Hessian, λ_2 , on the NCI surface discriminates steric/repulsive ($\lambda_2 > 0$), van-der-Waals like ($\lambda_2 \approx 0$), and attractive ($\lambda_2 < 0$) interactions from each other.

* Corresponding authors at: Institut für Anorganische Chemie und Kristallographie, Universität Bremen, Leobener Straße 7, 28359 Bremen, Germany (J. Beckmann).

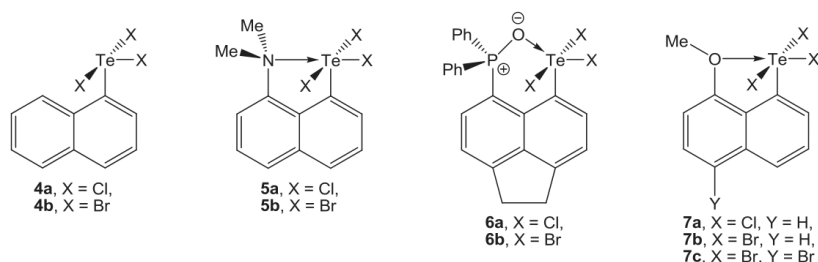
E-mail addresses: stebs@chemie.fu-berlin.de (S. Mebs), j.beckmann@uni-bremen.de (J. Beckmann).

<http://dx.doi.org/10.1016/j.ica.2017.08.011>

0020-1693/© 2017 Elsevier B.V. All rights reserved.



Scheme 1. Naphthyl-based diaryl ditellurides 1–3.



Scheme 2. (Ace-)Naphthyl-based aryltellurium trihalides 4–7.

Topological dissection of the pair density according to the Electron Localizability Indicator (ELI-D) [13] method provides core, bonding, and lone-pair basins, which can be integrated to give electron populations and volumes. ELI-D thus is especially useful for the analysis of covalent (including dative) bonds. Notably, ELI-D and NCI show complementary spatial distribution [14] suggesting spatial separation of covalent and non-covalent bonding aspects [15]. Dissecting ELI-D basins into contributions of AIM atoms forming this basin gives information about bond polarization and is called Raub-Jansen-Index (RJI) [16]. Homopolar contacts have values of 50%, which can become larger than 90–95% for dative bonds and larger than 99% for weak ionic and non-bonding contacts. Typical polar-covalent interactions are in the range between 70 and 90%. Mapping the electrostatic potential (ESP) on ED surfaces of the molecules under consideration or proper fragments helps to identify regions with increased Lewis acidity or basicity. Combining the mentioned RSBI facilitates monitoring (minute) electronic effects induced by small local changes in the geometry or electronic environment such as those induced by the intramolecular coordinating donor groups in *peri*-position.

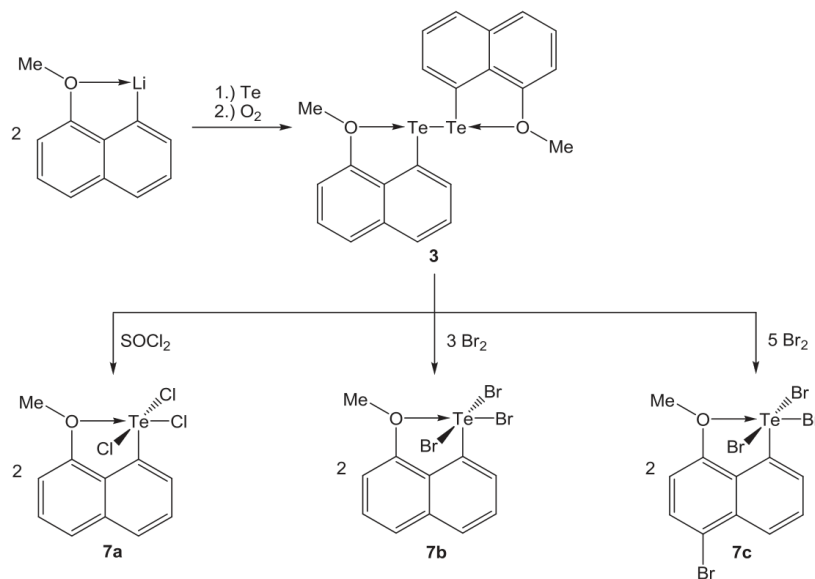
2. Results and discussion

2.1. Experimental aspects and characterization

The reaction of the well-known 8-methoxynaphthyl lithium [17] with Te powder and the subsequent oxidation of the lithium telluroate intermediate by molecular oxygen afforded bis(8-methoxynaphthyl)ditelluride (**4**) as orange-red crystalline solid in 51% yield (Scheme 3). It is characterized by a ^{125}Te chemical shift of $\delta = 415$ ppm, which compares well with that of bis(8-dimethylaminonaphthyl)ditelluride (**5**, $\delta = 433$ ppm) [18]. The molecular structure of **3** is shown in Fig. 1 and selected bond parameters of **1–3** are collected in Table 1 [3]. The C–Te–Te–C torsion angles of

3 ($100.55(5)^\circ$) is larger than 90° , which points to *transoid* conformation, whereas, the C–Te–Te–C torsion angles of the parent **1** ($86.96(1)^\circ$) [2] and **2** ($81.2(2)^\circ$) is smaller than 90° , which is indicative for a *cisoid* conformation [19]. The average Te–O coordination of **3** ($2.725(2)$ Å) and the average Te–N coordination of **2** ($2.721(5)$) are equal within the experimental error. The Te–Te bond length of the parent **1** ($2.711(1)$ Å) [2] is the shortest of all three ditellurides, but that of **3** ($2.713(1)$ Å) is nearly identical. However, the Te–Te bond length of **2** ($2.765(1)$ Å) is significantly longer, which is tentatively attributed to the fact that the N atom of **2** is a better donor than the O atom of **3**.

The chlorination of **3** to give 8-methoxy-naphthyltellurium trichloride (**7a**) was achieved with the rather unusual reagent thionyl chloride SOCl_2 (Scheme 2). In this way, **7a** was obtained as yellow crystalline solid in 91% yield. Neither the mechanism of the chlorination nor the by-products are known. The chlorination of **3** with the more rational reagent sulfuryl chloride SO_2Cl_2 gave mixtures of products, which contained **7a** and similar species that were chlorinated also at the aromatic ring. Attempts to separate these mixtures by fractional crystallization failed. The stoichiometry controlled bromination of **3** produced two products, namely, 8-methoxy-naphthyltellurium tribromide (**7b**) and 5-bromo-8-methoxy-naphthyltellurium tribromide (**7c**), which were isolated as yellow and orange crystals in yields of 33% and 82%, respectively (Scheme 3). The trichloride **7a** shows a ^{125}Te NMR chemical shift of $\delta = 1370$ ppm that is strongly reminiscent to those of **4a** (1373 ppm) and **5a** (1355 ppm). However, the tribromides **7b** and **7c** gave rise to ^{125}Te NMR chemical shifts of $\delta = 822$ and 733 ppm that differ substantially to those of **4b** (1348 ppm) and **5b** (1373 ppm) without any obvious reason. The molecular structures of **7a–7c** are shown in Fig. 2. In addition, the molecular structure of the previously known **5b** is presented in the ESI. Selected bond parameters of **4a–7a**, **4b–7b** and **7c** are collected in Table 2 [3]. Taking into account the CX_3 donor set (X = Cl, Br) and the lone pair, the spatial arrangement of the Te atoms can be described as



Scheme 3. Synthesis and halogenation of bis(8-methoxynaphthyl)ditelluride (3).

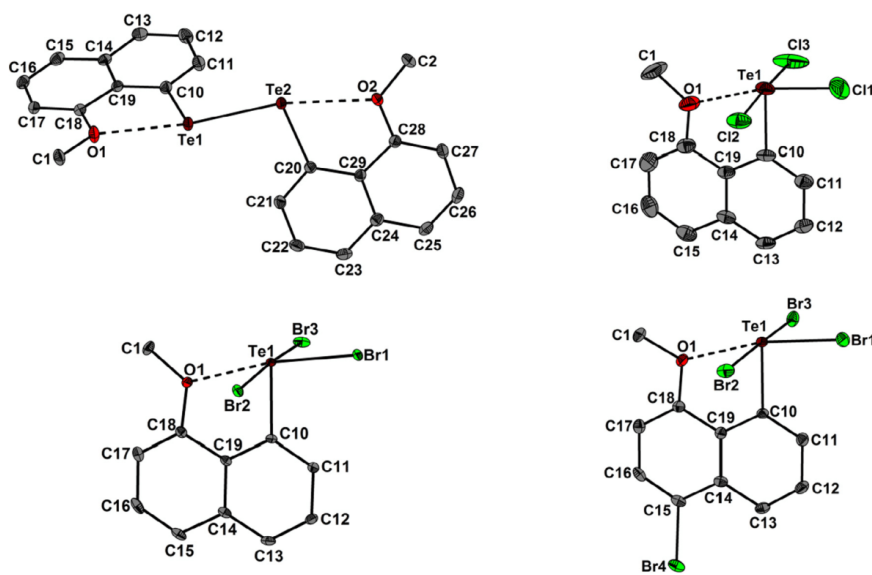


Fig. 1. Molecular structures of 3 (top left), 7a (top right), 7b (bottom left) and 7c (bottom right). The probability ellipsoids are set to 30% (7a) and 50% (3, 7b, 7c).

trigonal bipyramidal. Consistent with Bent's rule the equatorial Te–X_{eq} bond lengths are shorter than the axial Te–X_{ax} bond lengths. The Te–Cl_{eq} bond length increases in the order 7a (2.331(3) Å)

< 4a (2.334(3) Å) < 5a (2.442(2) Å) < 6a (2.466(1) Å). The Te–Br_{eq} bond length follows the same trend and increases in the order 7c (2.4913(4) Å) < 7b (2.4976(2) Å) < 4b (2.554(1) Å) < 5b (2.607

Table 1
Selected bond parameters [Å, °] of diaryl ditellurides 1–3.

	Te–Te	Te–C	Te–E	Te–Te–C	C–Te–Te–C
1 (E = null) [2]	2.711(1)	2.135(3)	–	97.96(9)	86.96(1)
2 (E = N) [3]	2.765(1)	2.126(5), 2.130(5)	2.699(5), 2.743(5)	99.5(1), 100.9(1)	81.2(2)
3 (E = N)	2.713(1)	2.159(1), 2.153(1)	2.718(1), 2.731(2)	100.85(4), 100.92(4)	100.55(5)

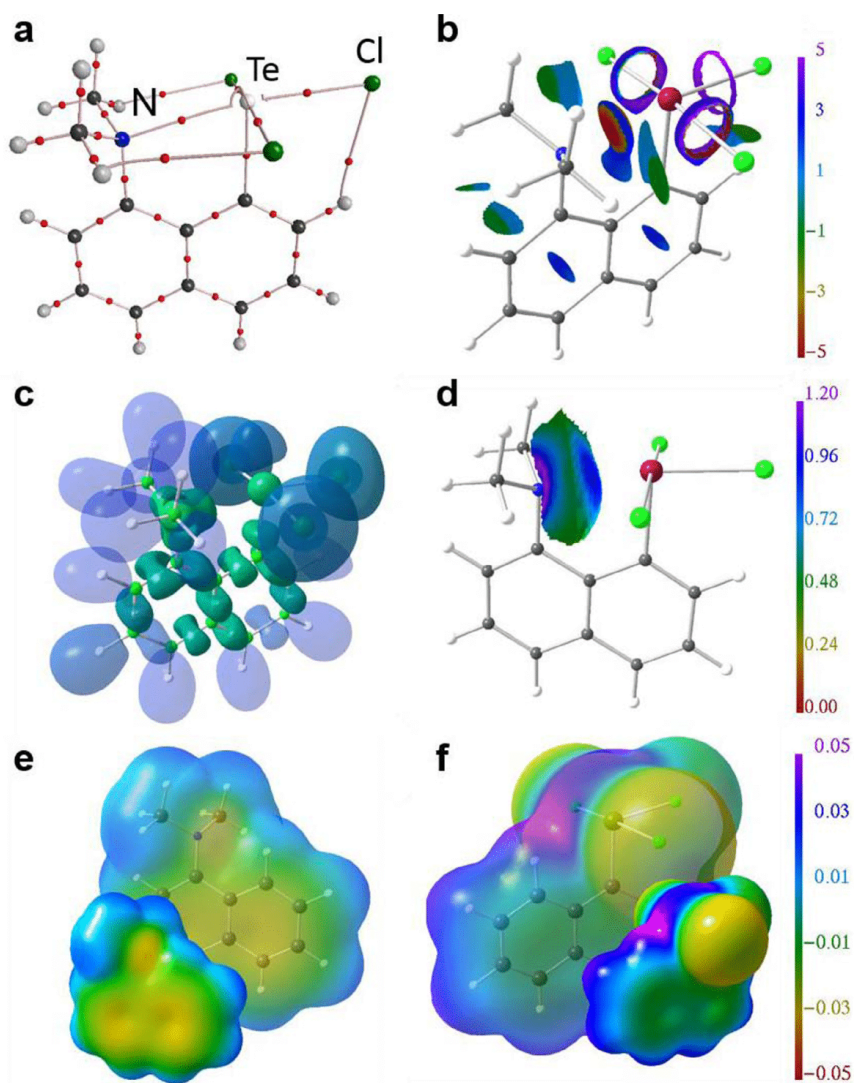


Fig. 2. (a) AIM-topology, (b) NCI *iso*-surface ($s(r) = 0.5$), (c) ELI-D *iso*-surface ($Y = 1.3$), and (d) ELI-D distribution mapped on relevant ELI-D basins for **5a**. (e) and (f) display the electrostatic potential in both transparent and solid mode mapped on 0.001 a.u. *iso*-surfaces of the electron density for compound fragments of **5a** lacking the donor or acceptor group. (e) Fragment is naphthylidimethylamine NapMe₂N (see Table 4) (f) Fragment is naphthyltellurium trichloride **4a**. Color-scheme: carbon – dark grey, hydrogen – light grey, tellurium – purple, chlorine – green, nitrogen – blue. (For interpretation of the references to color in this figure legend, the reader is referred to the web version of this article.)

Table 2
Selected bond parameters [Å, °] of the aryltellurium trihalides **4a–7a**, **4b–7b** and **7c**.

	Te–C	Te–E	Te–X _{eq}	Te–X _{ax}	E–Te–X _{eq}	X _{ax} –Te–X _{ax}
4a (E = null, X = Cl) [6]	2.115(5)	–	2.334(1)	2.382(1), 2.673(1)	–	171.93(5)
5a (E = N, X = Cl) [8]	2.105(3)	2.420(3)	2.442(2)	2.488(2), 2.529(2)	171.29(6)	172.17(3)
6a (E = N, X = Cl) [9]	2.137(2)	2.188(1)	2.466(1)	2.472(1), 2.532(1)	178.55(4)	174.73(2)
7a (E = O, X = Cl)	2.114(6)	2.466(6)	2.331(3)	2.446(2), 2.539(2)	169.41(13)	177.09(6)
4b (E = null, X = Br) [7]	2.130(1)	–	2.554(1)	2.517(1), 2.953(2)	–	173.11(5)
5b (E = N, X = Br) [3]	2.112(5)	2.434(5)	2.607(2)	2.646(2), 2.701(2)	172.6(1)	172.70(3)
6b (E = O, X = Br) [9]	2.143(2)	2.195(1)	2.626(1)	2.641(1), 2.701(1)	178.37(4)	177.143(8)
7b (E = O, X = Br)	2.124(2)	2.474(1)	2.4976(2)	2.6751(2), 2.6838(2)	171.70(3)	174.373(7)
7c (E = O, X = Br)	2.121(3)	2.519(2)	2.4913(4)	2.6713(4), 2.6806(4)	169.45(5)	174.847(13)

(2) Å) < **6b** (2.626(1) Å). In the parent aryltellurium trihalides, the difference between the axial Te–X_{ax} bond lengths is more pronounced than in the intramolecularly coordinated aryltellurium trihalides. The shortest intramolecular donor acceptor coordination is observed in the 6-diphenylphosphinoxy-acenaphthyl-5-tellurium trihalides **6a** and **6b**. The intramolecular Te–O contacts of 2.1881(1) and 2.195(1) Å nearly approach the 'standard' Te–O single bond lengths of [(*p*-MeOC₆H₄)₂TeO]_n (2.025(2) and 2.100(2) Å) [20]. Compared to these values, the intramolecular Te–O contacts of **7a** (2.466(6) Å), **7b** (2.474(1) Å) and **7c** (2.519(2) Å) are substantially longer. They are also slightly longer than the intramolecular Te–N contacts of **5a** (2.420(3) Å) and **5b** (2.434(5) Å), which reflects the better donor capability of the latter. In the solid state, two molecules of **7a–7c** are associated giving rise to the formation of centrosymmetric dimers via Te···Cl and Te···Br interactions of 3.557(2), 3.575(2) and 3.636(4) Å, respectively. Taking into account the CX₃E donor set of the first coordination sphere and the intermolecular X contact, the spatial arrangement of the Te atoms can also be described as distorted octahedral.

2.2. DFT calculations

The AIM bond topologies, NCI surfaces, ELI-D distributions, and ESPs mapped on the ED of fragments lacking the donor or acceptor group for DFT models **5a–7a** are displayed in Fig. 2–4. Topological and integrated AIM and ELI-D properties of all Te–X bonds (X = C, Cl) and Te–E contacts (E = O, N) are given in Table 3 and atomic or fragmental AIM charges are listed in Table 4. The Te–O and Te–N donor-acceptor interactions in **5a–7a** are dominated by non-covalent bonding aspects, which is reflected in low $\rho(\mathbf{r})$ values of 0.26–0.45 e Å³, positive signs of the Laplacian (1.7–3.9 e Å⁵), strongly positive $G/\rho(\mathbf{r})$ values of 0.51–0.80 a.u., low negative $H/\rho(\mathbf{r})$ values of –0.05 to –0.19 a.u., and RJI values above 99% (Table 3). This is further supported by the formation of NCI basins between Te and O/N (Figs. 2b–4b) and the formation of O and N lone-pair basins instead of Te–O and Te–N bonding basins (Figs. 2d–4d). Mapping the ESP on ED isosurfaces of molecular fragments lacking the intramolecularly coordinating donor group uncovers a Lewis acidic area opposite to the central chlorine atom (Figs. 2f–4f), suggesting σ -hole bonding to be present in all three compounds. Moreover, our DFT study shows that the electronic situation of the Te atom is similar in compound **7a** and **5a** despite the different donor atoms – O in **7a** and N in **5a**, and different from that in compound **6a** with a O atom. For **7a** and **5a** a disc-shaped Te–O/N NCI basin is observed, the red color of which indicates attractive non-covalent interactions, whereas a ring-shaped NCI basin is

observed for the ca. 0.3 Å shorter Te–O contact of **6a**, which indicates the onset of covalent bonding contributions. The ELI-D O and N lone-pair basin in **7a** and **5a** are flat in direction of the Te atom (Figs. 2d and 4d), but for **6a** a small deformation of the O atom lone-pair basin surface is visible (Fig. 3d). The reason for these differences is becoming evident by inspection of the ESP of the donor fragments, which only in the case of **6a** show a region of pronounced Lewis basicity at the terminal O atom, compare Fig. 3e with Figs. 2e and 4e. This leads to an enhanced polarization between donor and acceptor, which is also reflected in the AIM atomic charges of **7a**: $Q_{\text{AIM}}(\text{O}) = 1.16$ e, $Q_{\text{AIM}}(\text{Te}) = 1.69$ e and **6a**: $Q_{\text{AIM}}(\text{O}) = -1.46$ e, $Q_{\text{AIM}}(\text{Te}) = 1.76$ e, see Table 4. The Te–Cl bonds are also dominated by non-covalent contributions, as only for the Te–Cl bond opposite to the O–Te contact in **7a** a small Te–Cl ELI-D bonding basin is formed carrying 0.64 e, whereas for all other Te–Cl bonds the Cl atoms valence shells are denoted as lone-pair basins, see Table 3. Nevertheless, comparatively higher $\rho(\mathbf{r})$ values of 0.48–0.66 e Å³, smaller $G/\rho(\mathbf{r})$ values of 0.54–0.59 a.u., more negative $H/\rho(\mathbf{r})$ values of –0.32 to –0.45 a.u., RJI values between 95% and 98% and ring-shaped NCI basins are indicative for non-negligible covalent Te–Cl bond contributions. In all three cases the Te–Cl bond, which is located in the plane of the nap/ace-backbone is slightly shorter compared to the two Te–Cl bond perpendicular to the plane. On the contrary, the Te–C bonds are dominated by covalent contributions, which is characterized by high $\rho(\mathbf{r})$ values of 0.83–0.87 e Å³, negative signs of the Laplacian (–1.8 to –1.9 e Å⁵), even smaller $G/\rho(\mathbf{r})$ values of 0.39–0.41 a.u., even more negative $H/\rho(\mathbf{r})$ values of –0.54 to –0.55 a.u., and RJI values of 56–57% see Table 3. Accordingly, Te–C basins are formed in the ELI-D with electron populations of 2.2–2.3 e, but no T–C basins are observed in the NCI. In an overall picture both Te–Cl and Te–C bonds are hardly affected by the Te–O/N interaction. Tiny electron redistributions due to Te–O/N bond formation become apparent by comparing atomic and fragmental AIM charges of compounds **5a–7a** with the respective charges obtained for the fragments lacking the donor or acceptor group (Table 4). At first glance, the atomic charge of the donor atom (O or N) is little affected by the Te–O/N interaction (difference: 0.02–0.03 e). Whereas the P atom in **6a** gains 0.06 e, each Me or Ph group in **5a–7a** loses ca. 0.05 e, which results in an overall electron loss of 0.10 e (**5a**), 0.11 e (**6a**), and 0.02 e (**7a**) for the donor part. On the acceptor side the Te atoms are by 0.04–0.14 e more positive, whereas the central Cl atom (along the O/N–Te–Cl plane) gains ca. 0.15 e. The Cl atoms located perpendicular to the plane gain up to 0.04 e, resulting in an overall electron gain of 0.13 e (**5a**), 0.07 e (**6a**), and 0.07 e (**7a**) for the acceptor moiety. Notably, the

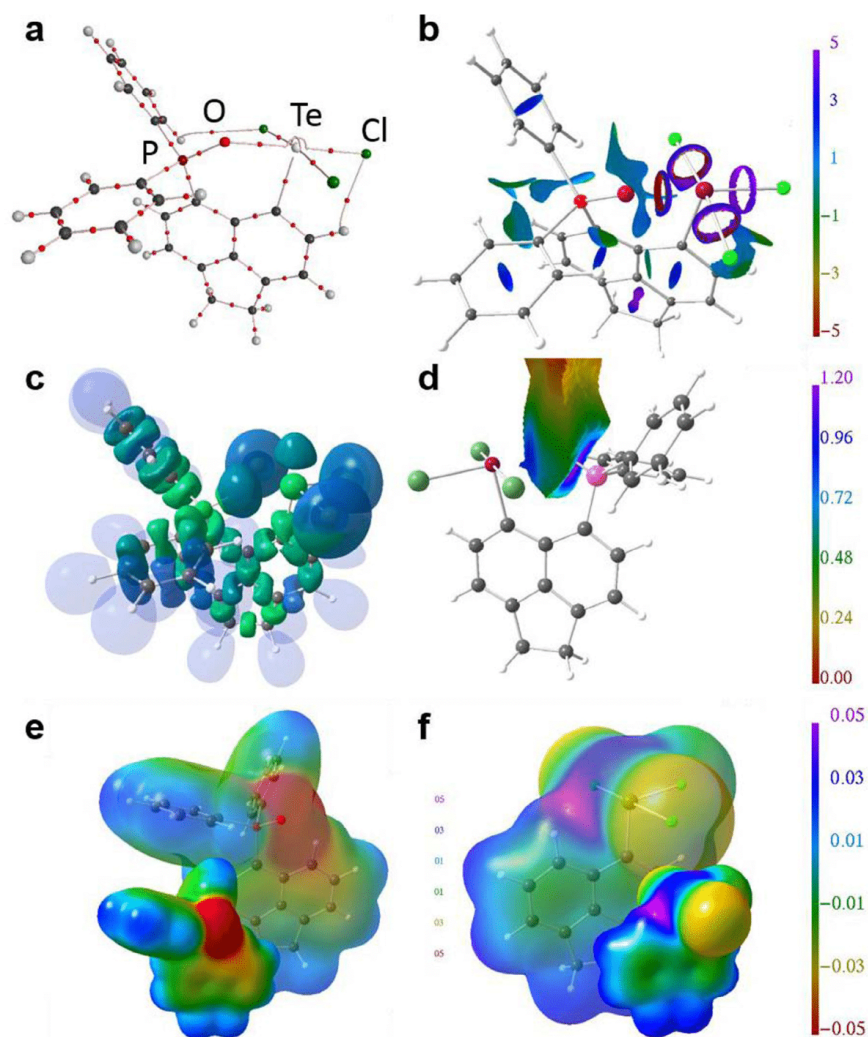


Fig. 3. (a) AIM-topology, (b) NCI iso-surface ($s(r) = 0.5$), (c) ELI-D iso-surface ($Y = 1.3$), and (d) ELI-D distribution mapped on relevant ELI-D basins for **6a**. (e) and (f) display the electrostatic potential in both transparent and solid mode mapped on 0.001 a.u. iso-surfaces of the electron density for compound fragments of **6a** lacking the donor or acceptor group. (e) Fragment is acenaphthylidiphenylphosphine oxide AcePh₂PO (see Table 4) (f) Fragment is acenaphthyltellurium trichloride **4a'**. Color-scheme: carbon - dark grey, hydrogen - light grey, tellurium - purple, chlorine - green, oxygen - red. (For interpretation of the references to color in this figure legend, the reader is referred to the web version of this article.)

AIM charges of the (ace)naphthyl backbones of models **5a–7a** can be estimated by adding the charges of the respective donor and acceptor fragments, e.g. for naphthyl in **5a**: 0.31 e (donor fragment) + -0.09 e (acceptor fragment) = 0.22 e (**5a**). Apparently, the electronic effect of donor and acceptor groups to the backbone parts simply add up to give the final charges (Table 4).

3. Conclusions

The first 8-methoxynaphthyltellurium compounds have been prepared, which add further examples to the rapidly growing com-

ound class of *peri*-substituted (ace)naphthyl species [21]. Due to the higher Lewis acidity of the Te atoms, the intramolecular Te–O coordination is shorter in the aryltellurium trihalides **7a–7c** than the diaryl ditelluride **3**. The calculated electrostatic potential of a fragment of **7a** lacking the OMe donor group shows that the Te–O interaction is determined by σ -hole bonding, which is induced by the coaxial Te–Cl bond. Corresponding computations of fragments **4a** and **4a'** lacking the TeCl_3 acceptor group proves the terminal O atom in the Ph₂PO group of **6a** to be a much stronger Lewis base compared to the methoxy atom in **7a**, which explains the significantly shorter Te–O contact in the former.

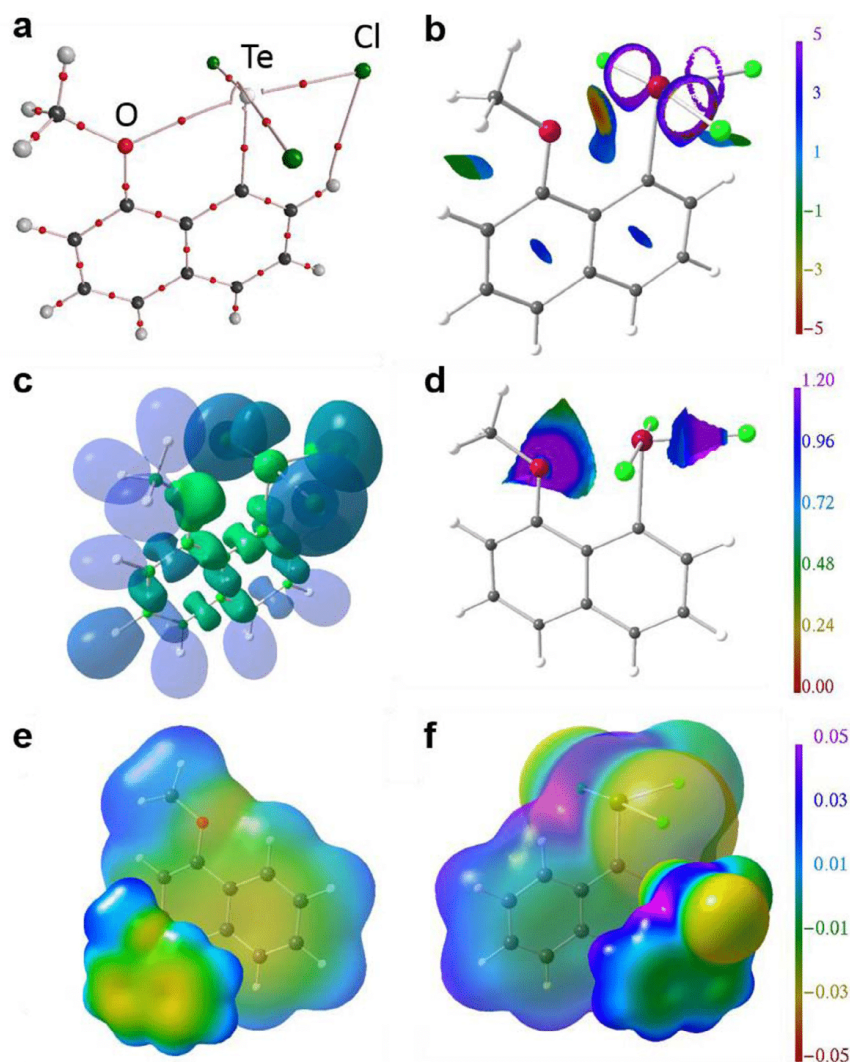


Fig. 4. (a) AIM-topology, (b) NCI iso-surface ($s(r) = 0.5$), (c) ELI-D iso-surface ($Y = 1.3$), and (d) ELI-D distribution mapped on relevant ELI-D basins for **7a**. (e) and (f) display the electrostatic potential in both transparent and solid mode mapped on 0.001 a.u. iso-surfaces of the electron density for compound fragments of **7a** lacking the donor or acceptor group. (e) Fragment is naphthylmethylether MeONap (see Table 4) (f) Fragment is naphthyltellurium trichloride **4a**. Color-scheme: carbon - dark grey, hydrogen - light grey, tellurium - purple, chlorine - green, oxygen - red. (For interpretation of the references to color in this figure legend, the reader is referred to the web version of this article.)

4. Experimental section

4.1. General

Reagents were obtained commercially and used as received. Dry Solvents were collected from a SPS800 mBraun solvent system. Manipulation of air-sensitive compounds was carried out under an argon atmosphere using standard Schlenk and glove-box techniques. ^1H -, ^{13}C - and ^{125}Te -NMR spectra were recorded at r.t. using a Bruker Avance-360 spectrometer and are referenced to tetram-

ethylsilane (^1H , ^{13}C) and dimethyl telluride (^{125}Te). Chemical shifts are reported in parts per million (ppm) and coupling constants (J) are given in Hertz (Hz). Electron impact mass spectroscopy (EIMS) was carried out using a Finnigan MAT 95.

4.2. Synthesis of bis(8-methoxy-naphthyl)ditellurid (**3**)

A solution of *tert*-butyl lithium (3.75 mL, 6.37 mmol) in hexane was slowly added to a solution of methoxynaphthalene (1.00 g, 6.37 mmol) in hexane (10 mL). Stirring for 36 h at room tempera-

Table 3
Electronic bond parameters of Te–X bonds (X = C, Cl) and Te–E contacts (E = O, N) of **5a–7a**.

	Contact	d [Å]	$\rho(r)$ [eÅ ⁻³]	$\nabla^2\rho(r)$ [eÅ ⁻⁵]	ϵ	G/ $\rho(r)$ [a.u.]	H/ $\rho(r)$ [a.u.]	N _{ELI} [e]	V _{ELI} [Å ³]	γ_{ELI}	RJI [%]
6a	Te–O	2.270	0.45	3.9	0.07	0.80	–0.19	6.13	15.9	1.63	99.5
5a	Te–N	2.565	0.33	1.7	0.09	0.51	–0.17	1.99	4.2	1.83	99.0
7a	Te–O	2.556	0.26	2.4	0.03	0.71	–0.05	4.70	5.1	1.70	99.9
6a	Te–Cl2	2.424	0.58	1.4	0.05	0.57	–0.40	7.78 [*]	17.6 [*]	1.69	94.9
5a	Te–Cl2	2.399	0.61	1.3	0.06	0.56	–0.41	7.78 [*]	17.4 [*]	1.67	94.6
7a	Te–Cl2	2.351	0.66	1.4	0.06	0.59	–0.45	7.13 [*]	16.5 [*]	1.68	98.1
								0.64	1.0	1.40	50.2
6a	Te–Cl3	2.504	0.50	1.4	0.06	0.54	–0.34	7.76 [*]	18.7 [*]	1.65	95.8
6a	Te–Cl4	2.528	0.48	1.5	0.06	0.54	–0.32	7.75 [*]	18.2 [*]	1.64	96.2
5a	Te–Cl3	2.508	0.50	1.5	0.04	0.55	–0.34	7.73 [*]	18.2 [*]	1.64	96.3
5a	Te–Cl4	2.508	0.50	1.5	0.04	0.55	–0.34	7.73 [*]	18.2 [*]	1.64	96.3
7a	Te–Cl3	2.493	0.51	1.5	0.04	0.55	–0.35	7.72 [*]	18.6 [*]	1.64	96.2
7a	Te–Cl4	2.493	0.51	1.5	0.04	0.55	–0.35	7.72 [*]	18.6 [*]	1.64	96.1
6a	Te–C	2.153	0.83	–1.8	0.06	0.39	–0.54	2.30	6.3	1.71	57.1
5a	Te–C	2.123	0.87	–1.8	0.05	0.41	–0.55	2.24	5.9	1.69	56.7
7a	Te–C	2.131	0.86	–1.9	0.05	0.40	–0.55	2.23	5.9	1.68	55.7

For all models: d is the atom–atom distance, $\rho(r)$ is the electron density (ED) at the bond critical point, $\nabla^2\rho(r)$ is the corresponding Laplacian, ϵ is the bond ellipticity, G/ $\rho(r)$ and H/ $\rho(r)$ are the kinetic and total energy density over ED ratios, N_{ELI} and V_{ELI} are electron populations and volumes of related ELI-D basins, γ_{ELI} is the ELI-D value at the attractor position, RJI is the Raub-Jansen Index.

^{*} Cl lone-pair basins added to one number.

Table 4
Atomic and fragmental AIM charges (in e) of **5a–7a**.

Compound backbone	NapMe ₂ N nap	AcePh ₂ PO ace	MeONap nap	4a nap	4a' ace	5a nap	6 ace	7a nap
Te				1.61	1.62	1.65	1.76	1.69
Cl1				–0.41	–0.38	–0.54	–0.52	–0.55
Cl2				–0.54	–0.55	–0.57	–0.55	–0.56
Cl3				–0.56	–0.57	–0.57	–0.59	–0.56
Acceptor				0.10	0.12	–0.03	0.05	0.03
nap/ace	0.31	–0.49	0.55	–0.09	–0.13	0.22	–0.64	0.46
N/O	–1.01	–1.49	–1.14			–0.99	–1.46	–1.16
P		3.01					2.95	
Me/Ph	0.35	–0.50	0.58			0.39	–0.45	0.62
Me/Ph	0.35	–0.51				0.39	–0.44	
Donor	–0.31	0.50	–0.56			–0.21	0.61	–0.54
Sum	0.00	0.01	0.00	0.01	–0.01	–0.02	0.02	–0.06

ture turned the solution into dark-yellow suspension. All volatile materials were removed under reduced pressure to leave a yellow solid, which was dissolved in THF (10 mL) before tellurium powder (810 mg, 6.37 mmol) was added. The resulting dark-red solution was stirred overnight before dried air was bubbled through for 30 min. The solvent was removed under reduced pressure and the crude product extracted with THF (40 mL). The solvent was removed nearly to dryness (about 3 mL). Addition of MeCN (3 mL) induced precipitation of an orange-red solid (Yield: 920 mg, 1.62 mmol, 51%; M.p. 142 °C).

¹H NMR (CDCl₃): δ = 7.96 (d, ³J_{HH} = 7.3 Hz, 2H; H5), 7.60 (d, ³J_{HH} = 8.0 Hz, 2H; H7), 7.44 (d, ³J_{HH} = 8.3 Hz, 2H; H4), 7.40 (t, ³J_{HH} = 8.1 Hz, 2H; H6), 7.12 (t, ³J_{HH} = 7.8 Hz, 2H; H3), 6.89 (d, ³J_{HH} = 7.2 Hz, 2H; H2), 4.10 ppm (s, 6H; CH₃). ¹³C-{¹H}-NMR (CDCl₃): δ = 154.3, 136.5, 135.7, 133.7, 127.9, 127.4, 126.8, 125.6, 121.5, 104.7, 54.4 ppm. ¹²⁵Te-{¹H}-NMR (CDCl₃): δ = 415 ppm. EI-MS: m/z (%) = 570 (69) [M]⁺, 444 (1 0 0) [M–Te]⁺, 315 (87) [M–2 Te]⁺.

4.3. Synthesis of 8-methoxy-naphthyltellurium trichloride (**7a**)

At 0 °C, thionyl chloride (25 μ L, 0.348 mmol) was slowly added to a stirred solution of **3** (200 mg, 0.348 mmol) in THF (10 mL). After the addition was finished the slightly yellow solution was stirred for 1 h at room temperature and the solvent was removed under reduced pressure. The solid residue was crystallized from CH₂Cl₂/hexane by slow evaporation to give yellow crystals of **7a** (250 mg, 0.318 mmol, 91%; Dec. 151 °C).

¹H NMR (CDCl₃): δ = 8.66 (d, ³J_{HH} = 7.4 Hz, 1H; H5), 8.08 (d, ³J_{HH} = 7.9 Hz, 1H; H7), 7.86 (t, ³J_{HH} = 7.4 Hz, 1H; H6), 7.67 (d,

³J_{HH} = 8.1 Hz, 1H; H4), 7.58 (t, ³J_{HH} = 7.9 Hz, 1H; H3), 6.14 (d, ³J_{HH} = 7.5 Hz, 1H; H2), 4.39 ppm (s, 3H; CH₃). ¹³C-{¹H}-NMR (CDCl₃): δ = 151.6, 139.4, 135.2, 131.7, 128.1, 127.0, 126.8, 123.4, 121.8, 108.3, 57.5 ppm. ¹²⁵Te-{¹H}-NMR (CDCl₃): δ = 1370 ppm. EI-MS: m/z (%) = 357 (25) [M–Cl]⁺, 192.2 (1 0 0) [M–TeCl₂]⁺.

4.4. Synthesis of 8-methoxynaphthyltellurium tribromide (**7b**)

At 0 °C, bromine (65 mg, 4.05 mmol) dissolved in CHCl₃ (15 mL) was slowly added to a stirred solution of **3** (920 mg, 1.62 mmol) in CDCl₃ (40 mL). After the addition was finished the suspension was stirred for 1 h at room temperature before the solid was collected by filtration and washed with CH₂Cl₂ (5 mL). The solid product was crystallized by diffusion of hexane into a solution of acetone to give yellow crystals of **7b** (Yield: 290 mg, 0.53 mmol, 33% M.p. 161 °C).

¹H NMR (CDCl₃): δ = 8.68 (d, ³J_{HH} = 7.6 Hz, 1H; H5), 8.08 (d, ³J_{HH} = 8.3 Hz, 1H; H7), 7.82 (t, ³J_{HH} = 7.9 Hz, 1H; H6), 7.66 (d, ³J_{HH} = 8.4 Hz, 1H; H4), 7.60 (t, ³J_{HH} = 7.3 Hz, 1H; H3), 7.19 (d, ³J_{HH} = 7.2 Hz, 1H; H2), 4.40 ppm (s, 3H; CH₃). ¹³C-{¹H}-NMR (CDCl₃): δ = 151.2, 135.3, 132.3, 131.7, 129.6, 129.0, 128.4, 122.7, 121.6, 108.3, 57.6 ppm. ¹²⁵Te-{¹H}-NMR ((D₆-acetone): δ = 822 ppm.

4.5. Synthesis of 5-bromo-8-methoxy-naphthyltellurium tribromide (**7c**)

At 0 °C, bromine (27 μ L, 1.05 mmol) was slowly added to a stirred solution of **3** (200 mg, 0.348 mmol) in CDCl₃ (15 mL). After the addition was finished the orange solution was stirred for 1 h at

Table 5
Crystal data and structure refinement of **3** and **7a–7c**.

	3	7a	7b	7c
Formula	C ₂₂ H ₁₈ O ₂ Te ₂	C ₁₁ H ₉ Cl ₃ O ₂ Te	C ₁₁ H ₉ Br ₃ O ₂ Te	C ₁₁ H ₉ Br ₄ O ₂ Te
Formula weight, g mol ⁻¹	569.56	391.13	524.51	603.41
Crystal system	Monoclinic	Monoclinic	Monoclinic	Monoclinic
Crystal size, mm	0.08 × 0.07 × 0.05	0.22 × 0.20 × 0.12	0.09 × 0.08 × 0.05	0.20 × 0.18 × 0.04
Space group	<i>P</i> 2 ₁ / <i>n</i>	<i>P</i> 2 ₁ / <i>c</i>	<i>P</i> 2 ₁ / <i>c</i>	<i>P</i> 2 ₁ / <i>c</i>
<i>a</i> , Å	12.0030(3)	11.5074(7)	7.6050(2)	15.0437(7)
<i>b</i> , Å	10.1347(2)	14.666(1)	15.3970(5)	12.0681(5)
<i>c</i> , Å	16.0911(4)	7.8816(7)	11.7728(4)	8.0954(4)
β, °	90	90	90	90
V, Å ³	106.469(1)	96.922(2)	104.021(1)	102.725(2)
Z	90	90	90	90
calcd., Mg m ⁻³	1877.12(8)	1320.4 (2)	1337.46(7)	1433.6(1)
(Mo Kα), mm ⁻¹	4	4	4	4
F(0 0 0)	2.015	1.968	2.605	2.796
range, deg	3.122	2.835	11.163	13.204
Index ranges	1080	744	960	1096
	2.40–30.05	2.78–27.54	2.22–28.35	2.78–30.05
	–16 ≤ <i>h</i> ≤ 16	–14 ≤ <i>h</i> ≤ 14	–10 ≤ <i>h</i> ≤ 10	–17 ≤ <i>h</i> ≤ 17
	–14 ≤ <i>k</i> ≤ 14	–19 ≤ <i>k</i> ≤ 19	–20 ≤ <i>k</i> ≤ 20	–17 ≤ <i>k</i> ≤ 17
	–22 ≤ <i>l</i> ≤ 22	–10 ≤ <i>l</i> ≤ 9	–15 ≤ <i>l</i> ≤ 15	–19 ≤ <i>l</i> ≤ 20
No. of refls collected	116089	16311	208249	57245
Completeness to max	99.9%	99.7%	99.9%	98.6%
No. indep. Reflins	5493	3027	3341	4152
No. obsd reflins with (<i>I</i> > 2(<i>I</i>))	5049	2426	3137	3487
No. refined params	237	146	146	155
Goof (<i>F</i> ²)	1.098	1.152	1.089	1.052
R ₁ (<i>F</i>) (<i>I</i> > 2(<i>I</i>))	0.0152	0.0599	0.0129	0.0262
wR ₂ (<i>F</i> ²) (all data)	0.0350	0.1439	0.0275	0.0595
Largest diff peak/hole, e Å ⁻³	0.974/–0.642	0.684/–1.636	0.517/–0.306	1.052/–0.965
CCDC number	1558299	1558300	1558301	1558302

room temperature and the solvent was removed under reduced pressure. The solid residue was crystallized from CH₂Cl₂/hexane by slow evaporation to give orange crystals of **7c** (300 mg, 0.286 mmol, 82%; Dec. 183 °C).

¹H NMR (CDCl₃): δ = 8.78 (d, ³*J*_{HH} = 7.4 Hz, 1H; H5), 8.50 (d, ³*J*_{HH} = 8.1 Hz, 1H; H7), 7.95–7.89 (m, 2H; H3 + H6), 7.08 (d, ³*J*_{HH} = 7.3 Hz, 1H; H2), 4.41 ppm (s, 3H; CH₃). ¹³C-{¹H}-NMR (CDCl₃): δ = 150.9, 133.4, 132.7, 131.4, 130.6, 130.3, 129.7, 122.6, 116.7, 108.9, 57.9 ppm. ¹²⁵Te-{¹H}-NMR ((D₆-acetone): δ = 773 ppm.

4.6. Crystallography

Intensity data of **3** and **7a–7c** was collected on a Bruker Venture D8 diffractometer at 100 K with graphite-monochromated Mo-Kα (0.7107 Å) radiation. All structures were solved by direct methods and refined based on *F*² by use of the SHELX program package as implemented in WinGX [22]. All non-hydrogen atoms were refined using anisotropic displacement parameters. Hydrogen atoms attached to carbon atoms were included in geometrically calculated positions using a riding model. Crystal and refinement data are collected in Table 5. Figures were created using DIAMOND [23]. Crystallographic data (excluding structure factors) for the structural analyses have been deposited with the Cambridge Crystallographic Data Centre. Copies of this information may be obtained free of charge from The Director, CCDC, 12 Union Road, Cambridge CB2 1EZ, UK (Fax: +44-1223-336033; e-mail: deposit@ccdc.cam.ac.uk or <http://www.ccdc.cam.ac.uk>).

4.7. Computational methodology

The atomic coordinates of compounds **5a–7a** were used as input for gas-phase calculations at the B3PW91/6-311+G(2df,p) [24] level of theory using Gaussian09 [25]. For the Te atoms effective core potentials (ECP28MDF) and a corresponding cc-pVTZ

basis set were applied [24]. The resulting wavefunction files were used for topological analysis of the electron density (ED) according to the Atoms-in-Molecules space-partitioning scheme using AIM2000 [26], whereas DGRID [27] was used to generate and analyze the Electron-Localizability-Indicator (ELI-D) related real-space bonding descriptors applying a grid step size of 0.05 a.u.. The NCI grids were computed with NCIPLOT [28]. Bond paths are displayed with AIM2000 [26], ELI-D and NCI figures are displayed with Molliso [29].

Acknowledgement

The Deutsche Forschungsgemeinschaft (DFG) is gratefully acknowledged for financial support.

References

- [1] I.D. Sadekov, V.I. Minkin, Sulfur Rep. 19 (1997) 285–230.
- [2] E. Schulz Lang, R.A. Burrow, E. Tarabal Silveira, Acta Crystallogr. C 58 (2002) o397–o398.
- [3] S.C. Menon, H.B. Singh, J.M. Jasinski, J.P. Jasinski, R.J. Butcher, Organometallics 15 (1996) 1707–1712.
- [4] G. Mugesh, H.B. Singh, Acc. Chem. Res. 35 (2002) 226–236.
- [5] C.J. Carmalt, A.H. Cowley, Main Group Chem. News 4 (1996) 4–10.
- [6] P. Singh, A.K.S. Chauhan, R.J. Butcher, A. Duthie, Polyhedron 62 (2013) 227–233.
- [7] S. Misra, A.K.S. Chauhan, R.C. Srivastava, A. Duthie, R.J. Butcher, RSC Adv. 1 (2011) 808–816.
- [8] J. Beckmann, J. Bolsinger, A. Duthie, Chem. Eur. J. 17 (2011) 930–940.
- [9] E. Hupf, T.G. Do, A. Nordheider, M. Wehrhahn, P. Sanz Camacho, S.E. Ashbrook, Sharon, E. Lork, A.M.Z. Slawin, S. Mebs, D.J. Woollins, J. Beckmann, Organometallics 36 (2017) 1566–1579.
- [10] R.W.F. Bader, Atoms in Molecules. A Quantum Theory, Cambridge University Press, Oxford, U.K., 1991.
- [11] C. Gatti, Z. Kristallogr. 220 (2005) 399–457.
- [12] E.R. Johnson, S. Keinan, P. Mori-Sanchez, J. Contreras-García, A.J. Cohen, W. Yang, J. Am. Chem. Soc. 132 (2010) 6498–6506.
- [13] (a) M. Kohout, Int. J. Quantum Chem. 97 (2004) 651–658;
(b) M. Kohout, F.R. Wagner, Y. Grin, Theor. Chem. Acc. 119 (2008) 413–420.
- [14] S. Mebs, Chem. Phys. Lett. 651 (2016) 172–177.

- [15] (a) P. de Silva, C. Corminboeuf, *J. Chem. Theory Comput.* 10 (2010) 3745–3756;
(b) N. Gillet, R. Chaudret, J. Contreras-García, W. Yang, B. Silvi, J.-P. Piquemal, *J. Chem. Theory Comput.* 8 (11) (2012) 3993–3997;
(c) D. Fang, R. Chaudret, J.-P. Piquemal, G.A. Cisneros, *Chem. Theory Comput.* 9 (2013) 2156–2160.
- [16] (a) S. Raub, G. Jansen, *Theor. Chem. Acc.* 106 (2001) 223–232;
(b) I. Vidal, S. Melchor, J.A. Dobado, *J. Phys. Chem. A* 109 (2005) 7500–7508.
- [17] (a) D.A. Shirley, C.F. Cheng, *J. Org. Chem.* 20 (1969) 251–252;
(b) P.C. Bell, W. Skranc, X. Formosa, J. O’Leary, J.D. Wallis, *J. Chem. Soc., Perkin Trans. 2* (2002) 878–886;
(c) F.R. Knight, A.L. Fuller, A.M.Z. Slawin, J.D. Woollins, *Polyhedron* 29 (2010) 1849–1853.
- [18] J. Beckmann, J. Bolsinger, A. Duthie, *Organometallics* 28 (2009) 4610–4612.
- [19] D.J. Sandman, L. Li, S. Tripathy, J.C. Stark, L.A. Acampora, B.M. Foxman, *Organometallics* 13 (1994) 398–353.
- [20] J. Beckmann, D. Dakternieks, A. Duthie, F. Ribot, M. Schürmann, N.A. Lewcenko, *Organometallics* 22 (2003) 3257–3261.
- [21] (a) V. Balasubramanian, *Chem. Rev.* 66 (1966) 567–641;
(b) J.D. Hoefelmeyer, M. Schulte, M. Tschinkl, F.P. Gabbai, *Coord. Chem. Rev.* 235 (2002) 93–103;
(c) P. Kilian, F.R. Knight, J.D. Woollins, *Coord. Chem. Rev.* 255 (2011) 1387–1413;
(d) P. Kilian, F.R. Knight, J.D. Woollins, *Chem. Eur. J.* 17 (2011) 2302–2328.
- [22] (a) G.M. Sheldrick, *Acta Crystallogr. A* 64 (2008) 112–122;
(b) G.M. Sheldrick, *Acta Crystallogr. C* 71 (2015) 3–8;
(c) L.J. Farrugia, *J. Appl. Crystallogr.* 32 (1999) 837–838.
- [23] K. Brandenburg, DIAMOND Version 3.2i, Crystal Impact GbR, Bonn Germany, 2012.
- [24] (a) J.P. Perdew, J.A. Chevary, S.H. Vosko, K.A. Jackson, M.R. Pederson, D.J. Singh, C. Fiolhais, *Phys. Rev. B* 46 (1992) 6671–6687;
(b) A.D. Becke, *J. Chem. Phys.* 98 (1993) 5648–5652;
(c) K.A. Peterson, D. Figgen, E. Goll, H. Stoll, M. Dolg, *J. Chem. Phys.* 119 (2003) 11113–11123;
(d) B. Metz, H. Stoll, M. Dolg, *J. Chem. Phys.* 113 (2000) 2563–2569;
(e) K.A. Peterson, *J. Chem. Phys.* 119 (2003) 11099–11112.
- [25] M.J. Frisch, G.W. Trucks, H.B. Schlegel, G.E. Scuseria, M.A. Robb, J.R. Cheeseman, G. Scalmani, V. Barone, B. Mennucci, G.A. Petersson, H. Nakatsuji, M. Caricato, X. Li, H.P. Hratchian, A.F. Izmaylov, J. Bloino, G. Zheng, J.L. Sonnenberg, M. Hada, M. Ehara, K. Toyota, R. Fukuda, J. Hasegawa, M. Ishida, T. Nakajima, Y. Honda, O. Kitao, H. Nakai, T. Vreven, J.A. Montgomery Jr., J.E. Peralta, F. Ogliaro, M. Bearpark, J.J. Heyd, E. Brothers, K.N. Kudin, V.N. Staroverov, R. Kobayashi, J. Normand, K. Raghavachari, A. Rendell, J.C. Burant, S.S. Iyengar, J. Tomasi, M. Cossi, N. Rega, J.M. Millam, M. Klene, J.E. Knox, J.B. Cross, V. Bakken, C. Adamo, J. Jaramillo, R. Gomperts, R.E. Stratmann, O. Yazyev, A.J. Austin, R. Cammi, C. Pomelli, J.W. Ochterski, R.L. Martin, K. Morokuma, V.G. Zakrzewski, G.A. Voth, P. Salvador, J.J. Dannenberg, S. Dapprich, A.D. Daniels, O. Farkas, J.B. Foresman, J.V. Ortiz, J. Cioslowski, D.J. Fox, Gaussian09, Revision B.01, Gaussian Inc, Wallingford, CT, 2010.
- [26] F. Biegler-König, J. Schönbohm, D. Bayles, *J. Comput. Chem.* 22 (2001) 545–559.
- [27] M. Kohout, DGRID-4.6 Radebeul, 2011.
- [28] J. Contreras-García, E. Johnson, S. Keinan, R. Chaudret, J.-P. Piquemal, D. Beratan, W. Yang, *J. Chem. Theory Comput.* 7 (2011) 625–632.
- [29] C.B. Hübschle, P. Luger, *J. Appl. Crystallogr.* 39 (2006) 901–904.

2.9. Synthesis and characterization of 5-Diphenylphosphino-6-phenylchalcogenacenaphthenes

2.9.1. Introduction & Results

For the study of element-element interactions *peri*-substituted (ace)naphthene compounds are well known in literature.^[151–157] Due to its rigid scaffold the elements in *peri*-position are forced to interact with each other and hence can be used as a precursor for obtaining stabilized radical cations.

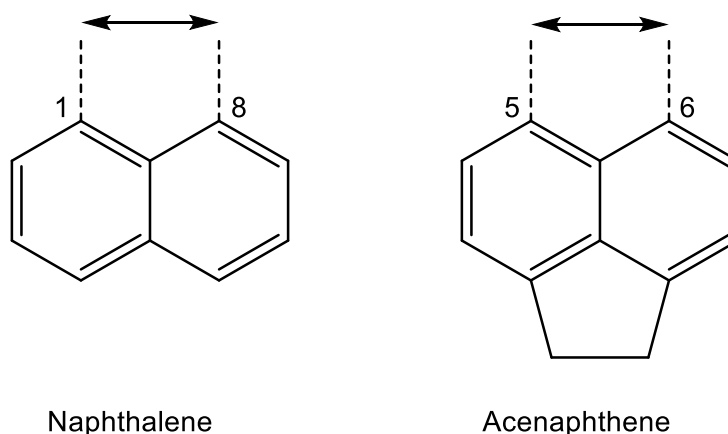


Figure 17. Naphthalene and acenaphthene scaffold.

The first ever reported naphthalene derivative with *peri*-substituted interactions was in 1966.^[158] Various *peri*-substituted naphthalene and acenaphthene aggregations were presented since then.

Woollins reported among numerous sterically crowded tin acenaphthenes^[159,160] some phosphorus substituted acenaphthenes with sulphur as can be seen in Figure 18 with intramolecular P···P distances of approx. 4.05 Å, which are among the longest ever reported *peri*-distances.^[161]

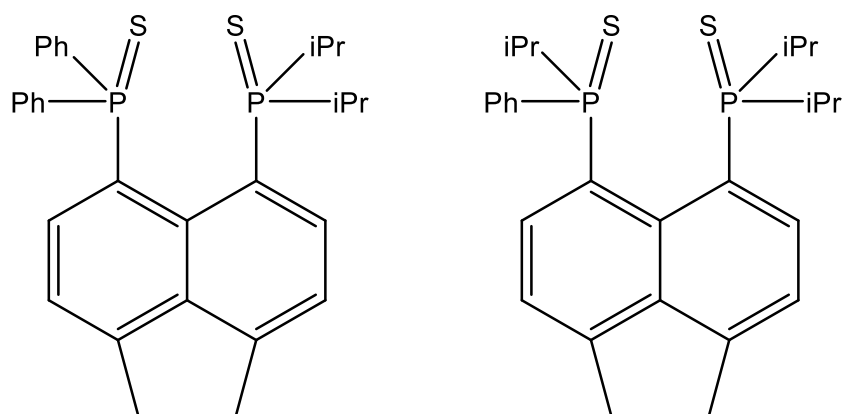
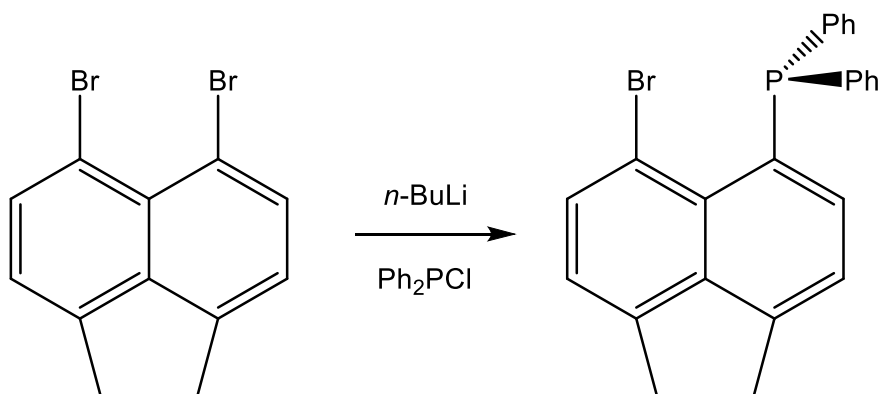


Figure 18. Phosphorus substituted acenaphthene with sulphur.^[161]

The study on tin acenaphthenes has also been enhanced to tin-chalcogene compounds creating some interesting bonding situations.^[160] In addition the first di- and mixsubstituted chalcogen acenaphthenes were introduced^[162,163], including a 1,2-ditelluraacenaphthene-1,2-dication.^[151]

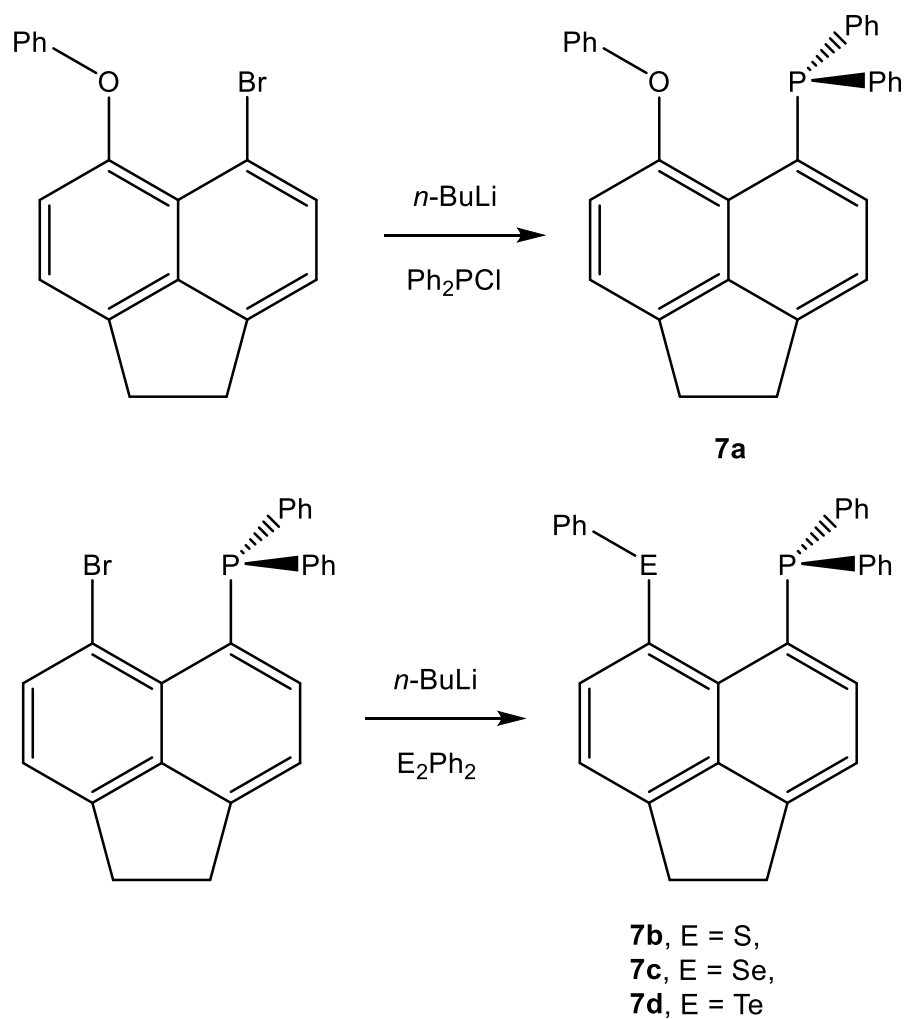
Although there are many *peri*-substituted (ace)naphthenes, no chalcogene radical cation has been reported. This work we focused on the 5-diphenylphosphino-6-chalcogeneacenaphthene scaffold.

For the synthesis acenaphthenes with *peri*-substituted halogens are commonly used. Starting from 5,6-dibromoacenaphthene the diphenylphosphino group is initially introduced by the reaction with *n*-buthyllithium and chlorodiphenylphosphine.^[164,165]



Scheme 17. Synthesis of 5-bromo-6-diphenylphosphinoacenaphthene.

The 5-bromo-6-diphenylphosphinoacenaphthene was then treated with *n*-buthyllithium again and the respective diphenyldichalcogene was added to receive the 5-chalcogenophenyl-6-diphenylphosphinoacenaphthene, as can be seen in Scheme 18. To obtain the oxygen-analogue, the phenoxy group was first introduced in the the *peri*-position^[164] followed by a reaction with *n*-buthyllithium and chlorodiphenylphosphine.



Scheme 18. Synthesis of 5-diphenylphosphino-6-chalcogenacenaphthene.

All obtained compounds were recrystallized from dichloromethane and hexane to give single crystals, which were measured by X-ray crystallography. The structures are shown below.

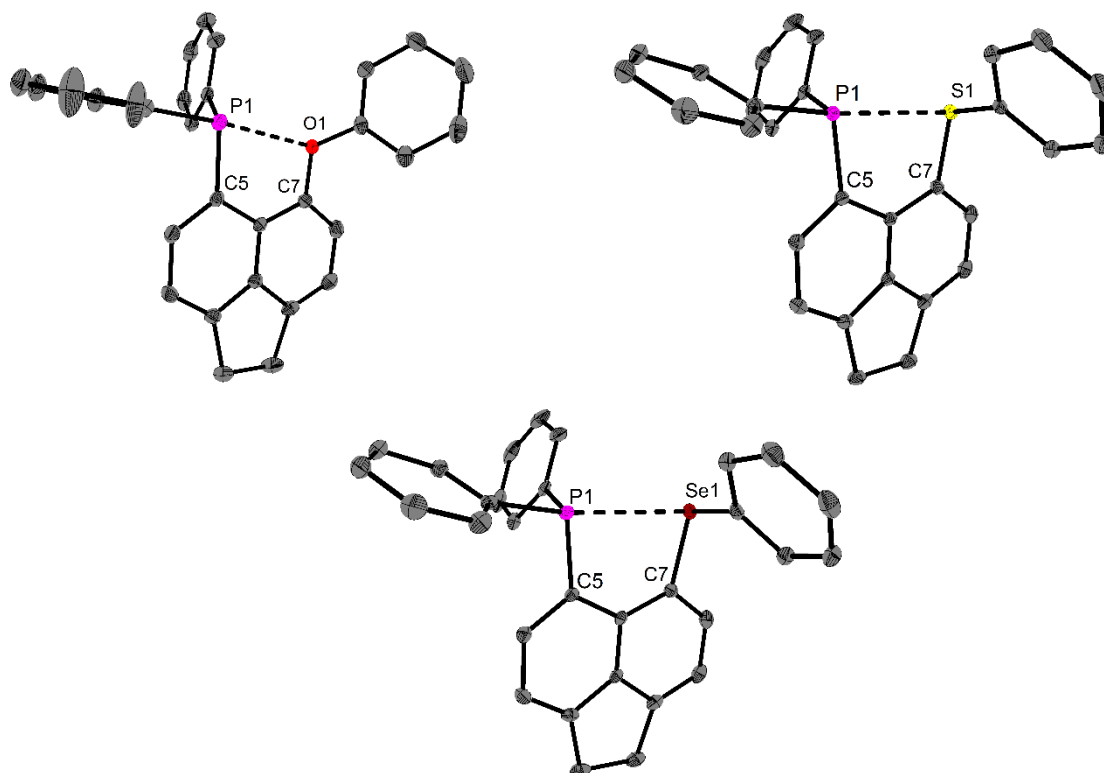
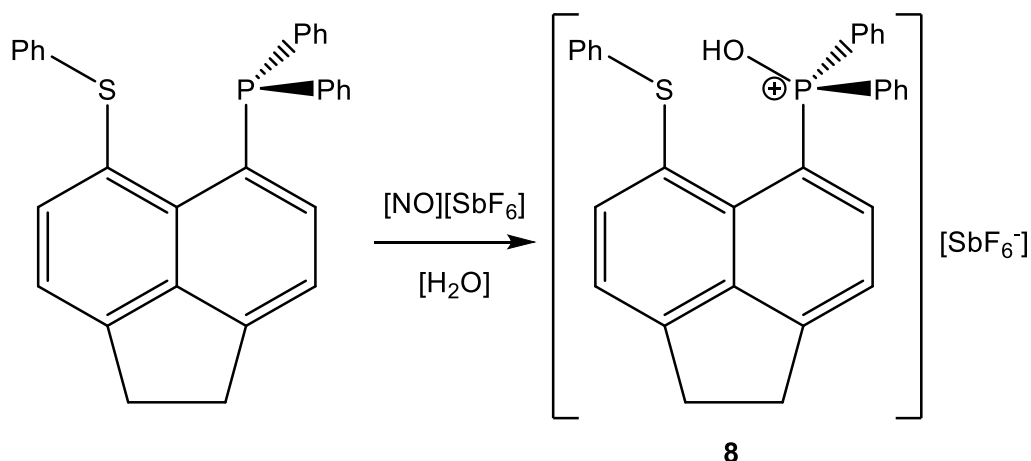


Figure 19. Molecular structure of 5-diphenylphosphino-6-phenylchalcogenacenaphthene ($(\text{Ph}_2\text{P})\text{Ace}(\text{E})\text{Ph}$) (**7a**, E = O; **7b**, E = S; **7c**, E = Se) showing 50 % probability ellipsoids and essential atom numbering. Selected bond parameters [\AA] of **7a**: P1-C5 1.837(7), O1-C7 1.389(1), P1-O1 2.871(5). Selected bond parameters [\AA] of **7b**: P1-C5 1.846(5), S1-C7 1.776(4), P1-S1 3.061(8). Selected bond parameters [\AA] of **7c**: P1-C5 1.846(7), Se1-C7 1.919(9), P1-Se1 3.140(5).

The $(\text{Ph}_2\text{P})\text{Ace}(\text{E})\text{Ph}$ (E = O, S, Se) compounds are all in the same spatial arrangement with phosphorus-chalcogen bond lengths of 2.87 - 3.14 \AA , with longer bond length for heavier chalcogen atoms.

Attempts of oxidizing the acenaphthenchalcogenes with nitrosonium salts to the respective radical cation led to no success, but the oxidation of the phosphorus atom to a phosphorus-oxygen bond.



Scheme 19. Reaction of 5-diphenylphosphino-6-phenylsulphideacenaphthene with nitronium hexafluoroantimonate.

The crystal structure of the product of the reaction with $(\text{Ph}_2\text{P})\text{Ace}(\text{SPh})$ is shown in Figure 20.

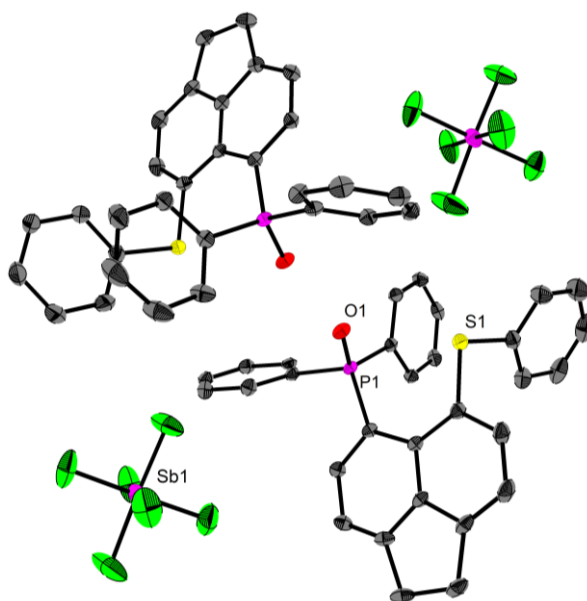


Figure 20. Molecular structure of the oxidation of $\text{C}_{30}\text{H}_{24}\text{SPOsbf}_6$ with nitronium hexafluoroantimonate showing 50 % probability ellipsoids and essential atom numbering. Selected bond parameters [Å]: P1-O1 1.520(1), P1-S1 3.239(1).

The sulphur phosphorus bond length of 3.24 Å is quite longer than the one of the educt with 3.06 Å.

2.9.2. Experimental

Reagents were obtained commercially (Sigma-Aldrich, Germany) and were used as received. Dry solvents were collected from a SPS800 mBraun solvent system. ^1H -, ^{13}C -, ^{31}P -, ^{77}Se - and ^{125}Te -NMR spectra were recorded at RT (unless otherwise stated) using a Bruker Avance-360 spectrometer and are referenced to tetramethylsilane (^1H , ^{13}C), phosphoric acid (85% in water) (^{31}P), diphenyldiselenide (^{77}Se) and telluric acid (^{125}Te). Chemical shifts are reported in parts per million (ppm) and coupling constants (J) are given in Hertz (Hz). Air sensitive substances were handled in gloveboxes "Labmaster" by M. Braun.

2.9.2.1 Synthesis of 5-diphenylphosphino-6-phenoxyacenaphthene (7a)

The synthesis of 5-bromo-6-phenoxyacenaphthene was carried out according to Kordts et al.^[164]

0.73 g (2.23 mmol) of 5-bromo-6-phenoxyacenaphthene were dissolved in 10 ml of dry THF and cooled to $-80\text{ }^\circ\text{C}$. 0.98 ml (2.45 mmol, 2.5-M in *n*-hexane) *n*-butyllithium was added and allowed to warm to room temperature. After stirring for one hour, the mixture was cooled to $-80\text{ }^\circ\text{C}$ again and 0.48 g (2.68 mmol) chlorodiphenylphosphine was added, while the solution turns brighter. The mixture was stirred for 30 minutes at $-80\text{ }^\circ\text{C}$ and warmed to room temperature. Aqueous workup and drying with magnesium sulphate resulted in an orange-yellow solid. Recrystallization from dichloromethane/hexane resulted in yellow crystals, yield 99 % (0.95 g).

$^1\text{H-NMR}$ (360 MHz, CDCl_3): δ = 7.33 (m, 10H), 7.21 (m, 4H), 7.06 (t, $^3J_{\text{H,H}} = 7.4\text{ Hz}$ 1H), 6.94 (dd, 1H), 6.85 (d, $^3J_{\text{H,H}} = 7.6\text{ Hz}$ 1H), 6.71 (d, $^3J_{\text{H,H}} = 7.8\text{ Hz}$ 2H), 3.44 (d, $^3J_{\text{H,H}} = 5.6\text{ Hz}$ 4H) ppm. $^{13}\text{C}\{-^1\text{H}\}$ -NMR (90 MHz, CDCl_3): δ = 157.0, 152.0, 151.9, 147.2, 141.0, 134.5, 134.4, 134.1, 129.4, 128.6, 128.4, 128.3, 122.9, 120.1, 119.6, 119.2, 116.0 (C_{Ar}), 30.7, 30.0 (CH_2) ppm. $^{31}\text{P-NMR}$ (81 MHz, CDCl_3): δ = 1.9 ppm.

2.9.2.2 Synthesis of 5-diphenylphosphino-6-phenylthioacenaphthene (7b)

0.50 g (1 eq, 0.12 mmol) of 5-bromo-6-diphenylphosphinoacenaphthene was dissolved in 10 ml of dry toluene and dropwise treated with 0.53 ml (1.1 eq, 0.13 mmol, 2.5-M in *n*-hexane) *n*-butyllithium. After stirring for 10 minutes 0.29 g (1.1 eq, 0.13 mmol) of diphenyl disulphate was added and the mixture was stirred overnight. Aqueous workup and evaporation of the solvent resulted in a yellow precipitate, which was then recrystallized from dichloromethane/*n*-hexane giving yellow crystals in 55 % (0.29 g) yield.

¹H-NMR (360 MHz, CDCl₃): δ = 7.72 (d, ³J_{H,H} = 7.2 Hz, 1H), 7.73 (d, ³J_{H,H} = 7.2 Hz, 1H), 7.26 (d, ³J_{H,H} = 3.8 Hz, 12H), 7.21 (d, ³J_{H,H} = 7.2 Hz, 1H), 7.08 (t, ³J_{H,H} = 7.5 Hz, 1H), 7.03 (t, ³J_{H,H} = 7.3 Hz, 1H), 6.83 (d, ³J_{H,H} = 7.5 Hz, 2H), 7.08 (s, 4H) ppm. **¹³C-{¹H}-NMR (90 MHz, CDCl₃):** δ = 148.9, 148.7, 141.2, 141.1, 140.9, 140.8, 139.6, 139.0, 138.9, 137.8, 135.9, 135.8, 134.1, 134.0, 128.5, 128.4, 128.3, 128.2, 127.5, 126.3, 125.0, 120.5, 120.1 (C_{Ar}), 30.3, 30.2 (CH₂) ppm. **³¹P-NMR (240 MHz, CDCl₃):** δ = 8.76 ppm.

2.9.2.2 Synthesis of 5-diphenylphosphino-6-phenylselenideacenaphthene (7c)

0.50 g (1 eq, 0.12 mmol) of 5-bromo-6-diphenylphosphinoacenaphthene was dissolved in 10 ml of dry toluene and dropwise treated with 0.53 ml (1.1 eq, 0.13 mmol, 2.5-M in *n*-hexane) *n*-butyllithium. After stirring for 10 minutes 0.41 g (1.1 eq, 0.13 mmol) of diphenyl diselenide was added and the mixture was stirred overnight. Aqueous workup and evaporation of the solvent resulted in an orange precipitate, which was then recrystallized from dichloromethane/ *n*-hexane giving orange crystals in 42 % (0.25 g).

¹H-NMR (360 MHz, CDCl₃): δ = 7.60 (d, ³J_{H,H} = 7.3 Hz, 1H), 7.33 (m, 14H), 7.27 (m, 2H), 7.23 (t, ³J_{H,H} = 7.4 Hz, 4H), 7.18 (m, 4H), 3.40 (s, 4H) ppm. **¹³C-{¹H}-NMR (90 MHz, CDCl₃):** δ = 149.1, 147.0, 140.6, 140.5, 138.6, 138.5, 138.4, 137.1, 136.2, 136.0, 135.8, 133.9, 133.8, 131.9, 129.0, 128.4, 128.3, 128.2, 126.9, 126.0, 120.6, 120.0 (C_{Ar}), 30.3, 30.0 (CH₂) ppm. **⁷⁷Se-NMR (69 MHz, CDCl₃):** δ = 418.0, 413.8 ppm. **³¹P-NMR (240 MHz, CDCl₃):** δ = - 100.6 ppm.

2.9.2.2 Synthesis of 5-diphenylphosphino-6-phenyltellurideacenaphthene (7d)

0.50 g (1 eq, 0.12 mmol) of 5-bromo-6-diphenylphosphinoacenaphthene was dissolved in 10 ml of dry toluene and dropwise treated with 0.53 ml (1.1 eq, 0.13 mmol, 2.5-M in *n*-hexane) *n*-butyllithium. After stirring for 10 minutes 0.54 g (1.1 eq, 0.13 mmol) was added and the mixture was stirred overnight. Aqueous workup and evaporation of the solvent resulted in an orange/brown precipitate, which was then recrystallized from dichloromethane/ *n*-hexane giving orange/brown crystals in 21 % (0.14 g).

¹H-NMR (360 MHz, CDCl₃): δ = 7.92 (d, ³J_{H,H} = 7.8 Hz, 2H), 7.70 (dd, ³J_{H,H} = 12.0, 7.7 Hz, 2H), 7.40 (m, 30H), 7.18 (t, ³J_{H,H} = 7.1 Hz, 1H), 7.08 (t, ³J_{H,H} = 7.7 Hz, 1H), 7.01 (d, ³J_{H,H} = 7.4 Hz, 1H), 3.39 (s, 4 H), 3.36 (d, ³J_{H,H} = 7.5 Hz, 2 H) ppm. **¹³C-{¹H}-NMR (90 MHz, CDCl₃):** δ = 150.0, 146.7, 145.6, 143.1, 140.0, 138.5, 138.4, 137.5, 137.4, 136.2, 133.4, 133.3, 132.4, 132.3, 131.6, 129.6, 129.5, 128.8, 128.5, 128.4, 128.3, 128.2, 128.1, 127.3, 127.0, 121.8, 121.1, 119.8, 112.3, 112.2 (C_{Ar}), 30.5, 29.6 (CH₂) ppm. **¹²⁵Te-NMR (110 MHz, CDCl₃):** δ = 638.1, 627.4 ppm. **³¹P-NMR (240 MHz, CDCl₃):** δ = 48.7, -118.5 ppm.

X-ray crystallography. Intensity data of **7a – 7c** was collected on a Bruker Venture D8 diffractometer with graphite-monochromated Mo-K α (0.7107 Å) radiation. The structure was solved by direct methods and difference Fourier synthesis with subsequent Full-matrix least-squares refinements on F^2 , using all data.^[140] All non-hydrogen atoms were refined using anisotropic displacement parameters. Hydrogen atoms were included in geometrically calculated positions using a riding model. Crystal and refinement data are collected in Table 8. Figures were created using DIAMOND.^[141]

Table 8. Crystal data and structure refinement of (Ph₂P)Ace(EPh) (**7a**, E = O; **7b**, E = S; **7c**, E = Se).

Formula	C ₃₀ H ₂₃ OP	C ₃₀ H ₂₃ SP	C ₃₀ H ₂₃ SeP
Formula weight, g mol ⁻¹	430.49	446.55	493.46
Crystal system	monoclinic	monoclinic	monoclinic
Crystal size, mm	0.2 × 0.15 × 0.15	0.09 × 0.08 × 0.06	0.07 × 0.07 × 0.06
Space group	P 1 21/n 1 (14)	P 1 21/n 1 (14)	P 1 21/n 1 (14)
a, Å	15.4697(5)	12.8899(5)	12.8373(2)
b, Å	9.2211(4)	9.6505(4)	9.6347(2)
c, Å	16.5627(5)	18.1240(7)	18.4277(3)
α, °	90	90	90
β, °	112.282(12)	101.008(1)	100.768(1)
γ, °	90	90	90
V, Å ³	2186.21(140)	2213.03(15)	2239.07(7)
Z	4	4	4
ρ _{calcd} , Mg m ⁻³	1.308	1.340	1.464
F(000)	904	936	1008
θ range, deg	2.49 to 27.58	2.29 to 30.07	2.25 to 28.35
Index ranges	-20 ≤ h ≤ 20	-17 ≤ h ≤ 18	-17 ≤ h ≤ 17
	-11 ≤ k ≤ 12	-13 ≤ k ≤ 13	-12 ≤ k ≤ 12
	-21 ≤ l ≤ 20	-25 ≤ l ≤ 25	-24 ≤ l ≤ 24
No. of reflns collected	47173	105948	135469
Completeness to θ _{max}	99,9%	99,6%	99,9%
No. indep. Reflns	5038	6486	5594
No. obsd reflns with (I > 2σ(I))	3883	5308	4752
No. refined params	289	289	289
GooF (F ²)	1.03	1.05	1.06
R ₁ (F) (I > 2σ(I))	0.049	0.037	0.030
wR ₂ (F ²) (all data)	0.131	0.092	0.071
Largest diff peak/hole, e Å ⁻³	0.65	0.55	0.50

Table 9. Crystal data and structure refinement of (Ph₂PO)Ace(SPh)[SbF₆] (**8**).

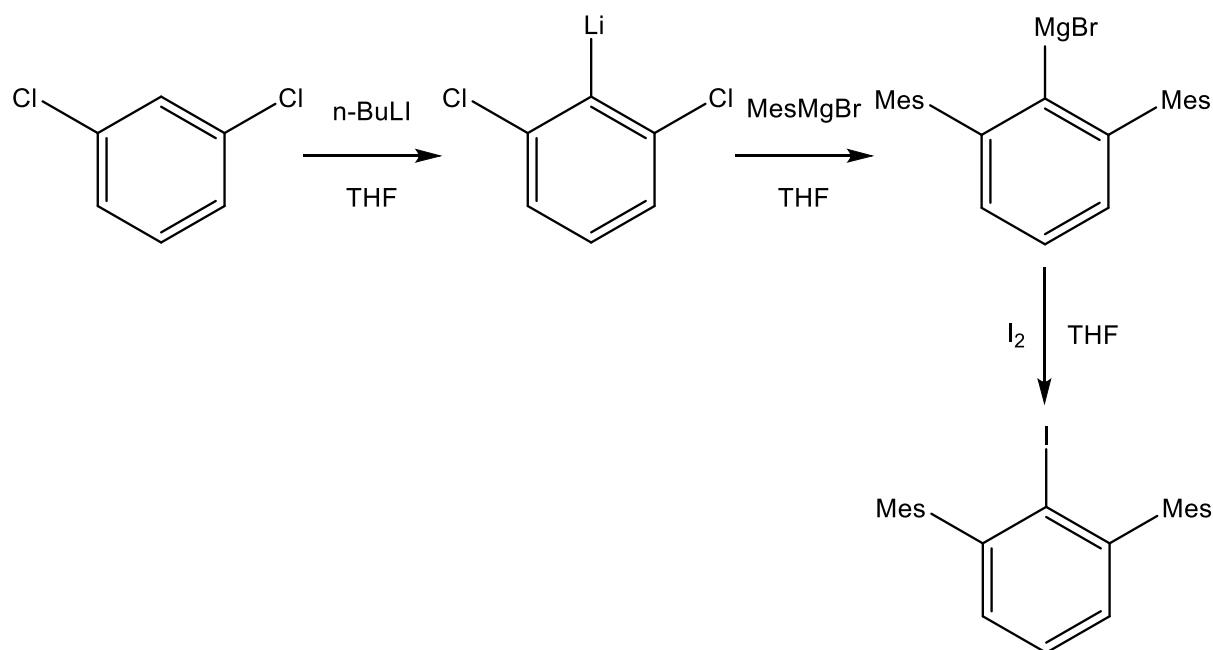
<i>Formula</i>	<i>C₃₀H₂₄SPOSbF₆</i>
<i>Formula weight, g mol⁻¹</i>	2323.70
<i>Crystal system</i>	triclinic
<i>Crystal size, mm</i>	0.35 × 0.25 × 0.10
<i>Space group</i>	<i>P</i> $\bar{1}$
<i>a, Å</i>	11.354(14)
<i>b, Å</i>	12.688(16)
<i>c, Å</i>	18.97(2)
<i>α, °</i>	81.09(5)
<i>β, °</i>	88.56(3)
<i>γ, °</i>	66.34(4)
<i>V, Å³</i>	2471(5)
<i>Z</i>	2
<i>ρ_{calcd}, Mg m⁻³</i>	1.561
<i>T, K</i>	293
<i>μ (Mo Kα), mm⁻¹</i>	0.777
<i>F(000)</i>	1180
<i>θ range, deg</i>	2.17 to 30.15
<i>Index ranges</i>	-15 ≤ h ≤ 15 -17 ≤ k ≤ 17 -26 ≤ l ≤ 26
<i>No. of reflns collected</i>	39412
<i>Completeness to θ_{max}</i>	98.7%
<i>No. indep. Reflns</i>	14406
<i>No. obsd reflns with (I > 2σ(I))</i>	11527
<i>No. refined params</i>	662
<i>GooF (F²)</i>	0.991
<i>R₁ (F) (I > 2σ(I))</i>	0.047
<i>wR₂ (F²) (all data)</i>	0.124
<i>Largest diff peak/hole, e Å⁻³</i>	2.84 / -1.68

2.10. Synthesis and Single-Electron Oxidation of Bulky Bis(*m*-terphenyl)chalcogenes

2.10.1. Introduction & Results

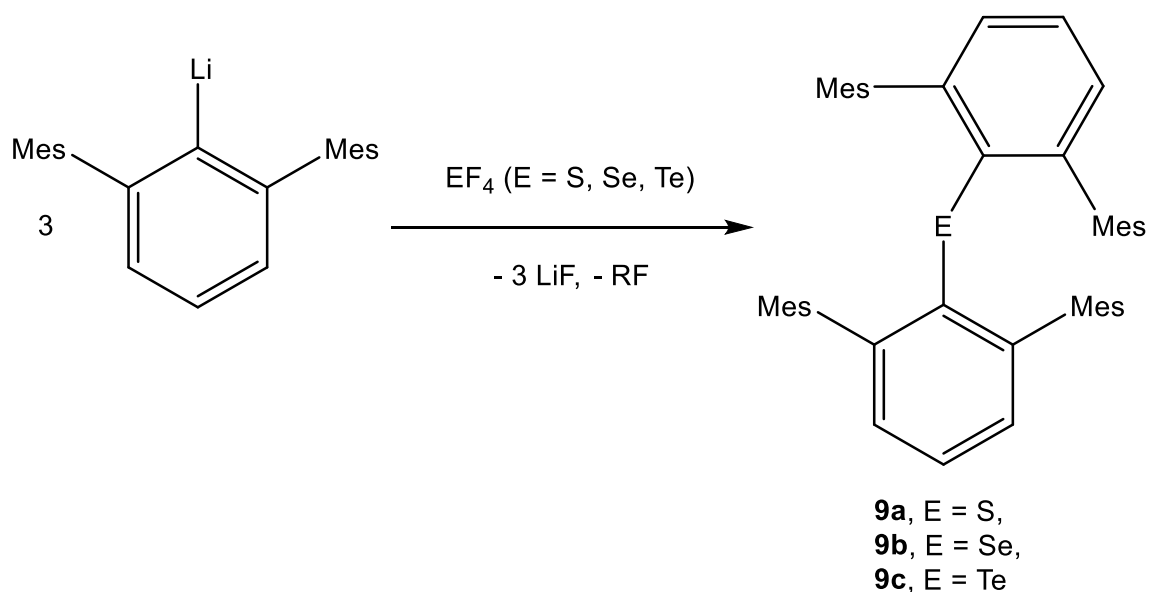
For the stabilization of labile diorganochalcogene radical cations, bulky substituents are necessary. In this work we present the synthesis and characterization of 2,6-dimesitylphenylchalcogenes (bis(*m*-terphenyl)chalcogenes) and its oxidation with known oxidation reagents.^[166–169]

The synthesis of the bulky substituent 2,6-dimesitylphenyl (*m*-terphenyl) was carried out according to a modified method of Saednya and Hart, described by M. Hesse. The lithiation of 1,3-dichlorobenzene and reaction with the Grignard-reagent of 2-bromomesitylene leads to *m*-terphenylmagnesiumbromide, which can be converted to the respective 2,6-dimesitylphenyl-iodine with elemental iodine (Scheme 20).^[167,168,170]



Scheme 20. Synthesis of 2,6-dimesitylphenyl iodide.

After lithiation with *n*-butyllithium the received 2,6-dimesitylphenyllithium (*m*TerLi) can be reacted with the respective EF₄ (E = S, Se, Te) to the targeted 2,6-dimesitylphenylchalcogene (Scheme 21).



Scheme 21. Synthesis of 2,6-dimesitylphenylchalcogene from 2,6-dimesitylphenyllithium and EF_4 (E = S, Se, Te).

In the first step the organolithium and chalcogen tetrafluoride react to the 2,6-dimesitylphenylchalcogenetrifluoride, which reacts subsequently to the difluoride with an additional equivalent of $mTerLi$. The third equivalent reduces the difluoride to the 2,6-dimesitylphenylchalcogene ($mTer_2E$).

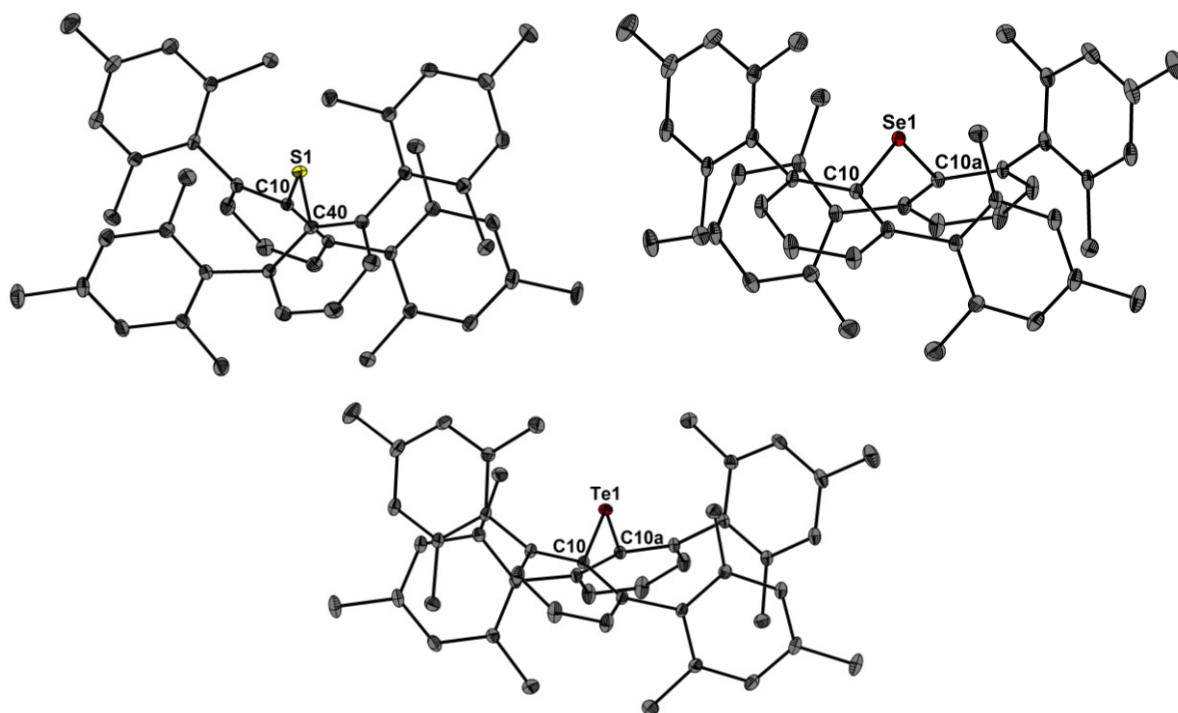


Figure 21. Molecular structure of $(2,6-Mes_2C_6H_3)_2E$ (**9a**, E = S; **9b**, E = Se; **9c**, E = Te) showing 50 % probability ellipsoids and the essential atom numbering. Selected bond parameters [Å, °] of **9a**: C10-S1 1.778(3), C40-S1 1.779(3), C10-S1-C40 109.2(1). Selected bond parameters [Å, °] of **9b**: Se1-C10 1.941(2), C10-Se1-C10a 116.3(1). Selected bond parameters [Å, °] of **9c**: Te1-C10 2.150(1), C10-Te1-C10a 116.16(5).

The bond length of 1.778(3) and 1.779(3) Å between the sulphur and carbon atoms C10 and C40 are nearly identical and are close to the sum of the covalent radii reported by Cordero et al. of 1.78 Å.^[171] The molecular structures of the heavier homologues (*mTer*₂Se and *mTer*₂Te) are similar to the structure of 2,6-dimesitylphenylsulfide. With a bond length of 1.941(2) Å (Se1-C10) for 2,6-dimesitylphenylselenide the sum of the covalent radii are also identical to the ones reported in literature (1.93 Å).^[171] The tellurium-carbon-distance of 2.150(1) Å in 2,6-dimesitylphenyltelluride is slightly higher than the sum of the covalent radii of 2.11 Å.^[171]

2.10.1.1 Electrochemical Oxidation

For the evaluation of the oxidative behaviour the 2,6-dimesitylphenylchalcogenes were investigated via cyclic voltammetric measurements. This method gives good information about the convenient choice of oxidation reagents and reveals the reversibility or quasi reversibility of the *mTer*₂E cations and radical cations (E = S, Se, Te).

The cyclic voltammetry measurements were carried out in a 0.1 M solution of tetrabutylammonium hexafluorophosphate in dichloromethane, with a scan rate of 0.1 volts per second. The received data was calculated with help of ferrocene as a calibrating reference and is shown in Figure 22.

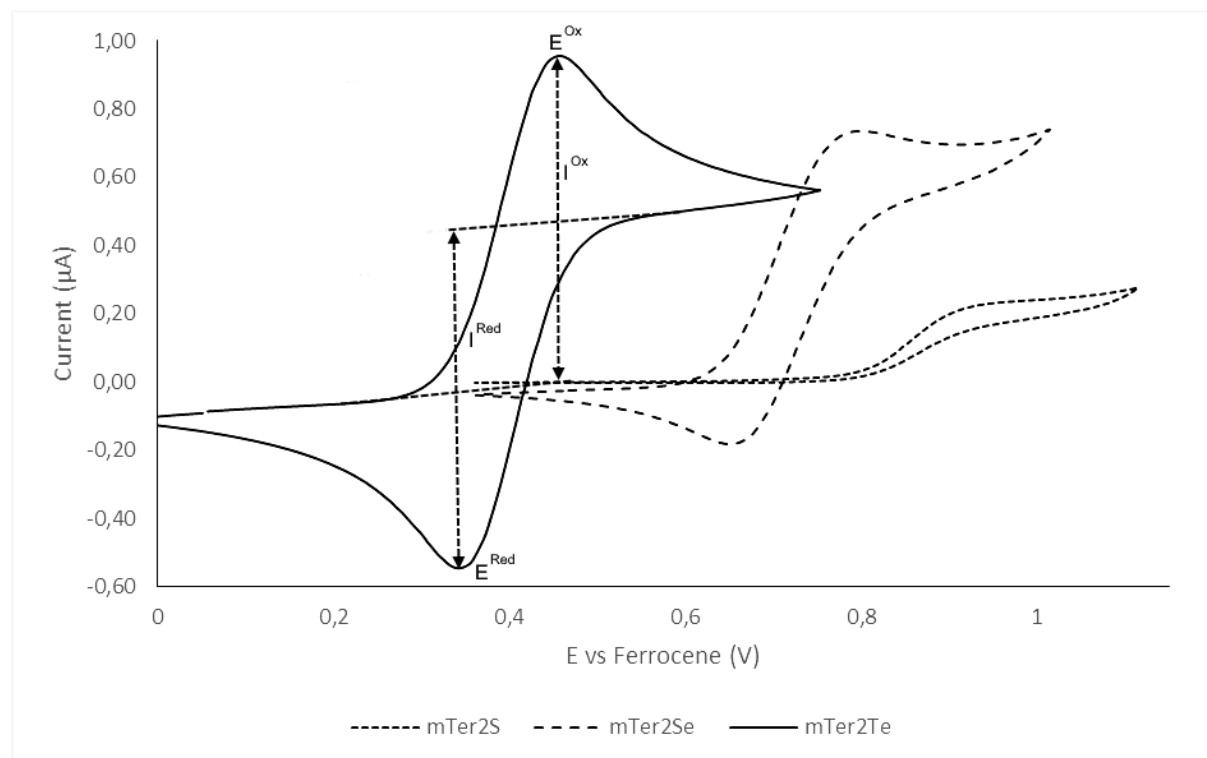


Figure 22. Cyclic Voltammetry measurements of *mTer*₂S, *mTer*₂Se and *mTer*₂Te at 0.1 V · s⁻¹ in dichloromethane, c = 5 · 10⁻³ mol · L⁻¹.

The measured voltages and currents are listed in the table below.

Table 10. Results of the cyclic voltammetric measurements of *mTer*₂S, *mTer*₂Se and *mTer*₂Te.

	E^{Ox} [V]	E^{Red} [V]	ΔE [V]	I^{Ox} [μA]	I^{Red} [μA]	$I^{\text{Red}}/I^{\text{Ox}}$
<i>mTer</i> ₂ S	0.931	0.806	0.125	0.23	0.17	0.74
<i>mTer</i> ₂ Se	0.793	0.657	0.136	0.75	0.72	0.96
<i>mTer</i> ₂ Te	0.462	0.348	0.114	1.04	1.01	0.97

The cyclic voltammetry measurements reveal the reversibility or quasi-reversibility of the 2,6-dimesitylphenylchalcogenes, with $I^{\text{Red}}/I^{\text{Ox}} = 0.7 - 1.0$.

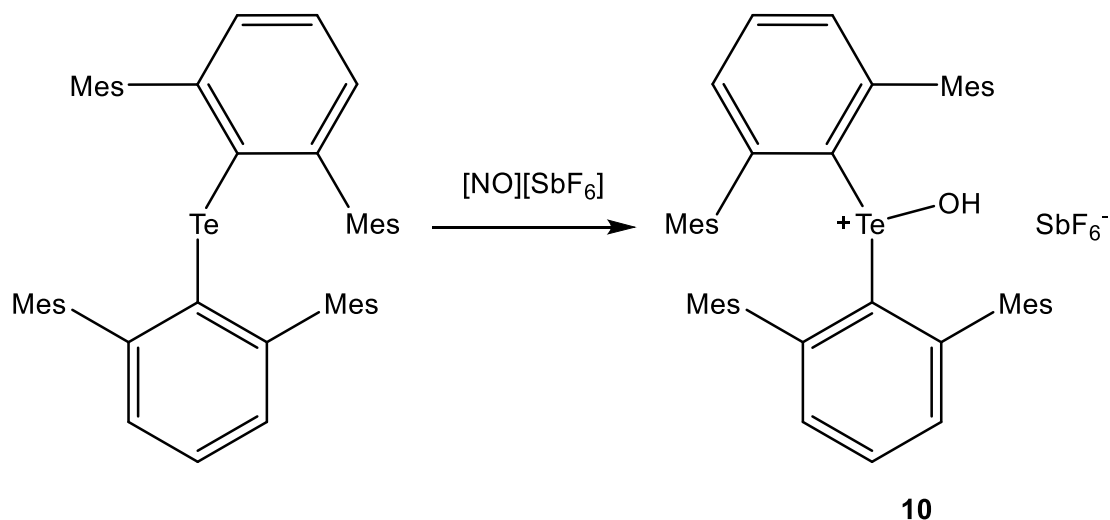
As described before by the workgroup of Jens Beckmann on the 2,6-dimesitylphenyldichalcogenes the 2,6-dimesitylphenylsulphide has the highest oxidation potential of + 0.93 V. With increasing period the oxidation potential decreases ($E^{\text{Ox}}(m\text{Ter}_2\text{Se}) = + 0.79$ V and $E^{\text{Ox}}(m\text{Ter}_2\text{Te}) = + 0.46$ V), which is also comparable to thianthrene and selenanthrene with oxidation potentials of + 0.69 and + 0.75 V.^[53]

Therefore, a suitable oxidizing reagent with an oxidation potential as high as + 0.93 V is needed to oxidize all three 2,6-dimesitylphenylchalcogenes.

2.10.1.2 Oxidation of 2,6-dimesitylphenyltelluride

Among the well known single electron oxidation reagents are the nitrosonium salts, which are described in numerous examples in literature.^[55,172–174]

The first attempt of oxidizing the *mTer*₂Te with nitrosonium hexafluoroantimonate resulted in [(2,6-Mes₂C₆H₃)₂TeOH][SbF₆], which could be crystalized in dichloromethane/*n*-hexane as can be seen in Scheme 22.



Scheme 22. Reaction of 2,6-dimesitylphenyltelluride with nitrosonium hexafluoroantimonate.

The crystal structure of the product of the reaction with nitrosonium hexafluoroantimonate is shown in Figure 23.

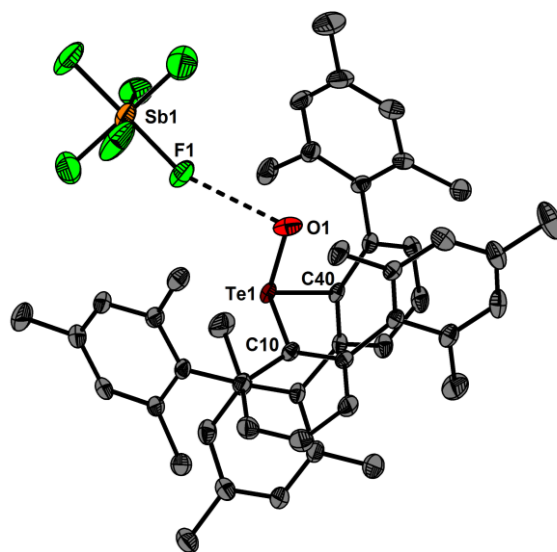


Figure 23. Molecular structure of $[(2,6\text{-Mes}_2\text{C}_6\text{H}_3)_2\text{TeOH}][\text{SbF}_6]$ (**10**) showing 50 % probability ellipsoids and the essential atom numbering. Selected bond parameters [\AA , $^\circ$]: Te1-C10 2.149(1), Te1-C40 2.118(1), C10-Te1-C40 108.1(5), Te1-O1 1.74(3), O1-F1 2.805(2).

In contrast to 2,6-dimesitylphenyldichalcogenides, which could be oxidized to the respective radical cations with nitrosonium hexafluoroantimonate in dichloromethane^[113], the oxidation of 2,6-dimesitylphenyltelluride led to no success.

2.10.2. Experimental

Reagents were obtained commercially (Sigma-Aldrich, Germany) and were used as received. Dry solvents were collected from a SPS800 mBraun solvent system. Diethyl ether was dried over potassium hydroxide and distilled of sodium/benzophenone. ^1H -, ^{13}C -, ^{77}Se - and ^{125}Te -NMR spectra were recorded at RT (unless otherwise stated) using a Bruker Avance-360 spectrometer and are referenced to tetramethylsilane (^1H , ^{13}C), diphenyldiselenide (^{77}Se) and telluric acid (^{125}Te). Chemical shifts are reported in parts per million (ppm) and coupling constants (J) are given in Hertz (Hz). Air sensitive substances were handled in gloveboxes "Labmaster" by M. Braun. The cyclic voltammetry measurements were carried out with a TSC 1600 Closed "Sealable Measuring Cell" by RHD Instruments with glass-sealed platinum-wires and a silver pseudo reference electrode. As potentiostat the Autolab PGSTAT101 by Metrohm was utilized, supported by the software Nova 2.1 by Metrohm. Tetrabutylammoniumhexafluorophosphate was used as conducting salt. The resulted cyclovoltgrams were referenced against the redox couple of ferrocene (Fc/Fc^+).

2.10.2.1 Synthesis of 2,6-dimesitylphenylsulphide (9a)

In a dried three-necked-flask, connected to a dropping funnel and a gas inlet 0.50 g (1.6 mmol) 2,6-dimesitylphenyllithium were dissolved in 20 ml dry diethyl ether and cooled to $-78\text{ }^{\circ}\text{C}$. Sulphur tetrafluoride was bubbled through the solution and the mixture was allowed to warm to room temperature overnight. The solvent was evaporated and the remaining solid was dried in vacuo, dissolved in 20 ml dry diethyl ether again and cooled to $-78\text{ }^{\circ}\text{C}$. Again 2,6-dimesitylphenyllithium, 1.5 g (4.7 mmol) dissolved in dry diethyl ether, was added dropwise. After stirring for 1 h the mixture was allowed to warm to room temperature and the solvent was evaporated. Unreacted 2,6-dimesitylphenyllithium was treated with dichloromethane. The solvent was evaporated and the resulting yellow solid was washed with ethanol and *n*-hexane. Recrystallization from tetrahydrofuran gave colourless crystals in 82 % (0.86 g) yield.

$^1\text{H-NMR}$ (360 MHz, CDCl_3): δ = 7.03 (t, $^3J_{\text{H,H}}$ = 7.6 Hz, 1H; *p*- C_6H_3), 6.77 (s, 4H; *m*-MesH), 6.75 (d, $^3J_{\text{H,H}}$ = 7.8 Hz, 2H; *m*- C_6H_3), 2.37 (s, 6H; *p*-ArCH₃), 1.66 (s, 12H; *o*-ArCH₃) ppm. **$^{13}\text{C}\{-^1\text{H}\}$ -NMR (90 MHz, CDCl_3):** δ = 145.4 (s; *ipso*- C_6H_3), 138.8 (s; *ipso*-Mes), 136.8 (s; *p*-Mes), 136.2 (s; *o*-Mes), 134.9 (s; *p*- C_6H_3), 131.6 (s; *m*-Mes), 128.3 (s; *m*- C_6H_3), 126.5 (s; *o*- C_6H_3), 21.4 (s; *o*-ArCH₃), 21.3 (s; *p*-ArCH₃) ppm.

2.10.2.2 Synthesis of 2,6-dimesitylphenylselenide (9b)

In a dried three-necked-flask under argon atmosphere connected to a dropping funnel 0.5 g (1.6 mmol) 2,6-dimesitylphenyllithium were dissolved in 20 ml dry diethyl ether and cooled to $-78\text{ }^{\circ}\text{C}$. To this solution 0.24 g (1.6 mmol) selenium tetrafluoride was added dropwise. The mixture was allowed to warm to room temperature overnight and the solvent was evaporated. The residue was dried in vacuo, dissolved in 20 ml dry diethyl ether and cooled to $-78\text{ }^{\circ}\text{C}$. Again 2,6-dimesitylphenyllithium 1.5 g (4.7 mmol) dissolved in dry diethyl ether was added dropwise. The resulting solution was allowed to warm to room temperature and the solvent was evaporated.

The unreacted 2,6-dimesitylphenyllithium was treated with 20 ml of dichloromethane and the solvent was evaporated once more. The residue was washed with ethanol and *n*-hexane. Recrystallization from tetrahydrofuran gave colourless crystals in 79 % (0.89 g) yield.

$^1\text{H-NMR}$ (360 MHz, CDCl_3): δ = 7.06 (t, $^3J_{\text{H,H}}$ = 7.5 Hz, 1H; *p*- C_6H_3), 6.75 (s, 4H; *m*-MesH), 6.74 (d, $^3J_{\text{H,H}}$ = 7.8 Hz, 2H; *m*- C_6H_3), 2.35 (s, 6H; *p*-ArCH₃), 1.66 (s, 12H; *o*-ArCH₃) ppm. **$^{13}\text{C}\{-^1\text{H}\}$ -NMR (90 MHz, CDCl_3):** δ = 146.0 (s; *ipso*- C_6H_3), 139.9 (s; *ipso*-Mes), 136.4 (s; *p*-Mes), 136.3 (s; *o*-Mes), 132.5 (s; *p*- C_6H_3), 130.8 (s; *m*-Mes), 128.2 (s; *m*- C_6H_3), 126.9 (s; *o*- C_6H_3), 21.4 (s; *o*-ArCH₃), 21.3 (s; *p*-ArCH₃) ppm. **$^{77}\text{Se-NMR}$ (69 MHz, CDCl_3):** δ = 423.9 ppm.

2.10.2.3 Synthesis of 2,6-dimesitylphenyltelluride (9c)

In a dried three-necked-flask under argon atmosphere connected to a dropping funnel 3.15 g (9.8 mmol) 2,6-dimesitylphenyllithium were dissolved in 30 ml dry diethyl ether and cooled to $-78\text{ }^{\circ}\text{C}$. To this solution a suspension of 0.50 g (2.5 mmol) tellurium tetrafluoride in dry diethyl ether was added dropwise, while the resulting solution turns dark red. The mixture was allowed to warm to room temperature overnight and the solvent was evaporated. The remaining solid was treated with 20 ml of dichloromethane to destroy the unreacted 2,6-dimesitylphenyllithium and evaporated again. After washing with ethanol and *n*-hexane a yellow solid was obtained. Recrystallization from dichloromethane gave bright yellow crystals in 89 % (0.89 g) yield.

$^1\text{H-NMR}$ (360 MHz, CDCl_3): $\delta = 7.33$ (t, $^3J_{\text{H,H}} = 7.5$ Hz, 1H; *p*- C_6H_3), 6.86 (d, $^3J_{\text{H,H}} = 7.6$ Hz, 2H; *m*- C_6H_3), 6.84 (s, 4H; *m*-MesH), 2.45 (s, 6H; *p*-ArCH₃), 1.68 (s, 12H; *o*-ArCH₃) ppm. **$^{13}\text{C}\{-^1\text{H}\}$ -NMR (90 MHz, CDCl_3):** $\delta = 144.6$ (s; *ipso*- C_6H_3), 138.4 (s; *ipso*-Mes), 137.8 (s; *p*-Mes), 136.7 (s; *o*-Mes), 131.1 (s; *p*- C_6H_3), 130.4 (s; *m*-Mes), 128.2 (s; *m*- C_6H_3), 128.1 (s; *o*- C_6H_3), 21.4 (s; *o*-ArCH₃), 20.7 (s; *p*-ArCH₃) ppm. **$^{125}\text{Te-NMR}$ (110 MHz, CDCl_3):** $\delta = 1291.3$ ppm.

2.10.2.4 Synthesis of 2,6-dimesitylphenylhydroxyltelluronium hexafluoroantimonate

In a 100 ml schlenk tube 284 mg (0.38 mmol) 2,6-dimesitylphenyltelluride and 100 mg (0.38 mmol) nitrosonium hexafluoroantimonate were stirred with 10 ml of dry dichloromethane for 30 minutes at $-78\text{ }^{\circ}\text{C}$. After warming to room temperature, the product was covered with dry *n*-hexane to gain light green crystals in 93 % (356 mg) yield.

$^1\text{H-NMR}$ (360 MHz, CDCl_3): $\delta = 7.61$ (t, $^3J_{\text{H,H}} = 7.5$ Hz, 1H; *p*- C_6H_3), 7.09 (d, $^3J_{\text{H,H}} = 7.5$ Hz, 2H; *m*- C_6H_3), 6.91 (d, $^3J_{\text{H,H}} = 4.9$ Hz, 2H; *m*-MesH), 2.37 (s, 6H; *p*-ArCH₃), 2.04 (s, 1H; TeOH), 1.75 (d, $^3J_{\text{H,H}} = 18.5$ Hz, 12H; *o*-ArCH₃) ppm. **$^{13}\text{C}\{-^1\text{H}\}$ -NMR (90 MHz, CDCl_3):** $\delta = 147.4$ (s; *ipso*- C_6H_3), 140.1 (s; *ipso*-Mes), 137.5 (s; *p*-Mes), 136.8 (s; *o*-Mes), 134.9 (s; *p*- C_6H_3), 133.9 (s; *m*-Mes), 133.6 (s; *m*- C_6H_3), 129.7 (d, $J = 21.0$ Hz; *o*- C_6H_3), 21.9 (d, $J = 14.4$ Hz; *o*-ArCH₃), 21.3 (s; *p*-ArCH₃) ppm. **$^{125}\text{Te-NMR}$ (110 MHz, CDCl_3):** $\delta = 1572.2$ ppm.

X-ray crystallography. Intensity data of $(2,6\text{-Mes}_2\text{C}_6\text{H}_3)_2\text{E}$ (**9a**, E = S; **9b**, E = Se; **9c**, E = Te) and $[(2,6\text{-Mes}_2\text{C}_6\text{H}_3)_2\text{TeOH}][\text{SbF}_6]$ (**10**) were collected on a Bruker Venture D8 diffractometer with graphite-monochromated Mo-K α (0.7107 Å) radiation. The structure was solved by direct methods and difference Fourier synthesis with subsequent Full-matrix least-squares refinements on F^2 , using all data.^[140] All non-hydrogen atoms were refined using anisotropic displacement parameters. Hydrogen atoms were included in geometrically calculated positions using a riding model. Crystal and refinement data are collected in Table 11. Figures were created using DIAMOND.^[141]

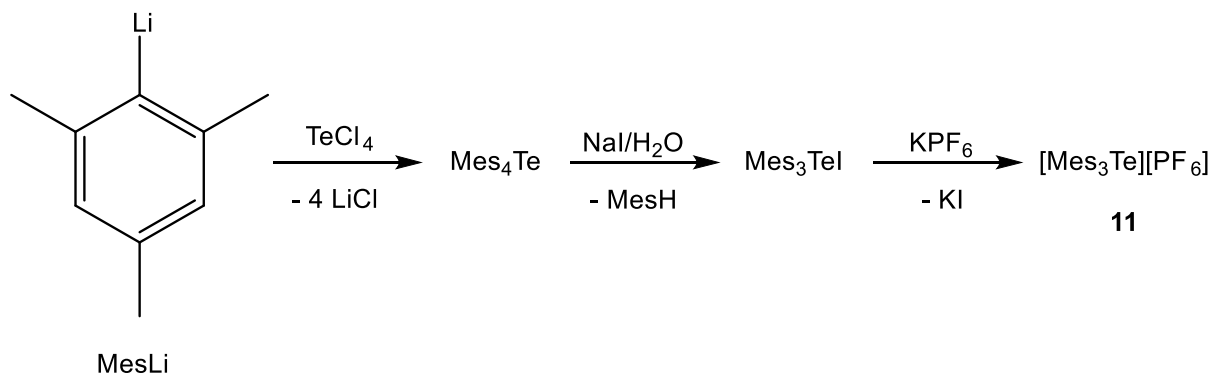
Table 11. Crystal data and structure refinement of 1a – 1c and 2.

	9a ·CH ₂ Cl ₂	9b	9c	10
<i>Formula</i>	C ₄₈ H ₅₀ S·CH ₂ Cl ₂	C ₄₈ H ₅₀ Se	C ₄₈ H ₅₀ Te	C ₄₈ H ₅₀ TeOHSbF ₆
<i>Formula weight, g mol⁻¹</i>	743.87	705.84	754.48	1007.29
<i>Crystal system</i>	Triclinic	Orthorhombic	Orthorhombic	Monoclinic
<i>Crystal size, mm</i>	0.06 × 0.06 × 0.05	0.07 × 0.06 × 0.04	0.07 × 0.05 × 0.04	
<i>Space group</i>	P-1	Fdd2	Fdd2	P 2/c
<i>a, Å</i>	9.1237(3)	20.3777(4)	20.657(5)	16.706(5)
<i>b, Å</i>	13.1914(6)	42.9059(8)	43.485(5)	13.988(5)
<i>c, Å</i>	17.1003(8)	8.3558(2)	8.277(5)	21.144(5)
<i>α, °</i>	92.204(2)	90	90	90
<i>β, °</i>	102.208(2)	90	90	92.111(5)
<i>γ, °</i>	91.970(2)	90	90	90
<i>V, Å³</i>	2008.2(2)	7305.7(3)	7435(5)	4937.65(300)
<i>Z</i>	2	8	8	4
<i>ρ_{calcd}, Mg m⁻³</i>	1.230	1.283	1.348	1.355
<i>μ (Mo Kα), mm⁻¹</i>	0.247	1.061	0.833	1.191
<i>F(000)</i>	792	2976	3120	2016
<i>θ range, deg</i>	2.29 to 30.03	2.68 to 29.87	2.18 to 37.57	2.15 to 28.36
<i>Index ranges</i>				
	-12 ≤ h ≤ 16	-28 ≤ h ≤ 28	-35 ≤ h ≤ 35	-22 ≤ h ≤ 22
	-18 ≤ k ≤ 19	-60 ≤ k ≤ 60	-74 ≤ k ≤ 74	-18 ≤ k ≤ 18
	-24 ≤ l ≤ 28	-11 ≤ l ≤ 11	-14 ≤ l ≤ 14	-28 ≤ l ≤ 28
<i>No. of reflns collected</i>	39968	206200	150801	390756
<i>Completeness to θ_{max}</i>	99.2%	99.9%	99.9%	99.7%
<i>No. indep. Reflns</i>	11647	5367	9813	12310
<i>No. obsd reflns with (I > 2σ(I))</i>	9566	5144	9507	9805
<i>No. refined params</i>	481	228	228	600
<i>GooF (F²)</i>	1.107	1.030	1.123	1.047
<i>R₁ (F) (I > 2σ(I))</i>	0.0595	0.0514	0.0156	0.0589
<i>wR₂ (F²) (all data)</i>	0.1600	0.1264	0.0404	0.1717
<i>Largest diff peak/hole, e Å⁻³</i>	1.114 / -0.674	2.428 / -1.825	0.358 / -0.552	1.220 / -1.029

2.11. Synthesis and Characterization of Trimesityltelluronium hexafluorophosphate

2.11.1. Introduction & Results

The synthesis of trimesityltelluronium iodide was reported by Wieber and Habersack in 1995^[175] which reacts with potassium hexafluorophosphate to trimesityltelluronium hexafluorophosphate in quantitative yield.



Scheme 23. Synthesis of trimesityltellurium hexafluorophosphate.

Starting from mesityllithium, which can be obtained by the reaction of 2-bromomesitylene with *n*-butyllithium, a slightly smaller amount of tellurium tetrachloride is added. The resulting tetramesityltellurium is treated with aqueous sodium iodide solution, leading to trimesityltelluronium iodide. Potassium hexafluorophosphate is added, generating trimesityltellurium hexafluorophosphate.

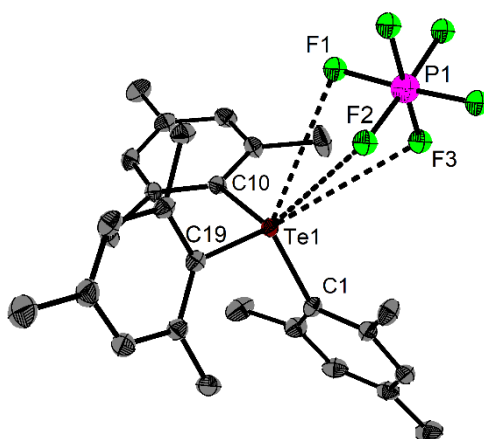


Figure 24. Molecular structure of [Mes₃Te][PF₆] showing 50 % probability ellipsoids and the essential atom numbering. Selected bond parameters [Å, °]: Te1-C1 2.132(3), Te1-C10 2.125(3), Te1-C19 2.131(3), C1-Te1-C10 104.26(1), Te1-F1 3.583(3), Te1-F2 3.554(1), Te1-F3 3.563(2).

The Te-C distances of 2.13 Å in all three mesityl groups are close to the sum of covalent radii (2.11 Å)^[171] and the distances to the three closest fluorides in hexafluorophosphate with 3.57 Å are noticeably smaller than the sum of Van-der-Waals-radii of 3.76 Å.^[176]

2.11.2. Experimental

Reagents were obtained commercially (Sigma-Aldrich, Germany) and were used as received. Dry solvents were collected from a SPS800 mBraun solvent system. Diethyl ether was dried over potassium hydroxide and distilled of sodium/benzophenone. ¹H-, ¹³C-, ¹⁹F-, ³¹P- and ¹²⁵Te-NMR spectra were recorded at RT (unless otherwise stated) using a Bruker Avance-360 spectrometer and are referenced to tetramethylsilane (¹H, ¹³C), phosphoric acid (85% in water) (³¹P), trichlorofluoromethane (¹⁹F) and telluric acid (¹²⁵Te). Chemical shifts are reported in parts per million (ppm) and coupling constants (*J*) are given in Hertz (Hz). Air sensitive substances were handled in gloveboxes "Labmaster" by M. Braun. The electrospray ionization mass spectrometry (ESI-MS) spectrum was obtained on the Bruker Impact II. Acetonitrile solutions were injected directly into the spectrometer at a flow rate of 3 μl min⁻¹. Nitrogen was used both as a drying gas and for nebulization with flow rates of approximately 4 L min⁻¹ and a pressure of 0.4 bar. The spectrum was collected for one minute and averaged.

2.11.2.1. Mesityllithium

In a dried schlenk tube 6.0 ml (39.8 mmol) 2-bromomesitylene was dissolved in 20 ml dry hexane. To this solution 17.6 ml *n*-butyllithium (2.5-M in *n*-hexane) was added and the mixture was stirred overnight. The resulting mesityllithium was filtrated and washed with dry *n*-hexane to gain 3.21 g (64 %).

2.11.2.2. Trimesityltelluronium iodide

The synthesis of trimesityltelluriniumiodide was carried out according to Wieber and Habersack.^[175] 1 g (7.9 mmol) mesityllithium was stirred in 10 ml dry diethyl ether and cooled down to -78 °C. To this suspension 0.43 g (1.6 mmol) tellurium tetrachloride in 10 ml dry diethyl ether was added dropwise. The solution was allowed to warm up to room temperature and stirred for additional two hours. After treating with aqueous sodium iodide solution, the reaction mixture was warmed to 40 °C, while the trimesityltelluroniumiodide precipitates. Extraction with dichloromethane and washing with water gave trimesityltelluroniumiodide in 86 % (1.14 g) yield.

2.11.2.3. Trimesityltelluronium hexafluorophosphate

Without further purification the trimesityltelluronium iodide was dissolved in dry toluene and treated with potassium hexafluorophosphate. Potassium iodide was filtered off. The solvent

was removed and the product was obtained in quantitative yield (1.19 g). Recrystallization from dichloromethane/*n*-hexane gave yellow crystals in 89 % (1.05 g) yield.

¹H-NMR (360 MHz, CDCl₃): δ = 7.04 (t, ³J_{H,H} = 7.6 Hz, 1H; *p*-C₆H₃), 6.77 (s, 4H; *m*-MesH), 6.74 (d, ³J_{H,H} = 7.8 Hz, 2H; *m*-C₆H₃), 2.37 (s, 6H; *p*-ArCH₃), 1.66 (s, 12H; *o*-ArCH₃) ppm. **¹³C-{¹H}-NMR (90 MHz, CDCl₃):** δ = 145.4 (s; *ipso*-C₆H₃), 138.8 (s; *ipso*-Mes), 136.8 (s; *p*-Mes), 136.2 ((s; *o*-Mes), 134.9 (s; *p*-C₆H₃), 131.6 (s; *m*-Mes), 128.3 (s; *m*-C₆H₃), 126.5 (s; *o*-C₆H₃), 21.38 (s; *o*-ArCH₃), 21.27 (s; *p*-ArCH₃) ppm. **¹⁹F-NMR (188 MHz, CDCl₃):** δ = 72.2 - 76.0 (d, J = 713.5 Hz, PF₆) ppm. **³¹P-NMR (240 MHz, CDCl₃):** δ = - 143.1 (hept, ¹J_{P,F} = 704.2 Hz) ppm. **¹²⁵Te-NMR (110 MHz, CDCl₃):** δ = 243.5 ppm. **MS (ESI, methanol, positive mode):** *m/z* (rel.Int.) = 487 (100) [Mes₃Te⁺]. **MS (ESI, methanol, negative mode):** *m/z* (rel.Int.) = 145 (100) [PF₆⁻].

X-ray crystallography. Intensity data of [Mes₃Te][PbF₆] was collected on a Bruker Venture D8 diffractometer with graphite-monochromated Mo-Kα (0.7107 Å) radiation. The structure was solved by direct methods and difference Fourier synthesis with subsequent Full-matrix least-squares refinements on *F*², using all data.^[140] All non-hydrogen atoms were refined using anisotropic displacement parameters. Hydrogen atoms were included in geometrically calculated positions using a riding model. Crystal and refinement data are collected in Table 1. Figures were created using DIAMOND.^[141]

Table 12. Crystal data and structure refinement of [Mes₃Te][PF₆] (**11**).

<i>Formula</i>	<i>C₂₇H₃₃Te PF₆</i>
<i>Formula weight, g mol⁻¹</i>	630.13
<i>Crystal system</i>	orthorhombic
<i>Crystal size, mm</i>	0.05 × 0.05 × 0.05
<i>Space group</i>	P b c a
<i>a, Å</i>	15.722(3)
<i>b, Å</i>	16.995(3)
<i>c, Å</i>	19.721(4)
<i>α, °</i>	90
<i>β, °</i>	90
<i>γ, °</i>	90
<i>V, Å³</i>	5269.36(170)
<i>Z</i>	8
<i>ρ_{calcd}, Mg m⁻³</i>	1.589
<i>F(000)</i>	2528
<i>θ range, deg</i>	2.40 to 30.80
<i>Index ranges</i>	-22 ≤ h ≤ 22 -24 ≤ k ≤ 24 -28 ≤ l ≤ 28
<i>No. of reflns collected</i>	520177
<i>Completeness to θ_{max}</i>	99,8%
<i>No. indep. Reflns</i>	8251
<i>No. obsd reflns with (I > 2σ(I))</i>	7500
<i>No. refined params</i>	8251
<i>GooF (F²)</i>	1.07
<i>R₁ (F) (I > 2σ(I))</i>	0.042
<i>wR₂ (F²) (all data)</i>	0.146
<i>Largest diff peak/hole, e Å⁻³</i>	3.81 / -1.53

3. Conclusion

In the course of this work various new compounds were synthesized and characterized by common methods. The well-defined dibenzodioxine type heterocycle phenoxatellurine (PT) was investigated in its behaviour towards single electron oxidating reagents, such as nitrosonium salts, resulting in diamagnetic double decker respectively triple decker structures which can be described as dimers of the elusive radical cation $[PT]^+$.

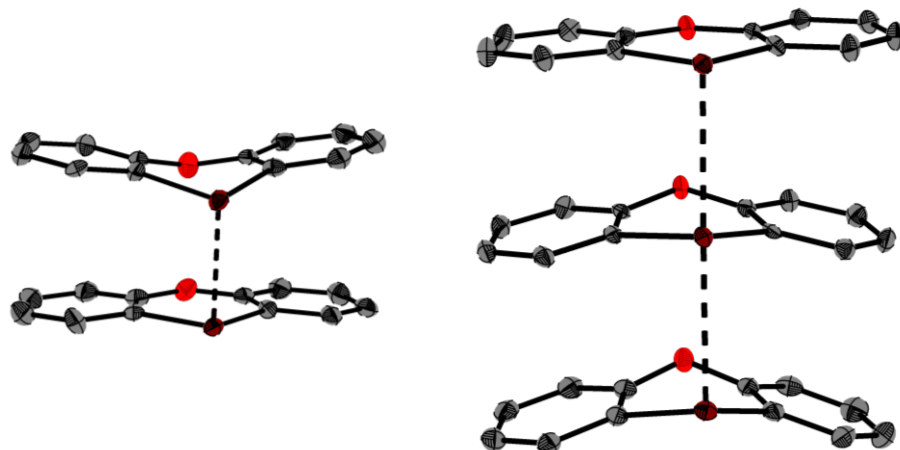


Figure 25. Phenoxatellurine double decker and triple decker structures (respective anions omitted).

The stacking derives not just from London dispersion interactions and non-covalent multi-centre bonding between the tellurium atoms, but also from SOMO-SOMO interactions between two radical cations $[PT]^+$, also known as “pancake” bonding,^[177] which can be realized due to the change in the conformation of the PT units upon oxidation. The oxidations with nitrosonium hexafluoroantimonate gave rise to a phenoxatellurine double decker cation, whereas the tetrafluoroborate salt gave rise to a triple decker structure.

The reaction of PT with triflic acid led to relatively air stable triple decker structures in three different modifications, which were investigated by Hirshfeld surface analysis.^[129] Upon exposure to moist air for several weeks an oxo-bridged dimer or trimer structure evolved.

Based on the well known behaviour as a donor^[178] the first PT charge-transfer complex with 1,2,5-thiadiazole derivatives was prepared and characterized. Upon gasphase cocrystallization a complex in ratio of 1:3 in favour of the thiadiazole acceptor was obtained. Furthermore an octahedral complex by the reaction of $(CO)_5MnBr$ with PT was obtained, that has two PT ligands situated in *cis*-position, similar to the structure described by Hieber and Kruck in 1962.^[142] In 1926 Drew discovered intensively colored solutions by dissolving PT in conc. sulphuric acid.^[134] Almost 100 years later the nature of one of those species, which is responsible for the

color, has been unravelled. X-ray diffraction reveal a PT double decker structure with hydrogensulphate ions associated via secondary interactions.

The condensation reaction of 4,4'-dimethyldiphenylether with tellurium tetrachloride afforded 2,8-dimethyl-10,10-dichlorophenoxatellurine which shows, compared to the unsubstituted PT, a planar structure in which the Cl atoms are arranged in the axial positions, while the two C atoms are arranged in the equatorial positions. Attempts on reducing the structure to 2,8-dimethylphenoxatellurine were unsuccessful.

Isoelectronic to the neutral PT, dibenzo[*b,e*][1,4]iodaoxin-5-ium 4-methylbenzenesulphonate [C₁₂H₈OI][O₃S(*p*-C₆H₄Me)] was prepared. The phenoxaiodonium ion possesses also a butterfly-like conformation with nearly identical I-C bond length compared to Te-C in phenoxatellurine.

The first 8-methoxanaphthyltellurium compounds have been introduced enhancing the variety of peri-substituted naphthyl and acenaphthyl species. Furthermore new acenaphthene compounds have been obtained with a diphenylphosphino-group in the 5-position and phenylchalcogenes in 6, opening a new path for oxidization to chalcogen radical cations. Unfortunately no acenaphthene radical cation was obtained upon the oxidation with nitrosonium salts.

The synthesis of a trimesityltelluronium cation was made accessible, which can be used as a precursor on the way to stable radical cations.

Moreover organotellurium compounds with bulky 2,6-dimesitylphenyl groups, namely 2,6-dimesitylsulphide, 2,6-dimesitylphenylselenide and 2,6-dimesitylphenyltelluride were synthesized and characterized. First attempts of oxidizing 2,6-dimesitylphenyltelluride with nitrosonium hexafluoroantimonate led to the 2,6-dimesitylphenylhydroxyltelluronium hexafluoroantimonate. The problem in this reaction can be the presence of the nitrosonium ion, which is quite reactive and can thus disturb the reaction. Furthermore a more suitable oxidizing reagent that coordinates weaker than hexafluoroantimonate, hexafluorophosphate or tetrafluoroborate could also lead to more stable radical cation, such as tetrakis(3,5-bis(trifluoromethyl)phenyl)borate ([BaAr^F₄]⁻).^[179]

4. Zusammenfassung

In der vorliegenden Arbeit konnten eine Reihe von neuen Verbindungstypen dargestellt und charakterisiert werden. Die Reaktion von Phenoxatellurin (PT) mit Ein-Elektronen-Oxidationsmitteln, wie verschiedene Nitrosylsalze, führte zur Bildung von Doppeldecker- bzw Trippeldeckerstrukturen, die als Dimer der entsprechenden Radikalkationen $[PT]^{\bullet+}$ angesehen werden können.

Diese Dimerisierung kann aufgrund der Änderung des Faltwinkels entlang der O-Te Achse erfolgen. Die dabei resultierenden Wechselwirkungen lassen sich nicht nur auf London-Kräfte und nicht kovalente Multizentrenbindungen zwischen den Telluratomen zurückführen, sondern sind auch von SOMO-SOMO-Wechselwirkungen zwischen den Radikalkationen $[PT]^{\bullet+}$, genannt „pancake bonding“^[177] geprägt.

Die Oxidation mit Nitrosylhexafluoroantimonat führt zur Bildung einer Doppeldecker- und mit dem Tetrafluoroboratsalz zu einer Trippeldeckerstruktur.

Die Reaktion mit Trifluormethansulphonsäure ergab ebenfalls Trippeldeckerstrukturen, wobei aber drei verschiedene Modifikationen erhalten wurden. Diese wurden mittels Crystal Explorer mit der Hirshfeld Surface Analyse^[129] auf ihre unterschiedlichen Wechselwirkungen untersucht. Nach längerem Kontakt an der Luft wurde ein Oxo-Dimer bzw. Oxo-Trimer erhalten, was ebenfalls kristallographisch nachgewiesen werden konnte.

Basierend auf den Donoreigenschaften des Phenoxatellurin konnte auch der erste Charge-Transfer Komplex mit 1,2,5-Thiadiazolederivaten dargestellt werden, wobei die hohe Stabilität sogar eine Gasphasen Kokristallization zuließ. Ferner ergab die Reaktion von $(CO)_5MnBr$ mit PT einen oktaedrischen Mangankomplex mit drei CO-Molekülliganden in facialer Anordnung und zwei PT Einheiten in *cis*-Stellung.

Drew entdeckte 1926, dass sich Phenoxatellurin, ähnlich wie Thianthren, in konzentrierter Schwefelsäure unter Bildung stark farbiger Lösungen löst, konnte allerdings, aufgrund von zu damaliger Zeit fehlenden analytischen Methoden, keine genauen Rückschlüsse über die erhaltenen Strukturen ziehen. Fast 100 Jahre nach der Entdeckung konnten die erhaltenen Strukturen mittels Röntgenstrukturanalyse ermittelt werden.

Die Kondensationsreaktion zwischen Di-*p*-tolylether und Tellurtetrachlorid führte zu 2,8-Dimethyl-10,10-Dichlorphenoxatellurin, das im Gegensatz zu dem 10,10-Dichlorphenoxatellurin eine planare Struktur aufweist. Der Versuch zur Reduktion zu 2,8-Dimethylphenoxatellurin führte jedoch zu keinem Erfolg.

Das zu dem PT isoelektronische Iodosoniumsalz $[\text{C}_{12}\text{H}_8\text{OI}][\text{O}_3\text{S}(p\text{-C}_6\text{H}_4\text{Me})]$ konnte im Zuge dieser Arbeit ebenfalls dargestellt werden. Die Diaryliodoniumsalze rückten aufgrund ihrer pharmakologischen Eigenschaften ins Interesse der Forschung.

Zudem konnte die erste 8-Methoxynaphtyltellurverbindung dargestellt werden. Auch konnten neue Acenaphthenverbindungen mit Diphenylphosphin in *peri*-Stellung zu Chalkogenphenylen synthetisiert werden. Allerdings konnten diese nicht mit den Nitrosylsalzen zum Radikalkation oxidiert werden.

Des Weiteren wurde Trimesityltellurioniumhexafluorophosphat aus dem entsprechenden Iodid gewonnen und charakterisiert.

Schließlich wurden Chalkogenverbindungen mit sterisch anspruchsvolleren 2,6-Dimesitylphenylresten (*m*-Terphenyl) dargestellt. Das dabei erhaltenen Bis(*m*-Terphenyl)sulphid, Bis(*m*-Terphenyl)selenid und Bis(*m*-Terphenyl)tellurid könnte, aufgrund des großen organischen Gerüsts die Radikalbildung der jeweiligen Chalkogene weit genug abschirmen, um diese zu stabilisieren. Allerdings führte die erste Umsetzung von Bis(*m*-Terphenyl)tellurid mit Nitrosylhexafluoroantimonat zu Bis(*m*-Terphenyl)hydroxotellurioniumhexafluoroantimonat.

Vermutlich ist die Wahl der Nitrosylsalze für diese Reaktionen eher ungeeignet, da das Nitrosyl die Reaktion stören könnte, obwohl in der Arbeitsgruppe die Bis(*m*-Terphenyl)dichalkogene bereits erfolgreich zu Radikalkationen oxidiert werden konnten.^[113] Durch die Verwendung schwach koordinierender Anionen, zum Beispiel dem Tetrakis(3,5-bis(trifluormethyl)phenyl)borat ($[\text{BAr}^{\text{F}}_4]^-$) könnten die gewünschten Radikale erhalten werden.

5. References

- [1] Nehb, W.; Vydra, K. Sulphur. *Ullmann's encyclopedia of industrial chemistry*; Wiley: Chichester **2010**; p 3748.
- [2] *Fertilizer manual*, UNIDO; International Fertilizer Development Center, 3. ed.; Kluwer Academic Publ: Dordrecht **1998**.
- [3] Lechner, M. D.; Gehrke, K.; Nordmeier, E. H. *Makromolekulare Chemie: Ein Lehrbuch für Chemiker, Physiker, Materialwissenschaftler und Verfahrenstechniker*, 4. überarbeitete und erweiterte Auflage; Birkhäuser Basel: Basel, **2010**.
- [4] Asinger, F.; Thiel, M. Einfache Synthesen und chemisches Verhalten neuer heterocyclischer Ringsysteme. *Angew. Chem.* **1958**, *70*, 667–683. DOI: 10.1002/ange.19580702202.
- [5] March, J. *Advanced organic chemistry: Reactions, mechanisms, and structure*, 4. ed.; A Wiley Interscience publication; Wiley: New York, **1992**.
- [6] Weeks, M. E. The discovery of the elements. VI. Tellurium and selenium. *J. Chem. Educ.* **1932**, *9*, 474. DOI: 10.1021/ed009p474.
- [7] Löwig, C. Ueber Schwefelwasserstoff- und Selenwasserstoffäther. *Ann. Phys. Chem.* **1836**, *113*, 550–553. DOI: 10.1002/andp.18361130315.
- [8] Comasseto, J. V. *et al.* Vinylic Selenides and Tellurides - Preparation, Reactivity and Synthetic Applications. *Synthesis* **1997**, *1997*, 373–403. DOI: 10.1055/s-1997-1210.
- [9] Riley, H. L.; Morley, J. F.; Friend, N. A. C. 255. Selenium dioxide, a new oxidising agent. Part I. Its reaction with aldehydes and ketones. *J. Chem. Soc.* **1932**, 1875. DOI: 10.1039/jr9320001875.
- [10] Simpson, R. E. *et al.* Interfacial phase-change memory. *Nature Nanotech* **2011**, *6*, 501–505. DOI: 10.1038/nnano.2011.96.
- [11] Lide, D. R., Ed. *CRC handbook of chemistry and physics: A ready-reference book of chemical and physical data*, 86. ed.; CRC Press: Boca Raton, **2005**.
- [12] Devillanova, F. A.; Du Mont, W.-W., Eds. *Handbook of chalcogen chemistry: New perspectives in sulphur, selenium and tellurium*, Second edition; Royal Society of Chemistry: Cambridge, **2013**.
- [13] Brownridge, S. *et al.* Recent advances in the understanding of the syntheses, structures, bonding and energetics of the homopolyatomic cations of Groups 16 and 17. *Coordination Chemistry Reviews* **2000**, *197*, 397–481. DOI: 10.1016/S0010-8545(00)00230-7.
- [14] Holleman, A. F.; Wiberg, E.; Wiberg, N. *Lehrbuch der anorganischen Chemie*, 102., stark umgearb. u. verb. Aufl.; de Gruyter: Berlin, **2007**.
- [15] Klaproth. XVIII. Extract from a memoir on a new metal called tellurium. *The Philosophical Magazine* **1798**, *1*, 78–82. DOI: 10.1080/14786447808676799.
- [16] Gillespie, R. J. *et al.* Polyatomic cations of tellurium. I. The +1/3, +1/2, and +1 oxidation states of tellurium. *Inorg. Chem.* **1971**, *10*, 362–367. DOI: 10.1021/ic50096a029.

- [17] Dean, P. A. W. *et al.* Polyatomic Cations of Sulphur, Selenium, and Tellurium. In *Inorganic syntheses: Volume 15*; Parshall, G. W., Ed.; Inorganic syntheses, 1934-4716 15; McGraw Hill: New York, **1974**; pp 213–222.
- [18] Burns, R. C.; Gillespie, R. J. Vibrational spectra and analyses of the S_4^{2+} , Se_4^{2+} , Te_4^{2+} , and trans- $Te_2Se_2^{2+}$ polyatomic cations. *Inorg. Chem.* **1982**, *21*, 3877–3886. DOI: 10.1021/ic00141a004.
- [19] Tomaszewicz, I. *et al.* Thermochemistry of tetrachalcogen-bis-hexafluoroarsenate salts $M_4(AsF_6)_2$ (M=Se or Te) containing lattice-stabilized cyclic M_4^{2+} cations. *The Journal of Chemical Thermodynamics* **1996**, *28*, 1019–1028. DOI: 10.1006/jcht.1996.0087.
- [20] Beck, J. *et al.* Synthese, Struktur und Phasenumwandlung von $Te_4[AsF_6]_2 \cdot SO_2$. *Z. anorg. allg. Chem.* **2003**, *629*, 1073–1079. DOI: 10.1002/zaac.200300044.
- [21] Passmore, J.; Sutherland, G.; White, P. S. Preparation and crystal structures of $(S_7)_4S_4(AsF_6)_6$ and $S_4(AsF_6)_2 \cdot 0.6SO_2$; a convenient synthesis of hexafluoroarsenate salts of chalcogen homoatomic cations. *J. Chem. Soc., Chem. Commun.* **1980**, 330–331. DOI: 10.1039/C39800000330.
- [22] Passmore, J.; Sutherland, G.; White, P. S. Preparation and x-ray crystal structure of μ -iodo-bis(4-iodo-cycloheptasulphur) tris(hexafluoroantimonate)-bis-(arsenic trifluoride), $[(S_7I)_2]_3(SbF_6)_3 \cdot 2AsF_3$, and $(S_7I)_4S_4(AsF_6)_6$ containing the iodo-cycloheptasulphur(1^+) and the tetrasulphur(2^+) cations. *Inorg. Chem.* **1982**, *21*, 2717–2723. DOI: 10.1021/ic00137a036.
- [23] Murchie, M. P. *et al.* Halogen-facilitated preparation of $S_4(AsF_6)_2 \cdot xSO_2$ ($x \leq 1$) and $S_4(Sb_2F_{11})_2$, and a convenient synthesis of $Se_4(AsF_6)_2$ and $Se_4(Sb_2F_{11})_2$. *J. Chem. Soc., Dalton Trans.* **1992**, *10*, 503–508. DOI: 10.1039/DT9920000503.
- [24] Cameron, T. S. *et al.* Preparation, X-ray Crystal Structure Determination, Lattice Potential Energy, and Energetics of Formation of the Salt $S_4(AsF_6)_2 \cdot AsF_3$ Containing the Lattice-Stabilized Tetrasulphur [2^+] Cation. Implications for the Understanding of the Stability of M_4^{2+} and M^{2+} (M = S, Se, and Te) Crystalline Salts. *Inorg. Chem.* **2000**, *39*, 2042–2052. DOI: 10.1021/ic990850j.
- [25] Cowley, A. H., Ed. *Inorganic syntheses: Volume 31*; Inorganic Syntheses v. 62; Wiley: New York, **1997**.
- [26] Barr, J.; Gillespie, R. J.; Ummat, P. K. The cation S_4^{2+} . *J. Chem. Soc. D* **1970**, 264. DOI: 10.1039/C29700000264.
- [27] Gillespie, R. J.; Passmore, J. The compounds $S_8(AsF_6)_2$ and $S_{16}(AsF_6)_2$. *J. Chem. Soc. D* **1969**, 1333. DOI: 10.1039/C29690001333.
- [28] Stenhouse, J. Products of the Destructive Distillation of the Sulphobenzolates. No. II. *Proceedings of the Royal Society of London* **1868**, *17*, 62–67. DOI: 10.1098/rspl.1868.0006.
- [29] Stenhouse, J. Ueber die Producte der trockenen Destillation der sulphobenzolsauren Salze. *Ann. Chem. Pharm.* **1869**, *149*, 247–255. DOI: 10.1002/jlac.18691490216.

- [30] Fries, K.; Volk, W. Über Thianthrene. *Ber. Dtsch. Chem. Ges.* **1909**, *42*, 1170–1176. DOI: 10.1002/cber.190904201190.
- [31] Fries, K.; Koch, H.; Slukenbrock, H. Zur Kenntnis des Thianthrens. *Ann. Chem. Pharm.* **1929**, *468*, 162–201. DOI: 10.1002/jlac.19294680108.
- [32] Diltthey, W. Bonner Chemische Gesellschaft. *Angew. Chem.* **1929**, *42*, 668–670. DOI: 10.1002/ange.19290422405.
- [33] Gomberg, M. Triphenylmethyl, ein Fall von dreiwertigem Kohlenstoff. *Ber. Dtsch. Chem. Ges.* **1900**, *33*, 3150–3163. DOI: 10.1002/cber.19000330369.
- [34] Gomberg, M. An Instance Of Trivalent Carbon: Triphenylmethyl. *J. Am. Chem. Soc.* **1900**, *22*, 757–771. DOI: 10.1021/ja02049a006.
- [35] Hirshon, J. M.; Gardner, D. M.; Fraenkel, G. K. Evidence for the Existence of Radicals in the Presence of Lewis Acids. *J. Am. Chem. Soc.* **1953**, *75*, 4115. DOI: 10.1021/ja01112a541.
- [36] Fava, A.; Sogo, P. B.; Calvin, M. Chemistry and Spin Resonance Spectroscopy of Radicals from Thioaromatic Compounds 1. *J. Am. Chem. Soc.* **1957**, *79*, 1078–1083. DOI: 10.1021/ja01562a019.
- [37] Shine, H. J.; Piette, L. Ion-radicals. The Reaction of Thioaromatic Compounds with Acids. II. Diphenyl Disulphide, Thianthrene and Thianthrene Oxides. *J. Am. Chem. Soc.* **1962**, *84*, 4798–4806. DOI: 10.1021/ja00883a034.
- [38] Rundel, W.; Scheffler, K. EPR-untersuchungen an substituierten thianthrenen. *Tetrahedron Letters* **1963**, *4*, 993–995. DOI: 10.1016/S0040-4039(01)90759-2.
- [39] Shine, H. J.; Dais, C. F.; Small, R. J. Ion Radicals. IV. 1 The Electron Spin Resonance Spectra of Substituted Thianthrenes in Sulphuric Acid Solution. *J. Org. Chem.* **1964**, *29*, 21–25. DOI: 10.1021/jo01024a004.
- [40] Kinoshita, M. The Electron Spin Resonance Absorption of the Complex of Thianthrene with Antimony Pentachloride. *BCSJ* **1962**, *35*, 1137–1140. DOI: 10.1246/bcsj.35.1137.
- [41] Lucken, E. A. C. 965. 1,4-Dithiinium radical-cations. *J. Chem. Soc.* **1962**, 4963. DOI: 10.1039/JR9620004963.
- [42] Giordan, J.; Bock, H. Radical ions, 51. Oxidative Rearrangement of Diphenyl Disulphides to Thianthrenes. *Ber. Dtsch. Chem. Ges.* **1982**, *115*, 2548–2559. DOI: 10.1002/cber.19821150718.
- [43] Davies, A. G.; McGuchan, D. C. Electron spin resonance spectra of mercurated arene radical cations. *Organometallics* **1991**, *10*, 329–336. DOI: 10.1021/om00047a068.
- [44] Rapta, P. *et al.* Dimerization of thianthrene radical cations as studied by in situ ESR and UV-Vis-NIR voltammetry at different temperatures. *Phys. Chem. Chem. Phys.* **2002**, *4*, 4181–4185. DOI: 10.1039/B204024G.

- [45] Rangappa, P.; Shine, H. J. An overview of some reactions of thianthrene cation radical. Products and mechanisms of their formation. *Journal of Sulphur Chemistry* **2006**, *27*, 617–664. DOI: 10.1080/17415990600987965.
- [46] Sato, Y. *et al.* Magnetic Susceptibilities of Crystalline Phenothiazine, N -Methylphenothiazine and Thianthrene Radical Salts with Antimony Pentachloride. *BCSJ* **1967**, *40*, 2539–2543. DOI: 10.1246/bcsj.40.2539.
- [47] Murata, Y.; Hughes, L.; Shine, H. J. Thianthrenium trichlorodiiodide ($C_{12}H_8S_2^+I_2Cl_3^-$). *Inorganic and Nuclear Chemistry Letters* **1968**, *4*, 573–576. DOI: 10.1016/0020-1650(68)90006-8.
- [48] Bandlish, B. K.; Shine, H. J. Ion radicals. 37. Preparation and isolation of cation radical tetrafluoroborates by the use of nitrosonium tetrafluoroborate. *J. Org. Chem.* **1977**, *42*, 561–563. DOI: 10.1021/jo00423a039.
- [49] Boduszek, B.; Shine, H. J. Preparation of solid thianthrene cation radical tetrafluoroborate. *J. Org. Chem.* **1988**, *53*, 5142–5143. DOI: 10.1021/jo00256a042.
- [50] Bock, H. *et al.* Thianthren-Radikalkation-Tetrachloroaluminat. *Ber. Dtsch. Chem. Ges.* **1994**, *127*, 2043–2049. DOI: 10.1002/cber.19941271029.
- [51] Rosokha, S. V. *et al.* Tris(thianthrene)²⁺ bis(dodecamethylcarba-closo-dodecaborate) dichloromethane tetrasolvate: a crossed triple-decker pi-trimer dication. *Acta crystallographica. Section C, Crystal structure communications* **2007**, *63*, o347-9. DOI: 10.1107/S0108270107018136.
- [52] Beck, J.; Bredow, T.; Tjahjanto, R. T. Thianthrene Radical Cation Hexafluorophosphate. *Zeitschrift für Naturforschung B* **2009**, *64*, 145–152. DOI: 10.1515/znb-2009-0201.
- [53] Tjahjanto, R. T. *et al.* The Reactions of Thianthrene and Selenanthrene with AlCl₃: Coordination Complexes, Radical Ions, and Investigations on the Unique Triple-Decker Molecule (Thianthrene)₃²⁺. *Eur. J. Inorg. Chem.* **2012**, *2012*, 3625–3635. DOI: 10.1002/ejic.201200067.
- [54] Poleschner, H.; Seppelt, K. XeF₂/Fluoride Acceptors as Versatile One-Electron Oxidants. *Angew. Chem. Int. Ed.* **2013**, *52*, 12838–12842. DOI: 10.1002/anie.201307161.
- [55] Connelly, N. G.; Geiger, W. E. Chemical Redox Agents for Organometallic Chemistry. *Chem. Rev.* **1996**, *96*, 877–910. DOI: 10.1021/cr940053x.
- [56] Lee, W. K. *et al.* Addition of Thianthrene Cation Radical to Cycloalkenes. An Unexpected Monoadduct. *J. Org. Chem.* **1999**, *64*, 9206–9210. DOI: 10.1021/jo9911241.
- [57] Qian, D.-Q. *et al.* Mono- and bisadducts from the addition of thianthrene cation radical salts to cycloalkenes and alkenes. *J. Org. Chem.* **2002**, *67*, 4030–4039.
- [58] Shine, H. J. *et al.* Adducts of Phenoxathiin and Thianthrene Cation Radicals with Alkenes and Cycloalkenes. *J. Org. Chem.* **2003**, *68*, 8910–8917. DOI: 10.1021/jo030173h.

- [59] Zhao, B.-J. *et al.* Addition of thianthrene cation radical to non-conjugated dienes—Part I: Addition to one double bond. *Journal of Sulphur Chemistry* **2006**, *27*, 127–138. DOI: 10.1080/17415990600578574.
- [60] Nishinaga, T.; Komatsu, K. Persistent π radical cations: self-association and its steric control in the condensed phase. *Org. Biomol. Chem.* **2005**, *3*, 561. DOI: 10.1039/B418872A.
- [61] Sebastiano, R.; Korp, J. D.; Kochi, J. K. The aromatic cation radical from bis(pentamethylphenyl)methane oxidation. Structural reassignment by X-ray crystallography. *J. Chem. Soc., Chem. Commun.* **1991**, 1481. DOI: 10.1039/c39910001481.
- [62] Modjewski, M. J. *et al.* Isolation and X-ray structural characterization of a dicationic homotrimer of 2,3,6,7-tetramethoxy-9,10-dimethylantracene cation radical. *Tetrahedron Letters* **2009**, *50*, 6687–6690. DOI: 10.1016/j.tetlet.2009.09.081.
- [63] Plasseraud, L. *et al.* A novel two-dimensional organostannoxane coordination network promoted by phenazine: Synthesis, characterization and X-ray structure of. *Journal of Organometallic Chemistry* **2009**, *694*, 2386–2394. DOI: 10.1016/j.jorganchem.2009.03.027.
- [64] Plasseraud, L. *et al.* Organotin(IV) trifluoromethanesulphonates chemistry: Isolation and characterization of a new di-n-butyl derivative presenting a Sn₃O₃ core. *Inorganica Chimica Acta* **2012**, *380*, 50–56. DOI: 10.1016/j.ica.2011.08.042.
- [65] Peintinger, M. F.; Beck, J.; Bredow, T. Charged stacks of dithiin, diselenin, thianthrene and selenanthrene radical cations: long range multicenter bonds. *Phys. Chem. Chem. Phys.* **2013**, *15*, 18702. DOI: 10.1039/C3CP53410C.
- [66] Lakkaraju, P. S.; Zhou, D.; Roth, H. D. Extended radical cation of diphenyl disulphide and oxidative cyclization on a pentasil zeolite: an EPR study. *J. Chem. Soc., Perkin Trans. 2* **1998**, 1119–1122. DOI: 10.1039/a800341f.
- [67] Lakkaraju, P. S. *et al.* Extended Diaryl Diselenide Radical Cations in Pentasil Zeolite Studied by EPR and Diffuse Reflectance Optical Spectroscopy. *J. Phys. Chem. A* **1999**, *103*, 7381–7384. DOI: 10.1021/jp991571k.
- [68] Martí, V. *et al.* UV-vis and IR spectroscopic characterization of diphenyl disulphide radical cation in acid zeolites and its rearrangement to thianthrenium radical cation. *J. Chem. Soc., Perkin Trans. 2* **1999**, 145–152. DOI: 10.1039/a806522e.
- [69] Shine, H. J.; Thompson, D. R. Ion radicals. VIII. The thianthrene dication in sulphuric acid. *Tetrahedron Letters* **1966**, *7*, 1591–1597. DOI: 10.1016/S0040-4039(01)99761-8.
- [70] Glass, R. S. *et al.* 2,3,7,8-Tetramethoxythianthrene dication. Isolable thianthrene dication. *J. Am. Chem. Soc.* **1973**, *95*, 2375–2376. DOI: 10.1021/ja00788a052.
- [71] Ito, A. *et al.* Tuning Spin-State Preference by Substituents: A Case Study of Thianthrene Dication. *J. Phys. Chem. A* **2002**, *106*, 8716–8720. DOI: 10.1021/jp0155967.
- [72] Weiss, R.; Schlierf, C. A Convenient Synthesis of Methyl-bis[methylthio]sulphonium Hexachloroantimonate. *Synthesis* **1976**, *1976*, 323–324. DOI: 10.1055/s-1976-24035.

- [73] Passmore, J.; Richardson, E. K.; Taylor, P. Oxidation of bis(perfluoroethyl) diselenide by antimony pentafluoride and by the dioxygen (1+) cation. Evidence for the novel cations $[\{\text{Se}(\text{C}_2\text{F}_5)_2\}_3]^+$ and $[\{\text{Se}(\text{C}_2\text{F}_5)_2\}_{4n}]^{2n+}$. *J. Chem. Soc., Dalton Trans.* **1976**, 1006. DOI: 10.1039/dt9760001006.
- [74] Mueller, B. *et al.* Syntheses and Structures of Two Dimethyl Diselenide-Diiodine Adducts and the First Well Characterized Diorgano Disulphide-Nitrosonium Adduct. *Eur. J. Inorg. Chem.* **2011**, 2011, 4970–4977. DOI: 10.1002/ejic.201100620.
- [75] Mueller, B.; Poleschner, H.; Seppelt, K. Dialkyl dichalcogen cations. *Dalton Trans.* **2008**, 83, 4424. DOI: 10.1039/B802259N.
- [76] Poleschner, H.; Seppelt, K. XeF_2 /Fluoridakzeptoren als vielseitige Einelektronen-Oxidationsmittel. *Angew. Chem.* **2013**, 125, 13072–13077. DOI: 10.1002/ange.201307161.
- [77] Gillespie, R. J. *et al.* The I_4^{2+} cation. X-Ray crystal structures of $(\text{I}_4^{2+})(\text{AsF}_6^-)_2$ and $(\text{I}_4^{2+})(\text{Sb}_3\text{F}_{14}^-)(\text{SbF}_6^-)$. *J. Chem. Soc., Chem. Commun.* **1983**, 8–9. DOI: 10.1039/C39830000008.
- [78] Faggiani, R. *et al.* Preparation and solid-state and solution studies of three compounds of the tetraiodine dication I_4^{2+} : $\text{I}_4^{2+}(\text{AsF}_6^-)_2$, $\text{I}_4^{2+}(\text{SbF}_6^-)_2$, and $\text{I}_4^{2+}(\text{Sb}_3\text{F}_{14}^-)(\text{SbF}_6^-)$. *Inorg. Chem.* **1988**, 27, 4350–4355. DOI: 10.1021/ic00297a005.
- [79] Block, E. *et al.* Synthesis, Properties, Oxidation, and Electrochemistry of 1,2-Dichalcogenins. *J. Am. Chem. Soc.* **2000**, 122, 5052–5064. DOI: 10.1021/ja994134s.
- [80] Shuvaev, K. V.; Passmore, J. RCN₃⁺: A novel class of stable sulphur rich radical cations. *Coordination Chemistry Reviews* **2013**, 257, 1067–1091. DOI: 10.1016/j.ccr.2012.07.003.
- [81] Houghton, D. S.; Humffray, A. A. Anodic oxidation of diaryl sulphides—I. diphenyl sulphide in sulphate and perchlorate media. *Electrochimica Acta* **1972**, 17, 1421–1433. DOI: 10.1016/0013-4686(72)80086-0.
- [82] Gilbert, B. C.; Hodgeman, D. K. C.; Norman, R. O. C. Electron spin resonance studies. Part XXXVIII. Evidence for the formation of dimeric radical-cations, $\text{R}_2\text{S}^+\text{S}_2^+$, in the one-electron oxidation of sulphides. *J. Chem. Soc., Perkin Trans. 2* **1973**, 1748–1752. DOI: 10.1039/P29730001748.
- [83] Nishikida, K.; Williams, F. The ESR spectrum and structure of the dimer radical cation of dimethyl selenide ($\text{Me}_2\text{Se}-\text{SeMe}_2^+$) in a γ -irradiated single crystal. *Chemical Physics Letters* **1975**, 34, 302–306. DOI: 10.1016/0009-2614(75)85279-1.
- [84] Bonifačić, M. *et al.* Formation of positive ions and other primary species in the oxidation of sulphides by hydroxyl radicals. *J. Chem. Soc., Perkin Trans. 2* **1975**, 675–685. DOI: 10.1039/P29750000675.
- [85] Asmus, K.-D. *et al.* Free radical oxidation of organic sulphur compounds in aqueous solution. *Faraday Discuss. Chem. Soc.* **1977**, 63, 213–225. DOI: 10.1039/DC9776300213.

- [86] Lanzalunga, O.; Lapi, A. Recent photo- and radiation chemical studies of sulphur radical cations. *Journal of Sulphur Chemistry* **2012**, *33*, 101–129. DOI: 10.1080/17415993.2011.619536.
- [87] Wang, J. T.; Williams, F. Comparison of proton hyperfine coupling constants for the monomer and dimer radical cations of dimethyl sulphide and dimethyl selenide. *J. Chem. Soc., Chem. Commun.* **1981**, 1184. DOI: 10.1039/C39810001184.
- [88] Almond, M. J. *et al.* Study of dialkyltellurium radical cations by electron spin resonance spectroscopy. *J. Chem. Soc., Dalton Trans.* **1992**, 1–4. DOI: 10.1039/DT9920000001.
- [89] Musker, W. K.; Wolford, T. L. Long-lived radical cations from mesocyclic dithioethers. *J. Am. Chem. Soc.* **1976**, *98*, 3055–3056. DOI: 10.1021/ja00426a084.
- [90] Fujihara, H. *et al.* Reactivity of Diselenide Dication Salt, 1,5-Diselenoniabicyclo[3.3.0]octane Bis(hexafluorophosphate) toward Aromatics. A New Mode of Aromatic Substitution and Redox Reaction. *Chem. Lett.* **1990**, *19*, 393–396. DOI: 10.1246/cl.1990.393.
- [91] Fujihara, H. *et al.* Chemical and electrochemical reduction of diselenide dication salt, 1,5-diselenoniabicyclo[3.3.0]Octane bis(hexafluorophosphate). *Tetrahedron Letters* **1990**, *31*, 6375–6378. DOI: 10.1016/S0040-4039(00)97068-0.
- [92] Iwasaki, F. *et al.* Structure of 1,5-diselenoniabicyclo[3.3.0]octane bis(tetrafluoroborate) acetonitrile solvate. *Acta crystallographica. Section C, Crystal structure communications* **1991**, *47*, 1463–1466. DOI: 10.1107/S0108270190012586.
- [93] Fujihara, H.; Akaishi, R.; Furukawa, N. Preparation and reactivity of dichalcogenide (S, Se) dication salts from medium-sized cyclic bis-sulphide and bis-selenides. *Tetrahedron* **1993**, *49*, 1605–1618. DOI: 10.1016/S0040-4020(01)80348-3.
- [94] Furukawa, N.; Sato, S. Chalcogenuranyl dications bearing unusual bonds and charges. *Heteroatom Chem.* **2002**, *13*, 406–413. DOI: 10.1002/hc.10089.
- [95] Nenajdenko, V. G. *et al.* 1,2-Dications in Organic Main Group Systems. *Chem. Rev.* **2003**, *103*, 229–282. DOI: 10.1021/cr0000628.
- [96] Detty, M. R. *et al.* Tellurium-centered radical cations. 1. The 1,3-ditellurole radical cation by chemical, electrochemical, and photochemical oxidation. *J. Am. Chem. Soc.* **1985**, *107*, 6298–6304. DOI: 10.1021/ja00308a023.
- [97] Fujihara, H. *et al.* First example of tetraalkyl substituted ditelluride dication salt from 1,5-ditelluracyclooctane. *Tetrahedron Letters* **1991**, *32*, 4537–4540. DOI: 10.1016/0040-4039(91)80033-3.
- [98] Evans, D. H. *et al.* Electrochemical and Chemical Oxidation of Dithia-, Diselena-, Ditel-lura-, Selenathia-, and Tellurathiamescycles and Stability of the Oxidized Species. *J. Org. Chem.* **2010**, *75*, 1997–2009. DOI: 10.1021/jo9026484.

- [99] Musker, W. K.; Wolford, T. L.; Roush, P. B. An investigation of mesocyclic and acyclic dithioether cation radicals and dications. *J. Am. Chem. Soc.* **1978**, *100*, 6416–6421. DOI: 10.1021/ja00488a024.
- [100] Wilson, G. S. *et al.* Electrochemical oxidation of some mesocyclic dithioethers and related compounds. *J. Am. Chem. Soc.* **1979**, *101*, 1040–1042. DOI: 10.1021/ja00498a046.
- [101] Musker, W. K. Chemistry of aliphatic thioether cation radicals and dications. *Acc. Chem. Res.* **1980**, *13*, 200–206. DOI: 10.1021/ar50151a002.
- [102] Ryan, M. D. *et al.* Studies of the EE mechanism. Evidence for reversible dimer formation in electrochemical oxidation of a cyclic dithioether. *J. Phys. Chem.* **1981**, *85*, 1069–1075. DOI: 10.1021/j150608a030.
- [103] Iwasaki, F. *et al.* The Crystal Structure of 1,5-Dithioniabicyclo[3.3.0]octane Bis(trifluoromethanesulphonate). The First Structural Characterization of Dithionia Dication and Strong S···O Interactions between Cations and Anions. *BCSJ* **1988**, *61*, 2563–2567. DOI: 10.1246/bcsj.61.2563.
- [104] Stowasser, R.; S. Glass, R.; Hoffmann, R. The dithiacyclooctane cation (DTCO⁺): conformational analysis, interconversion barriers and bonding. *J. Chem. Soc., Perkin Trans. 2* **1999**, 1559. DOI: 10.1039/A805100C.
- [105] Nakayama, N. *et al.* Ab initio study of the 1,5-dithiacyclooctane radical cation and its dimer dication. *Journal of Molecular Structure: THEOCHEM* **2001**, *542*, 215–226. DOI: 10.1016/S0166-1280(00)00844-7.
- [106] Maity, D. K. Structure, bonding, and spectra of cyclic dithia radical cations: a theoretical study. *J. Am. Chem. Soc.* **2002**, *124*, 8321–8328. DOI: 10.1021/ja0261067.
- [107] Tobien, T.; Hungerbühler, H.; Asmus, K.-D. Free Radical and Electrochemically Induced Oxidation of Organic Sulphur-, Selenium- and Phosphorus-Compounds. *Phosphorus, Sulphur, and Silicon and the Related Elements* **1994**, *95*, 249–263. DOI: 10.1080/10426509408034211.
- [108] Fujihara, H. *et al.* Hypervalent selenurane with chalcogenium cation (selenium⁺, sulphur⁺) from 1,11-(methanoselenomethano)-5H,7H-dibenzo[b,g][1,5]diselenocin and its sulphur derivative: interconvertible redox structures by multicenter chalcogenide participation. *J. Am. Chem. Soc.* **1992**, *114*, 3117–3118. DOI: 10.1021/ja00034a057.
- [109] Bergholdt, A. B. *et al.* Crystal Structures and abInitio Calculations of New Dicationic Telluranes (λ 4 -Tellane), [10-Te-4(C₂X₂)]²⁺ (X = S, Se): Positively Charged Hypervalent Bonding Systems. *J. Am. Chem. Soc.* **1998**, *120*, 1230–1236. DOI: 10.1021/ja972930x.
- [110] Kobayashi, K. *et al.* Synthesis of Dicationic Telluranes by Remote Oxidation through a π -Conjugated System. *Angew. Chem. Int. Ed.* **2000**, *39*, 1318–1320. DOI: 10.1002/(SICI)1521-3773(20000403)39:7<1318:AID-ANIE1318>3.0.CO;2-5.

- [111] Fujihara, H.; Chiu, J.-J.; Furukawa, N. Electrochemical Property and Formation of the Cation Radical and Dication of Dinaphtho[1,8- b , c]-1,5-dithiocin. *Chem. Lett.* **1990**, *19*, 2217–2220. DOI: 10.1246/cl.1990.2217.
- [112] Fujihara, H. *et al.* Peri interaction between selenium atoms in dinaphtho[1,8-b,c]-1,5-diselenocin and 1,8-bis(methylseleno)naphthalene. *Tetrahedron Letters* **1991**, *32*, 4345–4348. DOI: 10.1016/S0040-4039(00)92166-X.
- [113] Mallow, O. *et al.* Diaryldichalcogenide radical cations. *Chemical science* **2015**, *6*, 497–504. DOI: 10.1039/c4sc02964j.
- [114] Smith, M. R. *et al.* The crystal structure of phenoxatellurine, C₁₂H₈OTe. *Journal of Heterocyclic Chemistry* **1973**, *10*, 527–531. DOI: 10.1002/jhet.5570100418.
- [115] Mostaghimi, F. *et al.* The reaction of phenoxatellurine with single-electron oxidizers revisited. *New J. Chem.* **2019**, *43*, 12754–12766. DOI: 10.1039/C9NJ02401H.
- [116] Bernstein, J.; Hagler, A. T. Conformational polymorphism. The influence of crystal structure on molecular conformation. *J. Am. Chem. Soc.* **1978**, *100*, 673–681. DOI: 10.1021/ja00471a001.
- [117] Nangia, A. Conformational polymorphism in organic crystals. *Acc. Chem. Res.* **2008**, *41*, 595–604. DOI: 10.1021/ar700203k.
- [118] Bernstein, J. *Polymorphism in molecular crystals*, Repr; Monographs on crystallography 14; Clarendon Press: Oxford, **2006**.
- [119] Bernstein, J. Polymorphism – A Perspective. *Crystal Growth & Design* **2011**, *11*, 632–650. DOI: 10.1021/cg1013335.
- [120] Braga, D.; Grepioni, F. Organometallic polymorphism and phase transitions. *Chem. Soc. Rev.* **2000**, *29*, 229–238. DOI: 10.1039/a909042h.
- [121] Cruz-Cabeza, A. J.; Bernstein, J. Conformational polymorphism. *Chem. Rev.* **2014**, *114*, 2170–2191. DOI: 10.1021/cr400249d.
- [122] Beckmann, J.; Bolsinger, J.; Mebs, S. Two polymorphs of dimesityltellurium dichloride. *Main Group Metal Chemistry* **2013**, *36* DOI: 10.1515/mgmc-2012-0052.
- [123] Grabowsky, S. *et al.* Conformational trimorphism of bis(2,6-dimesitylphenyl)ditelluride. *Zeitschrift für Kristallographie - Crystalline Materials* **2018**, *233*, 707–721. DOI: 10.1515/zkri-2018-2077.
- [124] Kruse, F. H.; Marsh, R. E.; McCullough, J. D. The crystal structure of p,p'-dichlorodiphenyl diselenide and p,p'-dichlorodiphenyl ditelluride. *Acta Cryst* **1957**, *10*, 201–209. DOI: 10.1107/S0365110X5700064X.
- [125] Sandman, D. J. *et al.* Conformational polymorphism of di-2-naphthyl ditelluride. *Organometallics* **1994**, *13*, 348–353. DOI: 10.1021/om00013a051.

- [126] van den Bossche, G. *et al.* New form of bis(p-chlorophenyl) ditelluride, C₁₂H₈Cl₂Te₂. *Acta Crystallogr C Cryst Struct Commun* **1984**, *40*, 1011–1012. DOI: 10.1107/S0108270184006600.
- [127] McKinnon, J. J.; Mitchell, A. S.; Spackman, M. A. Hirshfeld Surfaces: A New Tool for Visualising and Exploring Molecular Crystals. *Chem. Eur. J.* **1998**, *4*, 2136–2141. DOI: 10.1002/(SICI)1521-3765(19981102)4:11<2136:AID-CHEM2136>3.0.CO;2-G.
- [128] McKinnon, J. J.; Spackman, M. A.; Mitchell, A. S. Novel tools for visualizing and exploring intermolecular interactions in molecular crystals. *Acta crystallographica. Section B, Structural science* **2004**, *60*, 627–668. DOI: 10.1107/S0108768104020300.
- [129] Spackman, M. A.; Jayatilaka, D. Hirshfeld surface analysis. *CrystEngComm* **2009**, *11*, 19–32. DOI: 10.1039/B818330A.
- [130] Spackman, M. A. Molecules in crystals. *Physica Scripta* **2013**, *87*, 48103. DOI: 10.1088/0031-8949/87/04/048103.
- [131] McKinnon, J. J.; Jayatilaka, D.; Spackman, M. A. Towards quantitative analysis of intermolecular interactions with Hirshfeld surfaces. *Chemical communications (Cambridge, England)* **2007**, 3814–3816. DOI: 10.1039/b704980c.
- [132] Threlfall, T. Structural and Thermodynamic Explanations of Ostwald's Rule. *Org. Process Res. Dev.* **2003**, *7*, 1017–1027. DOI: 10.1021/op030026l.
- [133] Kitaigorodsky, A. I. *Molecular crystals and molecules*; Physical chemistry 29; Academic Press: New York, **1973**.
- [134] Drew, H. D. K. CCCCIX.—Cyclic organo-metallic compounds. Part II. Tellurylium compounds, a new series of intensely coloured tellurium derivatives. The migration of anions in solids. *J. Chem. Soc.* **1926**, *129*, 3054–3071. DOI: 10.1039/JR9262903054.
- [135] Drew, H. D. K. XXXIII.—Cyclic organo-metallic compounds. Part I. Compounds of tellurium. *J. Chem. Soc.* **1926**, *129*, 223–231. DOI: 10.1039/JR9262900223.
- [136] Drew, H. D. K. LXV.—Cyclic organo-metallic compounds. Part IV. Tellurylium compounds (continued). *J. Chem. Soc.* **1928**, *0*, 506–510. DOI: 10.1039/JR9280000506.
- [137] Drew, H. D. K. LXVI.—Cyclic organo-metallic compounds. Part V. Phenoxselenine, and phenoxthionine from phenoxtellurine. Selenylium and thionylium compounds. *J. Chem. Soc.* **1928**, *0*, 511–524. DOI: 10.1039/JR9280000511.
- [138] Drew, H. D. K.; Thomason, R. W. XX.—Cyclic organo-metallic compounds. Part III. Nitro- and amino-derivatives of phenoxtellurine. *J. Chem. Soc.* **1927**, *0*, 116–125. DOI: 10.1039/JR9270000116.
- [139] Turner, M. J. *et al.* CrystalExplorer17, University of Western Australia **2017**.
- [140] Dolomanov, O. V. *et al.* OLEX2 : a complete structure solution, refinement and analysis program. *J Appl Crystallogr* **2009**, *42*, 339–341. DOI: 10.1107/S0021889808042726.

- [141] Brandenburg, K.; Putz, H. Diamond - Crystal and Molecular Structure Visualization. *Crystal Impact GbR* **2006**.
- [142] Hieber, W.; Kruck, T. Tellurorganyl-haltige Metallcarbonyl(1). *Ber. Dtsch. Chem. Ges.* **1962**, *95*, 2027–2041. DOI: 10.1002/cber.19620950826.
- [143] Merritt, E. A.; Olofsson, B. Diaryliodonium salts: a journey from obscurity to fame. *Angewandte Chemie (International ed. in English)* **2009**, *48*, 9052–9070. DOI: 10.1002/anie.200904689.
- [144] Moulton, P. *et al.* The inhibition of flavoproteins by phenoxaiodonium, a new iodonium analogue. *European Journal of Pharmacology* **2000**, *401*, 115–120. DOI: 10.1016/S0014-2999(00)00454-4.
- [145] Beringer, F. M.; Kravetz, L.; Topliss, G. B. Iodonium Salts Containing Heterocyclic Iodine 1-3. *J. Org. Chem.* **1965**, *30*, 1141–1148. DOI: 10.1021/jo01015a046.
- [146] Mostaghimi, F. *et al.* New insights into the oxidation of phenoxatellurine with sulphuric acid. *Main Group Metal Chemistry* **2019**, *42*, 150–152. DOI: 10.1515/mgmc-2019-0017.
- [147] Kitamura, T. *et al.* Electrophile-induced intramolecular cyclization of ortho-(aryloxy)phenylalkynes to dibenz[b,f] oxepines. *J. Chem. Soc., Perkin Trans. 1* **1992**, 1969. DOI: 10.1039/p19920001969.
- [148] Zhu, M.; Jalalian, N.; Olofsson, B. One-Pot Synthesis of Diaryliodonium Salts Using Toluene-sulphonic Acid: A Fast Entry to Electron-Rich Diaryliodonium Tosylates and Triflates. *Synlett* **2008**, *2008*, 592–596. DOI: 10.1055/s-2008-1032050.
- [149] Lang, E. S.; Burrow, R. A.; Silveira, E. T. Bis(1-naphthyl) ditelluride. *Acta crystallographica. Section C, Crystal structure communications* **2002**, *58*, o397-8. DOI: 10.1107/s0108270102008284.
- [150] Menon, S. C. *et al.* Intramolecularly Coordinated Low-Valent Organotellurium Complexes Derived from 1-(Dimethylamino)naphthalene. *Organometallics* **1996**, *15*, 1707–1712. DOI: 10.1021/om950841s.
- [151] Nordheider, A. *et al.* Peri-substituted phosphorus-tellurium systems-an experimental and theoretical investigation of the P···Te through-space interaction. *Inorg. Chem.* **2015**, *54*, 2435–2446. DOI: 10.1021/ic503056z.
- [152] Hazell, A. C. *et al.* A neutron diffraction study of the crystal and molecular structure of acenaphthene. *Acta Crystallogr C Cryst Struct Commun* **1986**, *42*, 690–693. DOI: 10.1107/S0108270186094908.
- [153] Capelli, S. C. *et al.* Molecular motion in crystalline naphthalene: analysis of multi-temperature X-ray and neutron diffraction data. *J. Phys. Chem. A* **2006**, *110*, 11695–11703. DOI: 10.1021/jp062953a.

- [154] Katz, H. E. Hydride sponge: complexation of 1,8-naphthalenediylbis(dimethylborane) with hydride, fluoride, and hydroxide. *J. Org. Chem.* **1985**, *50*, 5027–5032. DOI: 10.1021/jo00225a005.
- [155] Katz, H. E. 1,8-Naphthalenediylbis(dichloroborane) chloride: the first bis boron chloride chelate. *Organometallics* **1987**, *6*, 1134–1136. DOI: 10.1021/om00148a038.
- [156] Melaimi, M.; Gabbaï, F. P. A heteronuclear bidentate Lewis acid as a phosphorescent fluoride sensor. *J. Am. Chem. Soc.* **2005**, *127*, 9680–9681. DOI: 10.1021/ja053058s.
- [157] Zhao, H.; Gabbaï, F. P. A bidentate Lewis acid with a telluronium ion as an anion-binding site. *Nature Chem* **2010**, *2*, 984–990. DOI: 10.1038/nchem.838.
- [158] Balasubramaniyan, V. peri Interaction in Naphthalene Derivatives. *Chem. Rev.* **1966**, *66*, 567–641. DOI: 10.1021/cr60244a001.
- [159] Lechner, M.-L. *et al.* Sterically Crowded Tin Acenaphthenes. *Organometallics* **2012**, *31*, 2922–2930. DOI: 10.1021/om201253t.
- [160] Athukorala Arachchige, K. S. *et al.* Synthetic, Structural, and Spectroscopic Studies of Sterically Crowded Tin–Chalcogen Acenaphthenes. *Organometallics* **2014**, *33*, 6089–6102. DOI: 10.1021/om500755w.
- [161] Chalmers, B. A. *et al.* Sterically encumbered tin and phosphorus peri-substituted acenaphthenes. *Inorg. Chem.* **2014**, *53*, 8795–8808. DOI: 10.1021/ic5014768.
- [162] Aschenbach, L. K. *et al.* Onset of three-centre, four-electron bonding in peri-substituted acenaphthenes: a structural and computational investigation. *Dalton Trans.* **2012**, *41*, 3141–3153. DOI: 10.1039/c1dt11697e.
- [163] Stanford, M. W. *et al.* Probing interactions through space using spin-spin coupling. *Dalton Trans.* **2014**, *43*, 6548–6560. DOI: 10.1039/c4dt00408f.
- [164] Kordts, N. *et al.* Silyl Chalconium Ions: Synthesis, Structure and Application in Hydro-defluorination Reactions. *Chemistry (Weinheim an der Bergstrasse, Germany)* **2017**, *23*, 10068–10079. DOI: 10.1002/chem.201700995.
- [165] Beckmann, J. *et al.* Peri-Interactions in 8-Diphenylphosphino-1-bromonaphthalene, 6-Diphenylphosphino-5-bromoacenaphthene, and Derivatives. *Z. anorg. allg. Chem.* **2013**, *639*, 2233–2249. DOI: 10.1002/zaac.201300272.
- [166] Beckmann, J. *et al.* Aryltellurenyl Cation [RTe(CR'2)]⁺ Stabilized by an N-Heterocyclic Carbene. *Ber. Dtsch. Chem. Ges.* **2008**, *2008*, 1921–1925. DOI: 10.1002/ejic.200800038.
- [167] Beckmann, J. *et al.* Formation of mixed-valent aryltellurenyl halides RX₂TeTeR. *Angewandte Chemie (International ed. in English)* **2007**, *46*, 8277–8280. DOI: 10.1002/anie.200702341.
- [168] Hesse, M. *Zur Chemie der ersten wohl definierten Tellurin- und Stibonsäure* **2009**.
- [169] Poleschner, H. *et al.* Trip₂C₆H₃SeF: the first isolated selenenyl fluoride. *Angewandte Chemie (International ed. in English)* **2012**, *51*, 419–422. DOI: 10.1002/anie.201106708.

- [170] Saednya, A.; Hart, H. Two Efficient Routes to m-Terphenyls from 1,3-Dichlorobenzenes. *Synthesis* **1996**, 1996, 1455–1458. DOI: 10.1055/s-1996-4426.
- [171] Cordero, B. *et al.* Covalent radii revisited. *Dalton Trans.* **2008**, 2832–2838. DOI: 10.1039/b801115j.
- [172] Caulton, K. G. Synthetic methods in transition metal nitrosyl chemistry. *Coordination Chemistry Reviews* **1975**, 14, 317–355. DOI: 10.1016/S0010-8545(00)80265-9.
- [173] Connelly, N. G.; Davies, J. D. The nitrosonium ion, NO⁺, and its versatility in transition metal organometallic synthesis. *Journal of Organometallic Chemistry* **1972**, 38, 385–390. DOI: 10.1016/S0022-328X(00)83341-0.
- [174] Mocella, M. T.; Okamoto, M. S.; Barefield, E. K. Nitrosonium Salts as Reagents in Inorganic Synthesis. *Synthesis and Reactivity in Inorganic and Metal-Organic Chemistry* **1974**, 4, 69–90. DOI: 10.1080/00945717408069633.
- [175] Wieber, M.; Habersack, R. Ortho- und Para-Methylsubstituierte Triphenyltelluronium-halogenide. Kristallstrukturen von Trimesityltelluroniumiodid und Bis(2,4,6-Tri-Butylphenyl)telluran. *Phosphorus, Sulphur, and Silicon and the Related Elements* **1995**, 106, 233–241. DOI: 10.1080/10426509508027911.
- [176] Mantina, M. *et al.* Consistent van der Waals radii for the whole main group. *J. Phys. Chem. A* **2009**, 113, 5806–5812. DOI: 10.1021/jp8111556.
- [177] Kertesz, M. Pancake Bonding: An Unusual Pi-Stacking Interaction. *Chemistry (Weinheim an der Bergstrasse, Germany)* **2019**, 25, 400–416. DOI: 10.1002/chem.201802385.
- [178] Heller, C. A.; Zingaro, R. A.; Meyers, E. A. A Study of the Donor Properties of the Phenoxachalcogenines.: I. Tetracyanoethylene and Chloranil as Acceptors. *Can. J. Chem.* **1974**, 52, 3814–3824. DOI: 10.1139/v74-571.
- [179] Brookhart, M.; Grant, B.; Volpe, A. F. [(3,5-(CF₃)₂C₆H₃)₄B]-[H(OEt₂)₂]⁺: a convenient reagent for generation and stabilization of cationic, highly electrophilic organometallic complexes. *Organometallics* **1992**, 11, 3920–3922. DOI: 10.1021/om00059a071.

6. Supporting Information

CHEMISTRY

A **European** Journal

Supporting Information

New Charge-Transfer Complexes with 1,2,5-Thiadiazoles as Both Electron Acceptors and Donors Featuring an Unprecedented Addition Reaction

Elena A. Chulanova,^[a, b, c] Elena A. Pritchina,^[a] Lorraine A. Malaspina,^[d] Simon Grabowsky,^{*,[d]} Farzin Mostaghimi,^[d] Jens Beckmann,^{*,[d]} Irina Yu. Bagryanskaya,^[a, b] Margarita V. Shakhova,^[e] Lidia S. Konstantinova,^[f, g] Oleg A. Rakitin,^[f, g] Nina P. Gritsan,^{*,[c, e]} and Andrey V. Zibarev^{*,[b, e]}

chem_201604121_sm_miscellaneous_information.pdf

§1. Crystal lattice voids analysis with the *CrystalExplorer* program

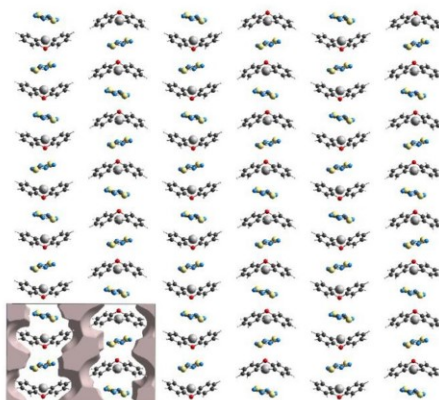


Figure S1. Voids in the crystal structure of **4** after artificially removing the A molecules that extend perpendicularly to the plane of the D molecule. Voids only shown within the unit cell, the view is down the a axis. The percentage of voids relative to the unit cell volume is 27.3 %. The voids are calculated with the *CrystalExplorer* program as explained in the main text at an electron density isosurface of 0.0003 au corresponding to the solvent-accessible surface.

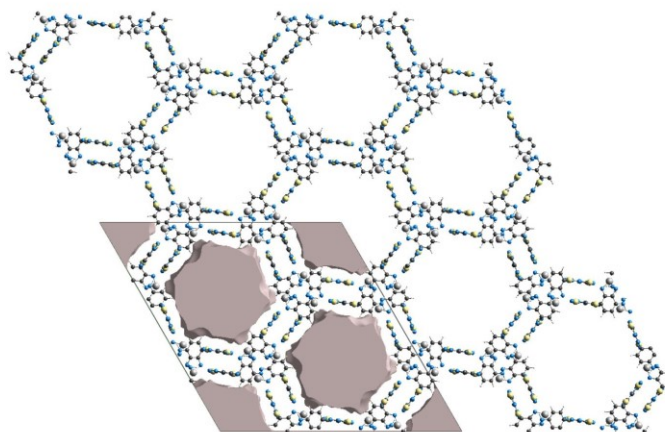


Figure S2. Voids in the crystal structure of **5** after artificially removing the disordered solvent molecules. Voids only shown within the unit cell, the view is down the c axis. The percentage of voids relative to the unit cell volume is 40.0 %. The voids are calculated with the *CrystalExplorer*

program as explained in the main text at an electron density isosurface of 0.0003 au corresponding to the solvent-accessible surface.

§2. Additional data of the calculation of model energies of pairwise interactions

The total energy of intermolecular interactions in the crystal was expressed in terms of four key components, *i.e.* electrostatic, polarization, dispersion and exchange repulsion, as $E_{\text{tot}} = E_{\text{ele}} + E_{\text{pol}} + E_{\text{dis}} + E_{\text{rep}}$.

Table S1. Scale factors used.^a

Energy Model	k_{ele}	k_{pol}	k_{disp}	k_{rep}
CE-B3LYP, B3LYP/6-31G(d,p), B3LYP/DGDZVP electron densities	1.063	0.756	0.843	0.595

^aCE: *CrystalExplorer 3.3* program used.

In the following Figures S3-S7, the D molecule is the central unit to which the intermolecular interactions are referred to. The molecules' color code is the same in Figures S3-S7 and in vertical bars in Tables S2-S6.

In the following Tables S2-S6, interaction energies are in kJ mol^{-1} and R is the distance in Å between molecular centers of mass. Partner molecules: A – acceptor, D – donor. The color scale for d_{norm} mapped onto the HSs is –0.4 to 1.2.

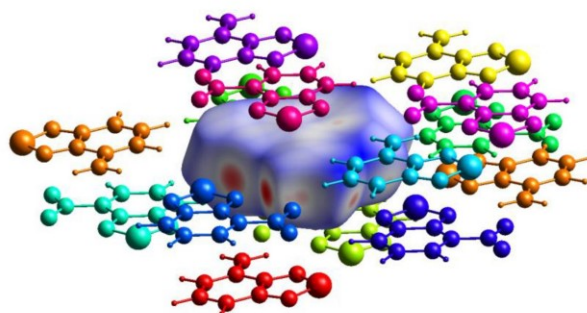


Figure S3 Complex 1: General situation around the central D unit.

Table S2. Complex 1. Electron densities are calculated at the B3LYP/6-31G(d,p) level of theory.

	R	E _{ele}	E _{pol}	E _{dis}	E _{rep}	E _{tot}	Partner molecule
	5.94	-0.3	-0.6	-10.1	2.8	-7.7	D1
	8.35	-1.1	-0.1	-5.4	5.3	-2.6	D2
	8.55	-1.0	-0.2	-5.6	2.2	-4.5	D3
	3.69	-6.8	-2.1	-42.1	28.3	-27.5	A1
	7.24	-13.4	-3.2	-12.0	13.1	-18.9	A2
	10.14	0.1	-0.2	-1.1	0.0	-1.0	D4
	7.47	-2.9	-0.3	-7.2	6.0	-5.8	A3
	9.40	1.8	-0.6	-2.2	0.1	-0.4	D5
	6.12	-37.5	-5.3	-16.1	37.1	-35.4	A4
	8.23	-8.5	-2.0	-9.6	13.1	-10.8	A5
	6.30	3.9	-1.0	-8.6	2.9	-2.1	D6

8.22	-1.3	-1.2	-6.0	2.5	-5.8	A6
3.86	-9.6	-1.4	-44.6	31.2	-30.3	A7

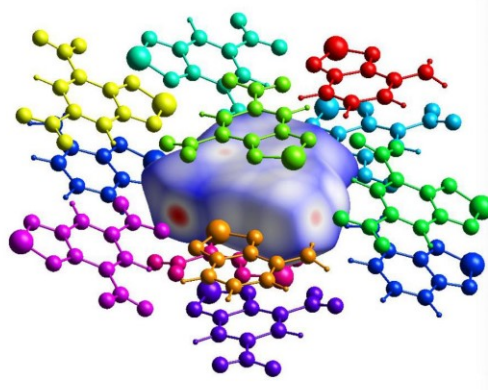


Figure S4 Complex 2: General situation around the central D unit.

Table S3. Complex 2. Electron densities are calculated at the B3LYP/6-31G(d,p) level of theory.

	R	E_{ele}	E_{pol}	E_{dis}	E_{rep}	E_{tot}	Partner molecule
	8.27	-1.7	-0.2	-7.3	4.3	-5.5	D1
	6.81	-4.7	-0.2	-8.5	11.5	-5.5	D2
	8.02	-4.3	-1.7	-9.8	9.6	-8.4	A1
	3.45	-16.2	-3.5	-52.6	39.4	-40.8	A2
	6.29	-10.4	-2.2	-16.0	16.5	-16.4	A3
	8.96	-3.9	-1.1	-6.1	4.5	-7.5	A4
	9.02	0.8	-0.5	-5.1	3.2	-1.9	A5
	7.38	-2.8	-1.5	-9.0	4.2	-9.2	D3
	6.62	-3.2	-1.1	-12.1	13.1	-6.7	A6

8.60	-10.0	-1.7	-6.7	8.0	-12.8	A7
3.94	-16.0	-3.3	-50.0	44.2	-35.3	A8

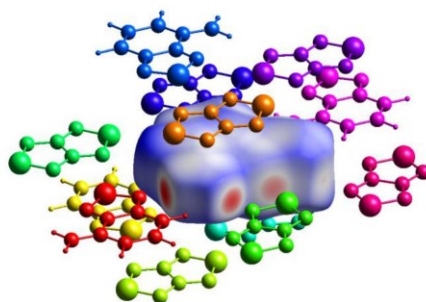


Figure S5 Complex **3**: General situation around the first symmetry-independent D molecule of the asymmetric unit as central D unit.

Table S4. Complex **3**. The first symmetry-independent D molecule of the asymmetric unit. Electron densities are calculated at the B3LYP/6-31G(d,p) level of theory.

	R	E_{ele}	E_{pol}	E_{dis}	E_{rep}	E_{tot}	Partner molecule
	7.45	-27.0	-6.7	-10.9	33.5	-23.1	D1
	4.01	-9.8	-1.8	-33.0	29.3	-22.2	A1
	6.50	-1.3	-0.5	-10.5	4.2	-8.1	A2
	6.29	-0.4	-0.9	-10.3	7.3	-5.4	A3
	6.29	-31.5	-3.8	-11.6	34.9	-25.4	A4
	7.92	-3.0	-0.7	-6.8	6.0	-5.9	A5
	3.71	-11.0	-1.8	-35.8	31.5	-24.4	A6
	8.61	-0.9	-0.1	-1.7	0.0	-2.4	A7
	6.37	-2.5	-0.3	-9.7	6.9	-6.8	D2
	6.91	-2.8	-1.1	-8.7	7.4	-6.7	A8

5.75	-5.1	-0.8	-11.4	9.1	-10.2	A9
7.46	-27.0	-6.8	-10.8	32.3	-23.7	D3
6.69	-5.1	-0.6	-7.4	11.7	-5.2	A10

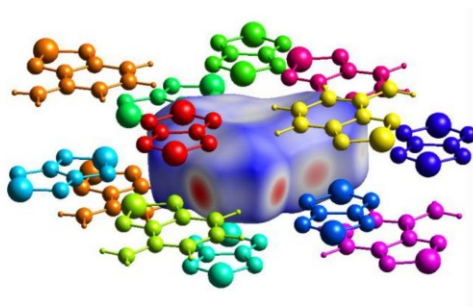


Figure S6 Complex **3**: General situation around the second symmetry-independent D molecule of the asymmetric unit as central D unit.

Table S5. Complex **3**. The second symmetry-independent D molecule of the asymmetric unit. Electron densities are calculated at the B3LYP/6-31G(d,p) level of theory.

R	E_{ele}	E_{pol}	E_{dis}	E_{rep}	E_{tot}	Partner molecule
6.75	-0.1	-0.8	-9.1	6.0	-4.9	A1
8.13	-0.5	-0.2	-4.7	0.6	-4.2	D1
6.50	-1.3	-0.5	-10.5	4.2	-8.1	D2
7.46	-27.0	-6.8	-10.8	32.3	-23.7	D3
4.09	-7.4	-1.4	-29.9	22.7	-20.7	A2
6.89	-2.8	-1.1	-9.1	8.4	-6.5	A3
4.24	-9.2	-1.7	-32.3	26.9	-22.3	A4

7.92	-3.1	-0.7	-7.1	6.7	-5.8	A5
6.30	-30.0	-3.5	-11.6	33.4	-24.4	A6
6.70	-4.9	-0.6	-7.3	11.4	-5.0	A7
6.39	-4.8	-0.7	-8.0	6.4	-8.6	A8
6.37	-2.5	-0.3	-9.7	6.9	-6.8	D4
7.45	-27.0	-6.7	-10.9	33.5	-23.1	D5

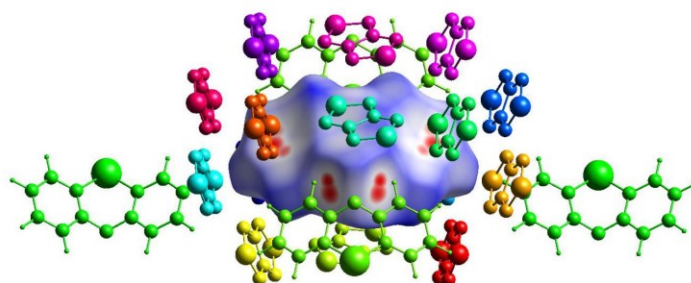



Figure S7 Complex 4: General situation around the central D unit.

Table S6. Complex 4. Electron densities are calculated at the B3LYP/DGDZVP level of theory.

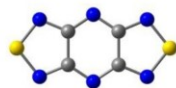
R	E_{ele}	E_{pol}	E_{dis}	E_{rep}	E_{tot}	Partner molecule
6.55	-5.4	-1.0	-11.8	10.4	-10.3	A1
6.05	-18.9	-1.6	-18.9	35.3	-16.3	A2
8.12	-0.3	-0.3	-4.4	2.9	-2.6	A3
6.43	-5.3	-1.0	-12.9	11.8	-10.2	A4



4.14	-34.5	-2.5	-33.6	57.3	-32.8	A5
6.51	-15.6	-1.2	-26.7	47.2	-11.9	D1
12.34	1.2	-0.1	-2.1	0.4	-0.3	D2
6.23	-18.1	-1.6	-18.4	34.1	-15.7	A6
5.04	-12.5	-1.3	-15.9	17.8	-17.1	A7
7.98	-0.1	-0.2	-4.0	2.0	-2.5	A8
8.14	-2.4	-0.5	-7.2	9.2	-3.5	A9
8.03	-5.1	-0.9	-10.2	11.4	-8.0	A10
8.06	-1.7	-0.4	-6.9	7.7	-3.3	A11
5.78	-5.5	-1.0	-14.4	10.0	-12.8	A12
7.20	-8.5	-1.7	-14.0	20.6	-9.8	A13
7.38	-7.4	-1.6	-12.6	17.0	-9.6	A14
5.80	-1.9	-1.1	-14.2	6.6	-10.9	A15
7.91	-3.8	-0.8	-10.2	8.7	-8.1	A16

§3. Additional data of the B97-D3/def2-TZVP calculations with the ORCA program for compounds in toluene solution

Compound 5a*



Atom	Coordinates, Å		
	x	y	z
C	-1.109145	-0.739788	0.000078
C	-1.109171	0.739780	0.000050
C	1.109129	0.739822	0.000002
C	1.109157	-0.739745	0.000011
N	-2.360587	-1.267527	-0.000457
N	-2.360635	1.267472	-0.000289
S	-3.359258	-0.000045	0.000606
N	0.000020	-1.481959	0.000026
N	-0.000037	1.481994	-0.000055
N	2.360620	-1.267437	0.000217
N	2.360571	1.267558	0.000217
S	3.359245	0.000076	-0.000280

For XRD structure, see Y. Yamashita, R. Saito, T. Suzuki, C. Kabuto, T. Mikai, T. Myashi, *Angew. Chem. Int. Ed.* **1988**, *27*, 434–435.

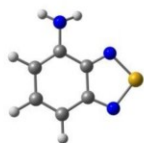
Collision diameter: 6.160 Å; ΔH (298 K, gas): -1277.137423, ΔG (298 K, gas): -1277.178540 au; ΔG_{solv} : -2.7 kcal mol⁻¹.

Radical anion [5a]^{-•}

Atom	Coordinates, Å		
	<i>x</i>	<i>y</i>	<i>z</i>
C	-1.121820	-0.742305	0.000041
C	-1.121894	0.742328	0.000036
C	1.121865	0.742450	-0.000009
C	1.121939	-0.742186	-0.000009
N	-2.359235	-1.276597	-0.000341
N	2.359375	1.276483	-0.000337
S	-3.403080	-0.000109	0.000559
N	0.000103	-1.484661	0.000002
N	-0.000059	1.484807	0.000000
N	2.359421	-1.276343	0.000289
N	2.359280	1.276740	0.000289
S	3.403125	0.000240	-0.000431

Collision diameter: 6.180 Å; $\langle S^2 \rangle$: 0.755251; E: -1277.299873 (with geometry of **5a**: -1277.296662), ΔG (298 K, gas): -1277.278662 au; ΔG_{solv} : -23.5 kcal mol⁻¹.

Compound 5d



Atom	Coordinates, Å		
	<i>x</i>	<i>y</i>	<i>z</i>
C	0.189757	-1.046082	-0.007661
C	0.469137	0.393514	-0.009470
C	1.831859	0.872509	-0.009291
C	2.836988	-0.077099	0.006450
C	2.549617	-1.470594	0.008259
C	1.270782	-1.973654	-0.002395
H	3.875154	0.247760	0.009449
H	3.390169	-2.160302	0.018409
H	1.065682	-3.038839	-0.001170
N	-1.103586	-1.385184	-0.002883
N	-0.576529	1.215028	0.000208
Se	-2.042873	0.157796	0.005273
N	2.044824	2.230877	-0.072492
H	1.249965	2.809446	0.160147
H	2.939245	2.576847	0.239128

Collision diameter: 6.586 Å; ΔH (298 K, gas): -2798.448804, ΔG (298 K, gas): -2798.490195 au;
 $\Delta G_{\text{solv}} = -1.6 \text{ kcal mol}^{-1}$.

Radical cation [5d]^{•+}

Atom	Coordinates, Å		
	<i>x</i>	<i>y</i>	<i>z</i>
C	0.187425	-1.022986	0.000264
C	0.450003	0.403862	0.000357
C	1.823651	0.878454	0.000256
C	2.867580	-0.090983	-0.000028
C	2.585492	-1.452230	-0.000186
C	1.270711	-1.945473	-0.000036
H	3.899451	0.250065	-0.000094
H	3.411958	-2.156297	-0.000404
H	1.067263	-3.012041	-0.000138
N	-1.101593	-1.374488	0.000470
N	-0.591279	1.216260	0.000613
Se	-2.057730	0.146829	0.000377
N	2.062624	2.185140	0.000407
H	1.284784	2.836925	0.000589
H	3.003985	2.556639	0.000287

Collision diameter: 6.607 Å; $\langle S^2 \rangle$: 0.760290; E: -2798.299873 (with geometry of **5d**: -2798.292261), ΔG (298 K, gas): -2798.227374 au; ΔG_{solv} : -23.4 kcal mol⁻¹.

Transition state TS1

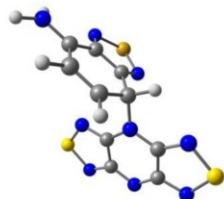


Atom	Coordinates, Å		
	x	y	z
C	-1.938731	1.822127	-0.546175
C	-0.839067	0.839448	-0.574891
C	-2.383231	-0.826859	-0.212632
C	-3.439333	0.193870	-0.206902
N	-1.489344	3.078736	-0.754444
N	0.360205	1.358839	-0.828830
S	0.123124	2.977800	-0.987873
N	-3.229064	1.510602	-0.365579
N	-1.055750	-0.497632	-0.368343
N	-4.658806	-0.356538	-0.031046
N	-2.802323	-2.071617	-0.030211
S	-4.440223	-1.964011	0.127698
C	0.034992	-1.373703	0.739121
C	1.412216	-1.139546	0.271844
C	2.195103	-0.056510	0.838178
C	1.643552	0.745823	1.903677
C	0.441420	0.316505	2.497592

C	-0.275013	-0.761864	2.009815
H	0.069534	0.856392	3.365751
H	-1.192883	-1.061634	2.504448
N	1.972729	-1.832390	-0.695005
N	3.398617	0.154994	0.327076
Se	3.609999	-1.089649	-0.976987
N	2.296648	1.869915	2.266961
H	3.187362	2.075449	1.839645
H	1.984182	2.431680	3.041687
H	-0.349437	-2.370957	0.552881

Imaginary mode: -394 cm^{-1} ; $r(\text{C}\dots\text{N})$: 1.7843 \AA ; $\Delta H(298\text{ K, gas})$: -4075.570602 au ; ΔG_{solV} : $-6.5\text{ kcal mol}^{-1}$.

Sigma-complex



Atom	Coordinates, Å		
	x	y	z
C	2.132916	1.828368	-0.577331
C	-0.985173	1.176130	0.066215
C	-2.306206	-0.732246	0.330880
C	3.406501	-0.006563	-0.320257
N	-1.833087	3.085253	-0.956657
N	0.107769	1.904862	0.161938
S	-0.283808	3.363000	-0.536308
N	-3.331290	1.254921	-0.772090
N	-1.092384	-0.117843	0.511809
N	-4.511452	-0.770887	-0.411141
N	-2.580732	-1.963986	0.709521
S	-4.162443	-2.214655	0.256914
C	0.062309	-0.837487	1.119343
C	1.249505	-0.816859	0.177767
C	2.555348	-0.370683	0.618603
C	2.747948	0.083083	1.960339
C	1.636621	0.093942	2.845897

C	0.383595	-0.302432	2.484980
H	1.802541	0.443643	3.863624
H	-0.434713	-0.274761	3.197468
N	1.124428	-1.198149	-1.064990
N	3.531430	-0.381599	-0.292904
Se	2.779499	-0.994391	-1.838878
N	3.998690	0.472088	2.353270
H	4.679584	0.616050	1.620393
H	4.102108	1.025941	3.188817
H	-0.296689	-1.870900	1.204486

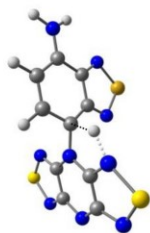
$\langle S^2 \rangle$ (high-spin): 2.0185; ΔH (298 K, gas): -4075.577091 au; ΔG_{solv} : -5.0 kcal mol⁻¹.

$\langle S^2 \rangle$ (broken symmetry): 0.8937.

E (high-spin): -4075.637544, E (broken symmetry): -4075.638676 au.

$J = -220.92 \text{ cm}^{-1}$ as $-(E_{\text{HS}} - E_{\text{BS}}) / (\langle S^2 \rangle_{\text{HS}} - \langle S^2 \rangle_{\text{BS}})$.

Transition state TS2



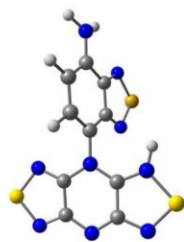
Atom	Coordinates, Å		
	x	y	z
C	-2.944995	1.267520	-0.230107
C	-1.601872	1.242494	0.379956
C	-1.812892	-1.076475	0.367224
C	-3.100322	-0.993726	-0.276867
N	-3.333972	2.532712	-0.441166
N	-1.023903	2.392537	0.601647
S	-2.132971	3.532470	0.068173
N	-3.676716	0.180045	-0.576194
N	-1.049236	0.004311	0.672232
N	-3.551289	-2.230343	-0.572745
N	-1.311597	-2.267595	0.601233
S	-2.482648	-3.368889	-0.047394
C	0.296109	-0.356068	1.065056
C	1.334522	-0.214692	0.042983
C	2.724293	-0.127292	0.456145
C	3.065543	-0.054740	1.854332

C	2.021267	-0.047371	2.803646
C	0.697651	-0.138036	2.421798
H	2.270825	0.046868	3.857622
H	-0.085515	-0.081465	3.172197
N	1.096540	-0.190577	-1.255172
N	3.641246	-0.058609	-0.508009
Se	2.722067	-0.067944	-2.071586
N	4.368507	0.026119	2.193852
H	5.054805	0.107681	1.458051
H	4.649552	0.195000	3.145682
H	-0.096257	-1.758802	0.976599

Imaginary mode: -1849 cm^{-1} , r (C...H...N): 1.4593 and 1.3700 Å, respectively; E (closed shell): -4075.599438 , ΔH (298 K, gas): -4075.546557 au ; ΔG_{solv} : $-6.4\text{ kcal mol}^{-1}$.

$\langle S^2 \rangle$ (broken symmetry): 0.3710, E (broken symmetry): -4075.600351 au .

Intermediate I1

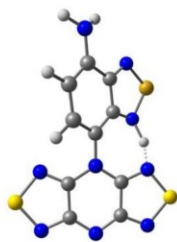


Atom	Coordinates, Å		
	<i>x</i>	<i>y</i>	<i>z</i>
C	3.411621	-0.626438	-0.302686
C	2.042048	-1.100379	-0.145839
C	1.445665	1.084949	0.443749
C	2.847823	1.483230	0.276227
N	4.213947	-1.617725	-0.713028
N	1.814871	-2.358742	-0.421278
S	3.297730	-2.977190	-0.872410
N	3.818018	0.642982	-0.080789
N	1.033829	-0.200258	0.282382
N	3.022880	2.796785	0.528771
N	0.663914	2.103847	0.799282
S	1.622869	3.559162	0.878647
C	-0.278065	-0.671490	0.617340
C	-1.460055	-0.066195	0.097976
C	-2.764295	-0.663754	0.411983
C	-2.861686	-1.839754	1.241774

C	-1.673038	-2.366265	1.725565
C	-0.424107	-1.794701	1.412263
H	-1.697382	-3.249153	2.358575
H	0.468262	-2.274738	1.796107
N	-1.504700	1.030936	-0.667348
N	-3.834463	-0.070259	-0.106193
Se	-3.246448	1.344306	-1.053470
N	-4.100922	-2.334054	1.533684
H	-4.875880	-1.995366	0.983398
H	-4.177494	-3.268273	1.902400
H	-0.327487	2.105946	0.551964

ΔH (298 K, gas): -4075.586974 au. ΔG_{solv} : -8.4 kcal mol⁻¹.

Transition state TS3



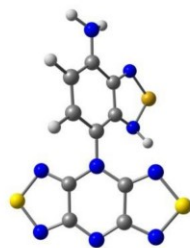
Atom	Coordinates, Å		
	<i>x</i>	<i>y</i>	<i>z</i>
C	3.557619	-0.276949	-0.194771
C	2.243368	-0.923914	-0.170078
C	1.322720	1.170884	0.339050
C	2.679933	1.731422	0.301724
N	4.517301	-1.145354	-0.549557
N	2.222638	-2.193945	-0.494003
S	3.806353	-2.599009	-0.817336
N	3.788856	1.021559	0.080039
N	1.093040	-0.180407	0.181068
N	2.666333	3.061247	0.519803
N	0.373693	2.072447	0.538529
S	1.130222	3.589774	0.693591
C	-0.164948	-0.827088	0.425789
C	-1.410259	-0.270668	0.032616
C	-2.644829	-1.037230	0.181771
C	2.622566	-2.355340	0.743962

C	-1.386380	-2.834273	1.165539
C	-0.205722	-2.095199	1.008946
H	-1.325744	-3.816013	1.627011
H	0.723118	-2.547362	1.328254
N	-1.609613	0.966361	-0.466950
N	-3.782883	-0.444509	-0.200413
Se	-3.403531	1.214240	-0.776244
N	-3.806287	-3.033454	0.897040
H	-4.598808	-2.684924	0.377976
H	-3.766623	-4.032274	1.025965
H	-0.766857	1.734870	-0.026183

Imaginary mode: -1185 cm^{-1} , r (N...H...N): 1.3167 and 1.2228 Å, respectively. E (closed shell): -4075.637385 , ΔH (298 K, gas): -4075.584228 au . ΔG_{solv} : $-6.2 \text{ kcal mol}^{-1}$.

$\langle S^2 \rangle$ (broken symmetry): 0.4038. E (broken symmetry): -4075.638598 au .

Intermediate I2



Atom	Coordinates, Å		
	x	y	z
C	3.451929	-0.402130	-0.411700
C	2.124620	-0.991977	-0.193180
C	1.391818	1.113946	0.513040
C	2.747998	1.618404	0.263656
N	4.321855	-1.311192	-0.891254
N	2.013084	-2.267471	-0.502893
S	3.515655	-2.718365	-1.040877
N	3.774930	0.880673	-0.181081
N	1.085139	-0.214094	0.298529
N	2.844698	2.932469	0.547675
N	0.526729	2.010914	0.953089
S	1.383525	3.437908	1.055866
C	-0.203686	-0.775127	0.581159
C	-1.374727	-0.231168	0.036859
C	-2.641618	-0.844514	0.293011
C	-2.712309	-2.022540	1.102864

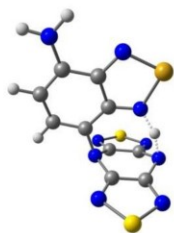
C	-1.519740	-2.536180	1.631198
C	-0.296284	-1.927047	1.376677
H	-1.554438	-3.423974	2.257175
H	0.609908	-2.350651	1.792966
N	-1.443611	0.875602	-0.803971
N	-3.760569	-0.289844	-0.235271
Se	-3.279908	1.186573	-1.175711
N	-3.943665	-2.560317	1.369875
H	-4.708353	-2.241795	0.792130
H	-3.991746	-3.510282	1.701005
H	-0.935904	1.688529	-0.442959

$\langle S^2 \rangle$ (high spin): 2.0139. E (high spin): -4075.647146, ΔH (298 K, gas): -4075.587188 au. ΔG_{solv} : -5.0 kcal mol⁻¹.

$\langle S^2 \rangle$ (broken symmetry): 0.8453. E (broken symmetry): -4075.648584 au.

$J = -270.05 \text{ cm}^{-1}$ as $-(E_{\text{HS}} - E_{\text{BS}}) / (\langle S^2 \rangle_{\text{HS}} - \langle S^2 \rangle_{\text{BS}})$.

Transition state TS4

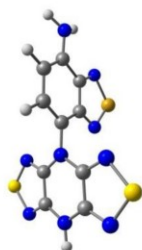


Atom	Coordinates, Å		
	x	y	z
C	-0.066124	0.067165	0.040784
C	1.381625	-0.010663	0.032145
C	1.446306	2.329556	-0.071339
C	0.000350	2.349205	-0.024491
N	-0.641418	-1.125947	-0.084200
N	1.888614	-1.216221	-0.088872
S	0.579527	-2.233266	-0.211879
N	-0.737630	1.238016	0.360965
N	2.155645	1.149374	0.296929
N	-0.501078	3.557552	-0.255691
N	2.028615	3.479875	-0.321790
S	0.786410	4.567149	-0.510147
C	2.650132	1.233711	1.651712
C	1.748933	1.203806	2.749152
C	2.245631	1.385377	4.104944
C	3.660563	1.577597	4.344526

C	4.497901	1.568615	3.237609
C	3.991668	1.406880	1.930218
H	5.566947	1.706377	3.376321
H	4.676504	1.423908	1.087819
N	0.410043	0.987557	2.707313
N	1.356074	1.389294	5.096635
Se	-0.272302	1.099423	4.406890
N	4.075257	1.795659	5.624330
H	3.423159	1.624790	6.373851
H	5.057464	1.759570	5.841846
H	-0.260830	1.144536	1.748982

Imaginary mode: -769 cm^{-1} , $r(\text{N}\dots\text{H}\dots\text{N})$: 1.1803 and 1.4706 Å, respectively. ΔH (298 K, gas): -4075.569816 au . ΔG_{soln} : $-7.2\text{ kcal mol}^{-1}$.

Compound 5



Atom	Coordinates, Å		
	<i>x</i>	<i>y</i>	<i>z</i>
C	-1.161912	0.345069	-3.022310
C	-1.184320	-0.290329	-1.721223
C	1.192085	-0.328456	-1.697575
C	1.215125	0.307041	-2.998640
N	-2.347072	0.627240	-3.509829
N	-2.390763	-0.479103	-1.240546
S	-3.457585	0.115087	-2.372238
N	0.037722	0.613377	-3.651087
N	-0.008084	-0.662695	-1.074785
N	2.417887	0.550599	-3.463109
N	2.382222	-0.556428	-1.193922
S	3.489267	0.003267	-2.304450
C	-0.030772	-1.085881	0.289816
C	-0.018725	-0.101690	1.322038
C	-0.052764	-0.537652	2.717988
C	-0.096939	-1.944774	3.046203

C	-0.112759	-2.843517	1.992373
C	-0.078585	-2.410882	0.642391
H	-0.147810	-3.910014	2.200478
H	-0.093820	-3.157082	-0.147030
N	0.016183	1.214719	1.117675
N	-0.050653	0.416418	3.643647
Se	0.004168	1.985324	2.749734
N	-0.080100	-2.303055	4.368309
H	-0.282951	-1.573044	5.035378
H	-0.378940	-3.232741	4.616906
H	0.054373	1.074517	-4.549124

ΔH (298 K, gas): -4075.705574 au. ΔG_{solv} : -5.0 kcal mol⁻¹.

Supporting Information

Content:

Additional experimental procedures.

Table S1. Crystal data and structure refinement of $\text{PtCl}_2 \cdot 1/2 \text{NCMe}$ and PT.

Figure S1. Molecular structure of $(\text{PT})\text{Cl}_2 \cdot 1/2 \text{NCMe}$.

Figure S2. Molecular structure of PT.

Figure S3. Scan rate dependence of CVs for PT at a GC electrode in $\text{CH}_2\text{Cl}_2/\text{nBu}_4\text{NPF}_6$.

Figure S4. Scan rate dependence of CVs for PT at a Pt electrode in $\text{CH}_2\text{Cl}_2/\text{nBu}_4\text{NPF}_6$.

Figure S5. Cyclic voltammetry measurement of PT and TA.

Figure S6. Spectroelectrochemical measurement of PT and TA.

Table S2. Simulated isotropic EPR Spectrum of $\text{PT}^{+\cdot}$ from DFT calculations

Table S3. Simulated isotropic EPR spectrum of $\text{TA}^{+\cdot}$ from DFT calculations

Additional experimental procedures.

Synthesis of 10,10-dichlorophenoxatellurine, (PT)Cl₂.^[27] Diphenyl ether (7.00 g, 41.2 mmol) and tellurium tetrachloride (11.1 g, 41.2 mmol) were set into a flask with an air-condenser, carrying a moisture guard-tube and heated at 150°C for two hours and at 200°C for four hours, while hydrogen chloride was evolved. The cooled melt was ground and stirred with diethyl ether. After filtration the residue was stirred with acetone and filtered again. The solvent was evaporated and left crude (PT)Cl₂ (14.4 g, 39.3 mmol) that was used without further purification in the next step. A small amount of the crude product was recrystallized from acetonitrile to give orange-brown needles of (PT)Cl₂·1/2 MeCN.

¹H-NMR (360 MHz, d₆-acetone): δ = 8.04 - 7.73 (m, 12H, C_{Ar}-H) ppm. ¹³C-NMR (90 MHz, Acetone-d₆): δ = 150.5, 133.3, 132.8, 124.7, 119.1 (C_{Ar}), 117.9 (C_{Ar}-CH-Te), ¹²⁵Te-NMR (110 MHz, d₆-acetone): δ = 594.4 ppm.

Synthesis of Phenoxatellurine (PT). A mixture of (PT)Cl₂ (2.00 g, 5.45 mmol) sodium sulfide nonahydrate (3.93 g, 16.35 mmol) were heated to 100°C for 15 minutes. After cooling to room temperature the solid was stirred with diethyl ether and washed with water. The organic layer was then separated and dried with magnesium sulfate. Evaporation of the ether left a dark reddish-brown solid, which on further purification by sublimation to give yellow spear-like needles of PT (1.60 g, 5.41 mmol, 99 %; Mp. 77°C. (78 - 79°C^[27]))

¹H-NMR (360 MHz, CDCl₃): δ = 7.68 - 7.06 (m, 12H, C_{Ar}-H) ppm. ¹³C-NMR (90 MHz, CDCl₃): δ = 165.8, 135.2, 129.4, 125.8, 119.9 (C_{Ar}), 106.6 (C_{Ar}-CH-Te), (C_{Ar}-CH-O) ppm. ¹²⁵Te-NMR (110 MHz, CDCl₃): δ = 420.0 ppm. MS (EI, 70 eV, 200 °C): m/z = 298 [M⁺], 168 [M-Te]⁺, 139 [M-Te-CHO]⁺. UV/VIS (CH₂Cl₂): λ_{max} = 279 nm, 343 nm.

Table S1. Crystal data and structure refinement of $\text{PtCl}_2 \cdot 1/2 \text{NCMe}$ and PT.

	$\text{PtCl}_2 \cdot 1/2 \text{NCMe}$	PT [#]
Formula	$\text{C}_{26}\text{H}_{19}\text{Cl}_4\text{NO}_2\text{Te}_2$	$\text{C}_{12}\text{H}_8\text{OTe}$
Formula weight, g mol^{-1}	774.42	295.78
Crystal system	monoclinic	orthorhombic
Crystal size, mm	$0.08 \times 0.08 \times 0.07$	$0.09 \times 0.07 \times 0.03$
Space group	$C2/c$	$P2_12_12_1$
a , Å	27.070(2)	5.9407(2)
b , Å	13.247(1)	8.0196(3)
c , Å	7.4254(7)	20.6459(6)
α , °	90	90
β , °	94.945(3)	90
γ , °	90	90
V , Å ³	2652.8(4)	983.61(6)
Z	4	4
ρ_{calcd} , Mg m^{-3}	1.939	1.997
μ (Mo $K\alpha$), mm^{-1}	2.628	2.983
$F(000)$	1480	560
θ range, deg	2.74 to 35.03	2.62 to 27.50
Index ranges	$-31 \leq h \leq 32$ $-10 \leq k \leq 15$ $-7 \leq l \leq 8$	$-10 \leq h \leq 10$ $-11 \leq k \leq 14$ $-36 \leq l \leq 29$
No. of reflns collected	4974	13802
Completeness to θ_{max}	94.2%	99.0%
No. indep. Reflns	1941	5780
No. obsd reflns with ($I > 2\sigma(I)$)	1703	5309
No. refined params	161	127
Goof (F^2)	1.143	1.038
R_1 (F) ($I > 2\sigma(I)$)	0.0329	0.0258
wR_2 (F^2) (all data)	0.0871	0.0490
Largest diff peak/hole, e Å^{-3}	0.942 / -0.526	0.989 / -0.424
CCDC number	1895457	1895458

[#] Reinvestigation with inclusion of hydrogen atoms.^[37]

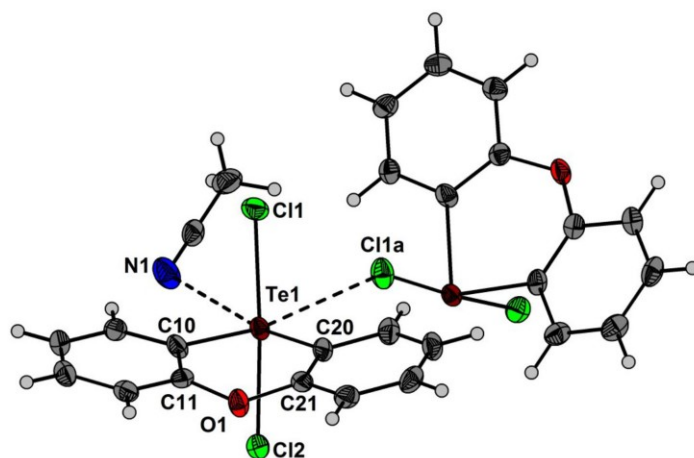


Figure S1. Molecular structure of (PT)Cl₂·1/2 NCMe showing 50% probability ellipsoids

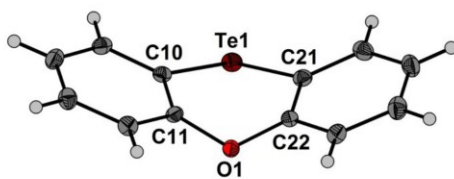


Figure S2. Molecular structure of PT showing 50% probability ellipsoids

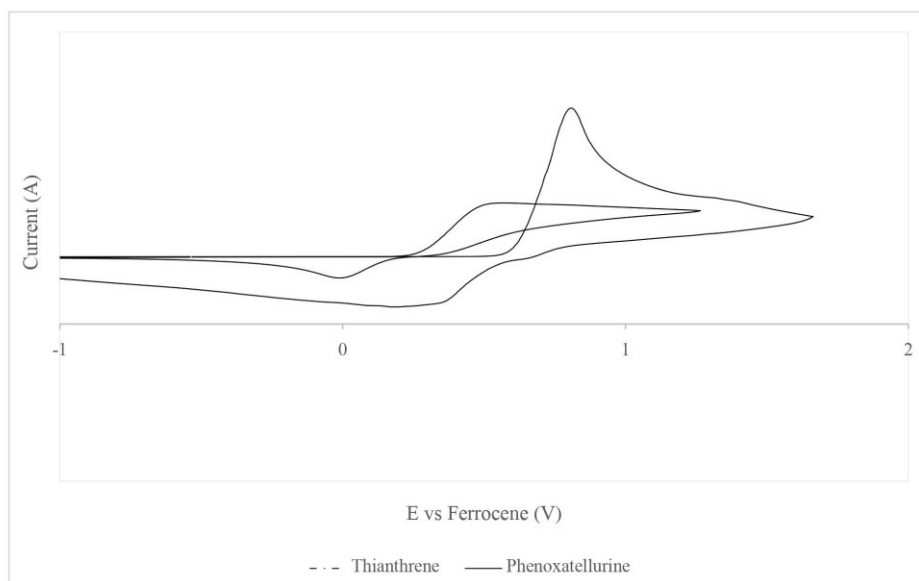


Figure S3. Cyclic voltammetry measurement of phenoxatellurine (5.5 mg/mL) and thianthrene (5.7 mg/mL), conducting salt (0.1 M Bu_4NPF_6) in dichloromethane. The peak potential data for the two scans are:

E_{p1}^a TA	+0.81 V	E_{p1}^a PT	+0.52 V
E_{p1}^c TA	+0.34 V	E_{p1}^c PT -	+0.01 V

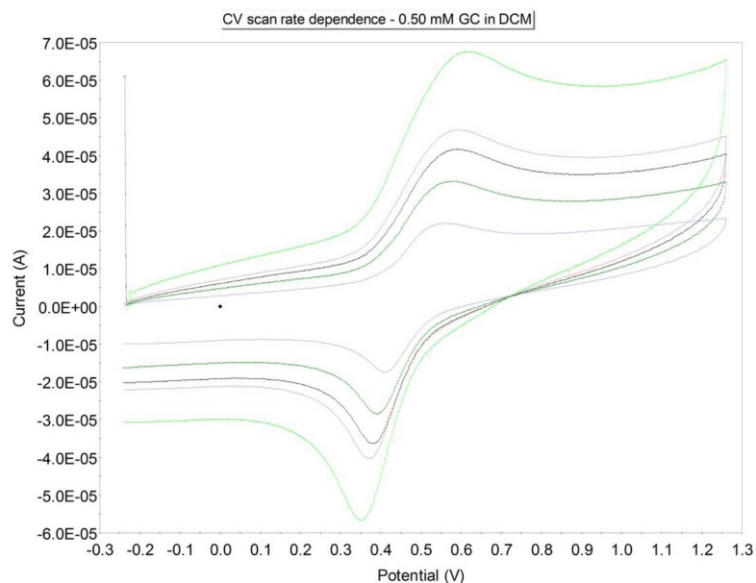


Figure S4. Scan rate dependence (0.2, 0.5, 0.8, 1.0 2.0 V/s) for CVs of PT in anodic scans through the first oxidation process in $\text{CH}_2\text{Cl}_2/[\text{nBu}_4\text{N}][\text{PF}_6]$ at a GC electrode. The ΔE^{a-c} (peak separation) varies as: 0.2: 152; 0.5: 189; 0.8, 200; 1.0, 228; 2.0, 262 mV.

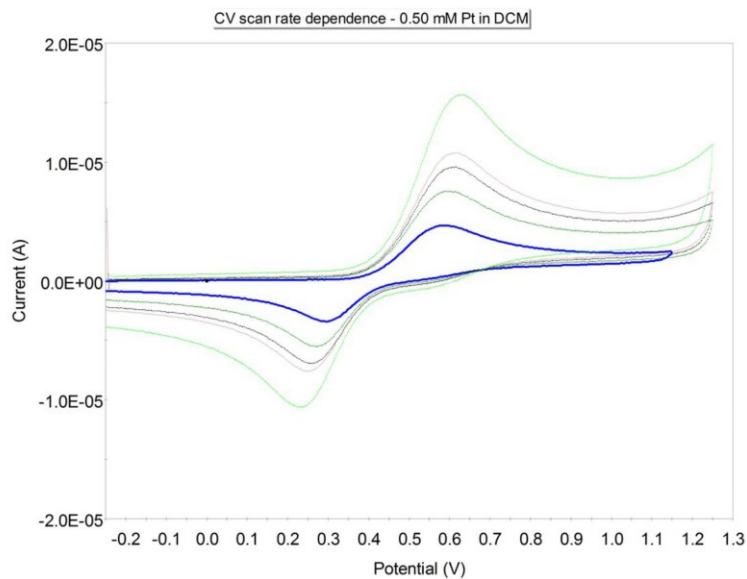


Figure S5. Scan rate dependence (0.2, 0.5, 0.8, 1.0 2.0 V/s) for CVs of PT in anodic scans through the first oxidation process in $\text{CH}_2\text{Cl}_2/[\text{nBu}_4\text{N}][\text{PF}_6]$ at a Pt electrode. The ΔE^{a-c} (peak separation) varies as: 0.2: 292; 0.5: 327; 0.8, 355; 1.0, 363; 2.0, 394 mV.

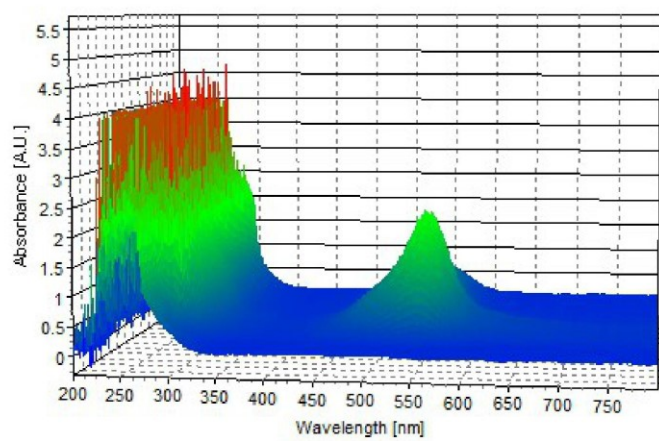
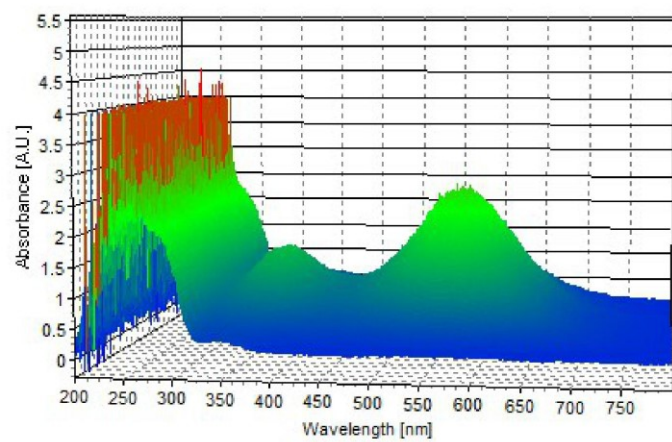
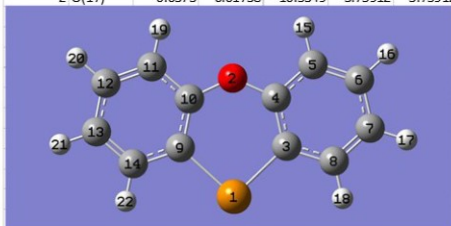


Figure S6. UV-Vis Spectroelectrochemical measurement of PT (top) and TA (bottom).

Table S2. Simulated isotropic EPR spectrum of PT^{•+} from DFT calculations

EPR Simulation: phenoxytellurine radical cation						
From:	Farzin_1_p1_opt	UB3PW91 6-311+G(2df,p) // Te = ?			Doublet	
Isotropic Fermi Contact Couplings						
Atom	Abundance a.u.	MegaHertz	Gauss	Gauss	Simulaed EPR spectrum of the phenoxytellurine radical from DFT	
16 H(1)	99.98	-0.00083	-3.72438	-1.32895	1.32895	
20 H(1)	99.98	-0.00076	-3.38561	-1.20807	1.20807	
17 H(1)	99.98	-0.00056	-2.50503	-0.89386	0.89386	
21 H(1)	99.98	-0.00055	-2.43668	-0.86947	0.86947	
15 H(1)	99.98	0.00012	0.53236	0.18996	0.18996	
19 H(1)	99.98	0.0001	0.45473	0.16226	0.16226	
18 H(1)	99.98	-0.00006	-0.26259	-0.0937	0.0937	
22 H(1)	99.98	-0.00005	-0.23849	-0.0851	0.0851	
1 Te(125)	7.07	-0.00015	0.2137	0.07625	0.07625	
5 C(13)	1.109	-0.00389	-4.37657	-1.56167	1.56167	
11 C(13)	1.109	-0.00368	-4.13592	-1.4758	1.4758	
3 C(13)	1.109	-0.00324	-3.64259	-1.29977	1.29977	
9 C(13)	1.109	-0.00313	-3.52181	-1.25667	1.25667	
8 C(13)	1.109	-0.00249	-2.79998	-0.9991	0.9991	
14 C(13)	1.109	-0.00244	-2.74417	-0.97919	0.97919	
10 C(13)	1.109	-0.00157	-1.76825	-0.63096	0.63096	
4 C(13)	1.109	-0.00137	-1.54085	-0.54981	0.54981	
6 C(13)	1.109	0.00085	0.95299	0.34005	0.34005	
12 C(13)	1.109	0.00065	0.73138	0.26097	0.26097	
7 C(13)	1.109	-0.00049	-0.54619	-0.19489	0.19489	
13 C(13)	1.109	-0.00045	-0.50345	-0.17964	0.17964	
2 O(17)	0.0373	0.01738	-10.5349	-3.75912	3.75912	



For sake of comparison, the same 0.5 GLW is used here for the simulation
 In reality, we expect the strong spin-orbit coupling of Te to significantly
 increase the LW of this radical compared to that of the thianthrene.
 This is expected to eliminate any resolvable hyperfine splitting in the signal.

Table S3. Simulated isotropic EPR spectrum of TA^{•+} from DFT calculations

EPR Simulation: thianthrene radical cation					
From:	17_SS_1_p1_m1_gas_opt	UB3PW91	6-311+G(2df,p)	Doublet	
Isotropic Fermi Contact Couplings					
Atom	Abundanc a.u.	MegaHertz	Gauss	Gauss	Simulated EPR spectrum of the thianthrene radical from DFT
20 H(1)	99.98	-0.00111	-4.97666	-1.77579	1.77579
17 H(1)	99.98	-0.00111	-4.97552	-1.77539	1.77539
21 H(1)	99.98	-0.00111	-4.97329	-1.77459	1.77459
16 H(1)	99.98	-0.00111	-4.97315	-1.77454	1.77454
15 H(1)	99.98	-0.00018	-0.80997	-0.28902	0.28902
22 H(1)	99.98	-0.00018	-0.80956	-0.28887	0.28887
18 H(1)	99.98	-0.00018	-0.80883	-0.28861	0.28861
19 H(1)	99.98	-0.00018	-0.80683	-0.2879	0.2879
10 C(13)	1.109	-0.00377	-4.23822	-1.5123	1.5123
7 C(13)	1.109	-0.00377	-4.2356	-1.51137	1.51137
13 C(13)	1.109	-0.00377	-4.23354	-1.51063	1.51063
4 C(13)	1.109	-0.00376	-4.23231	-1.51019	1.51019
11 C(13)	1.109	0.00082	0.9223	0.3291	0.3291
6 C(13)	1.109	0.00082	0.92091	0.3286	0.3286
12 C(13)	1.109	0.00082	0.91847	0.32773	0.32773
5 C(13)	1.109	0.00082	0.91808	0.32759	0.32759
3 C(13)	1.109	-0.00049	-0.55045	-0.19641	0.19641
14 C(13)	1.109	-0.00049	-0.54762	-0.1954	0.1954
8 C(13)	1.109	-0.00048	-0.54364	-0.19398	0.19398
9 C(13)	1.109	-0.00048	-0.54088	-0.193	0.193
2 S(33)	0.76	0.04978	17.09676	6.10055	6.10055
1 S(33)	0.76	0.04978	17.0964	6.10042	6.10042

Note that the linewidth is merely an arbitrary value, and is likely too narrow. The value here is 0.5 Gauss for a Lorentzian function.

List of Figures

Figure 1. Change of the folding angle along the E – E axis through oxidation (E = S, Se).	4
Figure 2. Crystal structure of the diamagnetic trimer (TA) ₃ [Al ₂ Cl ₇] ₂ with stacks of parallel and eclipsed TA units (parallel triple-decker structure). ^[53]	4
Figure 3. Crystal structure of the diamagnetic trimer (TA) ₃ [C ₁₃ H ₃₆ B ₁₁] ₂ containing stacks of parallel TA units, with an orthogonal central unit to the two outer eclipsed units (crossed triple-decker structure) (Solvent molecules are omitted). ^[51]	5
Figure 4. Crystal structure of the 1,2,3,4,5,6,7,8-octamethylantracene (OMA) double-decker structure (the counterions SbF ₆ are omitted). ^[61]	6
Figure 5. Unit cell of the double-decker structure (left) and the [(H-PA) ₂ (PA)][O ₃ SCF ₃] ₂ triple-decker structure (right). ^[63]	6
Figure 6. Crystal structure of the mixed triple-decker structure [(H-PA) ₂ (AC)][O ₃ SCF ₃] ₂	7
Figure 7. Molecular and crystal structure of the phenoxatellurine charge-transfer complex. .	12
Figure 8. Molecular structure of the one [PT ₃] ²⁺ dication of monoclinic [PT ₃](O ₃ SCF ₃) ₂ showing 50 % probability ellipsoids ([CF ₃ SO ₃] ⁻ omitted).....	40
Figure 9. 2D-packing motifs of the [PT ₃] ²⁺ dication in triclinic (top left), monoclinic (bottom) and orthorhombic (top right).	42
Figure 10. Hirshfeld Surfaces of the conformer in the triclinic, conformer 1 and 2, the monoclinic and the orthorhombic crystal structure. Significant interaction partners are shown if existent, d _{norm} mapped.	44
Figure 11. Hirshfeld surface fingerprint plots of [PT ₃] ²⁺	45
Figure 12. Crystal structures of [PT] ₂ O(O ₃ SCF ₃) ₂ (left) and [PT] ₃ O ₂ (O ₃ SCF ₃) ₂ (right) showing 50 % probability ellipsoids and the essential numbering scheme.....	46
Figure 13. Suggested orientation of the substituents in the bis-(phenoxatellurine)-tricarboxyl-manganese(II)-bromide (Mn(PT) ₂ (CO) ₃ Cl) structure. ^[142]	55
Figure 14. Molecular structure of 2,8-Dimethyl-10,10-dichlorophenoxatellurine.	59
Figure 15. Phenoxaiodonium cation (left) and isoelectronic neutral phenoxatellurine (right). 63	
Figure 16. Crystal structure of [6][O ₃ S(<i>p</i> -C ₆ H ₄ Me)]. Selected bond parameters [°, Å]: I1-C10 2.098(2), I1-C20 2.093(2), C10-I1-C20 87.66(7), I1···O2 2.726(2), I1···O3a 2.667(2).....	64
Figure 17. Naphthalene and acenaphthene scaffold.....	78
Figure 18. Phosphorus substituted acenaphthene with sulphur. ^[161]	78
Figure 19. Molecular structure of 5-diphenylphosphino-6-phenylchalcogenacene-naphthene (Ph ₂ P)Ace(EPh) (7a, E = O; 7b, E = S; 7c, E = Se) showing 50 % probability ellipsoids and essential atom numbering. Selected bond parameters [Å] of 7a: P1-C5 1.837(7), O1-C7 1.389(1), P1-O1 2.871(5). Selected bond parameters [Å] of 7b: P1-C5 1.846(5), S1-C7 1.776(4), P1-S1 3.061(8). Selected bond parameters [Å] of 7c: P1-C5 1.846(7), Se1-C7 1.919(9), P1-Se1 3.140(5).	81
Figure 20. Molecular structure of the oxidation of C ₃₀ H ₂₄ SPOsSbF ₆ with nitrosonium hexafluoroantimonate showing 50 % probability ellipsoids and essential atom numbering. Selected bond parameters [Å]: P1-O1 1.520(1), P1-S1 3.239(1).	82

Figure 21. Molecular structure of (2,6-Mes ₂ C ₆ H ₃) ₂ E (9a, E = S; 9b, E = Se; 9c, E = Te) showing 50 % probability ellipsoids and the essential atom numbering. Selected bond parameters [Å, °] of 9a: C10-S1 1.778(3), C40-S1 1.779(3), C10-S1-C40 109.2(1). Selected bond parameters [Å, °] of 9b: Se1-C10 1.941(2), C10-Se1-C10a 116.3(1). Selected bond parameters [Å, °] of 9c: Te1-C10 2.150(1), C10-Te1-C10a 116.16(5).	89
Figure 22. Cyclic Voltammetry measurements of <i>m</i> Ter ₂ S, <i>m</i> Ter ₂ Se and <i>m</i> Ter ₂ Te at 0.1 V · s ⁻¹ in dichloromethane, c = 5 · 10 ⁻³ mol · L ⁻¹	90
Figure 23. Molecular structure of [(2,6-Mes ₂ C ₆ H ₃) ₂ TeOH][SbF ₆] (10) showing 50 % probability ellipsoids and the essential atom numbering. Selected bond parameters [Å, °]: Te1-C10 2.149(1), Te1-C40 2.118(1), C10-Te1-C40 108.1(5), Te1-O1 1.74(3), O1-F1 2.805(2).....	92
Figure 24. Molecular structure of [Mes ₃ Te][PbF ₆] showing 50 % probability ellipsoids and the essential atom numbering. Selected bond parameters [Å, °]: Te1-C1 2.132(3), Te1-C10 2.125(3), Te1-C19 2.131(3), C1-Te1-C10 104.26(1), Te1-F1 3.583(3), Te1-F2 3.554(1), Te1-F3 3.563(2).....	96
Figure 25. Phenoxatellurine double decker and triple decker structures (respective anions omitted).....	100

List of Schemes

Scheme 1. Oxidation of diphenyl disulphide in concentrated sulphuric acid (intermediate species in brackets have not been isolated).	3
Scheme 2. Addition of thianthrene radical cation (TA) ^{•+} to cyclohexane. ^[56]	5
Scheme 3. Creation of the triple-decker structure [(H-PA) ₂ (PA)][O ₃ SCF ₃] ₂ (left) and the mixed triple-decker structure [(H-PA) ₂ (AC)][O ₃ SCF ₃] ₂ (right). ^[64]	7
Scheme 4. Oxidation of dimethyl disulphide (Me ₂ S ₂) with antimony pentachloride (SbCl ₅). ^[72]	8
Scheme 5. Oxidation of bis(perfluoroethyl) diselenide [(C ₂ F ₅) ₂ Se ₂] with antimony pentafluoride (SbF ₅). ^[73]	8
Scheme 6. Single-electron oxidation of di-neo-pentyl disulphide (Neo ₂ S ₂) with nitrosonium triflate ([NO][O ₃ SCF ₃]). ^[74]	8
Scheme 7. Single-electron oxidation of dialkyl dichalcogenides Me ₂ Se ₂ and R ₂ Te ₂ (R = Et, Pr, <i>i</i> -Bu) with nitrosonium triflate ([NO][O ₃ SCF ₃]). ^[75,76]	9
Scheme 8. Single-electron oxidation of dialkyl sulphide with titanium(III)-hydrogen peroxide. ^[82]	9
Scheme 9. Stepwise oxidation of 1,5-dithiacyclooctane (DTCO) with nitrosonium tetrafluoroborate [NO][BF ₄]. ^[89]	10
Scheme 10. Example of a selenurane and the stabilization of the dication. ^[108]	10
Scheme 11. Oxidation of dinaphtho[1,8- <i>b,c</i>]-1,5-dithiocin in conc. sulphuric acid. ^[111]	11
Scheme 12. Synthesis of the diaryldichalcogenide radical cations.....	11
Scheme 13. Reaction of phenoxatellurine with AlCl ₃ /CH ₂ Cl ₂ (1), [NO][SbF ₆] (2) and [NO][BF ₄] (3).	26
Scheme 14. Reaction of phenoxatellurine (PT) with triflic acid and gaseous oxygen.	40
Scheme 15. Reaction of [PT] ₃ (O ₃ SCF ₃) ₂ with moist air.	46
Scheme 16. Synthesis of phenoxaiodonium tosylate.	63
Scheme 17. Synthesis of 5-bromo-6-diphenylphosphinoacenaphthene.....	79
Scheme 18. Synthesis of 5-diphenylphosphino-6-chalcogenacenaphthene.....	80
Scheme 19. Reaction of 5-diphenylphosphino-6-phenylsulphideacenaphthene with nitrosonium hexafluoroantimonate.	82
Scheme 20. Synthesis of 2,6-dimesitylphenyliodide.	88
Scheme 21. Synthesis 2,6-dimesitylphenylchalcogene from 2,6-dimesitylphenyllithium and EF ₄ (E = S, Se, Te).	89
Scheme 22. Reaction of 2,6-dimesitylphenyltelluride with nitrosonium hexafluoroantimonate.	91
Scheme 23. Synthesis of trimesityltellurium hexafluorophosphate.....	96

List of Charts

Table 1. Selected bond parameters of the $[\text{PT}_3]^{2+}$ dications within the three modifications. .	41
Table 2. Percentage contributions of atom–atom interactions between a central $[\text{PT}_3]^{2+}$ dication with adjacent $[\text{PT}_3]^{2+}$ dications and triflate ions in the crystal lattice for all three modifications (^a conformer 1, ^b conformer 2).....	43
Table 3. Selected bond parameters for the oxo-bridged species ($[\text{PT}]_2\text{O}(\text{O}_3\text{SCF}_3)_2$ and $[\text{PT}]_3\text{O}_2(\text{O}_3\text{SCF}_3)_2$).	47
Table 4. Te···O bond lengths of the PT units towards the triflic anions.	47
Table 5. Crystal data and structure refinement of $[\text{PT}]_3(\text{O}_3\text{SCF}_3)_2$ (three modifications).....	49
Table 6. Crystal data and structure refinement of $[\text{PT}]_2\text{O}(\text{O}_3\text{SCF}_3)_3$ and $[\text{PT}]_3\text{O}_2(\text{O}_3\text{SCF}_3)_3$. .	50
Table 7. Crystal data and structure refinement of $[\text{6}][\text{O}_3\text{S}(p\text{-C}_6\text{H}_4\text{Me})]$	66
Table 8. Crystal data and structure refinement of $(\text{Ph}_2\text{P})\text{Ace}(\text{EPh})$ (7a, E = O; 7b, E = S; 7c, E = Se).....	86
Table 9. Crystal data and structure refinement of $(\text{Ph}_2\text{PO})\text{Ace}(\text{SPh})[\text{SbF}_6]$ (8).	87
Table 10. Results of the cyclic voltammetric measurements of <i>mTer</i> ₂ S, <i>mTer</i> ₂ Se and <i>mTer</i> ₂ Te.....	91
Table 11. Crystal data and structure refinement of 1a – 1c and 2.	95
Table 12. Crystal data and structure refinement of $[\text{Mes}_3\text{Te}][\text{PF}_6]$ (11).	99